CHEMICAL REVIEWS

pubs.acs.org/CR

Open Access

This article is licensed under CC-BY-NC-ND 4.0

Review

# Skin-Integrated Soft Wearable XR Interfaces for Seamless and Realistic User Experience

Kyung Rok Pyun, Jung Jae Park, Jiyong Ahn, Yoon Seon Lee, Hongchan Kim, Jinsol Kim, Sangjin Yoon, Kyoung-Ho Ha, Deog-Gyu Seo,* John A. Rogers,* and Seung Hwan Ko*

Cite This: *Chem. Rev.* 2025, 125, 11567−11665

Read Online

ACCESS | Metrics & More | Article Recommendations

**ABSTRACT:** Extended reality (XR) is an emerging field that connects the physical and digital worlds, enabling communication that transcends time and space. Commercial XR devices have been developed to support such experiences, but they are limited to specific sensations, mainly vibrational cues. Furthermore, these devices are realized mainly in rigid form factors, requiring external controllers or equipment, which hinders intuitive interaction and causes a mismatch with natural body movements. In this regard, skin-integrated human−machine interfaces with wearable electronics have played an important role in intuitive and immersive interaction in the XR environment, facilitating highly authentic sensory reconstruction and perception. Novel innovations in materials and structural design have enabled a wider range of sensory modalities and miniaturization, overcoming the limitations of conventional rigid XR systems. In this article, we thoroughly review human perception mechanisms to replicate hyper-realistic sensations. Then, we deal with the design and functionality for sensory feedback and input, specifically tailored for XR applications. In addition, we discuss precise system-level integration for untethered XR devices, alongside the role of artificial intelligence in real-time processing and rapid sensation conversion through predictive algorithms. Finally, we introduce promising XR applications and conclude with the challenges and prospects of future XR technologies.

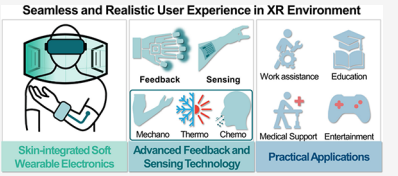


## CONTENTS



**Received:** December 13, 2024
**Revised:** November 5, 2025
**Accepted:** November 7, 2025
**Published:** December 4, 2025


Downloaded via NORTHWESTERN UNIV on December 27, 2025 at 12:58:49 (UTC).
See https://pubs.acs.org/sharingguidelines for options on how to legitimately share published articles.

ACS Publications

© 2025 The Authors. Published by American Chemical Society

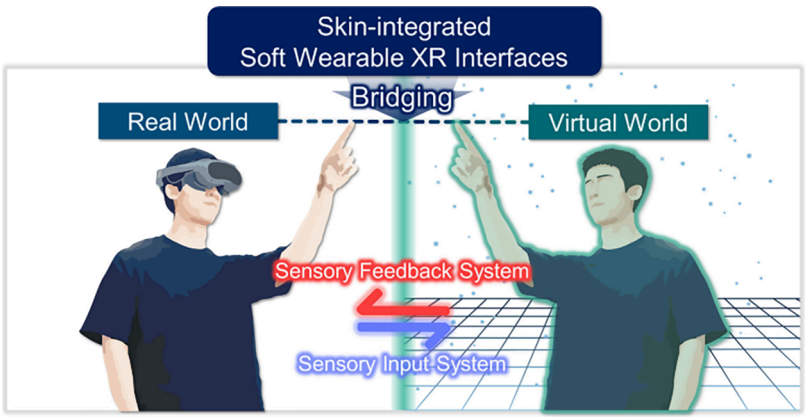


**Figure 1.** Conceptual illustration of a skin-interfaced soft wearable XR interface bridging the real and virtual worlds. Sensory information is delivered through the sensory feedback and input system, crossing the boundaries between the real (left) and virtual (right) worlds.



## 1. INTRODUCTION

Extended reality (XR) represents a collective term for technologies aimed at augmenting or replacing the human experience of reality, either by merging the virtual and the physical or by constructing entirely immersive spaces.[1] The rapid progress of XR is significantly revolutionizing human interaction with the world, introducing unprecedented changes to daily life.[2] Moreover, XR serves as a key enabler for emerging innovations such as the Metaverse, which necessitate novel and evolved communicative modalities.[3]

Central to the XR experience is the concept of immersion, which blurs the distinction between the virtual and physical worlds.[4] This immersion relies on the ability of technologies to replicate and perceive sensory information such as vision, audition, tactility, gustation, and olfaction, which are pathways for humans to interact with the surrounding environment.[5] Furthermore, a fully interactive and immersive experience within the XR environment requires a bidirectional exchange of sensory information through interfaces that deliver virtual stimuli to the user and capture user responses.[6]

The bidirectional attributes of XR highlight the importance of the human−machine interface (HMI), which functions as a direct conduit between humans and machines.[7] XR interfaces facilitated by soft wearable HMIs bridge the gap between the real world and the virtual world (Figure 1). The HMI in XR technologies is bifurcated into sensory feedback systems and input systems. Sensory feedback systems generate artificial sensations that transition experience from the real world to the virtual world. The feedback systems utilize mechanical, thermal, electrical, or chemical mechanisms to create various artificial sensations.[8−10] On the other hand, sensory input systems recognize human actions and environmental cues to reflect these interactions within the virtual world. These input systems employ sensors equipped with diverse mechanisms to capture extensive and responsive interactions.

Recent developments in soft wearable electronics, which include actuators and sensors, offer substantial potential for XR technologies to exchange sensory information with users.[11−14] Being conformally attached to the human body, soft wearable electronics can emulate and recognize the stimuli of the real world. Their high mechanical compliance ensures comfortable use and enhances wearability, while their conformity to the skin increases the authenticity of artificial sensations and improves the accuracy of sensing human interaction. Thereby, soft wearable electronics have evolved into qualified form factors for intuitive HMI, enabling the exchange of sensations that closely mimic real-world interactions, and thus facilitating natural communication through the XR interface. Furthermore, the seamless integration of user responses with the immersive XR experience can enhance both realism and the interactivity of the virtual world.

In the realm of XR devices, the challenge lies not simply in generating sensations, but in meticulously considering human perception to enhance the authenticity of these experiences.[15] Unlike other wearable applications, XR technologies must engage deeply with the nuances of human sensory feedback systems. The human sensory system is intricate, featuring a multimodal array of receptors that perceive and interpret various stimuli. For XR devices to deliver truly immersive and convincing sensations, they must closely align with the biological mechanisms of human perception. This requires a precise simulation of sensory data, such as signal frequency and stimulation strength, and feedback mechanism, tailored to resonate with the natural processing of the human body. In this regard, wearable XR devices, particularly in the domains of vision and audition, have advanced significantly, reaching stages of commercialization. However, the development of XR technologies for tactile, motion, olfactory, and gustatory senses


https://doi.org/10.1021/acs.chemrev.4c00966
Chem. Rev. 2025, 125, 11567−11665

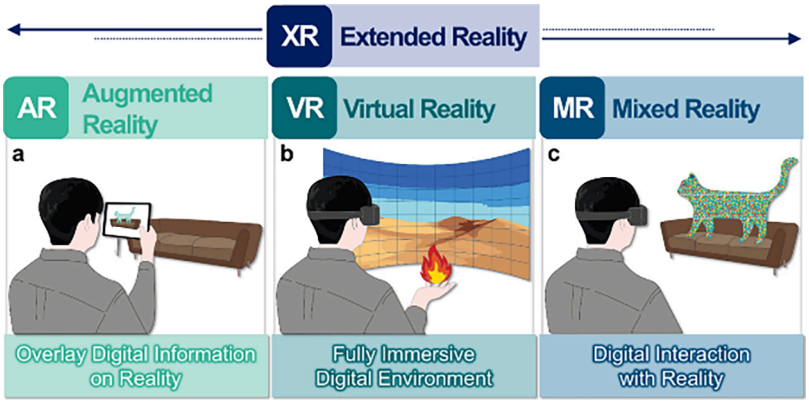


**Figure 2.** Overview of XR technologies. Illustrations that highlight the differences between (a) AR, (b) VR, and (c) MR. AR overlays virtual content onto the real world, while VR immerses the user in a fully digital environment. MR allows real-time interaction between physical and virtual elements. XR is a collective concept that encompasses AR, VR, and MR.

remains in the early stages. Therefore, this report focuses on the cutting-edge developments in soft wearable XR technologies equipped with feedback systems and sensors, specifically targeting tactility, motion, olfaction, and gustation.

First, we will elucidate the sophisticated human sensory system, as well as feedback and sensing mechanisms, and associated materials and devices that are essential for achieving realistic sensory feedback simulations in immersive XR applications. Furthermore, this review will delve into the essential components of system-level integration for untethered wearable XR systems. This includes an exploration of power sources, electrical circuit systems, and wireless communication technologies, all of which are crucial for the seamless functionality of these devices.

In addition, this paper will address the recent advancements in artificial intelligence (AI), particularly focusing on machine learning (ML) techniques, that have been instrumental in overcoming challenges such as user calibration, hysteresis, control issues, and nonlinearities arising from the inherent nature of the soft materials used in wearable electronics.[16] ML techniques have also enabled real-time signal processing and feature extraction from large volumes of random data, which are indispensable for the practical deployment of XR applications. Lastly, we will discuss XR technology-based wearable applications, the remaining challenges, and the outlook for a new class of soft wearable XR technologies, aiming to provide a comprehensive perspective on the evolving scope of this field.

## 2. OVERVIEW OF XR

The term 'Reality' has been modified with various prefixes to define new forms of reality that either merge with or diverge from our everyday reality.[17] XR represents all real and virtual combined environments with HMIs created through computer-based technology, which encompasses the entire spectrum of Augmented Reality (AR), Virtual Reality (VR), and Mixed Reality (MR).[1] This section will explore the commonly encountered Reality-related terms and define each reality to distinguish between them.

AR, VR, and MR are fundamentally all grounded in graphic and display technology, sharing a similar hardware and software infrastructure that includes feedback systems, sensors, cameras, processors, imaging technologies, and advanced algorithms for image processing, object recognition, and spatial mapping.[18] Each of these realities aims to immerse the user in an experience that enhances or alters their perception of reality. XR and its components possess transformative potential across numerous sectors, enhancing how users interact with and perceive surrounding environments, thereby blending the boundaries between physical and digital realities. AR augments the real world with digital overlays, VR creates a completely virtual environment, and MR seamlessly blends real and virtual elements to provide an immersive experience (Figure 2).

AR integrates virtual objects or information with the surrounding environment of users in real-time by overlaying computer graphics onto existing images of the world, thereby making digital objects or information appear as if they are part of the original environment (Figure 2a).[19] Basically, AR enhances the natural world with sounds, videos, and graphics as perceived through a camera or transparent lenses. Using smartphones or tablets, users can view and interact with AR content on their screen, which overlays virtual objects onto the live camera feed of the real environment.[20] Furthermore, glasses allow for a hands-free experience, where virtual objects are projected into the view of the user. Interaction with AR content is typically achieved through touch gestures, such as tapping, swiping, or pinching on the screen.

VR, in contrast, creates a completely virtual environment, isolating the user from the real world and immersing them in a fully digital experience (Figure 2b).[21] VR completely replaces the surroundings of the user with a digitally constructed environment. This immersive experience is achieved primarily through the use of VR headsets, which cover both the eyes and ears to deliver visual and auditory stimuli that simulate the real world. Users wear VR headsets or goggles that completely cover their vision, providing a 360° view of the virtual world. The visual experience is coupled with auditory input through headphones or integrated speakers. VR commonly uses handheld controllers, which allow users to grab or manipulate virtual objects, perform gestures, and interact with the virtual environment in a tactile way. The controllers often have buttons, triggers, and haptic feedback to enhance the user interaction.

MR represents a fusion of both real and virtual worlds, creating environments where physical and digital objects coexist and interact in real-time (Figure 2c).[22] This technology not only overlays but also anchors virtual objects to the real world, enabling them to interact with the physical environment and the user through advanced sensors and cameras.


https://doi.org/10.1021/acs.chemrev.4c00966
Chem. Rev. 2025, 125, 11567−11665

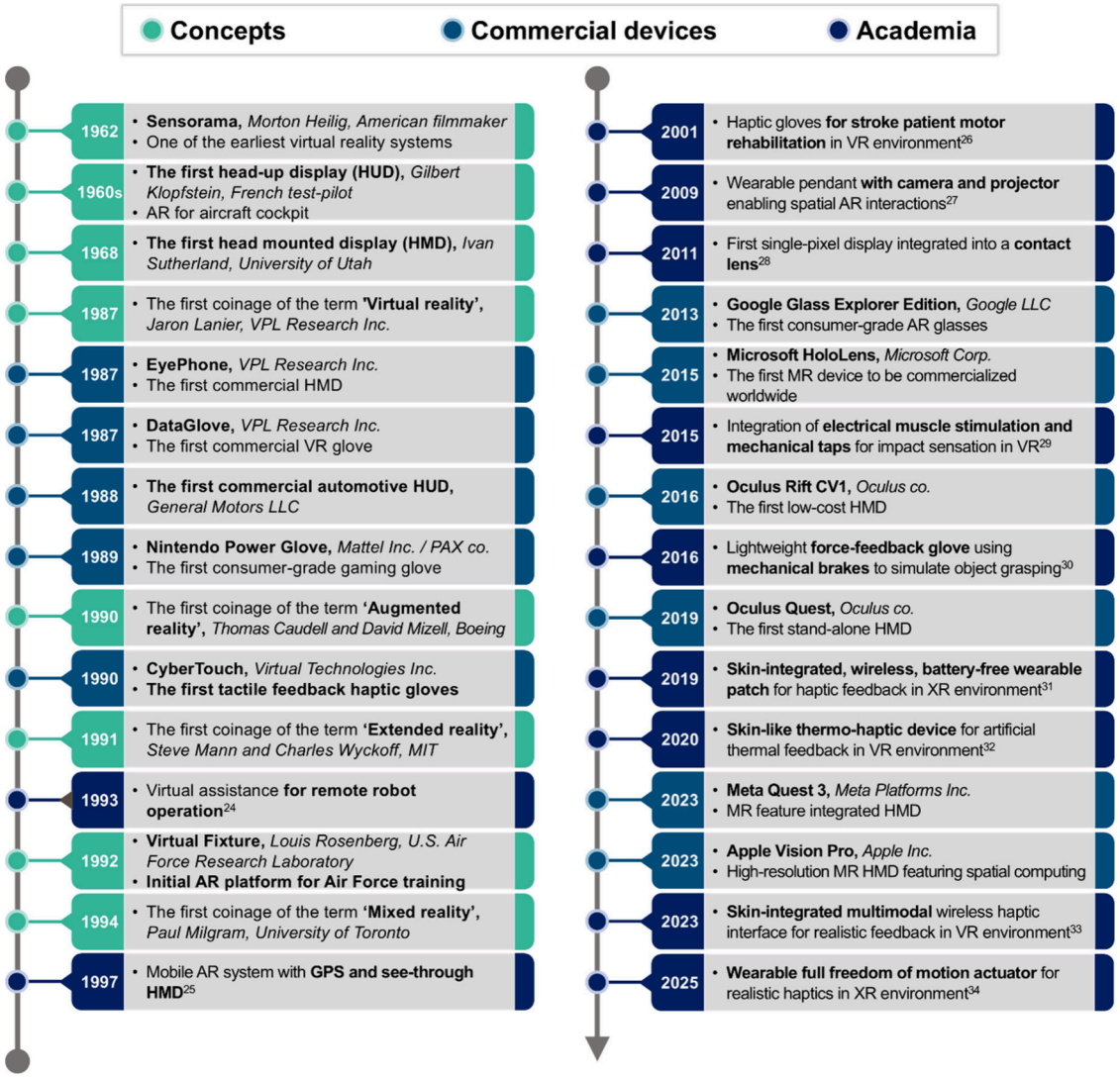


**Figure 3.** Timeline of key developments in the evolution of XR technologies. The advancement of XR technologies has been shaped by foundational concepts, academic research, and commercial deployment. Conceptual developments (green dots) introduced terms such as VR, AR, and MR. Commercial releases (blue dots) brought XR into practical use, ranging from headsets to wearable XR devices. Academic progress (dark blue dots) enabled immersive interaction through advances in display, haptic feedback, and input devices.[24−34] This timeline outlines the transition of XR concepts and technologies from early ideas to widely adopted technologies.

Furthermore, users can interact with virtual objects through natural hand gestures, and in some cases, directly touch or manipulate them as if they were real. This is possible due to the precise tracking and spatial mapping capabilities of MR technology. Interaction with these objects can be managed via voice commands, eye tracking, or external controllers that recognize hand gestures and movements.

Over the past few decades, the conceptual foundations of AR, VR, and MR have evolved into practical technologies through progressive developments in both commercial products and academic research (Figure 3). Interaction with virtual objects in AR, VR, and MR relies primarily on a combination of visual display technologies, sensory inputs, and input methods, including touchscreen interactions, human gestures, and voice commands.[23] Although these elements have collectively enhanced the immersion and realism of XR experiences, achieving a higher level of interaction requires more intuitive HMIs. For example, the commonly used rigid external controllers are inadequate for intuitive HMIs due to their limited functionality and programmed responses, which fail to align naturally with human gestures, such as requiring a button press instead of recognizing a natural grabbing motion. Thus, for XR devices, accurately identifying human behaviors as they occur is important for developing natural and intuitive HMIs. Moreover, the bulkiness and weight of current rigid wearable XR devices can impede human natural movement, thereby diminishing the immersive interaction. Therefore, soft wearable XR devices will play a crucial role in enhancing intuitive interaction and achieving high levels of immersion in XR applications.

In addition, simultaneous stimulation of the human five senses is important for wearable XR devices to implement a high-level immersion. In this respect, the development of comprehensive sensory stimulation, including touch, taste, and smell, is essential for the multistimulation of human senses. Incorporating advanced feedback systems and sensing technologies, soft wearable XR devices are expected to facilitate more natural and intuitive user interactions. There-


https://doi.org/10.1021/acs.chemrev.4c00966
Chem. Rev. 2025, 125, 11567−11665

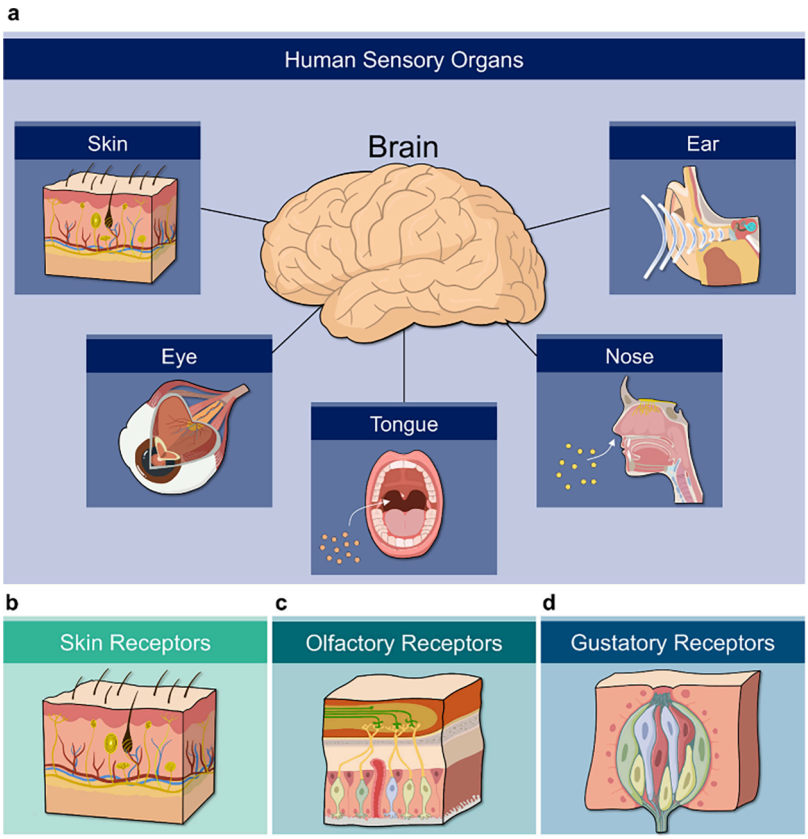


**Figure 4.** Human sensory organs and receptors in the human body. (a) Graphical illustration of sensory organs in humans connected to the brain. Magnified illustration of the organs with receptors in the (b) skin, (c) nose, and (d) tongue. Created with BioRender.com.

fore, soft wearable XR devices can integrate seamlessly with existing XR technologies, enabling users to interact with and manipulate both digital and physical elements within XR environments by closely mirroring natural human behavior and their surroundings.

## 3. BIOLOGICAL MECHANISMS OF HUMAN SENSORY SYSTEM

In the field of XR technology, the creation of artificial sensations by wearable sensory feedback systems is pivotal for achieving a high level of immersion.[35] The degree immersion is essentially determined by human perception, and thus it is difficult to technically quantify or objectify human feelings.[36] Given that the subject of sensory feedback in XR environments is the human being, a profound understanding of human sensory perception mechanisms is crucial for reproducing realistic sensations.[37] To achieve truly immersive and convincing artificial experiences, the XR feedback system must be designed with a deep understanding of how humans perceive and process sensory information. This knowledge is essential not only for enhancing realism but also for ensuring that the artificial sensations resonate authentically with users, thereby maximizing engagement and immersion.

Sensory perception refers to the process by which various stimuli such as touch, pain, temperature, light, taste, smell, and sound are transmitted through nerves to the central nervous system and then perceived by the brain.[38] Thus, the sensory nervous system can be understood as the biological information transmission pathway that detects changes in the external environment. All sensory stimuli must be converted into a form that can be transmitted through sensory nerves, which is a process known as transduction. This transduction begins at specialized sensory receptors located on specific parts of the body such as skin, eyes, tongue, nose, and ears (Figure 4a). To perceive a particular type of sensation, there must be a specific stimulus capable of triggering that sensation, and simultaneously, a specific receptor that can respond to that stimulus.

Basic sensory receptors can be categorized into several types based on the nature of the stimuli they detect. The first type is mechanoreceptors that respond to mechanical pressure or stretch.[39] The second type is thermoreceptors that respond to temperature changes.[40] The third type is chemoreceptors which detect chemical stimuli such as taste, smell, and blood oxygen levels.[41] The fourth type is nociceptors which react to physical or chemical damage to tissues.[42] The fifth type is electromagnetic receptors that respond to light and other electromagnetic waves.[43] The sixth type is auditory receptors, or hair cells in the inner ear, which specifically respond to sound waves.[44] Additionally, proprioceptors are often considered a specialized type of internal mechanoreceptor that monitors changes in the internal body environment, such as balance, position of the body, and muscle tension.[45]

In this chapter, we will concentrate on the mechanoreceptors and thermoreceptors situated in the skin (Figure 4b), alongside the chemoreceptors including the olfactory receptors in the nose (Figure 4c) and the gustatory receptors on the tongue (Figure 4d). These receptors are particularly pertinent to the primary focus of our paper on soft wearable XR devices. Therefore, we will examine their characteristics and explore the associated sensory perception processes.


https://doi.org/10.1021/acs.chemrev.4c00966
Chem. Rev. 2025, 125, 11567−11665

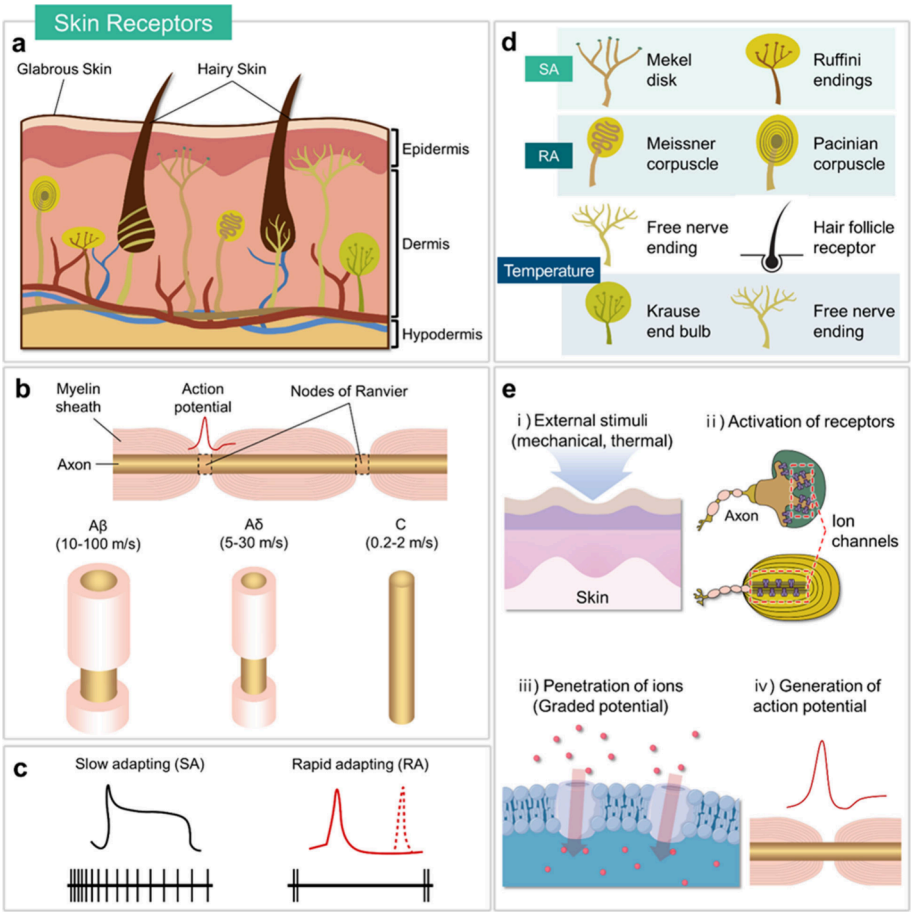


**Figure 5.** Mechanical receptors in human skin and their mechanisms. (a) Anatomy of human skin and its layers. (b) Anatomy of sensory fibers, categorized by conduction speed. The nodes of Ranvier are small gaps found between the myelin sheath that surrounds the axon of nerve cells. The myelin sheath, a fatty layer, accelerates the conduction of nerve signals (action potential). (c) Afferent responses of SA and RA receptors. (d) Various mechanoreceptors and thermoreceptors in human skin. (e) Mechanisms and processes involved in sensing external stimuli. Created with BioRender.com.

### 3.1. Mechanical and Thermal Receptors in Human Skin

Human skin is a complex organ composed of multiple layers, each fulfilling essential protective, sensory, and regulatory functions.[46] The skin is composed of the epidermis, dermis, and hypodermis, each of which serves distinct roles in protection and sensory perception (Figure 5a).[47] The epidermis, the outermost layer, functions as a protective barrier against environmental threats such as pathogens, ultraviolet (UV) radiation, and water loss. It is primarily composed of keratinocytes, which contribute to maintaining the integrity and resilience of the skin. Beneath the epidermis, the dermis provides structural support and contains essential components, including blood vessels, hair follicles, and sweat glands. This layer is rich in collagen and elastin, which are critical for maintaining the flexibility and tensile strength of the skin. The hypodermis, or subcutaneous layer, consists primarily of adipose tissue and connective tissue, offering insulation, cushioning, and energy storage for the body.

In terms of sensory perception, the skin contains numerous sensory receptors, particularly within the dermis.[48] These receptors detect various stimuli, including pressure, pain, touch, and temperature. For example, specialized nerve endings, such as Meissner corpuscles, which detect soft touch, and Pacinian corpuscles, which respond to intense pressure, relay sensory information to the central nervous system, enabling the body to react to external stimuli. These layers and the sensory receptors function collaboratively to allow the skin to detect a diverse range of stimuli, enhancing our interaction with the environment and contributing to our overall sensory experience.

Mechanoreceptors in human skin can be mainly classified into high-threshold mechanoreceptors (HTMRs) and low-threshold mechanoreceptors (LTMRs) based on their activation thresholds.[49−51] HTMRs have a high activation threshold, responding only to intense mechanical or noxious stimuli.[52] These receptors are activated by strong forces such as pinching or piercing, which have the potential to cause tissue damage. As a result, HTMRs play a critical role in triggering protective responses by functioning as nociceptors, detecting painful stimuli, and signaling the possibility of injury. HTMRs are predominantly found as free nerve endings.

In contrast, LTMRs possess a low activation threshold, responding readily to non-noxious mechanical stimuli such as light touch, mild pressure, or fine vibrations.[53] These receptors are responsible for detecting everyday tactile sensations, vibrations, and subtle changes on the surface of the skin. Merkel cells, Meissner corpuscles, Pacinian corpuscles, and Ruffini endings are common examples of LTMRs. Given that immersive user experiences in XR devices primarily aim to


https://doi.org/10.1021/acs.chemrev.4c00966
Chem. Rev. 2025, 125, 11567−11665

replicate non-harmful tactile sensations, the focus of this discussion will be on LTMRs.

**3.1.1. Sensory Fibers.** For the sensing mechanism, physical deformation of the skin results in structural perturbation of LTMRs. When a stimulus is applied to an LTMR and sustained, the sensory afferent initiates a series of action potentials at the first node of Ranvier, which are then propagated along nerve fibers to the central nervous system (Figure 5b).[54] Upon stimulation, sensory receptors generate electrical signals through membrane depolarization, leading to the production of action potentials in the corresponding sensory fibers. These signals are subsequently transmitted to the central nervous system, where they are processed and integrated to produce appropriate responses.

Sensory fibers are vital components of the nervous system that facilitate sensory perception by detecting both external and internal stimuli, subsequently conveying this information to the brain and spinal cord for interpretation and response.[55−57] These fibers are typically categorized into A, B, and C fibers based on their degree of myelination and diameter, with each type specialized for transmitting distinct types of sensory information.[48] A fibers are characterized by rapid conduction velocities, with A$\alpha$ fibers transmitting signals related to muscle function and proprioception, A$\beta$ fibers conveying sensations of touch, pressure, and vibration, and A$\delta$ fibers transmitting sharp pain and temperature changes. B fibers, which are myelinated but thinner than A fibers, are primarily responsible for transmitting autonomic functions and signals related to visceral sensations. In contrast, C fibers, which are unmyelinated, are associated with the transmission of slow, diffuse pain and chronic temperature sensations. These sensory fibers are intricately linked with various sensory receptors that transduce stimuli into electrical signals, which are then relayed along neural pathways to the central nervous system for processing and response. Notably, most tactile sensations are transmitted by A$\beta$ fibers, which are large myelinated nerve fibers.[58] Conversely, nociceptive and thermosensory information are primarily conveyed by A$\delta$ and C fibers, respectively.[59,60] LTMRs are classified into A$\beta$-LTMRs, A$\delta$-LTMRs, and C-LTMRs, depending on the type of sensory fibers they are associated with. Each LTMR subtype exhibits differences in the specific stimuli they detect and their conduction velocities. Heavily myelinated A$\beta$-LTMRs propagate action potentials at high velocities (15−100 m $s^{-1}$), while lightly myelinated A$\delta$-LTMRs and unmyelinated C-LTMRs conduct signals at intermediate (5−30 m $s^{-1}$) and slow (0.2−2 m $s^{-1}$) velocities, respectively.[48]

If the stimulus persists, the receptor potential diminishes, leading to a decrease in receptor firing, a phenomenon known as adaptation (Figure 5c).[61] Skin receptors demonstrate varying degrees of adaptation, which are influenced by their response to sustained mechanical stimuli. Slowly adapting (SA) A$\beta$-LTMRs (A$\beta$ SA-LTMRs) continue to spike during sustained indentation, while rapidly adapting (RA) A$\beta$-LTMRs (A$\beta$ RA-LTMRs) fire action potentials only at the onset and offset of indentation.[62,63] SA LTMRs such as Merkel disks and Ruffini endings maintain their response as long as the stimulus is present, detecting sustained pressure and touch.[64] On the other hand, RA LTMRs such as Pacinian corpuscles generate receptor potentials only when the stimulus begins or ends.[64] The viscous fluid between the concentric layers allows the energy from the mechanical stimulus to dissipate, facilitating rapid adaptation.[65] Receptive field properties further distinguish LTMRs. Both cutaneous A$\beta$ SA-LTMRs and A$\beta$ RA-LTMRs typically have small receptive fields, but the receptive fields of RA-LTMRs increase with force. Glabrous skin Meissner-associated RA-LTMRs have well-defined, restricted receptive fields (10−15 $mm^2$), unlike the extensive fields of Pacinian corpuscle RA-LTMRs (50−100 $mm^2$). Mechanoreceptors in human skin, such as Merkel disks, Meissner corpuscles, Pacinian corpuscles, Ruffini endings, free nerve endings, and hair follicles, which contain the aforementioned LTMR terminals, are responsible for their respective specialized sensations.[66] Specifically, Merkel disks, Ruffini endings, Meissner corpuscles, and Pacinian corpuscles are associated with the end of A$\beta$ SA type I (A$\beta$ SAI), A$\beta$ SA type II (A$\beta$ SAII), A$\beta$ RA type I (A$\beta$ RAI), and A$\beta$ RA type II (A$\beta$ RAII) LTMRs, respectively.[51]

**3.1.2. Receptors in Skin.** Various sensory receptors located within the human skin possess the ability to distinctly detect mechanical sensations and temperature (Figure 5d).[53,67] Merkel disks are flat, disk-shaped structures that form the Merkel cell-neurite complex, which consists of clusters of 50−70 Merkel cells interconnected by terminals from A$\beta$ SAI-LTMR. Merkel disks, located in the epidermis aligned with papillae beneath dermal ridges, account for about 25% of mechanoreceptors in the hand and are particularly dense in the fingertips. Meissner corpuscles respond to light touch, vibration, and skin indentation depth with the highest spatial resolution, enabling the skin to distinguish fine textures and subtle contact changes.[68,69] Ruffini endings consist of elongated, spindle-shaped capsules with A$\beta$ SAII-LTMRs situated within.[70,71] They are primarily located deep in the skin, ligaments, and tendons, and oriented parallel to skin stretch lines. These receptors exhibit relatively low density and are predominantly located in areas such as skin folds. They signal skin stretch more effectively than indentation, and through their stretch pattern perceive the direction of object motion. Meissner corpuscles are oval-shaped structures encapsulated by layers of Schwann cells, located in the dermal papillae near the surfaces of the hands and feet.[71,72] As A$\beta$ RAI-LTMRs, these receptors have a high density, especially in the fingertips and soles of the feet, allowing them to effectively detect low-frequency vibrations (30−50 Hz) and the movement of textured objects. Pacinian corpuscles are large oval-shaped encapsulated endings located in the subcutaneous tissues and deeper layers of the skin.[65,73] Classified as A$\beta$ RAII-LTMRs, these receptors have a low density, comprising approximately 10−15% of the mechanoreceptors in skin. They play a crucial role in sensing deep pressure, high-frequency vibrations (250−350 Hz), and transient pressure changes with high sensitivity, discerning fine surface textures, and dynamic tactile perception.

Unlike other LTMRs, free nerve endings are unencapsulated nerve fibers and represent one of the most prevalent types of sensory receptors in the skin. They lack specialized encapsulated structures and extend through both the epidermis and dermis. These receptors are responsible for detecting a wide range of sensory stimuli, including pain, touch, and pressure. Free nerve endings contribute to the protective mechanisms of the human body by responding to noxious stimuli and signaling potential harm or tissue damage. They are distributed throughout the skin, particularly in the epidermis, and are involved in mediating reflexive withdrawal responses to harmful stimuli. Their presence is essential for the perception of pain, positioning them as key contributors to both


https://doi.org/10.1021/acs.chemrev.4c00966
Chem. Rev. 2025, 125, 11567−11665

Table 1. Summary of Mechanical and Thermal Receptors in Human Skin

| sensation | receptors | location | detecting sensation | sensitivity | RA/SA | associated sensory fiber |
|---|---|---|---|---|---|---|
| mechanical sensation | Merkel disk | epidermis (basal layer) | xeep pressure, high-resolution tactile perception | very high sensitivity, precise tactile and shape detection | RA | Aβ SAI- LTMR |
| | Ruffini endings | dermis (reticular layer), hypodermis | skin stretch, detection of the direction of object movement | high sensitivity to skin stretch | RA | Aβ SAII-LTMR |
| | Meissner corpuscle | demis (papillary layer) | light touch, low-frequency vibration (30−50 Hz) | high sensitivity, detection of rapid movements | SA | Aβ RAI- LTMR |
| | Pacinian corpuscle | hypodermis, deep dermis | high-frequency vibration (250−350 Hz), rapid pressure changes | very high sensitivity, detection of fine vibrations | SA | Aβ RAII- LTMR |
| | free nerve ending | epidermis, dermis | touch, pain | low sensitivity to various mechanical stimuli | varied | Aδ-LTMR, C-LTMR |
| thermal sensation | Krause end bulb | xermis (mucous membranes) | cold temperature | moderate sensitivity to cold temperature | SA | Aβ |
| | cree nerve ending | epidermis, xermis | cold temperature (below 17 °C) | | varied | Aδ, C |
| | | | warm temperature (30−40 °C) | | varied | Aδ, C |
| | | | heat sensation (above 45 °C) | | varied | Aδ, C |

protective sensory functions and the broader mechanisms of tactile perception. Furthermore, in hairy skin, the connection of various LTMRs with hair follicles to form specialized terminals extends the sense of touch beyond the surface of the skin.[68,70] Hairy skin is particularly adapted for detecting subtle mechanical changes, such as the movement of individual hair shafts.[74−76] The hair shaft serves as a lever, magnifying the mechanical force applied to the follicle and its associated receptors. The diversity of LTMR subtypes with specific sensitivities and adaptation properties provides varied sensory input to the central nervous system.[48] For instance, Aβ RA-LTMRs create longitudinal lanceolate endings around hair follicles and respond to dynamic mechanical changes such as hair movement, allowing the detection of slight air currents and the presence of nearby objects. On the other hand, Aβ SAI-LTMRs form complexes with Merkel cells to make touch domes found at the base of hair follicles. These complexes are sensitive to skin indentation and provide detailed information about texture and shape, contributing to fine tactile discrimination. Unmyelinated C-LTMRs have free nerve endings that penetrate the epidermis and the neck of hair follicles and are implicated in the sensation of pleasant touch.[74]

On the other hand, the sensation of temperature in human skin is mediated through a complex network of thermoreceptors and nociceptors, which are primarily free nerve endings lacking terminal sensory end organs.[60,77] Four types of thermal sensations, cold, cool, warm, and hot, are perceived by various types of afferent fibers, which include low-threshold and high-threshold cold receptors, warm receptors, and heat nociceptors. Cold temperatures can cause pain at different thresholds, with glabrous skin experiencing pain between 10 and 15 °C and hairy skin around 18 °C.[78] Noxious cold stimuli can evoke various sensations such as pricking, burning, aching, and even a paradoxical feeling of heat, indicating that different nerve fibers are activated.[79] Mechanosensitive Aδ fibers, which respond to heat stimuli, can also be triggered by noxious cold. These Aδ fibers are likely responsible for the pricking sensation associated with cold, as blocking them significantly reduces this sensation. Besides Aδ fibers, certain C fiber nociceptors are also activated by noxious cold, contributing to the sensation of cold pain.[79] Like Aδ fibers, many cold-sensitive C fibers are polymodal, responding to mechanical and heat stimuli with varying threshold temperatures.[80] When Aδ fibers are blocked, leaving C fibers active, the perception of noxious cold is experienced as burning or heat. This suggests that Aδ fibers modulate or block C fiber input to the central nervous system, influencing the overall sensory experience of cold pain. Cool receptors, primarily found in free nerve endings, are activated by slightly lower temperatures around 25−30 °C. These receptors, often associated with Aδ fibers and some C fibers, respond to moderate drops in temperature without causing pain. This allows for the perception of gentle cooling sensations, which are critical for temperature regulation and environmental awareness. Warm receptors, on the other hand, are sensitive to mild increases in temperature, typically in the range of 30−40 °C. These receptors, which are mainly unmyelinated C fibers, detect gradual warmth without triggering discomfort. They play a key role in helping the body sense and adapt to warmer environmental conditions. At higher temperatures, hot sensations are mediated through heat nociceptors, which are activated when temperatures exceed 45 °C. These nociceptors, involving both Aδ and C fibers, respond to noxious heat, signaling burning pain to prevent tissue damage. Unlike the gentle warmth sensed by warm receptors, these heat nociceptors are designed to protect the body from dangerously high temperatures by triggering pain responses that encourage withdrawal from the heat source.

In addition to free nerve endings, Krause end bulbs also play a significant role in temperature sensation, particularly in detecting cold.[81] Krause end bulbs are encapsulated receptors found typically in the deeper layers of skin or mucous membranes, especially in cold-sensitive zones such as the fingertips and other peripheral regions of the body. These specialized thermoreceptors are thought to respond to cold temperatures and are associated with Aδ fibers, which mediate fast, sharp sensations like those felt during rapid cooling. Krause end bulbs are believed to contribute to the perception of cold sensations by detecting temperature drops in their localized areas and transmitting this information to the central nervous system via afferent pathways. Their encapsulated structure differentiates them from the more common free nerve endings and provides them with specialized sensitivity to cold stimuli, complementing the broader role of free nerve endings and polymodal C fibers in overall thermal perception. By integrating inputs from both free nerve endings and Krause


https://doi.org/10.1021/acs.chemrev.4c00966
Chem. Rev. 2025, 125, 11567−11665

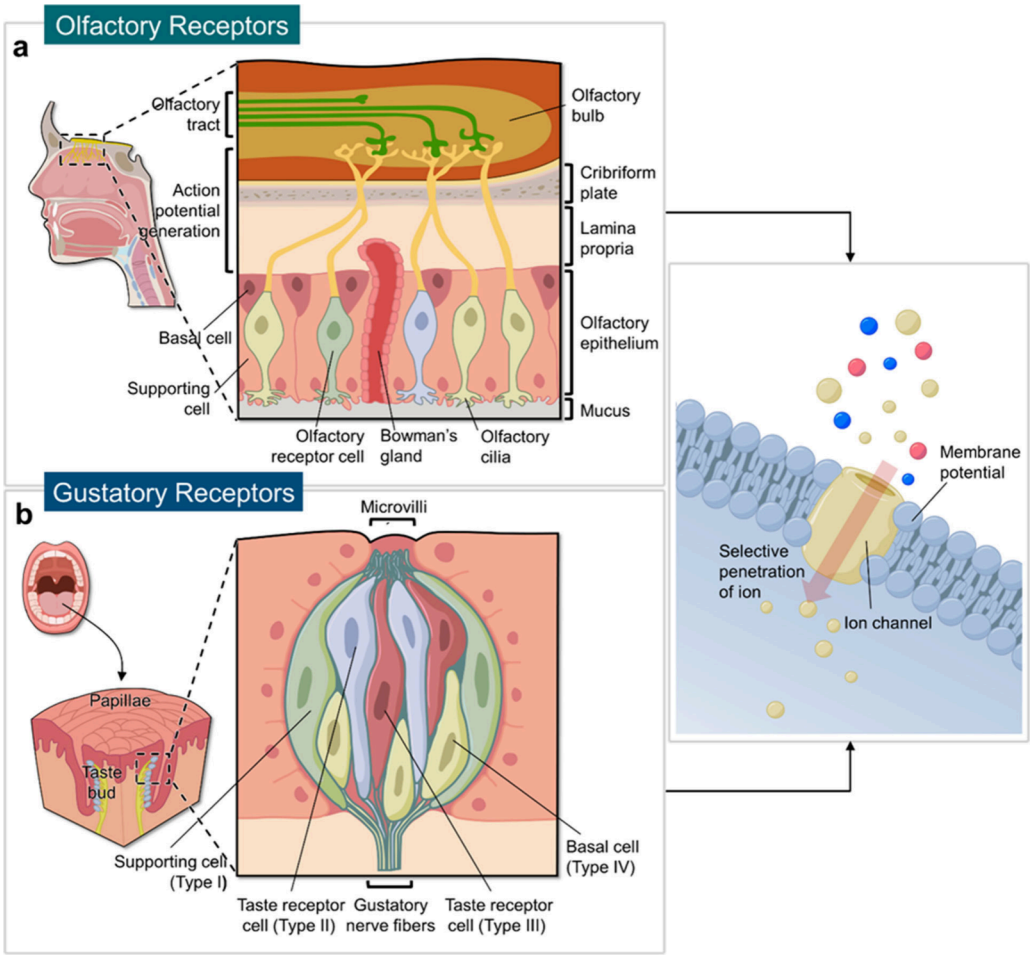


**Figure 6.** Chemical receptors in human nose and mouth, and their mechanisms. (a) Anatomy of the human nose and magnified view with various olfactory receptors. (b) Anatomy of the human mouth, featuring a magnified view of papillae with various gustatory receptors. Created with BioRender.com.

end bulbs, the body can detect a wide range of cold stimuli and respond accordingly.

In short, mechanoreceptors and thermoreceptors are responsible for detecting physical and temperature changes in the external environment (Figure 5e). These receptors respond to specific stimuli, including pressure, vibration, and temperature fluctuations, by generating electrical signals. Upon the application of physical stimuli or temperature changes, the receptors become activated, leading to deformation of the cell membrane and subsequent opening of ion channels. The opening of these ion channels facilitates the movement of ions across the membrane. When ions flow into the channel, the membrane potential experiences depolarization, leading to the generation of graded potentials, the amplitude of which is proportional to the intensity of the stimulus. When the graded potential at the receptor surpasses a defined threshold, it is transformed into an action potential. This action potential, characterized by a fixed magnitude, propagates uniformly along A, B, and C fibers, regardless of the distance and direction of the stimulus. The generated action potential travels along the nerve fibers to the central nervous system, where it is continuously maintained as an electrical signal throughout the transmission process. In summary, Table 1 provides an overview of the various receptors involved in detecting mechanical and thermal sensations. It details the location of each receptor, the specific sensations they detect, their sensitivity, the RA/SA classification, and associated sensory fibers.

**3.1.3. Ion Channels in Skin.** To explore in greater depth, mechano-transduction and thermo-transduction heavily rely on the function of specialized ion channels within sensory neurons.[82] The Piezo family of cation channels, including Piezo1 and Piezo2, is essential for detecting mechanical changes, particularly in conditions associated with mechanical hypersensitivity. Specifically, Piezo2 is predominantly located in the skin and RA LTMRs of the nervous system.[83] It has been identified as a vital component in light touch sensation, significantly contributing to tactile sensitivity, texture discrimination, and vibration detection. Activation of Piezo2 by mechanical forces leads to the depolarization of sensory neurons, facilitating subsequent signal transmission. Furthermore, transient receptor potential (TRP) family channels have been extensively studied for their roles in detecting mechanical changes, especially under pathological conditions related to mechanical hypersensitivity.[84,85] These channels regulate ion flow across the cell membrane in response to various stimuli, facilitating the generation of sensory neural signals. Canonical TRP (TRPC) channels are primarily implicated in sensing mechanical stimuli, with TRPC1 and TRPC4 expressed in mechanosensory neurons and activated by mechanical forces. These channels open in response to the deformation of the cell membrane, causing depolarization through ion influx. The


https://doi.org/10.1021/acs.chemrev.4c00966
Chem. Rev. 2025, 125, 11567−11665

mechanoreceptors of mechanosensory neurons collaborate with TRP channels to enhance their sensitivity to mechanical stimuli.

Furthermore, thermal or chemical stimuli activate specific TRP channels that are sensitive to different temperature ranges and chemical molecules.[77] Ankyrin TRP (TRPA) is primarily responsive to cold stimuli and certain chemical compounds. Specifically, TRPA1 is activated by cold temperatures around 17 °C or lower and reacts to substances such as icilin. It is predominantly expressed in sensory neurons that coexpress nociceptive markers like calcitonin gene-related peptide (CGRP) and substance P.[86] Melastatin TRP (TRPM) channels, particularly TRPM8, are activated by cooling temperatures and compounds like menthol, serving as key sensors for cool sensations. In contrast, Vanilloid TRP (TRPV) channels, particularly TRPV1 and TRPV2, are activated by heat. TRPV1, which responds to elevated temperatures, plays a critical role in nociception by signaling harmful thermal stimuli, such as those triggered by capsaicin in hot chili peppers. TRPV2 is activated at even higher temperature thresholds, contributing to the detection of noxious heat.

### 3.2. Chemical Receptors in Human Body

Chemical receptors in the human body are essential for recognizing and differentiating chemical signals, allowing us to experience and interpret sensory stimuli. Both olfaction and gustation rely on specialized receptors to detect chemical compounds in the environment, which then produce neural signals through G-protein-coupled receptor (GPCR) pathways.[87] These chemical-based olfactory and gustatory receptors are integral to identifying volatile compounds in the air and chemical substances in the mouth, enabling the detection of a wide range of odors and tastes, respectively.

Olfaction and gustation both engage distinct sets of receptors that bind with molecules to create sensory experiences, but their receptor distributions differ. These distinct distributions allow each system to detect and differentiate specific odors and tastes, resulting in subtle variations in how they process sensory information. For example, olfactory receptors are spread across the olfactory epithelium in the nasal passage, while taste receptors are mainly located on the tongue, roof of the mouth, and throat. This spatial arrangement plays a key role in how each system perceives and processes distinct chemical signals.

**3.2.1. Olfactory Receptors.** Olfaction is an external chemoreceptive sense that shares the characteristic of detecting chemicals dissolved in fluids.[88] Olfaction involves detecting highly volatile chemicals transmitted through the air. Inhaled odorant molecules must dissolve in the mucus lining the olfactory epithelium to stimulate the olfactory receptor cells (Figure 6a).[89]

Olfactory receptor cells in humans are primary sensory neurons with a width of 5−7 $\mu$m, primarily located in the lower two-thirds of the olfactory epithelium at a density of about 1−10 million $cm^{-2}$.[90,91] Each olfactory receptor cell extends a single dendrite, which branches out intricately and intermingles with other dendrites and supporting cells, gradually progressing toward the surface. The axons pass through the lamina propria and cribriform plate at the top of the nasal cavity and connect to the olfactory bulb below the frontal lobes, forming the first cranial nerve. Basal cells in the olfactory epithelium function as stem cells, capable of dividing and differentiating into other cell types, allowing the replacement of epithelial cells every 2−4 weeks. While supporting cells provide nourishment and structural support to olfactory cells, Bowman's glands produce mucus that lines the nasal cavity, protecting epithelial cells and trapping and dissolving odorants, which are then transmitted to the olfactory cilia.[92,93]

Odors are detected by olfactory receptor cells, where odor molecules bind to particular receptors located on the cell membrane.[94] This binding activates ion channels, allowing ions to move into or out of the cell, which in turn generates an electrical signal transmitted to the brain, resulting in the perception of smell. The structure and properties of odor molecules determine which olfactory receptors are activated, leading to the corresponding opening or closing of ion channels.[95] This interaction between olfactory receptors and ion channels is essential for distinguishing a wide range of odors.

For a substance to be smelled, it must be in a gaseous form and small enough to bind to odorant binding proteins (OBPs) in the mucus.[96] Therefore, only small molecules can produce a smell, with the upper limit being around 300 Da. The transduction of smell begins with the binding of odorant molecules to receptors located on the cilia of olfactory receptor cells. Olfactory receptors are among the largest gene families and can detect a wide variety of odors. The receptors are primarily composed of GPCRs, with more than 400 distinct types, each reacting specifically to different chemical compounds. The GPCRs activated by bound odorant molecules then stimulate the specific G-protein called Golf, which activates adenylyl cyclase, resulting in the formation of cyclic adenosine monophosphate (cAMP) within the cell.[97] cAMP is known as the most important secondary messenger in olfactory transduction, while other secondary messengers are also activated, such as $Ca^{2+}$, inositol-1,4,5-trisphosphate ($IP_3$), and cyclic guanosine monophosphate (cGMP). The increased cAMP opens cyclic nucleotide-gated cation channels on the olfactory cilia, allowing $Na^+$ and $Ca^{2+}$ to flow into the cell. The increase in cytoplasmic $Ca^{2+}$ concentration through cyclic nucleotide-gated channels enhances the signal by further opening the $Ca^{2+}$-activated $Cl^-$ channels.[98] The depolarizing receptor potentials generated in the olfactory cilia propagate to the soma through the dendrites of olfactory receptor cells, reaching action potentials. The cell returns to its resting state when $Ca^{2+}$-activated enzymes, phosphodiesterases (PDEs), break down cAMP. Concurrently, $Ca^{2+}$ binds to calmodulin, forming a complex that reduces the affinity of cyclic nucleotide-gated cation-selective channels for cAMP. Excess $Ca^{2+}$ is expelled through $Ca^{2+}/Na^+$ exchange pathways, restoring the cell to its resting potential.[99−101] Each receptor is specific to the functional groups or molecular structures of particular compounds. Multiple receptors can be activated simultaneously, enabling the brain to distinguish complex odors.

The second phase of the olfactory system involves the central nervous system. Once odorant signals are converted to electrochemical signals within the olfactory receptor neurons, the action potentials are then transmitted via unmyelinated axons that bundle into the olfactory nerve, passing through the cribriform plate to reach the olfactory bulb, where they combine. Within the glomeruli, synapses are formed with the dendrites of mitral cells. The mitral cells form the olfactory tract, projecting into the central nervous system and synapsing in five major brain regions including the anterior olfactory nucleus, piriform cortex, olfactory tubercle, parts of the


https://doi.org/10.1021/acs.chemrev.4c00966
Chem. Rev. 2025, 125, 11567−11665

Table 2. Summary of Olfactory and Gustatory Receptors in Human Body

| sensation | receptors | location | detecting sensation | function |
|---|---|---|---|---|
| olfactory sensation | olfactory receptors | olfactory epithelium | wide range of odors | • classification of odors with 400 different types of GPRs<br>• selective and simultaneous activation depending on chemical structure of odorant |
| gustatory sensation | type I cells | taste buds (fungiform papillae, front and side of tongue) | salty | • $Na^+$ ions enter through ENaC<br>• ion competition with $H^+$ ions modulates intensity |
| | type II cells | taste buds (fungiform papillae, front of tongue) | sweet | • T1R2−T1R3 protein complex activation<br>• activation of phospholipase C or adenylyl cyclase<br>• increase in cAMP and $Ca^{2+}$ levels |
| | | taste buds (circumvallate papillae, back of tongue) | bitter | • T2R receptors activate phospholipase C<br>• release of $Ca^{2+}$<br>• some substances block ion channels, causing depolarization |
| | type III cells | taste buds (foliate papillae, side of tongue) | sour | • $H^+$ ions activate specific ion channels<br>• blockage of $K^+$ channels causes depolarization |

amygdala, and the entorhinal cortex. Unlike other sensory systems, which project first to the thalamus before reaching the neocortex, the olfactory system projects directly to the cortex.[54]

**3.2.2. Gustatory Receptors.** To perceive taste, it is essential for the chemical substance to dissolve in saliva and reach the peripheral organs of gustation called taste buds (Figure 6b).[102] Of the four types of papillae on the tongue, taste buds are distributed among fungiform papillae, foliate papillae, and circumvallate papillae, excluding filiform papillae. They are clusters of elongated sensory cells located within the stratified epithelium of the tongue, palate, and epiglottis. Microvilli, which are small hair-like structures extending from the surface of the sensory cells, expand the surface area for chemical interaction and serve as the primary sites where taste molecules bind, triggering the cascade of cellular events that lead to taste perception.

Cells in the gustatory system can be classified into Type I, Type II, Type III, and Type IV, particularly based on their functions.[41,103,104] Each of these cell types performs distinct roles that contribute to overall flavor recognition. Type I cells primarily function as supporting cells, providing structural support and nourishment to other cells within the taste buds. They play an indirect role in detecting salty taste by sensing $Na^+$ concentrations, thereby helping to maintain the taste environment. Type II cells are specialized for detecting sweet, bitter, and umami stimuli. These cells utilize G-protein-coupled receptors to recognize taste stimuli and activate signaling pathways, such as phospholipase C, which increases intracellular calcium levels and ultimately generates neural signals. Type III cells primarily detect sour taste by sensing $H^+$ ion concentrations, leading to depolarization of the cell. While the detection of salty (NaCl) stimuli is associated with specific taste bud cells that have not yet been clearly identified, these cells are also involved in pathways related to salty taste detection. Lastly, Type IV cells, or basal cells, act as precursor cells that regenerate other cell types within the taste bud, contributing to the maintenance and renewal of the gustatory system. Gustatory nerve fibers are essential for transmitting the neural signals generated by these taste cells to the brain, where taste perception happens.

The transduction mechanism of salty taste in Type I cells is relatively simple, primarily involving the epithelial sodium channel (ENaC), which is blocked by amiloride. When $Na^+$ ions from salty foods enter the cell through ENaC, they cause depolarization, leading to the perception of a salty taste. The intensity of salty taste can vary depending on the ion species involved and their ability to pass through the channel, thus affecting $Na^+$ movement within the cell.[103]

In the context of sweet taste perception in Type II cells, heterodimeric taste receptor type 1 member 2 (T1R2) and taste receptor type 1 member 3 (T1R3) protein complex functions as a sweet taste receptor. When a sweet substance stimulates the G-protein coupled receptor, phospholipase C is activated, which in turn increases the levels of $IP_3$ and $Ca^{2+}$ within the cell, transmitting the sweet taste signal.[105] Additionally, sweet taste can be mediated by adenylyl cyclase activation, increasing cAMP levels, and activating protein kinase A, which decreases $K^+$ conductance in the taste cell membrane, leading to the depolarization and transmission of the sweet taste signal.[106−108]

In Type II cells, bitter taste receptors are thought to be about 30 different T2R protein receptors produced by T2R genes. These receptors form complexes with G-protein specific to bitter taste, leading to the activation of phospholipase C within the cell and subsequent release of intracellular calcium. In some cases, direct ion channel blockage by bitter substances causes cellular depolarization, transmitting the bitter taste signal.[107]

The transduction mechanism of sour taste in Type III cells involves two known pathways. The first pathway includes an $H^+$-sensitive ion channel, which is activated by $H^+$ ions and $Na^+$ ions, resulting in depolarization. The second pathway includes ENaC directly modulating $H^+$ uptake. This pathway is also involved in salty taste transduction. Hence, when $Na^+$ and $H^+$ ions compete, the salty taste is slightly diminished, a phenomenon often observed in daily life. Additionally, some sour taste receptors have $K^+$ channels that are blocked by $H^+$ ions, contributing to the sour taste transduction.[103,109]


https://doi.org/10.1021/acs.chemrev.4c00966
Chem. Rev. 2025, 125, 11567−11665

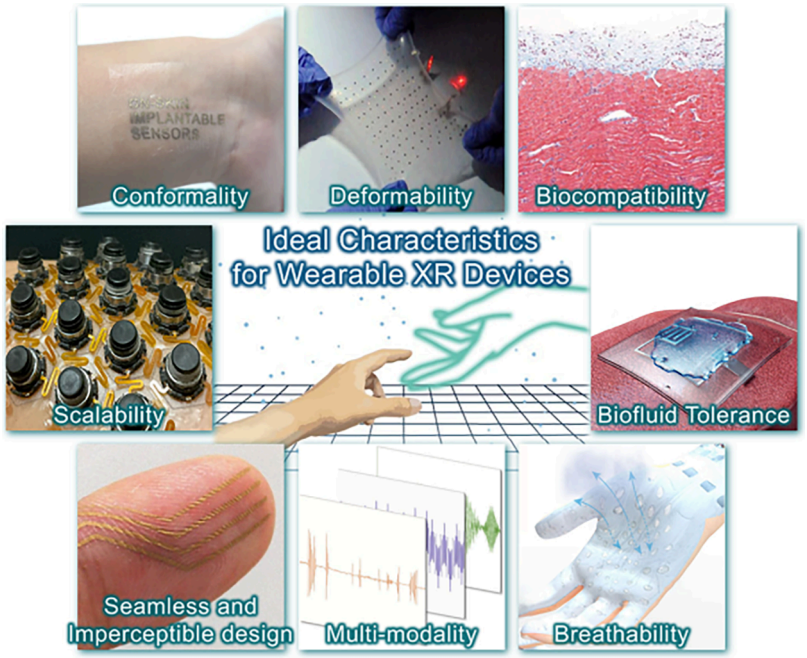


**Figure 7.** Ideal characteristics for wearable XR devices. Reproduced with permission from ref 170. Copyright 2022 Springer Nature. Reproduced with permission from ref 203. Copyright 2013 Springer Nature. Reproduced with permission from ref 146. Copyright 2018 Springer Nature. Reproduced with permission from ref 204. Copyright 2022 Wiley-VCH. Reproduced with permission from ref 161. Copyright 2024 The American Association for the Advancement of Science under CC BY-NC 4.0 license https://creativecommons.org/licenses/by-nc/4.0/. Reproduced with permission from ref 120. Copyright 2017 Springer Nature. Reproduced with permission from ref 199. Copyright 2024 Springer Nature.

In short, Table 2 summarizes olfactory and gustatory receptors, highlighting their distinct roles in detecting and processing stimuli for sensory perception. As discussed in this section, the human sensory organs exhibit intricate structures and mechanisms, necessitating efficient stimulation of each receptor to achieve realistic sensation reproduction. Moreover, within a single sensory organ, the location and operational mechanisms of each receptor vary, leading to distinct response patterns. Therefore, considering the location, sensitivity, and spatial distribution of each receptor is essential for the effective design of the mechanisms in wearable XR devices, ensuring the efficient reproduction of the desired and intended sensory stimuli.

## 4. IDEAL CHARACTERISTICS FOR SOFT WEARABLE XR DEVICES

Within the XR environment, generating realistic artificial sensations for sensory feedback and improving the accuracy of sensory input perception necessitate the development of novel functional materials and innovative XR device configurations.[2,6,12,110] Unlike conventional rigid wearable XR devices, the laboratory-level wearable XR devices currently under development rely on soft materials.[111,112] These soft wearable XR devices are typically used in direct contact with the interface between the body and the external environment, transmitting information through HMIs.[113] This working condition demands specific properties for soft wearable XR devices to effectively stimulate various sensory receptors in sensory organs and maintain proper functionality during continuous human activity (Figure 7). Therefore, in the following section, we will discuss the ideal properties for soft wearable XR devices and the relevant functional materials needed to meet these demands.

### 4.1. Conformality

In the context of soft wearable electronics, conformality refers to the ability to match the contours of the human body and movements.[114] For wearable XR devices, conformality is particularly important because sensory feedback and input information are transmitted via the interface between the human body and XR devices.[115,116] Highly conformal wearable XR devices can improve performance and effectiveness by enhancing the realism of artificial sensations and the perception accuracy of human activity. Therefore, even during intense human activities that can occur in an XR environment, conformal contact should always be maintained.

In this respect, materials with a low Young's modulus are suitable for housing XR devices. Human skin has a low Young's modulus from 1 kPa to 10 MPa, whereas most soft materials used for these devices have a higher Young's modulus compared to human skin.[117] This mechanical mismatch between the skin and the device can induce detachment of the device, which hinders its proper operation.[118] Furthermore, this mismatch can cause unwanted mechanical stimuli to the skin, such as pressure or irritation, reducing the overall immersion level in the XR environment.[119,120] These adverse effects not only diminish user comfort but also impair the functionality of the sensory feedback mechanisms, leading to a less effective XR experience.

Additionally, wearable devices are inevitably subject to continuous human motion, which can further induce delamination of the device.[121,122] This motion exacerbates the mechanical mismatch, making it even more challenging for the device to maintain stable contact with the skin. Therefore, materials with high adhesion properties such as hydrogels[117] or ultrathin thickness configuration[123] are required to prevent delamination and ensure that the device remains securely attached during wearing. High adhesion helps maintain


https://doi.org/10.1021/acs.chemrev.4c00966
Chem. Rev. 2025, 125, 11567−11665

consistent interface conditions, which are crucial for accurate sensory input and feedback. In turn, this enhances the reliability and performance of the XR device, ensuring a seamless and immersive user experience.

### 4.2. Deformability

Mechanical deformations, including bending, stretching, twisting, and compression, are unavoidable as users engage in dynamic, immersive XR environments. In soft wearable XR devices, deformability with high electrical conductivity is an important feature for ensuring reliable performance under frequent and varied mechanical deformations during use.[124,125] The ability to maintain consistent electrical performance under such conditions presents a significant technical challenge, highlighting the importance of stretchable conductors. Recent advancements in novel one-dimensional (1D) and two-dimensional (2D) materials have allowed continuous electrical functionality without failure, even when subjected to substantial mechanical strain.[126−128] Furthermore, intrinsically stretchable conductors, such as conductive polymers,[129,130] carbon-based materials,[131,132] liquid metals (LMs),[133,134] ionic conductors,[135,136] and metallic nanomaterials,[137,138] are critical due to their unique combination of mechanical flexibility and high electrical conductivity.

In addition, nonstretchable conductors, including traditional metals and semiconductors, can be incorporated into wearable XR devices through the use of innovative structural designs.[139,140] Configurations such as serpentine,[141] wavy,[142] mesh,[143] and kirigami[144] structures enable these otherwise rigid materials to endure mechanical stress by deforming in a controlled manner, without disrupting their electrical pathways. This adaptability is particularly important for ensuring long-term durability and device integrity, as wearable XR devices are subjected to continuous motion and deformation over extended periods.

Maintaining stable and robust electrical conductivity under mechanical deformation is thus essential for the successful operation of wearable XR devices, as it directly impacts critical performance metrics, such as data accuracy, power delivery, and the responsiveness of embedded sensors and actuators. Any degradation in conductivity due to mechanical deformation could result in latency issues, sensor malfunctions, or even complete device failure, thereby compromising the immersive experience for the user.[145] Consequently, the development and integration of reliable stretchable conductors are vital not only for improving user comfort and device functionality but also for ensuring the seamless operation of advanced XR technologies in real-world, dynamic settings.

### 4.3. Biocompatibility

Biocompatibility is another critical design consideration for wearable XR devices, as it directly influences user safety and comfort through the unavoidable mechanical, electrical, and chemical interactions between the device and the human body.[146] These interactions become increasingly significant given that wearable devices are often worn for extended periods, exposing the skin to continuous pressure, friction, and various environmental factors. Such exposure can lead to a range of adverse effects, including skin irritation, allergic reactions, and, in more severe cases, thermal burns resulting from electrical or thermal stimuli associated with the device.[147,148] Therefore, the materials employed in these devices must not only endure mechanical stresses but also remain nonreactive with the human skin and bodily fluids.

For example, while metal nanomaterials such as nanowires (NWs) and nanoparticles (NPs) provide benefits in terms of conductivity and flexibility, they can also present considerable biocompatibility risks.[149] These materials may dissolve in bodily fluids, releasing metal ions that can interact with cells and tissues, potentially inducing cytotoxicity and inflammatory responses.[146] This concern is particularly acute for devices in direct contact with human sensory organs, where prolonged exposure to reactive materials could result in tissue damage or irritation. Consequently, it is essential to use biocompatible materials to prevent provoking an immune response or other adverse reactions. In this regard, poly(3,4-ethylenedioxythiophene)−poly(styrenesulfonate) (PEDOT:PSS), a conducting polymer known for its high biocompatibility, is being extensively researched as a sensing material for wearable or implantable electronics to detect various physiological states.[150−152]

A key strategy to enhance biocompatibility is the incorporation of biocompatible polymeric materials for the encapsulation of potentially harmful components.[153] This protective barrier insulates the user from direct exposure to harmful materials. Additionally, selecting materials that are hypoallergenic, nontoxic, and gentle on the skin is crucial for mitigating inflammation and ensuring that users can wear the devices comfortably over extended periods without experiencing discomfort or health risks.[154]

### 4.4. Biofluid Tolerance

Unintended interactions between wearable XR devices and the human body can negatively affect the devices as well.[146] Therefore, biofluid tolerance should be considered as a crucial design factor to protect devices from biofluids including sweat, skin oils, and blood, which can degrade electronic components and compromise functionality. In this case, appropriate biofluid tolerance or isolation techniques ensure that these systems remain durable even with prolonged exposure to such fluids, without compromising the functional biointerface.

Advanced strategies involve developing biofluid-tolerant materials and robust encapsulation techniques to protect sensitive electronic components without hindering device functionality or user comfort. One promising approach involves employing hydrophobic coatings or encapsulation techniques to repel these fluids, thereby minimizing fluid absorption and preventing the degradation of active components. For example, materials with high chemical stability and biocompatibility, such as silicone elastomers[152,155,156] and dielectric composites,[157−159] are widely used to construct biofluid-resistant barriers. These materials prevent the penetration of moisture and corrosive elements into the electronic components, ensuring reliable performance even in humid environments. Furthermore, their stretchability allows for seamless integration into soft form factors, enhancing user comfort and wearability for XR devices.

The integration of biofluid isolation strategies must also balance device protection, functionality, and user comfort. Excessively thick barriers may compromise the stretchability and adherence to the skin, while overly thin layers may fail to provide sufficient protection.[123] Additionally, selective encapsulation of only the components requiring protection is crucial to preserving the mechanical, thermal, electrical, or chemical interactions between the devices and the human body. This necessitates precise patterning processes for insulating materials. In conclusion, balanced biofluid isolation is an


https://doi.org/10.1021/acs.chemrev.4c00966
Chem. Rev. 2025, 125, 11567−11665

important consideration for ensuring the long-term durability, functionality, and user comfort of wearable XR systems.

### 4.5. Breathability

Another factor that must be considered in the design of wearable XR devices is breathability, particularly due to the effect of human perspiration on skin health and overall device performance.[160,161] Even when using biocompatible polymers, prolonged wear of XR devices can negatively affect the skin without breathability.[120,162,163] For instance, sweat plays an essential role in regulating body temperature and preventing skin dryness, thus maintaining and protecting physiological functions.[164] Even without intense physical activity, the body continuously produces small amounts of sweat. However, the long-term use of wearable XR devices can impede air circulation to the skin, resulting in moisture accumulation that may lead to irritation and discomfort.[165]

Furthermore, the electrolytes present in sweat can interact with the materials in XR devices, potentially causing corrosion or other chemical reactions that can degrade device performance.[166] Moisture can also diminish the adhesion between the device and the skin, compromising the reliability and functionality of the wearable technology.[167] Particularly, preventing sweat accumulation at the skin-integrated XR interface is crucial for maintaining signal fidelity and operational reliability in wearable XR systems, both in actuators and sensors, and it is clearly demonstrated that such management significantly enhances device performance during prolonged use, including improved feedback accuracy, touch localization, and motion recognition accuracy.[122,168]

In this respect, it is imperative to incorporate skin-friendly and breathable materials into the design of wearable XR devices. Breathable materials with porous microstructures not only facilitate moisture evaporation but also support convective heat transfer, reducing local skin temperature rise. This thermal management is particularly critical in XR devices that include active components such as microheaters or power electronics. Innovative design strategies with permeable materials like graphene,[169] hydrogel,[159] and polydimethylsiloxane (PDMS)[170] as well as developing porous structures with micro and nano openings such as nanofiber matrices[163,171,172] and nanomesh[121,122] can significantly enhance sweat evaporation, moisture, and thermal management of the body. By integrating these features into the device construction, skin comfort and wearability of the device can be improved, ultimately elevating the overall user experience. The emphasis on breathability safeguards skin health as well as ensures that wearable XR devices remain functional and reliable during extended use, allowing users to engage with the XR technology seamlessly.

### 4.6. Multimodality

To enhance user immersion in XR technology, multimodality within a single wearable device is essential, especially given the limited area of human skin.[173,174] It is desirable for XR devices to simultaneously detect and deliver a variety of sensory information such as temperature, pressure, and touch. Achieving this requires advanced, compact technologies that enable seamless interaction and responsiveness.

For this purpose, integrating multiple independent sensors into a single device allows for the measurement of distinct factors.[175−177] Furthermore, a unified multimodal sensor system that decouples this information offers additional benefits in terms of spatial effectiveness and data processing.[178,179] Such a system simplifies the device architecture and improves efficiency by facilitating real-time data acquisition and analysis from multiple inputs. For example, a multimodal sensor could simultaneously monitor user-related signals, such as skin movement and temperature, offering a comprehensive understanding of the state of users in an XR environment.[179] Moreover, this system could also be employed to replicate sensations by detecting both environmental stimuli and user-generated outputs. By consolidating various sensing functions within a single device, wearable XR technology can reduce hardware complexity while providing more robust and enriched user feedback.

In addition to sensing, multimodality is equally important for actuation, as it generates sensations that enhance user immersion in XR environments.[180] Similar to sensors, multimodal actuators can provide a diverse range of sensory experiences, including vibrations, temperature changes, and tactile feedback, within a single device. For example, an integrated actuator could simultaneously simulate warmth and gentle pressure to more closely replicate real-world sensations.[33,181] This cohesive approach to generating multiple sensory outputs enhances realism and user engagement by delivering a seamless, synchronized experience. In contrast to independent actuators, a multimodal actuator system streamlines the design process and fosters a more immersive and interactive experience for users. In particular, a single actuator capable of delivering combined pressure, shear, vibration, and torque offers rich haptic feedback in a compact, lightweight, and wearable form.[34]

Lastly, the integration of multimodality in both sensing and actuation is essential for creating a comprehensive user experience.[182−184] Future wearable XR devices should incorporate these functions into a unified system, enabling the simultaneous detection of stimuli and the production of corresponding sensations. This dual functionality of sensing and actuation facilitates a more immersive, responsive, and intuitive experience for users, thereby enhancing applications that range from remote health monitoring to immersive gaming and training simulations. By prioritizing multimodality, wearable XR technology can fully leverage its potential to deliver richer and more engaging user experiences.

### 4.7. Seamless and Imperceptible Design

Ideally, removing any sensations induced by the wearable XR device itself is beneficial for achieving a high level of artificial sensation reconstruction. However, the incorporation of multiple functional components to facilitate multimodality in wearable XR devices often leads to greater system complexity, which inevitably increases overall weight and bulkiness. Although eliminating unintended sensations resulting from the weight and bulkiness of wearing XR devices itself is impossible, it is essential to ensure that these factors should not compromise the quality of XR experiences of users by causing undesirable sensations due to impeded use and burden. Thus, minimizing undesirable sensations is critical to achieving the intended experience, highlighting the importance of a seamless and imperceptible design.

For example, excessive weight can lead to undesirable sensations during use, as gravitational forces or inertia may significantly disrupt immersion in the XR environment.[6,11] A heavier device may induce discomfort and fatigue, which detracts from the intended user experience and may limit the duration of user engagement with the technology. Therefore,


https://doi.org/10.1021/acs.chemrev.4c00966
Chem. Rev. 2025, 125, 11567−11665

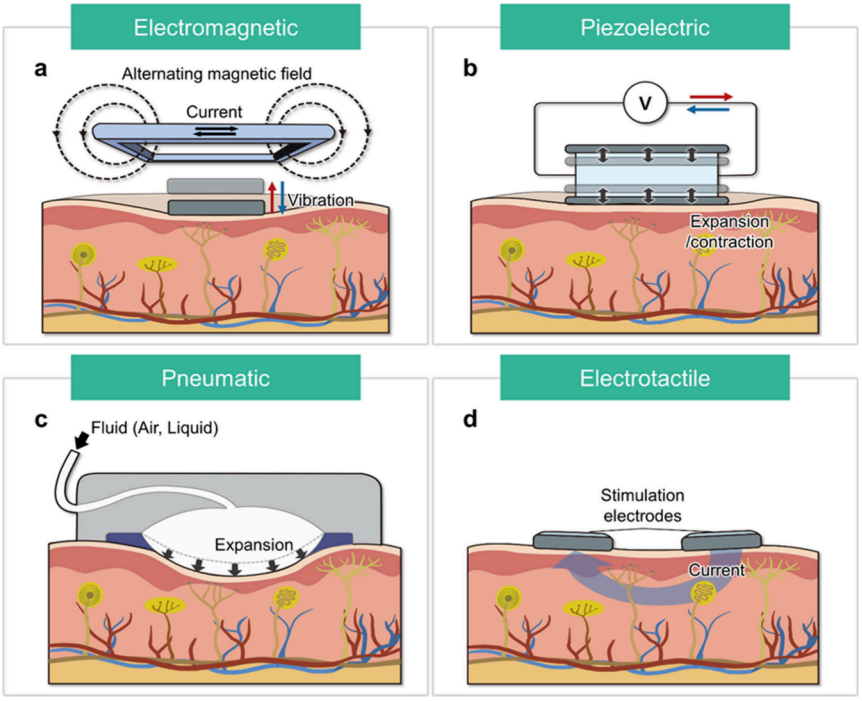


**Figure 8.** Mechanisms for the reconstruction of mechanical sensation with wearable XR feedback devices. (a) Electromagnetic-based feedback mechanism. (b) Piezoelectric-based feedback mechanism. (c) Pneumatic-based feedback mechanism. (d) Electrotactile-based feedback mechanism. Created with BioRender.com.

minimizing the weight of wearable XR devices is critical to ensuring a natural and comfortable user experience within XR environments. To this end, many innovative design strategies prioritize the use of lightweight materials and efficient engineering solutions. For instance, the adoption of advanced materials and fabrication techniques can substantially reduce weight without compromising structural integrity or functionality.[134,185−188] In particular, novel fabrication techniques such as laser direct patterning,[189] direct ink writing,[190] and 3D printing,[191] enabled high-resolution patterning to fabricate lightweight electronics. Moreover, optimizing the arrangement of electronic components and novel mechanisms can facilitate a lighter design by eliminating unnecessary bulk elements.[192−194]

Furthermore, a thinner design contributes to user comfort and device integration by decreasing the overall profile of the device, allowing more freedom of movement and reducing the sensation of bulk during prolonged wear. The mechanical resistance of the device under the deformation can be significantly lowered by reducing the thickness of device, allowing unimpeded use and lowering user burden for a seamless user experience.[195] In addition, thin geometry is an effective strategy for achieving a lightweight design. For full functionality, it is necessary to ensure that not only the substrate but also the functional elements are made thin. Combined with strategic component layout and integration, it plays a vital role in producing XR devices that offer both high functionality and user comfort without unnecessary bulk.

Lastly, unintended thermal sensation should be considered in the fabrication of wearable XR devices to maintain user comfort and ensure a seamless experience. When mounted on the skin, these devices must be designed to avoid distorting or interfering with natural body temperature and thermal fluctuations. A low thermal mass enables the device to quickly respond to external temperature changes, minimizing potential disruptions to the physiological state of users. This adaptability allows the device to integrate naturally with the body, preventing discomfort and temperature-related distractions.

Achieving a balance between functionality and wearability is vital for the successful adoption of wearable XR technologies, as it directly influences user engagement, satisfaction, and overall experience. A mechanically and thermally seamless design not only enhances user comfort but also encourages prolonged use, ultimately leading to more meaningful and unobtrusive interactions within the XR environment.

### 4.8. Scalability

Lastly, scalability is a crucial factor in the design and implementation of XR devices, particularly when it comes to both sensing and generating a comprehensive range of sensory experiences across various body regions.[112] For these devices to effectively gather and convey sensations across different areas of the body, it is essential to establish a scalable architecture that facilitates the integration of multiple components capable of both sensing and actuating diverse outputs.

To comprehensively and accurately simulate various forms of feedback on different parts of the human body, the XR system must accommodate numerous sensors and actuators that can independently monitor and generate sensations.[196−199] This is especially important, as each specific human body may require distinct sensory inputs and outputs to create a fully immersive experience.

By prioritizing scalability, XR technology can ensure that both sensory experiences and the corresponding feedback mechanisms are immersive, responsive, and customizable to individual user needs. To address this challenge, scalable fabrication techniques such as spray coating,[122] screen printing,[200] electrospinning,[201] and roll-to-roll manufacturing[202] have been utilized for the large-scale fabrication of


https://doi.org/10.1021/acs.chemrev.4c00966
Chem. Rev. 2025, 125, 11567−11665

wearable electronics. This scalability is vital not only for enhancing user engagement but also for guaranteeing accurate sensing capabilities in applications ranging from gaming to health monitoring. Ultimately, a scalable design is indispensable for the effective development of future wearable XR devices, as it allows for the seamless integration of diverse sensory functionalities.

## 5. SENSORY FEEDBACK AND INPUT DEVICES WITH WORKING MECHANISMS

### 5.1. Wearable Sensory Feedback Devices

In conjunction with the introduction of novel functional materials, XR devices should be equipped with innovative sensory feedback mechanisms to enhance user immersion and interaction. As we discussed, human sensory organs contain various types of receptors that respond differently to stimuli. Even within the same organ, each type of receptor has distinct locations and levels of sensitivity, contributing to the complexity of the human sensory mechanism. Furthermore, human receptors are highly sensitive, capable of detecting subtle changes, and therefore require a delicate and sophisticated feedback system for immersive experience. Therefore, beyond simple and monotonous feedback provided by conventional systems, future XR devices require the capability to effectively and selectively stimulate human receptors to replicate the rich sensations experienced in the physical world. In this section, we will delve into various novel feedback mechanisms to implement tactility, force, olfaction, and gustation. Moreover, we will explore how wearable XR devices transform XR experiences by closely mimicking real-world sensations.

**5.1.1. Mechanohaptic Feedback Devices.** Mechanohaptic feedback systems for XR devices rely on physical stimuli to deliver tactile or motional sensations to the skin, effectively enhancing the immersive experience. These systems can selectively stimulate various mechanical receptors in the skin by adjusting the frequency and intensity of the stimuli. Implementing mechanical feedback involves several methods, including electromagnetic actuators,[205−209] electrotactile stimulation,[210−212] pneumatic actuators,[213−216] and piezoelectric actuators.[217−219]

*5.1.1.1. Mechanisms and Materials for Mechanohaptic Feedback Devices.* Electromagnetic actuators utilize the principles of electromagnetism to produce mechanical stimuli on the skin (Figure 8a). This approach generates mechanical energy by converting electrical energy through magnetic field interactions. When an electric current passes through a coil, it creates a magnetic field that interacts with a magnet, resulting in movement. This movement generates vibrations or forces through coordinated motion with other components, which can be felt by the skin, providing precise and responsive haptic feedback.

For example, eccentric rotating mass (ERM) motors are among the most common techniques for generating haptic feedback due to their cost-effectiveness and ease of implementation. ERM motors utilize direct current (DC) motors to generate vibrations by rotating an off-center mass mounted on the shaft, creating a centrifugal force. This unbalanced mass generates centrifugal force during rotation, producing mechanical stimuli. On the skin, the ERM motor causes displacement both in and out of the plane of the skin, effectively stimulating mechanoreceptors. The forces generated by an ERM actuator can be significant, and both the intensity and frequency of these forces can be controlled by adjusting the DC voltage. However, because the torque and speed of the mass are coupled, the vibration amplitude and frequency cannot be controlled independently. Additionally, ERM motors suffer from nonlinear vibration responses and slower response times, which are critical factors for the precise control of feedback.

Linear resonant actuators (LRAs) present a promising alternative to ERM motors due to their faster response time and enhanced energy efficiency. Unlike ERM motors, LRAs generate vibrations through a resonating mass that moves linearly within a magnetic field, which is created by alternating currents (AC) passing through coils. This linear movement results in consistent, precise, and efficient vibrations. One significant advantage of LRAs is their capability to provide high-fidelity haptic feedback with a controllable amplitude, which is not coupled with frequency. LRAs can generate a precise waveform with varying amplitude over time with a fixed frequency range. Furthermore, these actuators are energy-efficient when operated at their resonant frequency, producing vibrations of comparable magnitude to ERM motors with lower energy consumption. However, the frequency of vibrations is constrained to the resonant frequency, because they must be driven at the resonant frequency range for generating a substantial amount of force.

Piezoelectric actuators leverage the piezoelectric effect to generate mechanical feedback, offering a high-precision and high-frequency response with low power consumption (Figure 8b).[7,220] The piezoelectric effect involves the deformation of piezoelectric materials, such as certain ceramics or polymers, when an electric field is applied. This deformation results in mechanical displacement, which can be used to generate vibrations[217,218,221] or other tactile sensations[219,222] on the skin.

The piezoelectric coefficient is primarily determined by the inherent electric asymmetry within a molecule and the redistribution of charge in response to external stimuli.[223] Electric asymmetry is fundamental to the piezoelectric effect, as a molecule must possess an asymmetric electric dipole to induce polarization under external electric fields, which subsequently leads to mechanical deformation. The mobility of domain walls within piezoelectric materials is also a crucial factor. Domain walls, which are boundaries between regions of different polarization orientations in the crystal structure, facilitate larger mechanical responses when they can move freely under external forces. An asymmetric crystal lattice structure is essential for achieving electrical changes due to mechanical deformation.[224,225] For instance, the perovskite structure possesses this asymmetry, allowing the central metal ion to shift under an external electric field, resulting in a strong piezoelectric response.[226] Additionally, for a material to exhibit a high piezoelectric coefficient, it must have structural flexibility to rearrange under strain. In polymers, the $\beta$-phase configuration can enhance piezoelectric properties, as observed in polyvinylidene fluoride (PVDF), where the $\beta$-phase responds strongly to applied electric fields.[227−229] Certain piezoelectric materials also exhibit phase transition capabilities that enhance their response to external stimuli.[230−232] Barium titanate ($BaTiO_3$), for example, undergoes phase transitions from tetragonal to cubic at specific temperatures, significantly increasing its piezoelectric properties and sensitivity to electric fields. These phase transitions amplify the asymmetry and


https://doi.org/10.1021/acs.chemrev.4c00966
Chem. Rev. 2025, 125, 11567−11665

polarization of the materials, enhancing the piezoelectric response.

Piezoelectric actuators can produce delicate vibrations with high frequency due to their precise controllability. This means that these actuators are suitable for applications requiring detailed haptic feedback, such as imitating textures or fine surface details in XR environments. The high precision and responsiveness of piezoelectric actuators significantly enhance the realism and immersion of the haptic experience. Additionally, they consume lower power during operation because they do not rely on large moving parts or the generation of substantial forces. Consequently, they are ideal for portable and wearable XR devices that are often constrained by size and battery life. Despite their unique properties and advantages, the displacement generated by piezoelectric actuators is typically small, which can be a limitation in applications requiring larger tactile sensations. To address this issue, various amplification mechanisms that enhance output displacement, such as mechanical levers or resonance techniques, can be employed.

Pneumatic actuators are a powerful method utilizing compressed air for generating mechanical feedback, especially pressure sensations (Figure 8c). These actuators operate by expanding and contracting a chamber or membrane filled with a fluid, producing mechanical movements that can be felt on the skin. This approach allows for mechanical feedback originating from large displacement and force.

Flexible and durable polymeric materials such as PDMS, Ecoflex, and Dragon Skin are promising candidates for pneumatic actuators due to their mechanical strength and elasticity, which enable them to withstand repeated expansion and contraction.[233] The performance of pneumatic actuators is highly dependent on the mechanical properties of the polymeric materials interacting with the working fluid. These properties can be enhanced by incorporating nanomaterials or fiber reinforcements into pure elastomers, significantly improving their mechanical strength and durability.[234] For example, a fiber matrix can support soft polymeric materials, converting deformation generated by pressurized air into finger-like motion. The sealing capability of polymeric materials against the working fluid is also a crucial factor that determines the performance and operational longevity of pneumatic actuators.[235,236] To address potential damage from sharp objects, soft self-healing materials can be employed for enhanced resilience.[237]

The capability to generate large deformations and forces makes these actuators ideal for applications requiring strong and noticeable feedback. For instance, pneumatic actuators can provide the sensation of objects pushing against the skin[238] or the feeling of being touched with varying degrees of pressure.[239] However, the implementation of pneumatic actuators in wearable XR devices comes with certain challenges. One significant drawback is the bulky and complex design of pneumatic systems, which require pumps, valves, and controllers to manage the airflow. This complexity can result in larger and less comfortable devices for the user. Additionally, the response time is slower compared to other types of actuators, as the fluid must be moved into and out of the chambers. Due to these challenges, pneumatic actuators are not widely used in skin-integrated devices. Nevertheless, they could be applied through advances in more compact and faster pneumatic systems suitable for integration into wearable devices. By focusing on miniaturizing the systems and optimizing the integration of various components, it is possible to overcome the current limitations.

Electrotactile stimulators, while not providing mechanical stimuli, create the perception of mechanical sensations by stimulating nerve endings of the skin through controlled electric currents (Figure 8d). This method involves placing arrays of electrodes on the skin to deliver precise electrical pulses that mimic various tactile sensations, ranging from light touch to more complex patterns. By modulating the intensity, frequency, and waveform of the currents, specific nerves are activated, resulting in haptic sensations such as pressure, vibration, and texture.

Electrodes for electrotactile stimulation must be in direct contact with the skin, making the biocompatibility of soft conductive materials essential. For instance, materials such as Au-based thin films,[177,240] conductive hydrogels,[161,241,242] and PEDOT:PSS[243,244] have shown no significant inflammatory responses, indicating high biocompatibility and positioning them as promising candidates. Additionally, an electrical conductivity of biocompatible materials is a critical factor for high performance of electrotactile stimulation. Recently, various techniques, such as doping,[245] laser-induced phase separation,[152] have enabled the development of skin-friendly electrodes with exceptionally high electrical conductivity and low mechanical modulus, making them highly suitable for applications requiring direct skin contact and electrotactile stimulation.

Electrotactile stimulators can provide diverse sensations without mechanical movement, which reduces the bulk and complexity of the haptic feedback systems. Electrotactile systems typically consume less power compared to mechanical actuators, as they do not rely on moving parts. Furthermore, the fine control over the electrode patterns and the electrical parameters allows for highly customizable feedback, enhancing the realism of the user experience. However, electrotactile mechanisms primarily target the mechanoreceptors situated in the superficial layers of the skin. These electrical signals lack the penetration depth required to effectively activate deeper receptors. Furthermore, the variability in skin impedance among different users and even over time for the same user can affect the consistency of the tactile feedback. Additionally, improper calibration of the electric currents can cause discomfort or pain. Because of these issues, adaptive control algorithms are necessary to adjust the electrical stimulation in real-time, and extensive testing is essential to fine-tune the system.

As summarized in Table 3, each mechanohaptic feedback mechanism presents distinct advantages and limitations, which must be carefully considered when designing wearable XR systems. By leveraging these technologies, wearable XR devices can provide users with nuanced mechanohaptic feedback, thereby increasing the sense of presence and interactivity in VR and AR applications. The integration of diverse actuators allows for a comprehensive range of tactile sensations. Each method has unique strengths and challenges, but advances in material science and device integration are making these technologies more viable for wearable XR devices. Building on this, Table 4 provides a comprehensive overview of widely studied mechanohaptic feedback devices, detailing their mechanisms, materials, and key performance metrics relevant to soft wearable XR interfaces.

*5.1.1.2. Vibrotactile Feedback Devices.* Vibrotactile feedback is a widely used form of mechanical feedback that


https://doi.org/10.1021/acs.chemrev.4c00966
Chem. Rev. 2025, 125, 11567−11665

**Table 3. Summary of Advantages and Disadvantages of Mechanohaptic Feedback Devices**

| mechanism | advantages | disadvantages |
|---|---|---|
| electromagnetic | • precise and responsive feedback | • structurally complex due to coils and magnets |
| | • direct electrical-to-mechanical conversion | • use of bulky and rigid components |
| | • battery-free and self-sustainable operation | • current-dependent heating and response delay |
| piezoelectric | • high precision and frequency response | • limited output displacement amplitude |
| | • compact and suitable for XR or wearable use | • need for amplification mechanisms |
| pneumatic | • strong and noticeable mechanical feedback capability | • bulky and complex system architecture |
| | • electrically safe and free of onboard power circuits | • slow response time due to air dynamics |
| electrotactile | • no mechanical movement required | • sensitive to skin impedance variations |
| | • low power consumption and compact form factor | • limited penetration depth |
| | • highly tunable tactile feedback | • risk of discomfort or pain if miscalibrated |

generates vibrations to provide tactile sensations on the skin.[209,246−250] This feedback stimulates mechanoreceptors in the skin, specifically Pacinian corpuscles and Meissner corpuscles, to convey various haptic experiences. As we discussed, Pacinian corpuscles, located deep in the skin, are highly sensitive to rapid and strong vibrations, detecting frequencies ranging from 80 to 450 Hz.[65,251,252] Meissner corpuscles, on the other hand, are located near the surface of the skin, especially in sensitive areas such as fingertips, palms, and soles. They are sensitive to low-frequency ranges of 10−80 Hz and light touch stimuli.[251] Vibrotactile devices primarily aim to stimulate these receptors using electromagnetic actuators[205−209] and piezoelectric actuators[217−219] generating controlled vibrations.

The method of converting oscillating electromagnetic waves into mechanical motions is well-suited for implementing vibrotactile feedback. Specifically, LRAs are appropriate for skin-integrated XR interfaces due to their ability to produce precise and energy-efficient vibrations. For example, utilizing the LRAs, the skin-integrated haptic devices provided a sense of virtual touch in a social communication scenario within a virtual environment (Figure 9a).[31] In this study, soft and skin-conformal vibrotactile actuators were developed, which could be attached to various body parts, including the hands and arms. The actuators utilized Lorentz forces generated by a time-varying current passing through a coil surrounding a permanent magnet. The magnet was attached to a thin polyimide (PI) disk with a semicircular cut, and the remaining frame was composed of soft elastomer (Figure 9b). This cantilever structure produced out-of-plane mechanical vibrations that were perceived as touch sensations, which enhanced vibratory amplitudes and bandwidths. The actuators were designed to resonate at frequencies between 100 and 300 Hz, which were most effective for stimulating mechanoreceptors in human skin. Furthermore, despite providing sufficient tactile feedback to users, these actuators required only about 1.7 mW of power due to their optimal design.

Since the shape and performance of LRAs are adjustable and customizable, they can be compactly integrated with other functional and electronic components. Using these attributes of the LRAs, self-sensing and haptic-generating actuators were achieved based on Faraday's law by reversing the principle of LRAs (Figure 9c).[156] The developed device was capable of detecting dynamic pressing, and the resonant frequency of the actuators could be easily adjusted by controlling the thickness of the magnet-attached elastomeric film. Consequently, the authors designed vibrotactile actuators with a thickness of less than 3 mm, vibrating at a resonant frequency of approximately 200 Hz with an amplitude of 200 $\mu$m. They successfully demonstrated touch transmission scenarios by integrating these self-sensing and vibrotactile feedback actuators with wireless communication modules (Figure 9d).

Furthermore, utilizing ERM vibrators, a ring-shaped haptic feedback device was designed with a simple structure and low driving voltage (Figure 9e).[253] The authors observed a nearly linear relationship between the driving voltage of the vibrator and the actual vibration amplitude. This linearity allowed for the control of both amplitude and vibration frequency, ranging from 130 to 230 Hz by varying the supply voltage. As a result, they demonstrated a portable wearable device for VR piano training (Figure 9f). Despite being powered by a low voltage, the device could provide significant vibrations sufficient to simulate the sensation of keystrokes in a VR environment.

In addition, the development of a haptic interface that delivers tactile sensations across large areas of the human body using an array of ERM motors has been reported.[254] The authors arranged the motors, each less than 10 mm in diameter and 2 mm in thickness, at a density exceeding the two-point discrimination threshold for mechanical sensation on the skin, which was sufficient to create a realistic tactile experience across most of the body (Figure 9g). Despite their small size and light weight, each motor could generate vibrational accelerations exceeding 1 G and produce large displacements on the order of several hundred micrometers. This enabled effective mechanical sensation even in less sensitive areas such as the back, abdomen, and arms (Figure 9h). By individually controlling these high-density ERM motors, the authors developed a haptic interface that conveyed information to humans through spatiotemporal vibration stimulation (Figure 9i).

On the other hand, piezoelectric actuators have gained prominence for producing vibrotactile feedback in regions with delicate sensory perception, such as the hands or fingers, due to their ability to generate precise vibrations without large displacements. In this regard, smart gloves that could provide vibrational haptic feedback using piezoelectric actuators were proposed (Figure 9j).[221] The authors employed piezoelectric PZT vibrational chips, which were activated by applying an electrical pulse width modulation signal at their resonant frequency, converting the signal into vibrational stimulation. Furthermore, the intensity of the vibrations was adjusted by varying the driving voltage, allowing the feedback to reflect the degree of interaction within a VR environment. As a demonstration, the gloves delivered the sensation changes in response to releasing and touching interactions in the VR environment, thereby enhancing the realism of the experience (Figure 9k).


https://doi.org/10.1021/acs.chemrev.4c00966
Chem. Rev. 2025, 125, 11567−11665

Table 4. Summary of Mechanohaptic Feedback Devices and Their Characterization for Soft Wearable XR Interfaces

| | | | | performance | | | | |
|---|---|---|---|---|---|---|---|---|
| type | mechanism | material | stretchability | force (pressure) | displacement | frequency | spatial resolution | ref |
| mechanohaptic feedback | | | | | | | | |
| vibrotactile | electromagnetic (LRA) | Cu coil, PDMS, magnet, PI | stretchable | 135 mN | 35 $\mu$m | 100−300 Hz | 2.1−21 mm | 31 |
| | | Cu coil, PDMS, magnet, PI | stretchable | 12.1 mM | 60−606 $\mu$m | 100−300 Hz | 6−18 mm | 156 |
| | electromagnetic (ERM) | commercial ERM vibrator | flexible | | | 130−230 Hz | | 253 |
| | | commercial ERM vibrator | stretchable | | 3−7 $\mu$m | 70−130 Hz | 13 mm | 254 |
| | piezoelectric | Cu, Cr/Au | flexible | 0.1−3.5 N | | 270 Hz | 5 mm | 221 |
| | | PZT, Ag, PI | flexible | 0−592 kPa | | 1−1000 Hz | 1.8 mm | 222 |
| | pneumatic | air, Dragon Skin | flexible | 298.1 mN | | 130 Hz | | 250 |
| pressure | pneumatic | TPU film, teflon sheet, foam | flexible | 0−2500 mN | 2 mm | 1−10 Hz | 4 mm | 239 |
| | | ecoflex, nichrome, nickel fabric | flexible | 0.69−0.3 N | 1−5 mm | 2 Hz | 7 mm | 238 |
| | hydraulic | mylar/PVDF, dielectric fluid | stretchable | 300 mN | 500 $\mu$m | 0−200 Hz | 6 mm | 266 |
| | | TPU, PDMS, Ecoflex, dielectric oil, Ag electrodes | stretchable (15%) | 1080 kPa | 493 $\mu$m | | 3 mm | 267 |
| | SMA | SMA wire, glass−fiber composite sheet | stretchable (300%) | 0.05−2 N | 0.2 mm | 0.1−30 Hz | 0.025−1 mm | 278 |
| | DEA | SWCNT, PDMS | stretchable (25%) | 9 mN | 6 $\mu$m | 1−500 Hz | 3 mm | 279 |
| kinesthetic | LCE | LCE, TPU, Ag heater | stretchable (50%) | 7 N | 5 mm | | 12 mm | 297 |
| | pneumatic | silicone elastomer, air chamber, nylon fabric | flexible | 0−5 N | 6 cm | 5 Hz | 10 mm | 298 |
| | tendon-driven | silicone, teflon tube, commercial actuators | stretchable | 29.5 N | | | 14 mm | 299 |
| electrotactile | | PDMS, Au, PAAm hydrogel | stretchable (425%) | 0−13.5 mA | | 25−200 Hz | 13 mm | 242 |
| | | FPC, Cu, Ag, TPU | stretchable (30%) | 10 V | | 4 kHz | 4 mm | 301 |
| | | PTFE, Cu, PET, ball electrode | stretchable (100%) | 5 $\mu$A | | 60 Hz | 15 mm | 302 |
| | | graphene, SWCNT, Ag NW, PLA, PMMA, PDMS, epoxy | stretchable (30%) | 18−40 mA | | 0−120 Hz | 30 mm | 304 |
| | | Cr/Au, PVA | stretchable (21%) | 3 mA | | 20 Hz | 1 mm | 177 |

Moreover, by stacking piezoelectric ceramics with micrometer-scale thickness, submillimeter-scale piezoelectric actuators were fabricated for flexible vibrotactile feedback devices (Figure 9l).[222] The actuator array was composed of submillimeter-sized piezoelectric ceramics stacked in a multilayer configuration, which was flexible enough to wrap around a fingertip and sufficiently small. Typically, reducing the area of piezoelectric ceramics for miniaturization can lead to a decrease in output performance. However, this serially stacked ceramic-based vibrotactile feedback device could generate dynamic vibrations across a wide frequency range, from 100 to 1000 Hz, and enveloped vibrations with a frequency below 10 Hz through amplitude modulation. This capability allowed for the generation of high-frequency dynamic pressure and low-frequency static pressure, thus providing a more realistic tactile sensation (Figure 9m).

*5.1.1.3. Pressure Feedback Devices.* Pressure feedback is a commonly utilized type of mechanical feedback that exerts a force on the skin, delivering sensory information about pressure and force distribution. The feedback is typically achieved through low-frequency and large-displacement mechanisms, which are effective in stimulating the mechanoreceptors in the deeper skin. To accomplish this, pressure feedback systems employ various types of actuators, such as pneumatic actuators,[214,215] hydraulic systems,[255−258] shape-memory materials,[259−261] and dielectric elastomer actuators (DEAs),[262−265] which are designed to generate controlled pressure and force. In addition, they can replicate sensations such as grasping, compression, or contact with an object depending on the shape and the structure of the deforming component. The ability to modulate the pressure and force enables more realistic and immersive interactions with virtual objects.

Pneumatic actuators are well-suited for implementing pressure feedback that requires low frequency but large deformations. The actuators also offer flexibility in adjusting pressure distribution over a wide range of scales, from small to large areas on the body, by modifying the size and shape of air chambers. A study reported the development of tactile feedback devices using pneumatic actuators, which provided multiscale feedback from the fingertip to the forearm and body (Figure 10a).[239] The feedback devices consisted of two types of pneumatic actuators, tailored to different body areas. Patch-type pneumatic actuators, composed of interconnected air capsules, were utilized for larger areas such as palms and arms. In contrast, pixel-type actuators, which featured individually


https://doi.org/10.1021/acs.chemrev.4c00966
Chem. Rev. 2025, 125, 11567−11665


**Figure 9.** Vibrotactile feedback devices. (a) Skin-integrated vibrotactile haptic device for social communication scenario. (b) Vibrotactile haptic actuators based on LRAs utilizing Lorenz forces. Inset: exploded view of the vibrotactile actuator. Reproduced with permission from ref 31. Copyright 2019 Springer Nature. (c) Haptic feedback patch with self-sensing mechanism employing Faraday's law. (d) Reproduction of virtual touch via LRA-based haptic feedback patch. Reproduced with permission from ref 156. Copyright 2022 The American Association for the Advancement of Science under CC BY 4.0 license https://creativecommons.org/licenses/by/4.0/. (e) Wearable tactile feedback device using ERM vibrators. (f) Demonstration of a piano training application in a VR environment. Inset: Optical image of the ERM vibrator Reproduced with permission from ref 253. Copyright 2022 Springer Nature under CC BY 4.0 license https://creativecommons.org/licenses/by/4.0/. (g) Schematic of a haptic interface composed of ERM motor array. (h) Digital image of the haptic interface delivering vibrotactile sensations to large areas of various body parts. (i) Wireless touch transmission through spatiotemporal vibration stimulation by individually controlling ERM motors. Reproduced with permission from ref 254. Copyright 2022 Springer Nature. (j) Smart glove providing precise vibrational feedback via piezoelectric


https://doi.org/10.1021/acs.chemrev.4c00966
Chem. Rev. 2025, 125, 11567−11665

**Figure** 9. continued

actuators (scale bar: 3 cm). Inset: magnified view of the vibrotactile actuators (scale bar: 1 cm). (k) Recreation of tactile sensations in response to releasing and touching interactions (top). Corresponding voltage signals to generate the tactile sensations (bottom). Reproduced with permission from ref 221. Copyright 2020 The American Association for the Advancement of Science under CC BY-NC 4.0 license https://creativecommons.org/licenses/by-nc/4.0/. (l) Optical image of submillimeter-scale piezoelectric actuators (scale bar: 5 mm). (m) Vibrotactile rendering using dynamic and static pressure generation for a realistic tactile sensation. Reproduced with permission from ref 222. Copyright 2022 Springer Nature under CC BY 4.0 license https://creativecommons.org/licenses/by/4.0/.

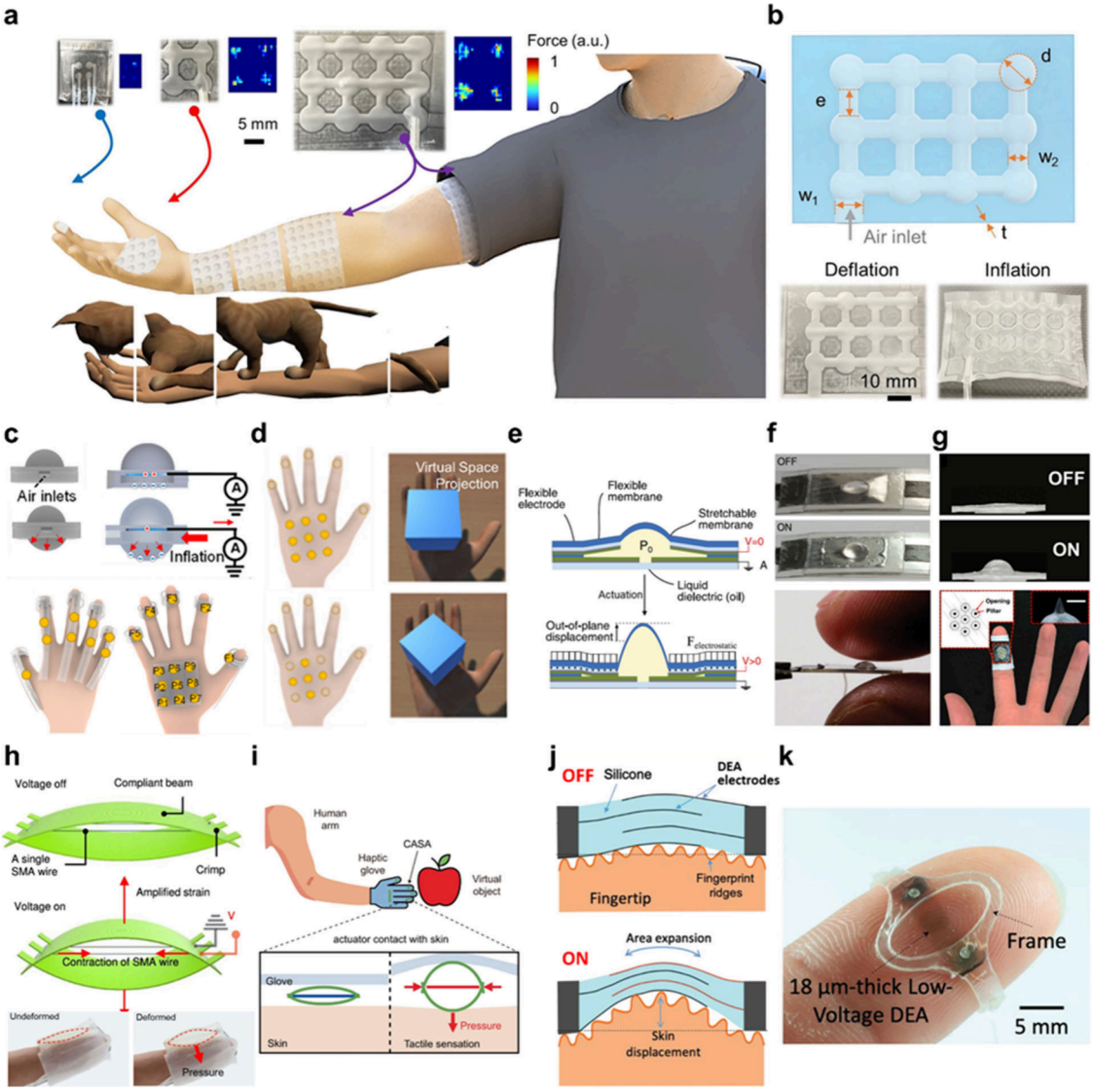


**Figure 10.** Pressure feedback devices. (a) Pneumatic actuator-based pressure haptic devices conveying multiscale feedback from the fingertip to the forearm and body. (b) Design parameters of the pneumatic actuator (top). Optical images of the actuators at deflation (bottom left) and inflation states (bottom right) (scale bar: 10 mm). Reproduced with permission from ref 239. Copyright 2024 Elsevier. (c) Pressure-inducing mechanism (top) and pneumatic haptic glove providing pressure feedback to the fingers and palm (bottom). (d) Reproduction of tactile sensations stimulated by a virtual object on the palm (left). Corresponding images showing that the virtual object is placed on the palm (right). Reproduced with permission from ref 238. Copyright 2022 American Chemical Society. (e) The actuation mechanism of hydraulic actuator utilizing electrostatic forces for idle (top) and activation (bottom) states. (f) Digital images of the hydraulic actuator in OFF state (top), ON state (middle), and during pressure feedback generation (bottom). Reproduced with permission from ref 266. Copyright 2020 Wiley-VCH. (g) Actuation states of skin-integrated hydraulic electrostatic actuator: OFF (top), ON (middle), and worn state (bottom) (scale bar: 1 mm). Reproduced with permission from ref 267. Copyright 2023 Springer Nature under CC BY 4.0 license https://creativecommons.org/licenses/by/4.0/. (h) Operating mechanism based on deformation-amplifying structure (top), with the SMA actuator in undeformed (bottom left) and deformed (bottom right) configurations. (i) Schematic illustration of the interaction with a virtual object through the SMA actuator-based haptic glove. Inset: magnified view of the contact area. Reproduced with permission from ref 278. Copyright 2022 Springer Nature under CC BY 4.0 license https://creativecommons.org/licenses/by/4.0/. (j) Schematic diagram of the pressure inducing mechanism by DEA-based soft actuator: OFF (top) and ON (bottom) modes. (k) Pressure haptic device attached to the fingertip (scale bar: 5 mm). Reproduced with permission from ref 279. Copyright 2020 Wiley-VCH.


https://doi.org/10.1021/acs.chemrev.4c00966
Chem. Rev. 2025, 125, 11567−11665

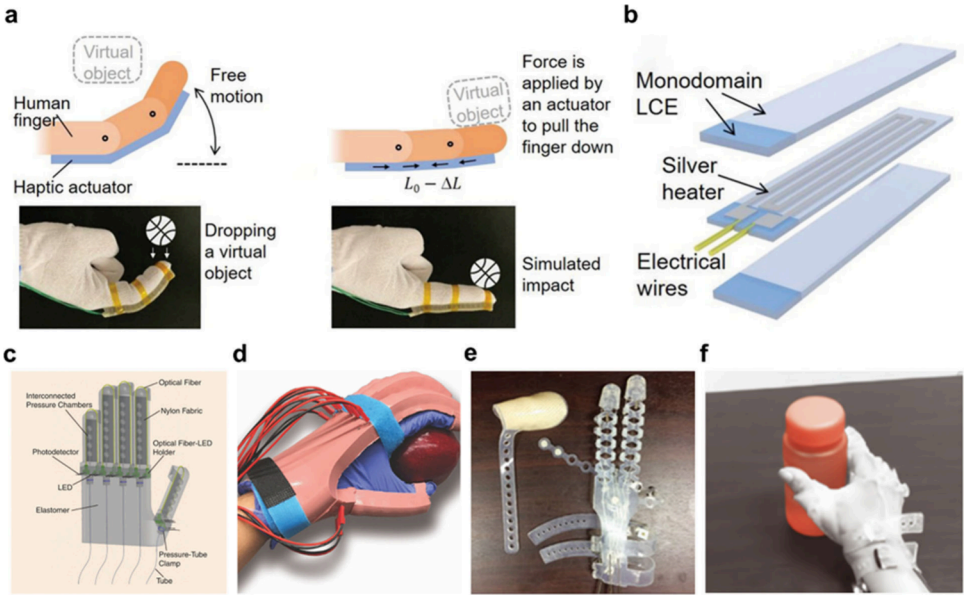


**Figure 11.** Kinesthetic feedback devices. (a) Schematic illustration (top) and corresponding images (bottom) of the interaction scenario where a falling virtual object exerts force on the finger. (b) Exploded view of the kinesthetic actuator employing heat-responsive LCE. Reproduced with permission from ref 297. Copyright 2020 Wiley-VCH. (c) Elastomer-based soft haptic glove based on pneumatic actuators for kinesthetic feedback. (d) Demonstration of assistance in grasping motion through the soft haptic glove. Reproduced with permission from ref 298. Copyright 2016 IEEE. (e) Optical image of a tendon-driven polymeric glove. (f) Reproduction of grasping motion using the tendon-driven glove. Reproduced with permission from ref 299. Copyright 2019 The American Association for the Advancement of Science.

controlled air capsules connected to independent channels, were employed for localized pressure on smaller regions like fingertips. In this study, a range of sensory experiences were achieved by manipulating design parameters including inlet channel width, airway width, capsule diameter, and spacing (Figure 10b).

In another study, two types of pneumatic actuators were proposed for a glove-type haptic feedback interface.[238] To simulate various sensations on the hand in virtual spaces, different designs were developed for the fingers and the palm (Figure 10c). Pneumatic actuators were arranged along the length of the device to provide localized pressure stimuli to the fingers and fingertips, while a 2D array of actuators was adopted to generate the required pressure distribution over a large area. Notably, the glove-type device demonstrated the ability to monitor the operation of individual pneumatic actuators without the need for a pressure sensor. Each actuator was composed of two triboelectrification layers. As air inflated the chamber, the distance between the two layers increased, generating triboelectric output, which enabled the detection of the pneumatic actuation state. The actuating mechanism without a sensor allowed for a more precise rendering of contact in VR environments while facilitating the design of more compact systems (Figure 10d).

In mechanical systems that require high pressure and force, hydraulic actuators typically rely on pumps to apply pressure to a liquid. However, in haptic systems where wearability and miniaturization are essential, hydraulic electrostatic mechanisms that generate pressure and deformation using electrostatic forces without mechanical components are promising.[266,267] For instance, hydraulic electrostatic actuators, less than a millimeter thick, have been developed to provide haptic feedback through pressure.[266] The central part of these actuators consisted of a stretchable elastomer to allow deformation, while the rest was composed of a membrane coated with flexible conductors. The liquid dielectric acted as a working fluid, filling the internal cavity inside the device. When voltage was applied to the actuators, the electrostatic force induced movement of the liquid, causing deformation in the stretchable part (Figure 10e). Furthermore, the electrostatic actuators generated both out-of-plane and in-plane displacements, providing normal and shear forces to localized regions of the body. Despite their light weight and small size at the millimeter scale, the actuators delivered substantial mechanical feedback with a force density of around 3 kN $kg^{-1}$ (Figure 10f). In a similar study, skin-integrated hydraulic electrostatic actuators were developed to account for the tactile sensitivity of skin.[267] When voltage was applied to electrodes placed parallel on both sides of a liquid-filled pouch, out-of-plane deformation occurred (Figure 10g). This deformation produced feedback to the skin with a pressure of 1 MPa, exceeding the tactile threshold of the skin and thereby providing information on surface textures and object shapes.

Additionally, shape-memory materials typically return to their preset shape when activated by external stimuli, including temperature,[260,268−271] light,[272−274] and electrical activation.[275−277] These responsive and deformable properties have been widely explored for actuators, particularly due to the ability to generate force and deformation in small form factors, making them promising candidates for actuating components in haptic feedback devices.[260,278] For example, compact shape memory alloy (SMA) actuators that respond to electrical stimuli have been designed to deliver immersive tactile feedback.[278] While SMA wires possess excellent power density and ease of use, they typically do not lead to significant deformation. However, the authors engineered a structure that amplified the deformation induced by the contraction of SMA wires (Figure 10h). When voltage was applied, the contraction of the SMA wires caused a compliant beam to produce amplified deformation in a direction perpendicular to the


https://doi.org/10.1021/acs.chemrev.4c00966
Chem. Rev. 2025, 125, 11567−11665

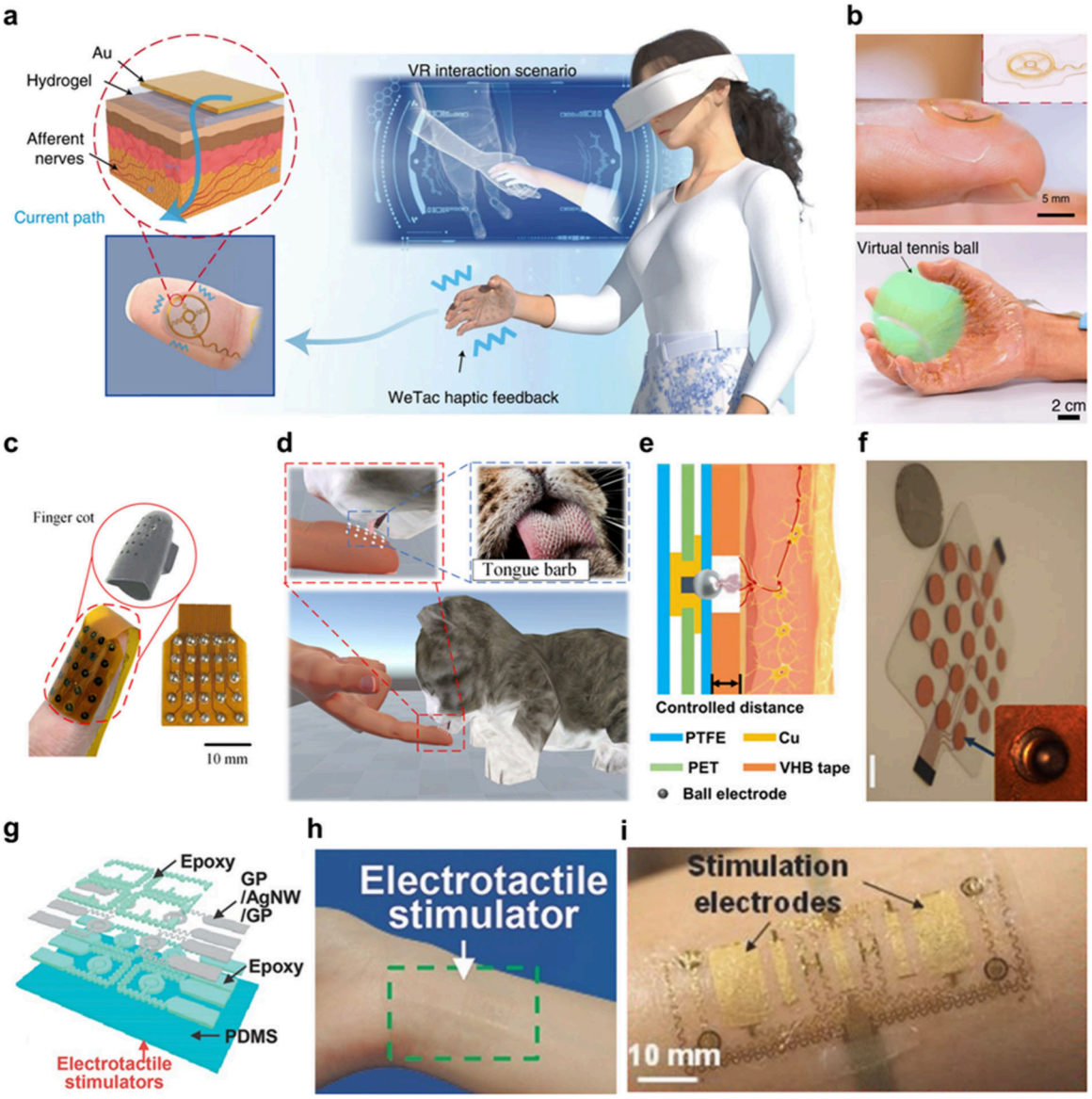


**Figure 12.** Electrotactile feedback devices. (a) Skin-integrated electrotactile system stimulating afferent nerves beneath the skin. (b) Electrotactile haptic device attached to the fingertip (top) (scale bar: 5 mm). Inset: digital image of the electrotactile feedback device. Reproduction of the tactile sensation of slowly grasping a virtual ball through the electrotactile device (bottom) (scale bar: 2 cm). Reproduced with permission from ref 242. Copyright 2024 Springer Nature. (c) Optical images of an electrotactile haptic device where the stimulation electrodes are arranged with a high spatial resolution (scale bar: 10 mm). (d) Tactile rendering of sensations like the feeling of a virtual cat licking the finger. Insets: magnified view of the action (red) and a close-up image of the tongue barb of a cat (blue). Reproduced with permission from ref 301. Copyright 2022 The American Association for the Advancement of Science under CC BY-NC 4.0 license https://creativecommons.org/licenses/by-nc/4.0/. (e) Schematic illustration of stimulation mechanism to produce haptic sensations. (f) TENG-based electrotactile system in the form of a wearable band for the forearm. Inset: magnified view of a stimulation electrode of the electrotactile system. Reproduced with permission from ref 302. Copyright 2021 The American Association for the Advancement of Science under CC BY-NC 4.0 license https://creativecommons.org/licenses/by-nc/4.0/. (g) Exploded view of transparent electrotactile stimulator with a sandwiched structure composed of graphene and Ag NWs. (h) Imperceptible electrotactile device attached to the skin. Reproduced with permission from ref 304. Copyright 2014 Wiley-VCH. (i) Digital image of electrotactile stimulator designed for larger muscle activation (scale bar: 10 mm). Reproduced with permission from ref 177. Copyright 2015 Wiley-VCH.

contraction. This structure allowed the actuators to maintain a thin form factor in the idle state while delivering sufficient pressure feedback when actuated. Consequently, the authors fabricated actuators that effectively utilized the high-power density of SMAs and the large displacement of the compliant structure. Despite weighing less than 0.25 g, these actuators demonstrated exceptional power density, above 1.5 kW $kg^{-1}$, making them suitable for haptic devices that realistically render contact with virtual objects (Figure 10i).

In addition, DEAs are soft actuators driven by the deformation of dielectric elastomers under an applied electric field.[262,279] DEAs consist of a dielectric elastomer sandwiched between two electrode layers. When voltage is applied to the electrodes, electrostatic forces compress the elastomer in thickness, resulting in actuation. DEAs can be fabricated in very thin forms, exhibit a wide range of response frequencies, and generate relatively large actuation strain, making them suitable for miniaturized tactile feedback devices for fingertips. For instance, fingertip haptic devices utilizing DEAs composed


https://doi.org/10.1021/acs.chemrev.4c00966
Chem. Rev. 2025, 125, 11567−11665

of alternating single-walled carbon nanotube (SWCNT) electrodes and dielectric membranes with 20 $\mu$m thickness have been reported (Figure 10j).[279] When in the off state, the DEA remained in conformal contact with the fingertip without any mechanical constraint. In the on state, the area expansion caused by a decrease in thickness pulls the skin in the normal direction, producing a feedback sensation. Notably, the actuators provided a localized pressing or pulling sensation at low frequencies from 1 to 20 Hz, and they also generated vibrations across the entire fingertip at high frequencies above 100 Hz. Consequently, the DEAs were demonstrated as microscale haptic devices that delivered rich tactile feedback, including pressure and vibration (Figure 10k).

*5.1.1.4. Kinesthetic Feedback Devices.* Kinesthetic feedback encompasses the sensations of force, motion, or vibration that users experience when interacting with VR environments. However, this section specifically focuses on kinesthetic feedback associated with the restriction or assistance of body movements perceived through joints, emphasizing the provision of large deformations or forces. Traditional actuators, such as pneumatic actuators, hydraulic systems, or motors, have been widely used to generate joint motion for kinesthetic feedback.[241,280−283] For skin-integrated soft haptic devices, soft actuators such as liquid crystal elastomer (LCE) actuators are gaining attention.[284,285] LCEs possess characteristics of both liquid crystals and elastomers, enabling them to change shape and mechanical properties triggered by external stimuli such as heat,[286−289] light,[290−293] and electrical activation.[294−296] Based on these characteristics, LCE actuators can mimic muscle-like behavior, making them ideal for delivering controlled movements to the user. For example, an LCE actuator, activated by thermal stimuli, has been developed for reconstructing kinesthetic sensations in the finger (Figure 11a).[297] When a virtual object was not in contact with the finger, the LCE actuator did not constrain the motion, behaving like a conventional elastomer. Upon contact of the virtual object with the fingertip, the LCE actuator contracted and applied force to extend the finger, thereby generating the sensation of the object pressing against it. For the actuation, a flexible heater was embedded within the actuator to trigger the heat-responsive LCE (Figure 11b).

Elastomer-based pneumatic actuators can also be employed in soft haptic gloves for kinesthetic feedback.[298] Elastomer-based haptic gloves were designed with the palm side of each finger made from relatively nonstretchable fabric and interconnected air chambers embedded within the fingers (Figure 11c). When the air was injected from an external pump, the air chambers inflated, bending the fingers, with the stiff fabric acting as a neutral plane to generate a grasping motion. By controlling each finger individually, various hand gestures could be produced. As a result, the glove not only provided mechanical feedback for simulating interactions with virtual spaces but also served as a soft orthosis to assist in grasping motions in real life (Figure 11d). A similar polymeric glove for kinesthetic feedback was developed by applying a tendon-driven mechanism, instead of pneumatic systems (Figure 11e).[299] The glove generated grasping and releasing motions by adjusting the tension of the tendon using an external motor. Since the tendon-driven actuator operated without air chambers, it offered a more compact form factor compared to a pneumatic system. Therefore, the tendon-driven polymeric gloves generated sufficient force to control the human hand to grab a rigid object without slippage (Figure 11f). However, both designs require additional components, such as air pumps or motors to control the tendon wires, which limits the transition to fully skin-integrated systems. Though bulky devices are still necessary for kinesthetic feedback, ongoing research aims to develop these technologies into skin-integrated systems.

*5.1.1.5. Electrotactile Feedback Devices.* Electrotactile feedback, which stimulates nerves with electric currents to provide tactile sensations, can be implemented in more compact form factors as it requires only electrodes rather than mechanical components.[210−212] Because of this property, the design of electrotactile feedback systems emphasizes the resolution of the electrode array and the stability of the interface between the electrodes and the skin.[242,300] By considering these technical aspects, a study developed a soft and compact skin-integrated hydrogel-based electrotactile system (Figure 12a).[242] The authors placed a hydrogel between the metal electrodes and the skin to reduce impedance and enhance current flow. Additionally, the hydrogel patch, being soft and adhesive, ensured stable conformal contact between the electrotactile unit and the skin, even during deformation of the skin. Miniaturizing the electrodes enabled the electrotactile system to achieve a high spatial density in the electrode array. Based on the superior stability and high resolution of the haptic device, the authors built a model that converted pressure distribution on the hand into a corresponding current map during interaction with virtual objects. As a result, they successfully rendered the tactile sensation of slowly gripping a tennis ball using electrotactile feedback (Figure 12b).

Another study introduced an electrotactile haptic system with high spatial resolution by analyzing the mechanisms through which humans perceive mechanical sensations via the skin (Figure 12c).[301] Inspired by the process of generating action potentials in receptors, the authors fabricated electrotactile haptic devices that replicated a natural sense of touch by stimulating localized regions around mechanoreceptors with electric currents, thereby inducing action potentials along the same neural pathways. The developed haptic devices with a 5 × 5 electrode array were designed to be worn on the fingertip. Using the current steering concept that selectively directs electrical currents to specific regions, the device achieved a spatial resolution of nearly 80 stimulation points per square centimeter using only 25 electrodes. By asymmetrically controlling currents through one target electrode and four adjacent electrodes, the system created stimulation points in the regions between physical electrodes. This approach enabled the generation of delicate sensations with high-resolution tactile feedback approaching the density of mechanoreceptors in the fingertip skin, allowing for the rendering of sensations like the feeling of a virtual cat licking the skin (Figure 12d).

Moreover, triboelectric nanogenerators (TENGs), which generate electrical energy by converting mechanical energy through the electrostatic induction and triboelectric effect, can be effectively applied to electrotactile feedback devices. In this respect, a skin-integrated and self-powered XR interface providing mechanohaptic feedback based on electrotactile techniques was demonstrated.[302] Electrostatic signals generated by touch and sliding motions in the TENG were transmitted to the connected electrotactile unit, causing discharging between the ball electrodes and the skin, which in turn produced haptic sensations (Figure 12e). In addition,


https://doi.org/10.1021/acs.chemrev.4c00966
Chem. Rev. 2025, 125, 11567−11665

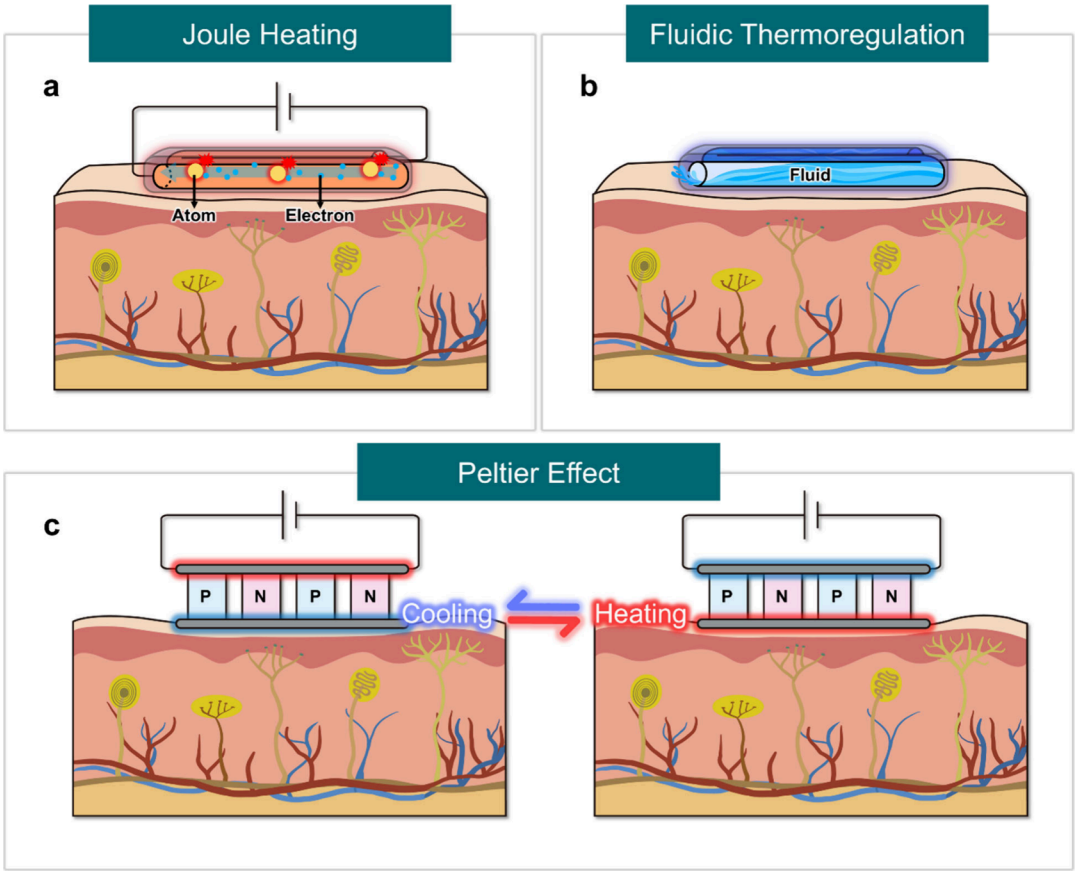


**Figure 13.** Mechanisms for the reconstruction of thermal sensation with wearable XR feedback devices. (a) Joule heating-based feedback mechanism. (b) Fluidic thermoregulation-based feedback mechanism. (c) Peltier effect-based feedback mechanism for cooling (left) and heating (right). Created with BioRender.com.

the electrical characteristics of the TENG, such as high voltage and low current, made it suitable for safe electrotactile stimulation. As a result, a TENG-based electrotactile system, designed as a wearable band for the forearm, demonstrated the potential to convey augmented tactile sensations from real-world contacts while wearing protective equipment like spacesuits (Figure 12f).

For electrotactile devices, it is crucial to maintain conformal contact between the skin and the device to effectively deliver electrical stimulation. To achieve this, it is important to avoid using rigid components. Furthermore, minimizing the thickness of the soft device to reduce mechanical resistance is essential for conformal contact.[303] To address these issues, an ultrathin and transparent electrotactile device was proposed using graphene and silver NWs (Ag NWs).[304] A structure in which Ag NWs are sandwiched between the top and bottom graphene layers was designed to improve the charge injection performance of the electrodes for effective feedback performance (Figure 12g). Based on these materials, the electrotactile device exhibited high transmittance over 90% in the visible light range, and was imperceptible when applied to the skin (Figure 12h). In addition, the device was sufficiently stretchable and thin to conformally attach to the skin, ensuring stable electrotactile stimulation during dynamic motions. Electrotactile feedback can also be applied to muscle activation through precise control.[177] While electrotactile stimulation typically provides haptic sensations via nerve stimulation, it can also trigger muscle contraction or provide proprioceptive feedback. An electrotactile stimulator designed for larger muscle activation could help users apply consistent force to their muscles via electrotactile feedback, suggesting the potential for advanced feedback beyond sensory input in VR environment (Figure 12i).

**5.1.2. Thermohaptic Feedback Devices.** Alongside mechanical tactile feedback, thermal sensations are among the most significant sensory experiences when humans touch or interact with objects. Mechanical tactile feedback provides texture and physical information of objects, while thermal sensations convey the temperature of objects and the atmosphere of the environment. For instance, similar to the distinct sensations perceived by humans when touching metal and wood at the same temperature, the integration of two distinct types of sensory feedback can offer users a more realistic and immersive experience.[305,306] Typically, mechanisms for wearable XR devices to implement thermal sensations include Joule heating,[307−326] fluid-based heat transfer,[327−332] and the Peltier effect.[32,333−336]

*5.1.2.1. Mechanisms and Materials for Thermohaptic Feedback Devices.* Joule heating, or resistive heating, is the phenomenon where heat is generated due to the resistance encountered by electric current flowing through a conductor.[337,338] This heat generation occurs because the electrons moving through the conductor collide with atoms or ions, transferring energy to them (Figure 13a). This energy is converted into vibrational energy of the atoms or ions, leading to a rapid increase in temperature.

For wearable Joule heating-based thermohaptic sensation, a percolation network structure with 1D nanomaterials is highly


https://doi.org/10.1021/acs.chemrev.4c00966
Chem. Rev. 2025, 125, 11567−11665

beneficial in terms of electrical conductivity and stretchability.[339−341] The percolation network functions by having junctions that act as hinges, allowing it to maintain electrical conductivity even under deformation.[139,342] In the meantime, these junctions efficiently generate localized heat when an electrical current is applied, while the remaining parts serve as excellent conductors, facilitating stable operation.[343] Furthermore, LMs provide high thermal and electrical conductivity while maintaining intrinsic stretchability.[133] Their fluid nature allows them to conform to complex geometries and deform without losing functionality, making them ideal for stretchable applications.[344,345] When embedded in microfluidic channels or patterned within polymer substrates, LM-based circuits can deliver precise and uniform thermal stimulation by efficiently distributing heat.[346,347]

The fast response time of Joule heating makes it particularly suitable for haptic feedback systems in wearable XR devices. By adjusting the voltage or current, the heat output can be precisely controlled, allowing for fine thermal sensations that enhance the immersive experience in VR environments. However, a limitation of Joule heating is that it can only implement heating sensations and not cooling.

In addition, fluidic heat transfer systems operate by adjusting the temperature of a fluid to transfer thermal sensations to the skin (Figure 13b). These systems commonly employ channels that enable fluids, such as water or air, to flow and make direct contact with the skin. Wearable thermohaptic systems utilizing fluids can deliver both heating and cooling sensations by changing the temperature of the fluid, offering a uniform temperature change over a wide area. Various working fluids, including air,[331] water,[327,330] can be used for thermal regulation. However, these systems are often bulky due to the incorporation of chambers and pumps required for storing and circulating the fluid, which can result in slower response times. Furthermore, regulating the temperature of the fluid within the device poses challenges, limiting the ability to achieve a diverse range of temperatures.

Lastly, the Peltier effect refers to the process where electric current passing through the junction between two different metals or semiconductors causes heat to be absorbed or released (Figure 13c).[173,348] The working principle of the Peltier effect utilizes the different heat transfer properties of the charge carriers in N-type and P-type semiconductors. In N-type semiconductors, electron movement results in heating at the junction opposite the current direction, while cooling occurs at the other junction. In P-type semiconductors, the movement of positive charge carriers causes cooling at the junction in the current direction and heating at the other junction. By arranging P-type and N-type semiconductor elements appropriately, both heated and cooled sides can be achieved with a single current.

To maximize the temperature difference in Peltier materials, it is essential to focus on minimizing thermal conductivity, enhancing electrical conductivity, and bandgap engineering.[349,350] Minimizing thermal conductivity involves techniques such as nanostructuring and alloying.[351,352] Nanostructuring introduces nanoscale interfaces that scatter phonons, thereby reducing lattice thermal conductivity without significantly affecting electrical conductivity.[353] Similarly, alloying with elements of differing atomic masses disrupts phonon propagation, further reducing heat leakage. In addition, enhancing electrical conductivity can be achieved through doping.[354] Doping adjusts the carrier concentration, balancing electrical conductivity with the Seebeck coefficient to achieve maximum efficiency.[355,356] Lastly, advanced bandgap engineering contributes significantly to enhancing the temperature gradient in Peltier materials by optimizing the electronic structure to maximize the Seebeck coefficient and carrier efficiency across a range of temperatures.[357,358]

The Peltier effect allows precise control over the thermal feedback by adjusting the direction of voltage or current, making it a highly promising mechanism for wearable XR devices.[32,33,335,336,359] It can generate both heating and cooling sensations within a single device configuration, enhancing the immersive experience. However, prolonged use may cause heat accumulation on the heated side to flow back to the cooled side, reducing the cooling effect. Thus, incorporating heat sinks to dissipate this backflow heat is crucial for stable and high-performance thermal feedback.

In terms of the delivery of thermal sensation, wearable thermohaptic XR devices rely heavily on the thermal properties of polymeric substrates that are commonly used due to their flexibility and biocompatibility. However, their inherently low thermal conductivity can hinder efficient heat transfer from functional materials or working fluids.[360−362] To overcome this limitation, the incorporation of highly thermally conductive fillers, such as metallic particles or ceramic-based fibers, has been explored.[363−366] These fillers significantly enhance the overall thermal conductivity of the polymer matrix, thereby improving heat transfer efficiency and enabling a more effective thermal response in wearable thermohaptic devices.

Table 5 outlines the key advantages and limitations of representative thermohaptic approaches, including Joule heating, fluidic thermoregulation, and the Peltier effect. Furthermore, Table 6 presents a detailed comparison of recent thermohaptic devices, highlighting their material platforms, stretchability, thermal performance, and target sensations, all of which are critical for integration into soft wearable XR interfaces. These thermal sensation implementation technologies are suitable with "for significantly enhancing the realism experienced by users in XR environments. By making users feel temperature changes as if they were real, the immersive

**Table 5. Summary of Advantages and Disadvantages of Thermohaptic Feedback Devices**

| mechanism | advantages | disadvantages |
|---|---|---|
| Joule heating | • fast and controllable thermal response | • heating only, no cooling capability |
| | • simple and compact device structure | • risk of hot spots or overheating |
| | • low-voltage operation with high output | • thermal loss and continuous power consumption |
| fluidic thermoregulation | • bidirectional thermal feedback | • bulky and complex system |
| | • uniform temperature distribution | • slow response time |
| | • flexible choice of working fluids | • limited precision in temperature control |
| Peltier effect | • bidirectional thermal control | • limited cooling performance and duration |
| | • no mechanically moving parts | • heat backflow and accumulation |
| | • no refrigerants required | • need for external heat sinks |


https://doi.org/10.1021/acs.chemrev.4c00966
Chem. Rev. 2025, 125, 11567−11665

Table 6. Summary of Thermohaptic Feedback Devices and Their Characterization for Soft Wearable XR Interfaces

| mechanism | material | stretchability | target sensation | performance | spatial resolution | ref |
|---|---|---|---|---|---|---|
| Thermohaptic Feedback | | | | | | |
| Joule heating | Cu NW | stretchable (120%) | heating | ~120 °C (@ 7 V) | 664 $\mu$m | 308 |
| | EGaIn | stretchable (100%) | heating | ~120 °C (@ 2 W) | | 310 |
| | CNT fiber | stretchable (150%) | heating | ~135 °C (@ 5 V) | | 372 |
| | | | | response time: 1030 °C $s^{-1}$ (@ 8 V) | | |
| | Cu, polyacrylate | flexible | heating | ~40 °C | 5 mm | 307 |
| | Ag NW | stretchable (400%) | heating | ~80 °C (@ 9 V) | | 373 |
| fluidic cooling | working fluid: air | flexible | heating/cooling | 28−40 °C; response time, 1−2 °C $s^{-1}$ | | 331 |
| | working fluid: PFP, $N_2$ | flexible | cooling | response time, 3 °C $s^{-1}$ (@ 300 $\mu$L $min^{-1}$) | | 329 |
| | working fluid: Novec 7100 engineering fluid | flexible | heating/cooling | 12−42 °C | | 328 |
| | working fluid: water | flexible | cooling | maintain ~35 °C (@ inlet 20 °C) | | 330 |
| | working fluid: water | stretchable | cooling | ~14 °C (@ 1.75 mL $min^{-1}$) | | 327 |
| Peltier effect | commercial TE alloys | flexible | heating/cooling | 26−43 °C ($\Delta T$: ~10 °C) | | 334 |
| | $Bi_2Te_3/Sb_2Te_3$, $Bi_2Te_3/Bi_2Te_{2.83}Se_{0.17}$ | flexible | cooling | 11−16 °C, 5.95 °C $s^{-1}$ | | 335 |
| | $Bi_2Te_3$ | stretchable (230%) | heating/cooling | 10−40 °C ($\Delta T$: ~15 °C) | | 32 |
| | $Bi_2Te_3/Sb_2Te_3$ | flexible | heating/cooling | 15−35 °C ($\Delta T$: ~13 °C) | | 336 |

experience is deepened. This can elicit emotional responses and create more vivid physical interactions, providing users with a richer and more authentic experience.

*5.1.2.2. Joule Heating-Based Feedback Devices.* For soft wearable XR devices, the Joule heating mechanism can be simply implemented using various materials such as CNTs,[367−369] NWs,[315,316,318,321,323−325] and LMs.[310,370,371] For instance, devices using hierarchically twisted CNT fibers offer rapid heating performance with response rates of 1030 °C $s^{-1}$ and improved wearability due to their stretchable helical structure.[372] Similarly, devices using Ag NWs and ultrathin colorless PI layers provide stable thermal performance even under 200% strain, offering excellent skin interfaces.[373] However, beyond simple broad thermal sensations over the skin, it is crucial to reproduce various thermal forms and scenarios through pixelated multiple thermal sensations to implement realistic thermal sensations in XR devices.

From this perspective, a flexible and adaptive Joule heating-based thermohaptic glove was developed by embedding eutectic Gallium−Indium (EGaIn) wires in silicone-based elastomer (Figure 14a).[310] EGaIn is generally known to have high electrical and thermal conductivity even under mechanical deformation, while the silicone elastomer offers flexibility, which allows stable operation under deformation according to user hand movements.[374] This device achieved 83.24 °C with 1 W power and maintained the target temperature precisely within an error of 1.74% through PID control. Furthermore, the thermohaptic glove recreated a scenario where the sensation of holding a 55 °C metal ball immersed in 45 °C hot water was implemented, mimicking the sensation of dipping hands into the water and feeling the temperature change when holding the metal ball (Figure 14b). Additionally, the device was able to adjust the heat flux by varying the rate of temperature control, allowing it to reproduce different types of objects in the VR environment with varying intensities of touch and thermal conductivity (Figure 14c).

Similarly, copper NWs (Cu NWs) can be used for a wearable Joule heating-based thermohaptic device using a serpentine structure, providing precise temperature control and enhanced wearability even in stretchable states (Figure 14d).[308] The glove consisting of 12 thermal sensation pixels recreated various thermal scenarios in VR environments. In a VR environment, as the hand approaches and moves away from a campfire, the thermohaptic glove is designed to adjust the temperature accordingly to provide a thermal sensation (Figure 14e). In addition, by independently controlling the Cu NW-based heater attached to the palm, the glove was able to simulate the sensation of pouring hot water in the VR environment (Figure 14f).

Although devices using the Joule heating mechanism can quickly reach the target heating temperature, it takes a long time for the heated device to return to its original temperature. The residual heat remaining in the device becomes a factor that hinders the performance of subsequent thermal scenarios until the generated heat dissipates, disrupting the high level of immersion in the VR environment.[9,375,376]

To address this issue, a wearable thermohaptic patch was designed, introducing cooling hydrogel to a Joule heating device to achieve efficient passive cooling (Figure 14g).[307] This system offered precise control over skin thermal stimulation by using a thin, flexible resistance heater and efficient cooling elements. The resistance heater was constructed using copper electrodes patterned in a fractal structure, similar to the Peano curve, on a PI substrate. This assembly was integrated into a flexible printed circuit board (f-PCB) and encapsulated with soft silicone-based composite materials to enhance skin


https://doi.org/10.1021/acs.chemrev.4c00966
Chem. Rev. 2025, 125, 11567−11665

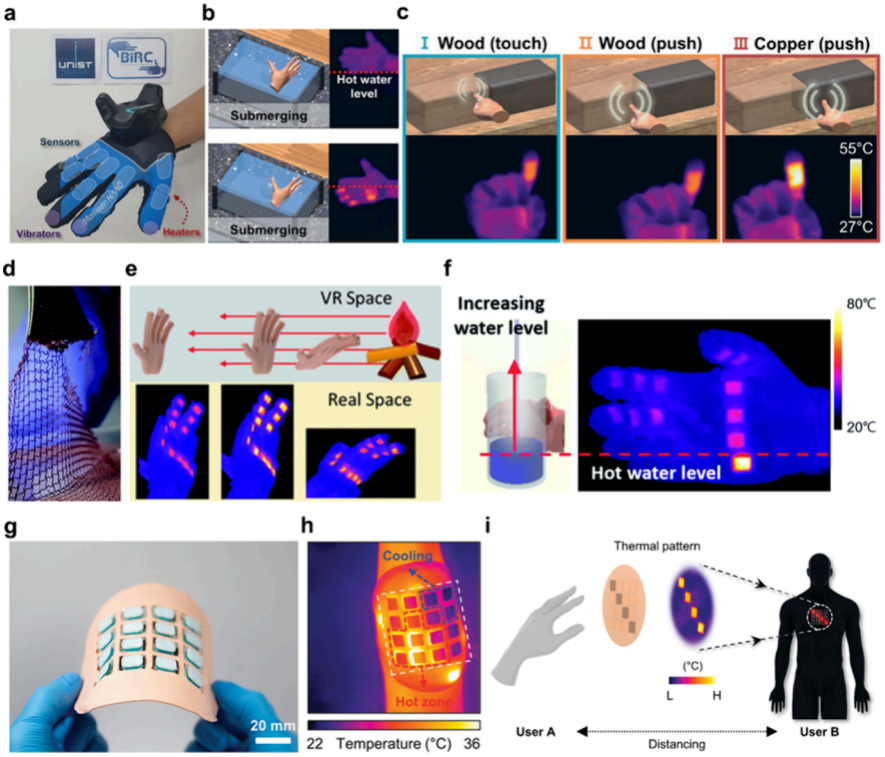


**Figure 14.** Joule heating-based feedback devices. (a) Flexible thermohaptic glove with EGaIn. (b) Virtual thermal sensation modeling before (top) and after (bottom) hand is submerged in hot water using an EGaIn-based glove. (c) Reproduction of virtual objects with various thermal sensations through heat flux adjustment of the EGaIn-based glove. Reproduced with permission from ref 310. Copyright 2021 Wiley-VCH. (d) Wearable Cu NW-based Joule heating device with a serpentine structure. (e) Recreation of a virtual campfire thermal scenario in a VR environment using Cu NW heaters. (f) Independent Cu NW Joule heating control simulating the sensation of pouring hot water. Reproduced with permission from ref 308. Copyright 2020 The Royal Society of Chemistry. (g) Thermohaptic patch with passive cooling enabled by cooling hydrogel (scale bar: 20 mm). (h) An infrared (IR) image showing thermal sensation patterns generated by a thermohaptic patch. (i) Wireless transmission and reproduction of thermal sensations through the thermohaptic patch. Reproduced with permission from ref 307. Copyright 2023 Proceedings of the National Academy of Sciences.

adhesion. In this device, the cooling element harnesses the phase change energy of a low-boiling-point liquid within the cooling gel. The cooling gel was applied to the underside of the resistance heater to regulate thermal transfer between the gel and the heater. Therefore, this system efficiently removed the residual heat in the heating elements and lowered skin temperature to facilitate the next thermal stimulus, providing a diverse pattern of thermal sensations (Figure 14h). Moreover, this patch implemented a system that transmits thermal sensation patterns wirelessly between two locations, allowing a thermal pattern generated at one location to be reproduced on the skin of a user at another location (Figure 14i). This suggests a new form of remote interaction, especially for remote social interactions, sensory experience sharing, and applications in a VR environment.

*5.1.2.3. Fluidic Thermoregulation-Based Feedback Devices.* Temperature control using fluids is one of the most commonly used systems, utilized across various fields, including industrial air conditioning and heating and cooling applications, due to its efficiency in regulating temperature.[305,377] This fluid-based thermal management system has been applied to wearable devices to deliver thermal sensations to the skin.[327−332] These devices operate by transferring or absorbing heat through fine fluid channels to directly alter the temperature of human skin, allowing users to experience the desired temperatures with minimal external environmental influence.

Regarding this, a thermohaptic glove system that provides thermal sensations by inflating air bladders with air at different temperatures was proposed (Figure 15a).[331] The system created warm or cool sensations by pumping hot or cold air to a specific part of the human body (Figure 15b). Using the air as working fluid, this system achieved a response rate of 2.75 °C $s^{-1}$ and successfully implemented thermal sensations with various materials, including copper, glass, and foam, within a VR environment by deriving the rate and magnitude of temperature change based on the thermal conductivity of these materials during user interaction (Figure 15c). With the air-based glove system, the authors were able to provide thermal sensations within a temperature range from 28 to 40 °C, owing to the low thermal conductivity and heat capacity of the air.

In contrast, water, which possesses higher thermal conductivity and heat capacity than air, can absorb and transfer more heat more quickly and effectively within the same volume. Most water-based cooling systems circulate fluids through tubes, making the thermal conductivity of the tubes crucial for implementing thermal sensations.[378] A wearable system utilizing water as the circulating medium was devised, enhancing the thermal conductivity of the tubes to achieve more efficient cooling (Figure 15d).[330] This study employed composite tubes containing aluminum powder dispersed in silicone, achieving a maximum thermal conductivity about 0.7 W $m^{-1}$·$K^{-1}$. As a result, the composite tube


https://doi.org/10.1021/acs.chemrev.4c00966
Chem. Rev. 2025, 125, 11567−11665

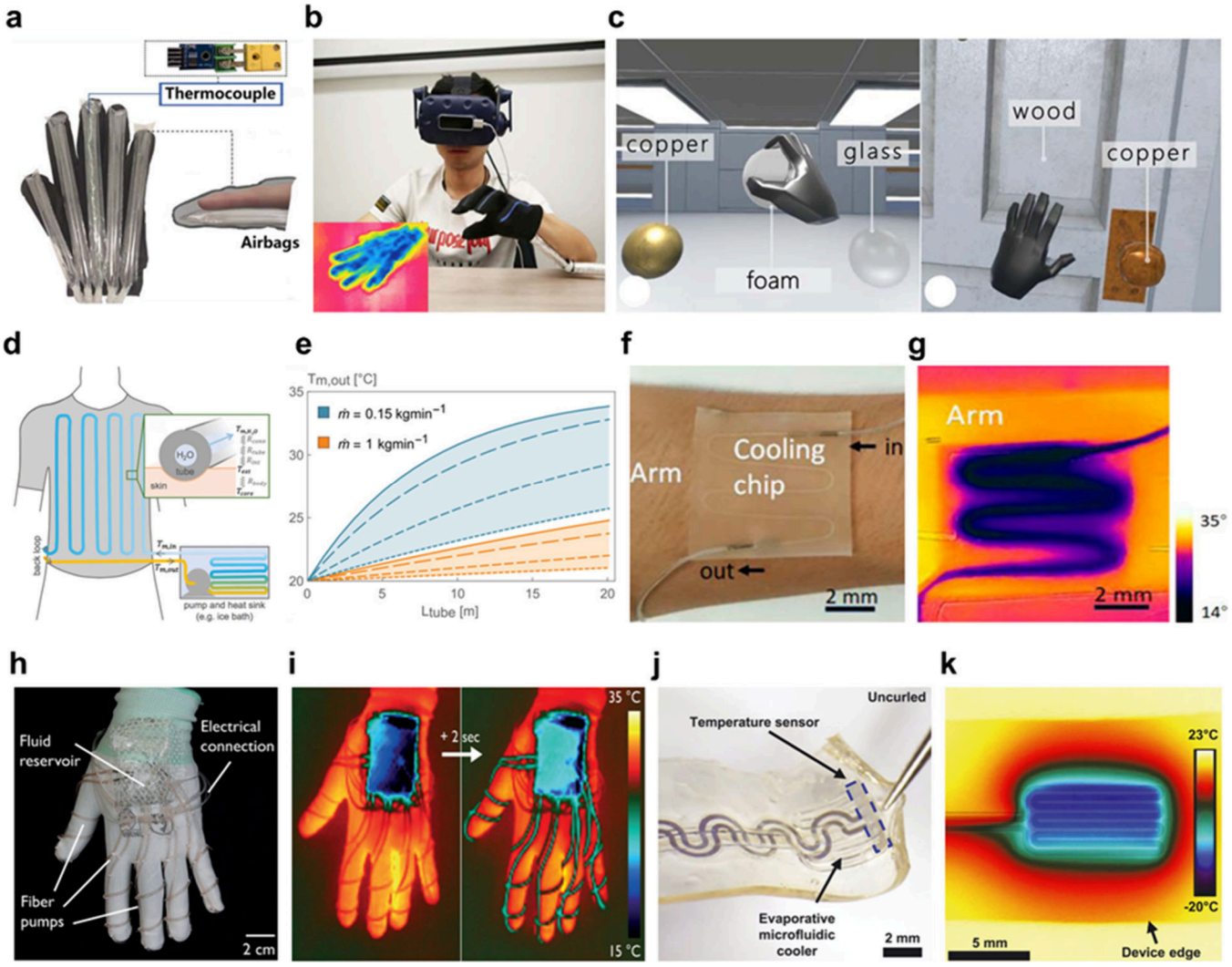


**Figure 15.** Fluidic thermoregulation-based feedback devices. (a) Air-based glove system providing thermal sensations through airbag inflation. (b) A user wearing the glove system with VR glasses. Inset: Thermal sensation through the delivery of hot or cold air to the hand. (c) Implementation of thermal sensations in a VR environment through thermal property analysis: three spheres with different materials (left) and a wood door with a copper handle. Reproduced with permission from ref 331. Copyright 2020 IEEE. (d) Water-based cooling feedback jacket with enhanced thermal conductivity composite tubes. Inset: the thermal interface of the tube between the skin and the fluid (top) and the structure of the pump and heatsink (bottom). (e) Improved cooling performance resulting from composite tubes. Reproduced with permission from ref 330. Copyright 2019 Wiley-VCH. (f) Digital image of the wearable micro cooling chip including fluidic channel (scale bar: 2 mm). (g) IR image of thermal sensation generated by liquid flow (scale bar: 2 mm). Reproduced with permission from ref 327. Copyright 2022 Frontier under CC BY 4.0 license https://creativecommons.org/licenses/by/4.0/. (h) Main components of EHD-powered thermohaptic fiber pump (scale bar: 2 cm). (i) Thermal images showing heat distribution before (left) and after (right) pump activation. Reproduced with permission from ref 328. Copyright 2023 The American Association for the Advancement of Science. (j) Evaporative soft microfluidic cooling system based on a mixture of PFP and $N_2$ gases (scale bar: 2 mm). (k) Thermal image showing the high performance of a system capable of cooling down to −20 °C (scale bar: 5 mm). Reproduced with permission from ref 329. Copyright 2023 The American Association for the Advancement of Science.

enabled more efficient heat removal under both laminar (0.15 kg $min^{-1}$) and turbulent (1 kg $min^{-1}$) flow conditions (Figure 15e). This allowed for the creation of more efficient and lighter cooling systems with shorter tube lengths using composite tubes.

The large volume of the system and the significant diameter of the circulation tubes still pose limitations for miniaturization and high-resolution local thermal sensation implementation in forms like gloves. Thus, transitioning from bulky wearable tube-based XR devices to microchannel-based designs is essential for significantly enhancing user comfort and mobility. Microchannels allow for more compact and lighter forms, reducing the overall weight of the device and seamlessly integrating with wearable technology.[379,380] Additionally, microchannel-based devices provide localized thermal sensations essential for immersive XR experiences. For example, a wearable microchannel cooling chip was developed to facilitate water flow and provide thermal sensations on human skin (Figure 15f).[327] By injecting and circulating cold water at 0 °C using a syringe pump, the wearable microfluidic cooler enabled local cooling on the human arm, effectively lowering the skin surface temperature to 20.3 °C at a flow rate of 1.75 mL $min^{-1}$ (Figure 15g).

In microfluidic wearable XR devices, decreasing the diameter of fluid channels necessitates higher pressure to sustain fluid flow. Furthermore, the increased complexity of channel


https://doi.org/10.1021/acs.chemrev.4c00966
Chem. Rev. 2025, 125, 11567−11665

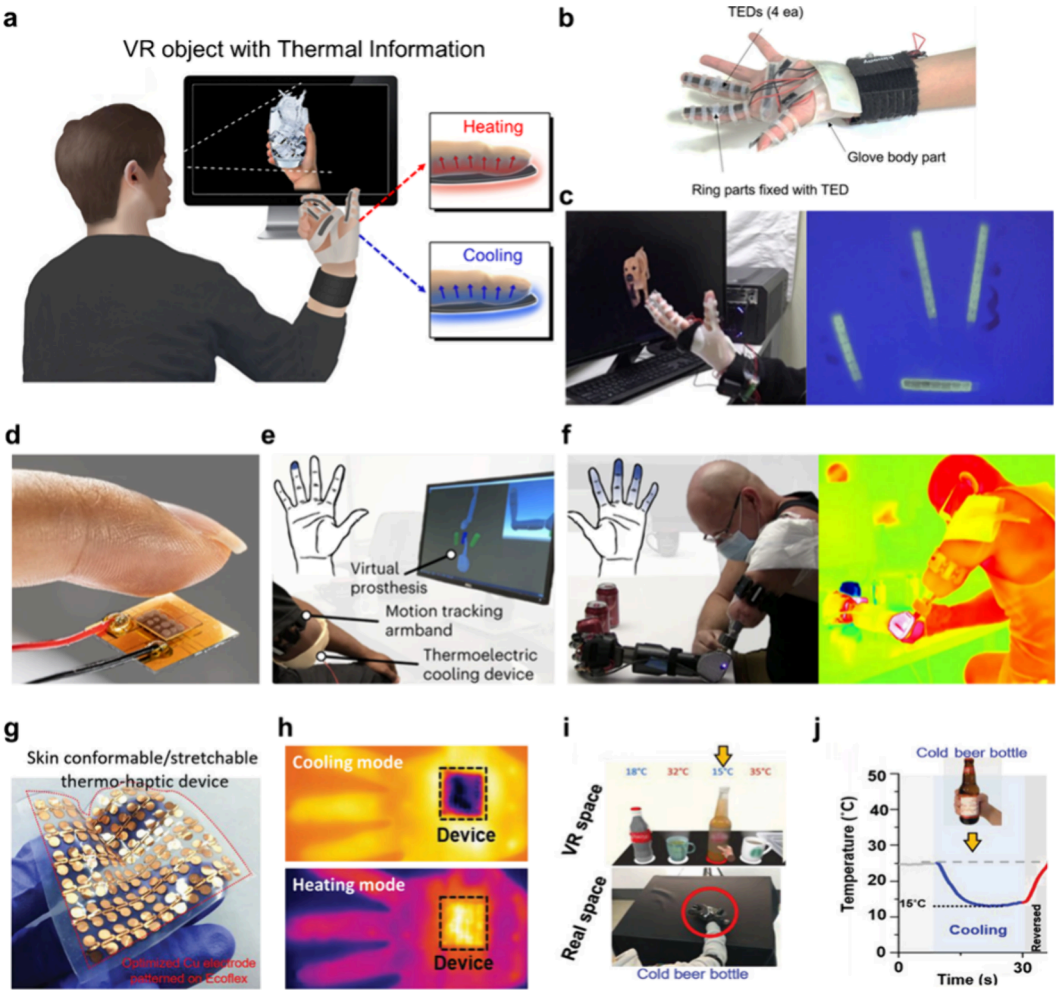


**Figure 16.** Peltier feedback devices. (a) Flexible TE feedback devices. Insets: schematic of heating (top) and cooling (bottom) sensations. (b) Flexible TE glove enabling independent temperature control for each finger. (c) User petting a virtual dog in a VR environment (left) and thermographic image of the thermal sensation generated through the flexible TE glove (right). Reproduced with permission from ref 336. Copyright 2020 Springer Nature under CC BY 4.0 license https://creativecommons.org/licenses/by/4.0/. (d) Thin-film TED with high cooling power density and fast response time. (e) The use of a thin-film TED with the Myo armband in a VR environment to control a virtual modular prosthetic limb and detect cold virtual objects. (f) Digital image of a patient experiencing rapid and intense cooling sensations through the thin-film TED (left) and corresponding thermal image (right). Reproduced with permission from ref 335, Copyright 2023 Springer Nature. (g) Stretchable thermohaptic device based on the Peltier effect. (h) The performance involved both heating and cooling within a single element, rapidly adjusting temperatures between 15 °C (top) and 45 °C (bottom) on the human palm. (i) Scenario of holding a cold beer bottle in a VR space (top) and a user interacting with it in real space through a thermohaptic device (bottom). (j) Temperature profile of thermal feedback provided by the stretchable thermohaptic device when grabbing a cold beer bottle in a VR environment. Reproduced with permission from ref 32. Copyright 2020 Wiley-VCH.

structures raises flow resistance, thereby requiring more energy. Thus, an effective pump system is essential for generating and maintaining flow in fluid-based wearable cooling XR devices. To address this issue, fiber pumps using electrohydrodynamics (EHD) have been reported to induce efficient flow through narrow channels (Figure 15h).[328] These fiber pumps incorporated continuous helical copper electrodes into the walls of polyurethane (PU) tubes. In this device, the dielectric fluid inside the tube was ionized when a DC electric field was applied across the electrodes. Negatively charged ions migrated toward the positive electrode, dragging surrounding fluid molecules and generating circulation. As the ions reached the positive electrode and discharged, they promoted the movement of fluid molecules, resulting in a continuous flow. Thereby, these pumps generated 100 kPa of pressure to produce a flow rate of 55 mL $min^{-1}$, achieving a high-power density of 15 W $kg^{-1}$. From this working mechanism, the cooling liquid rapidly filled the channels, enabling fast-response thermal sensations and demonstrating significant potential as a next-generation wearable XR device (Figure 15i).

Furthermore, to provide extreme temperatures that can be experienced in a VR environment, it is essential to achieve cooling at very low temperatures. However, implementing such low-temperature cooling in wearable technology poses significant challenges. By utilizing the phase change energy during the evaporation of a mixture of perfluoropentane (PFP) and nitrogen gases, a soft microfluidic cooling system achieved exceptionally high cooling performance in a wearable fluid-based device (Figure 15j).[329] The surface temperature of the microfluidic dropped to −20 °C, effectively lowering the temperature of the object to −1.4 °C (Figure 15k). Although this microfluidic system was developed as a nonopioid pain


https://doi.org/10.1021/acs.chemrev.4c00966
Chem. Rev. 2025, 125, 11567−11665

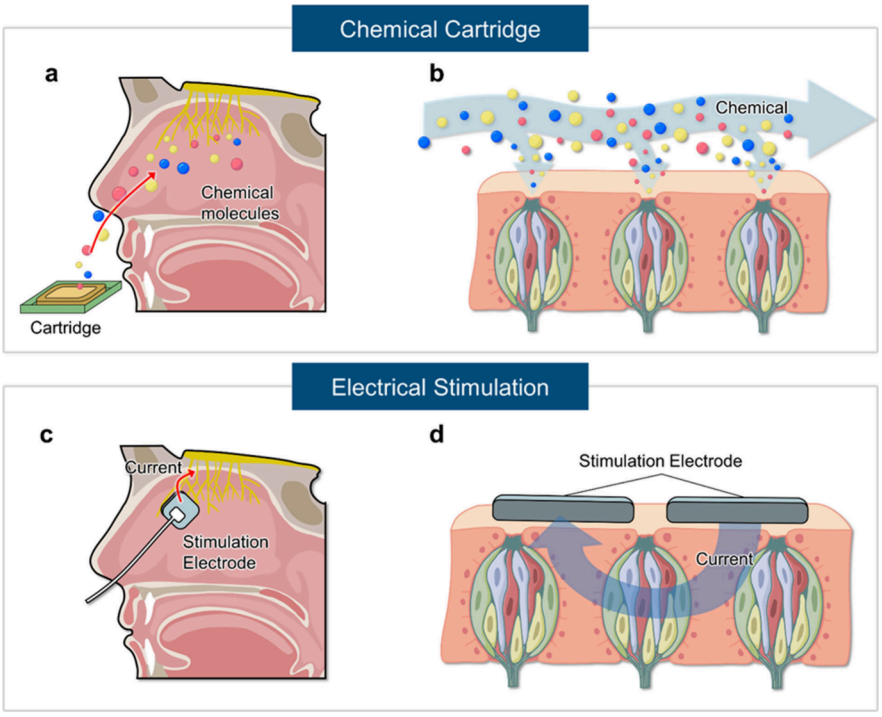


**Figure 17.** Mechanisms for the reconstruction of olfactory and gustatory sensation with XR feedback devices. (a) Mass transfer-based olfactory feedback mechanism with cartridge. (b) Mass transfer-based gustatory feedback mechanism with the cartridge. (c) Electrical stimulation-based olfactory feedback mechanism. (d) Electrical stimulation-based gustatory feedback mechanism. Created with BioRender.com.

management technology, the application of soft, stretchable materials and microfluidic technology for localized temperature control has significant potential to enhance the comfort and user experience of XR devices.

Likewise, wearable flow-based devices demonstrated excellent temperature control capabilities and successfully provided thermal sensations. However, given that the fluid must be actively circulated, further improvements in response times are necessary to increase the accuracy of real-time feedback. Moreover, the energy requirements to maintain consistent fluid flows in complex microchannel structures and the complexity of pump systems to guide flows present significant engineering challenges, potentially limiting scalability and practicality in compact and wearable forms.

*5.1.2.4. Peltier Feedback Devices.* Based on the analysis so far, an ideal thermo-feedback device should actively operate with a fast response time, which can switch heating and cooling modes. Phase change materials can be utilized as cooling feedback devices by leveraging phase transitions such as evaporation.[381−386] However, their slow and passive operation pose limitations as thermo-feedback devices. Electrocaloric cooling-based feedback devices enable active thermal control along with cooling and heating sensations through electrical input.[387−390] Yet, these devices require the actuation of electrocaloric materials and have limitations in delivering continuous and intense thermal sensations.[9]

In contrast, the Peltier effect, similar to Joule heating, facilitates fast-response control of thermal sensations through electrical input.[112,391] Furthermore, the Peltier effect generates both heating and cooling within a single device by simply controlling the direction of the electrical current, making it one of the most promising mechanisms for wearable XR devices. To enhance the performance of the Peltier effect, thermoelectric (TE) materials with fast response times and high figure-of-merit values are essential.[392,393] However, most of these materials are rigid semiconductors such as bismuth telluride ($Bi_2Te_3$),[32,394] antimony telluride ($Sb_2Te_3$),[395,396] and lead telluride (PbTe).[397,398] Therefore, various strategies have been employed to fabricate soft wearable Peltier feedback devices using rigid TE semiconductors.[32,333−336]

Wearable TE devices (TEDs) can be implemented to provide both heating and cooling thermal sensations in VR environments (Figure 16a).[336] The authors employed commercially available pellets with patterned copper electrodes on the PI substrate to fabricate flexible glove-type TED, and each finger was equipped with four TEDs for independent temperature control (Figure 16b). The TEDs were controlled by a microcontroller unit (MCU), demonstrating warming to 25−28 °C when petting a dog in a VR environment (Figure 16c). In addition, a thin-film TED with high cooling power density and fast response time was proposed (Figure 16d).[335] This thin-film TED was able to cool from ambient temperature to 10−20 °C within 3 s. In the VR environment, the thin-film TED was used with the Myo armband to control the virtual modular prosthetic limb and identify cold virtual objects (Figure 16e). Participants experienced rapid and intense cooling sensations through the thin-film TED compared to traditional bulk TED, a difference attributed to the thin-film configuration. The combination of the rapid cooling response of TED and VR technology played a significant role in effective and non-invasive restoration of thermal sensations for patients (Figure 16f).

Improving the thermal interface between the skin and devices is a highly effective method to enhance thermal sensation immersion in virtual environments.[115] From this perspective, designing devices to be stretchable is a promising strategy. For example, the substrate of a device can be made using stretchable materials.[334] However, to fabricate highly


https://doi.org/10.1021/acs.chemrev.4c00966
Chem. Rev. 2025, 125, 11567−11665

stretchable feedback devices, the electrodes must also be stretchable. A highly stretchable TED suitable for integration into VR environments was developed using an elastomeric Ecoflex and a serpentine electrode structure, offering 230% stretchability and excellent skin compatibility (Figure 16g).[32] The authors enhanced the thermal interface of the device by increasing the thermal conductivity of Ecoflex through the incorporation of Ag flakes. Thereby, the device performed both heating and cooling as a single element, quickly adjusting temperatures from 15 to 45 °C on the human palm (Figure 16h). In the VR environment, they simulated scenarios such as touching a cold beer bottle or a hot coffee cup, combined with finger motion-tracking gloves (Figure 16i). For instance, when a user grasps a cold beer bottle in the VR environment, the stretchable TED adjusted the temperature accordingly and rapidly returned to ambient temperature upon the release of the bottle (Figure 16j). Thus, the stretchable TED demonstrated highly realistic thermal sensations, featuring rapid and precise temperature control that is suitable for VR applications.

As discussed in this section, wearable TEDs hold great promise for implementing thermal sensations in wearable XR devices. However, the inherent rigidity of the TE materials used to generate the Peltier effect can restrict wearability in curved areas, such as the fingertips. Furthermore, in such TEDs, effective heat dissipation mechanisms such as heat sinks are essential for maintaining device performance and preventing overheating.[9] Therefore, developing flexible and efficient TE materials[399−401] and efficient thermal management technologies[375,402,403] will create more immersive thermal feedback devices with enhanced wearability.

**5.1.3. Chemohaptic Feedback Devices.** In contrast to mechanical and thermal sensations, which rely on physical contact, olfactory and gustatory sensations mainly operate through the transfer of molecules to the olfactory receptors in the nose and the gustatory receptors in the mouth. These types of sensations convey the atmosphere of the surrounding environment, influencing emotions and memories to create a more immersive and memorable experience.[404−411] However, XR devices that implement artificial feedback must be approached with caution, as the transfer of molecules for olfactory and gustatory sensations is directly linked to human health, with even small quantities of these chemicals posing potential health risks. Consequently, the implementation of olfactory and gustatory feedback in wearable XR devices has been quite limited to date. Common mechanisms for implementing olfactory and gustatory feedback in wearable XR devices include diffusion-based chemical cartridges[412−416] and electrical stimulation.[417−421]

*5.1.3.1. Mechanisms for Chemohaptic Feedback Devices.* Specifically, the chemical cartridge method relies on mass diffusion to generate flavors by releasing chemical molecules from cartridges into the human nose (Figure 17a) or mouth (Figure 17b).[412−416] The operating mechanism involves releasing suitable chemical compounds to replicate desired odors and flavors in precise amounts at the appropriate times. However, unless the chemical compounds are synthesized within the cartridge, the range of available scents and tastes is limited, which restricts operation to a programmable approach. On the other hand, electrical stimulation systems generate odors or flavors by directly stimulating olfactory cells (Figure 17c) or gustatory cells (Figure 17d) using electrodes. By adjusting the intensity, duration, and frequency of the electrical stimulation, various flavors can be replicated using this method alone.[417−421] However, for direct stimulation, the electrodes must be placed close to the receptors in the nose and mouth, potentially causing discomfort and disrupting immersion. Additionally, this approach requires a deep understanding of the complex connections between the olfactory or gustatory systems and the brain.[422,423] Table 7 summarizes the respective strengths and limitations of chemical cartridge and electrical stimulation-based chemohaptic feedback systems. In addition, Table 8 offers a detailed overview of representative implementations, including their material composition, targeted odor and taste sensations, and suitability for integration into soft wearable XR interfaces.

**Table 7. Summary of Advantages and Disadvantages of Chemohaptic Feedback Devices**

| mechanism | advantages | disadvantages |
|---|---|---|
| chemical cartridge | • realistic odor/taste generation<br>• simple diffusion-based operation | • limited scent/flavor variety<br>• bulky form factor/poor wearability |
| electrical stimulation | • chemical-free flavor and odor delivery<br>• precise control of intensity and timing | • limited to salty and sour sensations<br>• discomfort due to electrode placement |

*5.1.3.2. Olfactory Feedback Devices.* In wearable olfactory XR feedback devices, the chemical cartridge is the most conventional approach. Commercially available devices are based on liquid sprayers to disperse fine droplets of perfume and blow them toward the user.[415] However, these systems have the drawback of a fully rigid package design and are bulky.[424−427] To surpass simple odor generation and implement realistic olfactory feedback in XR devices, it is crucial to enable more localized and selective odor production, with the capacity to remotely control multiple distinct scents based on specific requirements.[402]

From this perspective, a flexible, thin, and soft electronic sheet containing an array of millimeter-sized odor generators (OGs), controlled wirelessly, has been developed as an olfactory interface (Figure 18a).[402] The authors miniaturized the OGs by creating a thin layer composed of a mixture of paraffin and liquid perfume, allowing it to generate sufficient odors while occupying minimal space. Additionally, they placed gold traces and a small thermistor on a PI substrate, enabling precise temperature control even in a very compact area. This allowed the heat source to quickly melt the paraffin and release the odor. Furthermore, the cantilever structure, designed with copper coils and magnets, was made highly compact to minimize the size of the device while ensuring quick temperature adjustments for the thermal actuator. As a result of this compact design, the OGs were manufactured in a size of approximately 20 mm, enabling integration into a thin and flexible electronic sheet that could conform to curved surfaces like facial skin (Figure 18b). Moreover, this system enabled wireless data transmission and interaction with a computer, allowing users to receive olfactory feedback in virtual environments. Through this, the system-controlled temperature, scent concentration, and operation time in real-time, enabling users to experience scents that match specific situations in the VR environment (Figure 18c).


https://doi.org/10.1021/acs.chemrev.4c00966
Chem. Rev. 2025, 125, 11567−11665

**Table 8. Summary of Chemohaptic Feedback Devices and Their Characterization for Soft Wearable XR Interfaces**

| | | | target sensation | | | |
|---|---|---|---|---|---|---|
| mechanism | material | stretchability | odor | taste | spatial resolution | ref |
| Chemohaptic Feedback | | | | | | |
| chemical cartridge (mass transfer) | Ag electrode, commercial liquid scents | | squid ink, lime, vanilla, chocolate | salty, sour | | 413 |
| | Au electrode, commercial odorous paraffin wax | flexible | 30 smells (ethanol, pineapple, grape...) | | 1.5 cm | 412 |
| | Au/Cr electrode, ethanol, commercial perfumes | flexible | 32 smells (ethanol, pineapple, grape...) | | 2 cm | 414 |
| | agarose hydrogel, food-grade chemicals | | | sSweet, salty, sour, bitter, umami, fruity... | 5 mm | 437 |
| electrical stimulation | Ag electrode, commercial Peltier module | | | sour, bitter, salty, sweet, minty, spicy | | 420 |
| | Ag electrode, commercial Peltier module | | | sour, bitter, salty | | 417 |
| | Ag electrode, RGB LEDs | | | Sour, bitter, salty | | 431 |
| | Ag electrode, RGB LEDs | | | sour, bitter, salty | | 432 |
| | Ag electrode | | | sour, salty | | 419 |
| | Ag electrode | | 10 smells (chemical, sweet, fragrant...) | | | 418 |

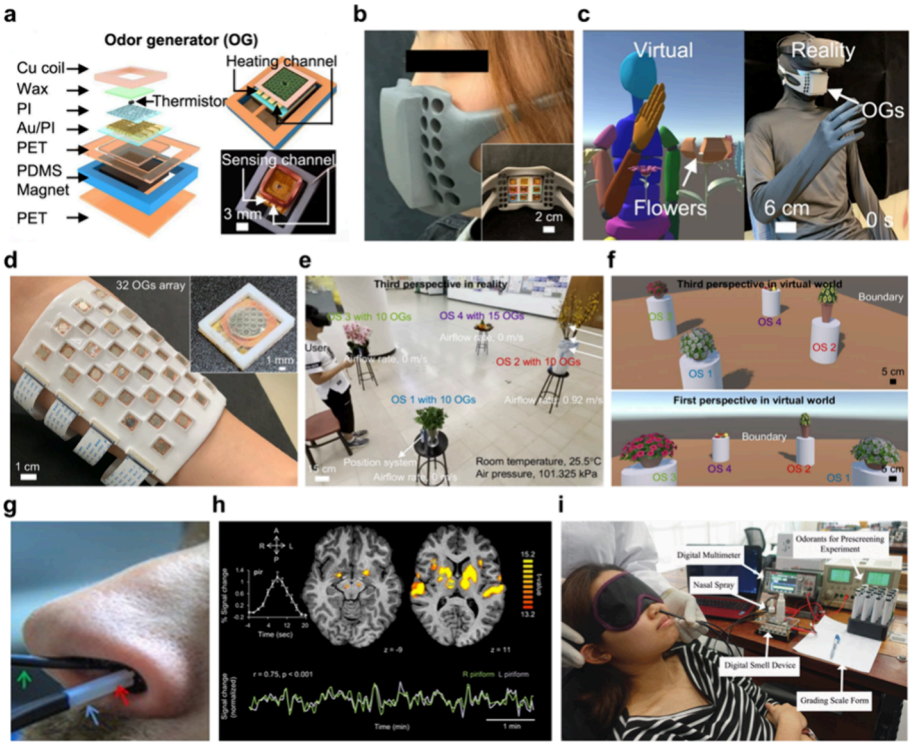


**Figure 18.** Olfactory feedback devices. (a) Schematic illustration of skin-interfaced OG releasing scents through heating. Inset: sensing channel of the OG (scale bar: 3 mm). (b) Prototype of an olfactory feedback mask combined with the OG. Inset: magnified view of the inside of the mask releasing scents through the OG (scale bar: 2 cm). (c) Flowers in VR environment (left) and corresponding scent reproduction in the real world (right) (scale bar: 6 cm). Reproduced with permission from ref 412. Copyright 2024 Springer Nature under CC BY 4.0 license https://creativecommons.org/licenses/by/4.0/. (d) Wearable olfaction interface with 32-OGs array mounted on the human forearm (scale bar: 1 cm). Inset: inner view of the OG (scale bar: 1 mm). (e) VR user wandering around a real environment with four odor sources. (f) The third perspective view (top) and first perspective view (bottom) of a user interacting with four odor sources in the virtual world. Reproduced with permission from ref 414. Copyright 2024 Springer Nature under CC BY 4.0 license https://creativecommons.org/licenses/by/4.0/. (g) Optical image of intranasal electrical stimulator. (h) Group activation map of brain response to olfactory stimulation. Reproduced with permission from ref 423. Copyright 2016 Oxford University Press. (i) Digital image of a digital smell device and artificial odor generation using it. Reproduced with permission from ref 418. Copyright 2023 IEEE under CC BY 4.0 license https://creativecommons.org/licenses/by/4.0/.

Despite the development of such skin-interfaced systems, the feedback latency compromises the real-time experience and could cause the olfactory feedback to seem unnatural. To address this issue, the previous authors developed miniaturized OGs with millisecond-level response times (Figure 18d).[414] The introduction of a solenoid valve structure allowed the


https://doi.org/10.1021/acs.chemrev.4c00966
Chem. Rev. 2025, 125, 11567−11665

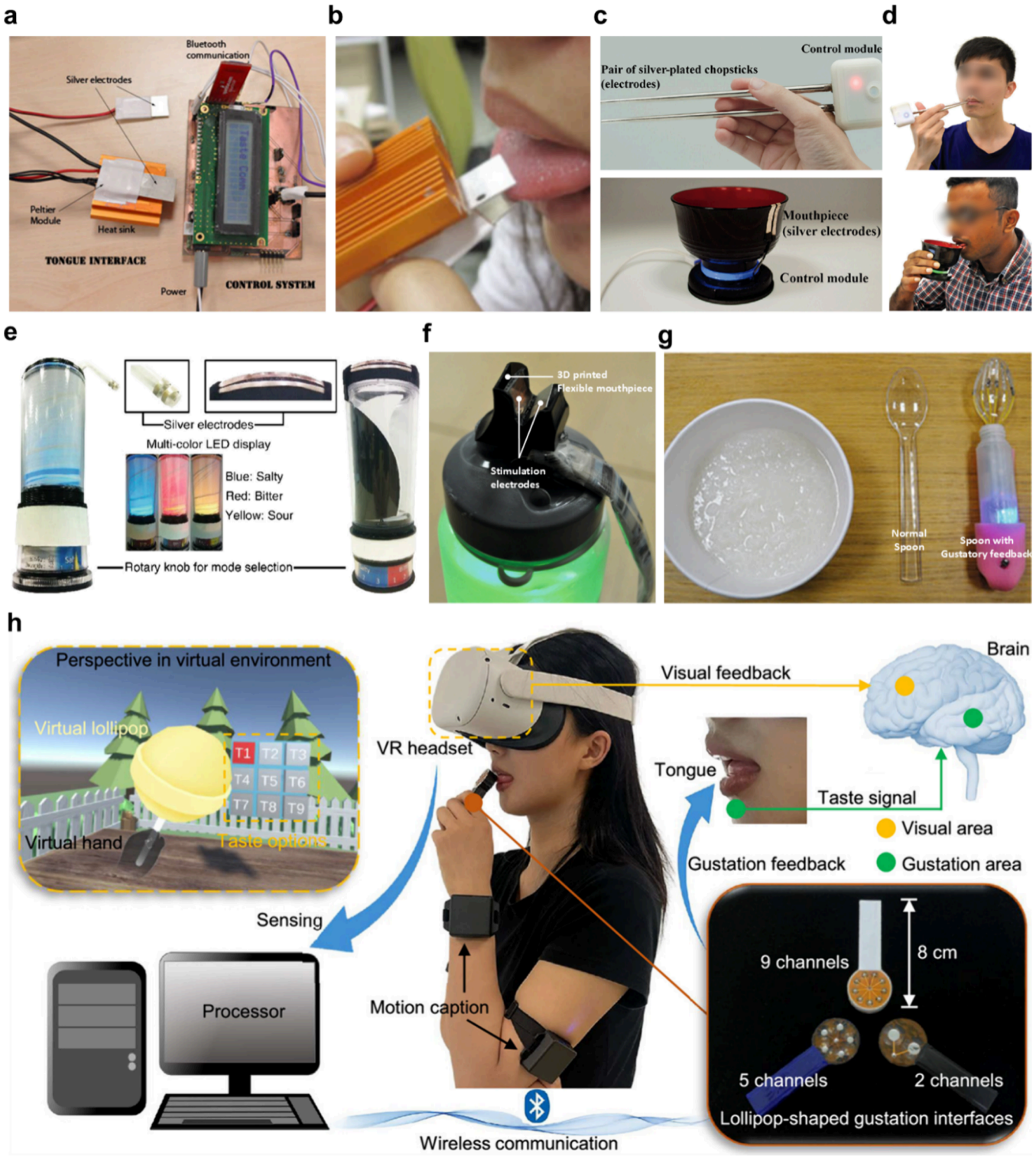


**Figure 19.** Gustatory feedback devices. (a) Gustatory stimulation system that integrates electrical and thermal stimulation using a Peltier module to create diverse artificial tastes. (b) Silver electrodes of the gustatory stimulation system that deliver current to the tongue. Reproduced with permission from ref 417. Copyright 2011 Springer Nature. (c) Chopsticks (top) and a bowl (bottom) equipped with an electrical stimulation system to mimic the eating behavior. (d) Users experiencing taste through current delivered via silver electrodes of chopsticks (top) and bowl (bottom). Reproduced with permission from ref 419. Copyright 2019 Elsevier. (e) Bottle-shaped multimodal digital taste feedback devices combining electrical stimulation and light projection. Reproduced with permission from ref 431. Copyright 2015 Springer Nature. (f) Virtual ingredient feedback bottle designed to be compatible with real beverage. (g) Virtual ingredient feedback spoon designed to integrate or enhance specific flavors in real food. Reproduced with permission from ref 432. Copyright 2016 Springer Nature. (h) Real-time activation of the taste interface triggered by virtual interactions, synchronized with user motion and visual feedback in the VR environment. Reproduced with permission from ref 437. Copyright 2024 Proceeding of the National Academy of Sciences under CC BY-NC-ND 4.0 license https://creativecommons.org/licenses/by/4.0/.



https://doi.org/10.1021/acs.chemrev.4c00966
Chem. Rev. 2025, 125, 11567−11665

system to rapidly open and close the odor-release holes by controlling the magnet through an electromagnetic coil, achieving a response time of approximately 70 ms. Furthermore, the system was integrated with AI algorithms that predict real-time movements and generate odors in advance based on these predictions to minimize the delay during interaction. In the experiment, four odor OGs were placed in the real environment (Figure 18e), with corresponding OGs positioned in the VR space (Figure 18f). Participants navigated within this environment, and the system was able to instantly adjust the olfactory feedback based on position and exploration path. As a result, the system successfully provided fast and seamless olfactory feedback, confirming its ability to minimize delays and deliver a natural experience. In this way, chemical-based wearable olfactory feedback devices have demonstrated excellent odor-generation capabilities and provided rapid feedback.

As mentioned above, electrical stimulation is considered another effective approach for replicating artificial olfactory sensations. Theoretically, this approach overcomes limitations related to the variety of scents and system maintenance, such as the need for refills of chemical compounds. Recent studies have been conducted in which electrodes were attached to the nasal cavity to apply electrical stimulation, followed by research on brain activity and olfactory perception (Figure 18g).[423] The results showed that although electrical stimulation does not directly induce olfactory perception, it can interact with the olfactory pathway and affect brain activity (Figure 18h). While this study did not achieve artificial olfaction through electrical stimulation, other studies have reported that electrical stimulation of the nasal mucosa has successfully induced smells like almond and vanilla.[428] Furthermore, a digital olfactory feedback device that induces artificial olfaction by adjusting the intensity, frequency, and pulse width of the current has been introduced (Figure 18i).[418] This system involved inserting electrodes into the middle nasal concha and applying a current of 1 mA at frequencies of 10 or 70 Hz, successfully eliciting sensations of sweet, fruity, and minty smells. These findings suggest that electrical stimulation can elicit a wide range of olfactory sensations under specific conditions.

Thus, the use of electrical stimulation to create artificial olfaction is promising because it allows for the reproduction of various smells solely through electrical signals, which could be advantageous for structural simplification and miniaturization. However, there are still challenges in understanding the complex correlation between electrical stimulation and brain responses, which complicates the precise control and generation of olfactory sensations.[429] Furthermore, due to the close structural connection of the olfactory nerve to the brain, careful consideration is required when electrically stimulating these nerves. For instance, most participants reported experiencing pain, while some reported visual flashes at higher current and frequency combinations (4 mA and 70 Hz).[418] Therefore, further investigation such as optimizing the parameters of electrical stimulation to minimize discomfort and prevent unintended sensory interference should be conducted in advance to achieve more realistic olfactory sensations.

*5.1.3.3. Gustatory Feedback Devices.* The feedback system for taste operates in a manner similar to that of the olfactory feedback system. However, the ingestion of chemical compounds to create artificial gustatory sensations poses health risks and is ineffective in terms of replication of sensation. Therefore, the electrical stimulation method has been actively employed in the research on gustatory feedback systems.

For example, a digital gustatory stimulation system that combines electrical current stimulation with thermal stimulation via a Peltier module to induce various artificial tastes has been proposed (Figure 19a).[417] This combined system aimed to replicate realistic sensations through the temperature and flavor of food. The electrical stimulation system passed current through the tongue using silver electrodes (Figure 19b). The intensity of the current ranged from 20 to 200 $\mu$A and the frequency could be set between 50 and 1200 Hz. In addition, the thermal stimulation system utilizing a Peltier element adjusted the temperature of the tongue between 20 and 35 °C, inducing cooling or heating sensations to enhance taste perception. By stimulating taste using both electrical and thermal stimulation, participants reported perceiving sour and salty tastes. In the case of thermal stimulation, cooling the tongue led to the sensation of sweetness, while heating produced a mild spicy sensation. Furthermore, a computer-integrated digital taste synthesizer demonstrated that sour taste was perceived across a broad range of currents and frequencies, while salty, spicy, and sweet tastes were modulated by specific electrical and thermal stimuli.[420]

In addition, a novel taste display to enhance gustatory experiences in XR environments has been proposed.[430] The ion electrophoresis technique was utilized to control the five basic tastes and deliver arbitrary flavors to the human tongue. When voltage is applied to the gel in the device, the cations migrate toward the cathode, resulting in a diminished perception of specific flavors. This mechanism enabled the individual suppression of each taste, allowing for the reproduction of arbitrary flavors.

Beyond simply reproducing sensations, there have also been attempts to enhance the level of immersion by incorporating the actions of eating and drinking. In this regard, electric taste utensils such as chopsticks and a soup bowl have been developed to mimic eating behaviors (Figure 19c).[419] When utensils equipped with silver-plated electrodes touch the human tongue during eating, the contact completed the circuit and then allowed current to flow through the tongue (Figure 19d). As a result, a microampere-level current induced a salty taste at lower intensities (40 $\mu$A) and a sour taste at higher intensities (180 $\mu$A). These devices are expected to offer higher immersion in virtual eating scenarios within XR environments, where users can use the utensils as if they were dining.

To create more complex virtual gustatory experiences, other types of stimulation such as colors,[413,431,432] smell,[433] and chewing texture[434] can be added to such gustatory feedback devices. These additional types of stimulation significantly influence taste perception, further enhancing the overall taste experience.[435,436] Considering this effect, a multimodal digital taste system has been proposed, combining electrical stimulation with color projection (Figure 19e).[431] Silver electrodes for electrical stimulation were attached to both the straw and the rim of the tumbler, along with a controller for adjusting taste settings and an LED that changes color based on the selected taste. In order to enhance the taste experience, the authors have proposed a virtual cocktail system that simulates salty, sour, and bitter tastes through electrical stimulation, and projects colors onto the beverage, and releases


https://doi.org/10.1021/acs.chemrev.4c00966
Chem. Rev. 2025, 125, 11567−11665

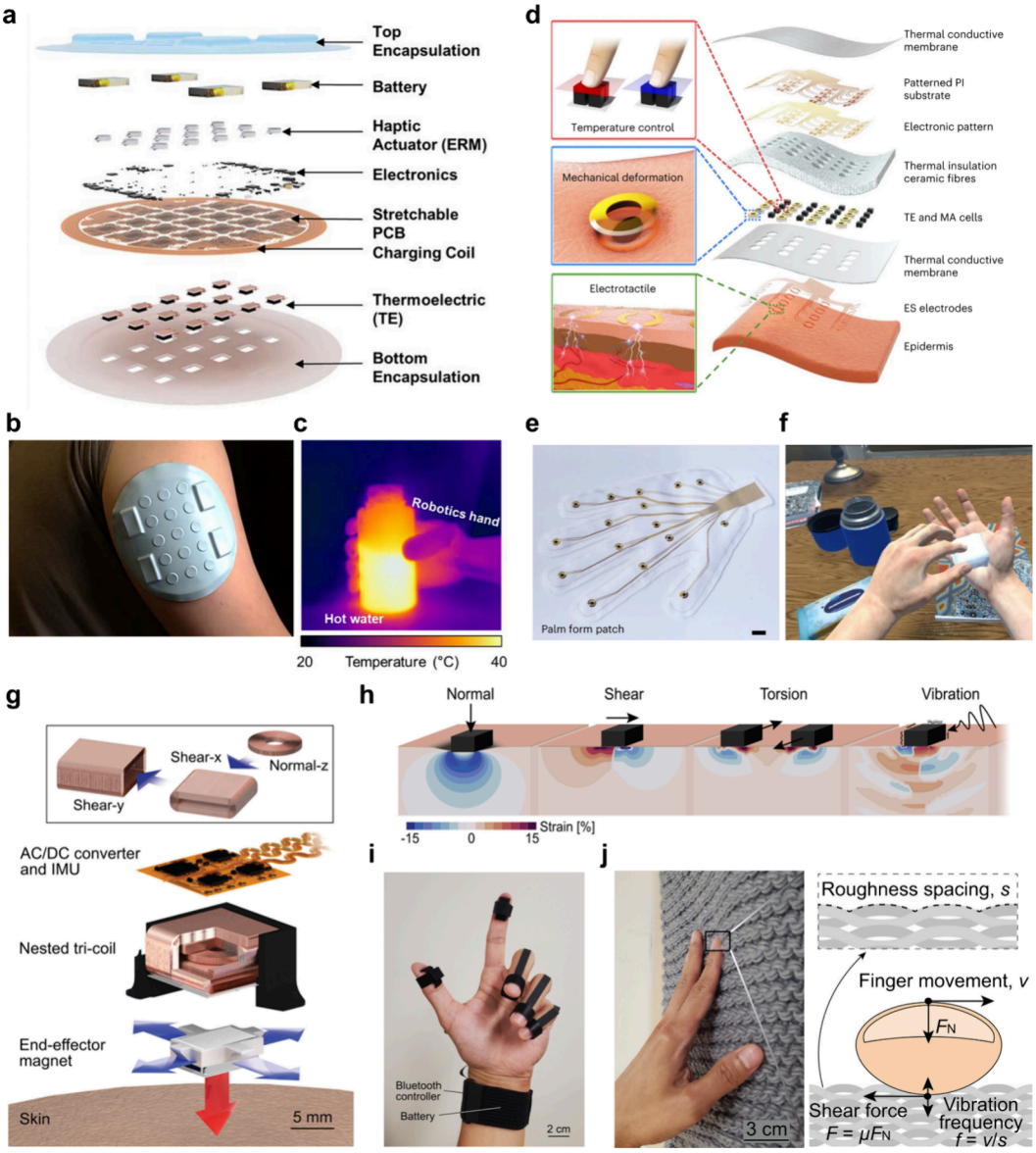


**Figure 20.** Multimodal feedback devices. (a) Schematics of Peltier-vibrotactile multimodal feedback system. (b) Digital image of the wearable multimodal feedback system attached to the arm. (c) Robotic arm remotely grasping a hot water bottle and measuring temperature and pressure information. Reproduced with permission from ref 359. Copyright 2024 Proceeding of the National Academy of Sciences under CC BY-NC-ND 4.0 license https://creativecommons.org/licenses/by/4.0/. (d) System design of a haptic system with three types of actuation units: Peltier (top), vibrotactile (middle), and electrotactile (bottom). (e) Palm-shaped VR interface patch integrated with 16 multimodal haptic units (scale bar: 1 cm). (f) Interaction in a virtual environment using the palm-shaped VR interface patch. Reproduced with permission from ref 33. Copyright 2023 Springer Nature. (g) Schematic of the tricoil actuator with integrated IMU for generating multidirectional haptic output. (h) Simulated strain distributions in the skin under normal, shear, torsion, and vibration stimuli. (i) Photograph of a fingertip-mounted FOM actuator with wireless controller and battery. (j) Physical model relating friction and finger velocity for texture-specific tactile stimulation. Reproduced with permission from ref 34. Copyright 2025 The American Association for the Advancement of Science.

scents using air pumps.[413] Participants reported that when mismatched scents and visual stimuli were combined with electrical taste stimulation, the perceived intensity of the taste was diminished. However, when the taste, scent, and visual stimuli were harmonious, they experienced richer and more complex flavors.

However, it is difficult for such electrical utensils designed for artificial gustatory sensation to convey the texture of food, which is another important aspect of taste perception. It has been proved that the food texture can be simulated through electrical muscle stimulation of the masseter muscle.[434] However, regardless of the quality of texture simulation, it cannot fully replicate the texture of actual food. Due to this limitation, electrical bottles and spoons have been developed to be compatible with real food.[432] The utensils could be used in conjunction with real food to enhance flavor through virtual ingredients. For example, while a person was drinking pure water, electrical stimulation mimicked the flavors of various beverages (Figure 19f). Furthermore, when various flavors were added to white rice, the electrical utensil demonstrated the potential for diverse forms of gustatory feedback that can enhance the flavors of actual food (Figure 19g). Consequently, with the introduction of complementary methods, these


https://doi.org/10.1021/acs.chemrev.4c00966
Chem. Rev. 2025, 125, 11567−11665

technologies are paving the way for enhanced MR-based gustatory experiences.

Unlike conventional electrical methods that stimulate oral tissues directly, the newly introduced lollipop-type gustation interface (LGI) presents a more user-friendly and realistic alternative by employing iontophoresis to release edible flavor compounds (Figure 19h).[437] This technique bypasses the need for current to flow through the human body, instead guiding taste-active molecules from food-grade agarose gels to the tongue surface via electrical fields. As a result, users can perceive genuine taste sensations simply by contacting the device with their tongue, achieving near-instantaneous feedback without discomfort or delay. To create an immersive experience, the LGI is wirelessly connected to external VR hardware and is able to track user motion, enabling interactive scenarios where gustatory stimuli are triggered in sync with hand movements or object selections in the virtual world. Its durable construction, streamlined form factor, and capability to independently control multiple taste modules further support stable and precise operation, expanding the potential of multisensory feedback in XR systems.

**5.1.4. Multimodal Feedback Devices.** So far, various feedback systems that generate different types of artificial sensations have been discussed. While it is possible to mimic certain sensations with a single type of feedback, in reality, even simple touch involves the intertwining of multiple senses, which combine synergistically to produce more complex sensations.[173,179,359,438−440] Therefore, to develop a more immersive XR feedback system that seamlessly emulates real-world sensations, it is essential to incorporate multimodal feedback that stimulates several senses simultaneously. Developing such a device requires integrating the previously discussed feedback mechanisms into a single system and incorporating efficient processing technologies capable of delivering multiple types of feedback in an organized manner.[441−444] Several studies have developed devices that provide multimodal feedback by integrating various mechanisms in a single device.[439,445] However, these devices remain rigid and bulky with significant limitations. To advance the next generation of XR technologies, the development of skin-integrated multimodal feedback devices is indispensable. Since skin-integrated multimodal feedback devices are still in the early stages of research, this chapter will focus on how previously existing feedback devices have been integrated into a single system.

The most common approach is to integrate individual feedback systems into a single device. For example, a wearable multimodal feedback system capable of simultaneously providing both mechanical and thermal sensations has been developed using an ERM vibrotactile motor and TE materials, respectively (Figure 20a).[359] The system integrates ERM actuators and TE materials into vertically stacked arrays along with soft silicone materials, resulting in an interface that can be comfortably mounted on various parts of the body (Figure 20b). A low-power wireless communication system was integrated into this device, enabling the real-time reception of temperature and pressure distribution data transmitted from remote objects (Figure 20c). Then, the collected data was fed back through the thermal and mechanical actuators to provide detailed spatiotemporal sensory feedback by independently controlling components in the device. This strategy allows for the reproduction of complex tactile sensations involving both mechanical and thermal stimuli, making it a valuable method for real-time sensory feedback in XR environments.

Moreover, even when forming similar types of sensations, applying multiple feedback mechanisms simultaneously can be an effective approach to achieve a more realistic sensation by activating different receptors in the skin.[31,177,242,302,440,446,447] For example, by simultaneously combining vibrotactile and electrotactile feedback for mechanical sensations, each mechanism can address aspects that the other cannot fully encompass, thereby facilitating the creation of a new type of sensation that has previously been challenging to implement (Figure 20d).[33] This system used a magnetic actuator to deliver high-frequency stimuli (100−250 Hz) to the skin, simulating the texture of objects. In contrast, the electrotactile actuator delivers low-frequency stimuli (0−100 Hz), simulating pressure or strong forces. Through user studies, the authors demonstrated that each stimulus activates different receptors within the skin and that the combination and intensity of these stimuli affect the mechanical sensation experienced by individuals. Furthermore, the authors integrated TE materials into the devices for thermal sensation along with two mechanical actuators, achieving more complex sensations at the same time. The integrated multimodal actuators were compact, with each unit smaller than 1 $cm^2$, allowing the creation of a VR interface glove patch with a total of 16 haptic units (Figure 20e). Thereby, this system demonstrated its multimodality in VR scenarios that include various textures and temperatures (Figure 20f). The 16 multimodal haptic units allowed for heat map analysis of the temperature distribution and mechanical vibration amplitude on the human palm, providing realistic heat distribution and fine tactile stimuli.

Instead of combining multiple feedback modules, a single, skin-mounted actuator capable of delivering multimodal tactile stimuli has been introduced.[34] The core component, a full freedom-of-motion (FOM) actuator, utilizes a tricoil electromagnetic structure to independently generate normal, shear, torsional, and vibrational forces via programmable Lorentz forces (Figure 20g). Each coil is aligned to produce direction-specific actuation, and by tuning the waveform and amplitude of the driving current, the system can generate well-calibrated static and dynamic tactile cues that match the response profiles of individual skin mechanoreceptors, as characterized in perception threshold studies (Figure 20h). An integrated inertial measurement unit (IMU) enables the actuator to adapt its output in real time based on the motion and hand posture of users in XR environments, while the compact, skin-conformal form factor allows it to be comfortably mounted on wearable platforms (Figure 20i). To simulate realistic surface textures, the system interprets finger motion across different materials using physical models that relate friction-induced shear forces and vibration frequency to material roughness and finger speed (Figure 20j). This enables real-time generation of texture-specific tactile feedback, such as roughness or anisotropic surface feel, using only a single, compact actuator.

Likewise, to simulate real-world sensations, multiple sensations must be delivered simultaneously. However, rather than simply combining mechanisms, enhancing realism in XR devices requires a design that considers the properties of the receptors responsible for eliciting the desired sensations. Therefore, a comprehensive understanding of how humans experience these sensations is essential, as discussed earlier. These multimodal feedback devices, which can deliver various


https://doi.org/10.1021/acs.chemrev.4c00966
Chem. Rev. 2025, 125, 11567−11665

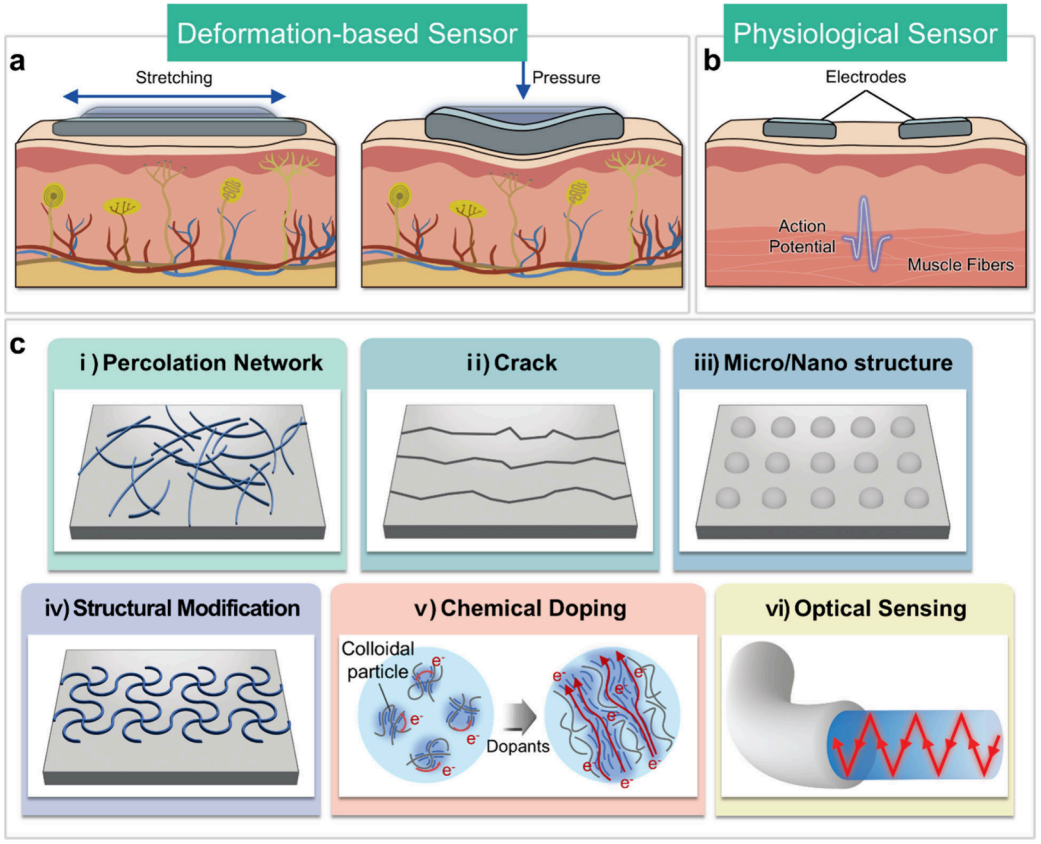


**Figure 21.** Mechanisms for body motion monitoring with wearable XR input devices. (a) Deformation-based sensors to detect strain (left) and pressure (right). (b) Physiological sensors to detect EMG signals. (c) Representative material design strategies for enhancing motion-sensing performance: (i) percolation networks, (ii) crack-based structures, (iii) micro/nano structuring, (iv) structural modification, (v) chemical doping, and (vi) optical sensing mechanisms. Created with BioRender.com.

types of feedback to users from a single device, represent the goal of wearable XR technology. In addition to the integration and efficient communication methods mentioned earlier, the development of wearable XR input devices capable of collecting sensory data for feedback is essential to accurately deliver diverse stimuli to users.

## 5.2. Sensory Input Devices with Working Mechanisms

In wearable XR interfaces, sensory input devices are essential for creating immersive and interactive experiences in AR and VR environments. Sensory input data serves as a bridge that transfers information from the physical world to virtual reality, with wearable sensory input devices being the primary technology facilitating this interaction. These sensing devices play a pivotal role in capturing and interpreting various physiological and environmental signals, which are crucial for providing a responsive and engaging experience. Furthermore, wearable input devices, such as motion sensors, facilitate intuitive and natural interactions with virtual objects and spaces. For example, when a user reaches out to touch a virtual object, the sensors track hand and body movements, translating them into precise actions within the XR environment. Additionally, these wearable sensory input devices continuously monitor human motion or physiological data such as skin temperature, facilitating real-time interactions and enhancing user engagement. Ultimately, the integration of wearable sensors is essential for bridging the gap between the physical and virtual worlds. In this section, we will explore the types of interactions that are possible through these sensors and examine how various sensory data can be translated for XR experiences.

**5.2.1. Human Motion Input Devices and Interpretation Techniques.** *5.2.1.1. Mechanisms and Materials for Mechanical Motion Input Devices.* Recent advancements in electromechanical sensors have evolved beyond merely measuring skin deformation, to a level capturing motions or gestures of specific human body parts. Deformation-based sensors are widely used to detect physical changes such as stretching, bending, and pressure (Figure 21a). The key sensing mechanism involves measuring changes in resistance or capacitance resulting from alterations in length, thickness, volume, or shape. To detect mechanical deformation, advanced materials with tunable electromechanical properties, such as metal NWs,[448−452] LMs,[453−458] piezoelectric materials,[209,214,459] and conducting polymers,[460−462] are employed with distinct mechanisms. Additionally, specific structures that respond to target deformations are applied in sensor design.[463−467] Deformation-based sensors can be categorized as strain gauges or pressure sensors depending on the target deformation. Strain sensors, which conform to the skin and detect even minute deformations, are particularly useful for sensing tactile input or recognizing gestures and facial expressions. Pressure sensors, which measure forces or vertical deformations, are better suited for detecting touch or contact with surfaces.

Physiological sensors are another key technology for human motion recognition or body monitoring, aimed at capturing biometric data such as heart rate, skin temperature, or muscle


https://doi.org/10.1021/acs.chemrev.4c00966
Chem. Rev. 2025, 125, 11567−11665

activity. In this section, we specifically consider electrophysiological sensors that detect and measure bioelectrical signals, primarily used to monitor the electrical activities of nerves, muscles, and the heart. During physiological activity, small electrical signals are generated within biological tissues due to potential differences created by the flow of ions between cells. These signals are typically produced by depolarization and repolarization processes of cell membranes. Electrophysiological input devices detect the signals through electrodes attached to the tissue, then amplify and process them (Figure 21b). Depending on the type of physiological activity, various bioelectrical signals can be captured, including electroencephalograms (EEG), electrocardiograms (ECG), electromyograms (EMG), and electrooculograms (EOG). These devices are valuable for tracking external movements and monitoring internal physiological states, offering a more comprehensive understanding of user engagement and experience.[113,373,468,469] Since the electrophysiological signals are minute and susceptible to noise and environmental interference, reducing unnecessary noise and improving signal quality are critical in sensor development. For example, EMG sensors measure bioelectrical signals generated by muscle contractions, and the sensor measurement must not be disrupted by motion or skin deformation. Reliabley EMG signals allow systems to infer more subtle actions, such as hand gestures or facial motions, without the need for obvious movements.[469]

Reliable acquisition of diverse motion and physiological signals begins with the precise tuning of sensor materials and device architectures. These foundational components must support not only signal transduction, but also stretchability, sensitivity, and stability under dynamic conditions. Recent advances in materials science have addressed these challenges through the engineering of soft, deformable, and highly conductive nanostructures. We delve into how nanoscale architecture, including percolation networks, crack-based sensors, and microstructured geometries, enables the realization of high-performance mechanical motion input devices. We further explore structural design strategies, chemical doping approaches, and optical sensing mechanisms (Figure 21c).

Percolation network is a structure formed when enough conductive nanomaterials are evenly dispersed in a nonconductive material so that electricity can flow through the entire system (Figure 21c-i). These networks are sensitive to small mechanical changes such as stretching or bending, which makes them useful for wearable sensors or other soft electronic components. Percolation networks provide effective strategies for introducing electrical conductivity into soft materials without compromising their mechanical softness. The performance of a percolation network depends on how well the nanomaterials, including CNTs,[470] metal NWs,[146,471] graphene,[472−474] and MXene,[475,476] are shaped and spread out within the soft polymer matrix. Materials with a high aspect ratio, like CNTs and NWs, are especially effective because they form networks at lower concentrations, which helps maintain flexibility and stretchability.[146,470,471] Achieving uniform dispersion, stable interfacial bonding, and optimal filler alignment is important for forming conductive pathways that exhibit metallic electrical conductivity and resilience under mechanical stress. Some recent studies achieve these characteristics by embedding dense NW layers into ultrathin elastomer membranes[146] or by leveraging controlled phase separation to form microstructured conductive domains within soft elastomers.[471] Additionally, printable materials designed to promote the spontaneous formation of percolation pathways through finely entangled nanofillers within an elastic matrix have demonstrated that uniform dispersion can yield high conductivity and mechanical adaptability.[470] This highlights the role of micro- and nanoscale architecture in balancing conductivity with mechanical softness.

Crack-based sensors exploit controlled micro- and nanoscale cracks in a thin conductive film on an elastomeric substrate to achieve ultrahigh gauge factors (Figure 21c-ii). By mimicking the slit organs of spiders, these sensors transduce minute mechanical deformations into large resistance changes.[477] Key design parameters include the prestrain applied during deposition, which determines initial crack density, the thickness and material of the conductive film, and the method of filler incorporation. Increasing prestrain raises crack density, amplifying $\Delta R/R_0$ for small strains, while tuning film thickness sets the threshold at which cracks propagate to maximize the gauge factor without sacrificing durability. Incorporating high-aspect-ratio fillers at crack junctions helps maintain percolation networks as cracks open, sustaining conductivity and enhancing mechanical resilience.[478] Engineering the substrate also presents a promising strategy to improve sensing performance. One study introduced a mechanical meta-substrate with a negative Poisson's ratio to facilitate effective decoupling of crack edges.[479] This meta-substrate enabled orientation-independent crack opening, even under infinitesimal strains, thereby allowing the authors to demonstrate parallel meta-crack circuits to overcome the traditional trade-off between resolution and maximum sensing range.

Micro- and nanostructure engineering has emerged as a crucial strategy to enhance electromechanical sensitivity and minimize signal noise, particularly through the control of interfacial contact area (Figure 21c-iii). By patterning elastomeric dielectrics or electrodes with micro- to nanoscale geometries such as microdomes,[480−482] pyramids,[463,483,484] and wavy ridges,[466] the authors have achieved advanced pressure or touch sensors. For example, a laser-programmed iontronic sensor with gradient micropyramidal structures was developed.[483] These geometries provided stepwise deformation under pressure, ensuring linear responses with high sensitivity. The structure allowed for an ultralow detection limit and ultrahigh pressure resolution. A hierarchical micropyramidal structure can also realize strain-insensitive pressure detection.[463] The integration of stiffening electrodes beneath ionic micropyramids allowed for a stable electrical double layer interface for consistent pressure sensing. This design maintained unaltered contact area between the top electrode and pyramid tip, resulting in high sensitivity and a low detection limit of 0.2 Pa, suitable for skin-mounted systems. The unique stress-focusing geometry, which is hourglass-shaped microstructures inspired by the starfish surface morphology, enhanced the sensitivity and broadened the detection range from sub-kPa up to 100 kPa.[485] To spatially localize strain within sensor arrays, microcage architectures formed by photoreticulated PDMS layers were utilized.[486] This structural confinement minimized mechanical crosstalk, ensuring that localized pressure induced distinct electrical outputs without interference from adjacent pixels.

One of the primary strategies to impart stretchability into intrinsically rigid or brittle electronic materials is the geometric reconfiguration into mechanically compliant architectures (Figure 21c-iv). This structural modification approach allows


https://doi.org/10.1021/acs.chemrev.4c00966
Chem. Rev. 2025, 125, 11567−11665

nonstretchable materials like metals, semiconductors, and oxide films to deform reversibly under mechanical strain without fracture. Representative designs include serpentine[123,487,488] or kirigami-inspired structures,[489−491] which transform in-plane strain into out-of-plane displacement, thereby localizing deformation into low-strain regions. These strategies are grounded in the fundamental mechanics that any material becomes flexible when sufficiently thinned, as bending-induced strain decreases linearly with thickness.[114] Therefore, metal thin films patterned into serpentine structures on elastomeric substrates can stretch and compress elastically. Furthermore, fractal-inspired serpentine designs, characterized by self-similar and hierarchical geometry, can distribute strain uniformly and suppress crack formation. These multiscale architectures enhance both the mechanical reliability and electrical performance of rigid electronic materials, making them particularly valuable for integration with soft materials and curvilinear surfaces.[492] Kirigami structures based on periodic cuts offer engineering elasticity in electronic materials.[490] They enable significant enhancement of stretchability without substantial degradation of electrical conductivity. Importantly, kirigami designs can be applied to strain-insensitive structures, as they maintain conductive pathways across the entire deformation range.

In addition to geometric and structural approaches, electronic performance can also be modulated via chemical doping (Figure 21c-v). Unlike structural reconfiguration, doping directly alters the electronic structure and carrier concentration of the sensing material, enabling enhancements in electrical conductivity, particularly in conducting polymers. Among these, PEDOT:PSS is widely used due to its biocompatibility, solution processability, and favorable electrical characteristics. However, its intrinsic conductivity is relatively low compared to metallic materials, and mechanical properties are often insufficient for stretchable applications. To overcome these limitations, chemical dopants have been introduced to enhance both electrical conductivity and stretchability. One representative approach involves the incorporation of ionic additives, such as sulfonate-based ionic liquids or surfactants.[493] These dopants induce phase separation between PEDOT and PSS domains, promoting the formation of conductive PEDOT-rich networks embedded within a soft matrix. Polar solvents, such as dimethyl sulfoxide (DMSO), have also been reported to enhance the conductivity of PEDOT:PSS by facilitating polymer chain reorganization.[494] Pure PEDOT:PSS hydrogels synthesized via DMSO-assisted annealing achieve interconnected nanofibrillar networks with improved mechanical integrity and electrical pathways for bioelectronic interfaces in wearable systems.[151] Beyond conducting polymers, chemical doping of carbon-based materials, such as graphene, has shown substantial improvements in stability and performance.[495] For instance, macromolecular dopants like perfluorinated polymeric sulfonic acid provide stable p-type doping in graphene films, lowering sheet resistance while preserving high optical transparency and achieving thermal, chemical, and environmental stability.

Optical sensing is another robust strategy for wearable human motion detection, leveraging optical properties such as intensity, wavelength, and refractive index (Figure 21c-vi). Compared to electronic sensors, optical sensing offers immunity to electromagnetic interference, inherent electrical safety, and multiplexing capabilities, making it highly attractive for wearable applications.[496,497]

In optical sensing, fiber Bragg grating (FBG) sensors utilize periodic refractive index modulations inscribed into optical fibers to reflect specific wavelengths of light, where the reflected wavelength shifts in response to mechanical strain or temperature-induced changes in optical path length.[498−500] In FBG sensors, mechanical strain or temperature changes alter the grating period and the effective refractive index of the fiber core due to the photoelastic effect. When the fiber is stretched, the grating period increases and the refractive index decreases, both leading to a shift in the Bragg reflection wavelength, which can be converted into mechanical information. To improve mechanical coupling, strain transfer, and performance, polymer optical fibers have been fabricated by embedding FBGs into soft elastomeric matrices.[501] Furthermore, the fiber core has been doped with photosensitive materials to improve grating inscription fidelity and spectral resolution.[502]

Interferometric sensing mechanisms rely on the detection of changes in optical path length, which occur as coherent light waves recombine and produce interference patterns.[503,504] Interferometric sensors measure phase shifts that result from changes in the optical path length, which is determined by the product of the physical length and the effective refractive index of the optical medium. Mechanical deformation modifies the geometry and induces strain-dependent refractive index variations via the photoelastic effect.[504−506] These changes alter the phase of the propagating light, producing measurable shifts in the resulting interference pattern.[507−509] In this mechanism, photonic-crystal or multicore fibers have been used to enhance modal discrimination and interference clarity.[510] The choice of core and cladding materials, along with precise control over refractive index profiles, enables fine-tuning of optical path sensitivity.[511] Integrating these optical fibers into soft polymer matrices is an effective strategy to enhance their deformability.[512] The polymer matrix efficiently transmits external mechanical stimuli, leading to greater changes in the optical path within the fiber without the need for additional optical modulation structures.

Mechanoluminescent optical fibers sense mechanical deformation by converting applied stress into visible light emission through the mechanoluminescent properties of doped phosphors.[513−515] Mechanical energy is transferred to the phosphor lattice, causing triboluminescence or piezoluminescence, where stress-induced crystal field distortion leads to electron excitation and subsequent visible light emission.[516,517] This self-powered mechanism enables wireless optical sensing without the need for external power or electrical circuitry. To improve its performance, recent designs incorporate mechanoluminescent particles into stretchable elastomeric fibers, where controlled particle dispersion, optimized doping concentration, and core−shell structures have been employed to enhance emission efficiency, repeatability, and mechanical compliance.[518]

Intensity-modulated optical sensing mechanisms operate by detecting variations in transmitted light intensity caused by mechanical deformation, which modulates optical path geometry, absorption, or reflection within the sensor structure.[519−521] This approach does not require coherent light sources or spectral analysis, making it compatible with compact and low-complexity system designs. Deformation-induced changes can lead to microbending losses, modal dispersion, or changes in total internal reflection, thereby modulating light transmission.[522,523] In dye-doped systems, mechanical strain alters the effective absorption path length,


https://doi.org/10.1021/acs.chemrev.4c00966
Chem. Rev. 2025, 125, 11567−11665

resulting in intensity variations governed by the Beer−Lambert law.[524] Performance can be further improved through material design strategies, including refractive index contrast tuning, optimized dye distribution, and multicore or patterned elastomeric geometries for enhanced sensitivity and mode isolation.[525]

Monitoring human motion within XR systems is a complex task requiring the integration of advanced sensor technologies and data interpretation methods to identify motions, gestures, and facial expressions that convey user intent. Converting basic data, such as strain and bending, obtained from sensors into higher-dimensional information, such as motion, object, and texture recognition, requires the capabilities of AI techniques.[526−529] In this section, we provide a brief introduction to the AI algorithms employed in the information transformation process, with a more detailed discussion to follow in the subsequent section. By capturing inputs such as gestures, facial expressions, and physiological data, XR systems can deliver more intuitive and immersive interactions. Ongoing advancements in sensory input technology and processing algorithms will continue to improve the accuracy, responsiveness, and comfort of these systems, driving the next generation of XR experiences. In this section, we focus on the input devices commonly used in XR applications, such as touch, hand or arm gestures, and facial expressions. By accurately tracking these specific inputs, XR systems can better interpret user actions and intentions, delivering outputs that correspond to real-world actions. The systems can modify the VR environment to react to the intended actions, thereby enhancing the sense of presence and realism in the XR experience. Table 9 summarizes the sensing mechanisms and performance trade-offs of representative electromechanical sensors, including deformation-based, physiological, and optical types. Table 10 complements this by providing detailed specifications of mechanical input devices tailored for XR applications, such as those capturing touch, gestures, and facial expressions.

**Table 9. Summary of Advantages and Disadvantages of Electromechanical Sensors for Monitoring Body Motion**

| mechanism | advantages | disadvantages |
|---|---|---|
| deformation-based sensors | • responsive to various mechanical stimuli | • signal interference under simultaneous strain and pressure |
| | • high mechanical conformability for skin | • nonlinearity and hysteresis during repeated deformation |
| | • high sensitivity and fast response time | • performance degradation due to fatigue and repeated use |
| physiological sensor | • accurate bioelectrical signal detection | • sensitive to motion artifacts |
| | • soft, stretchable, skin-like interface | • signal susceptibility to noise |
| | • compatible with multifunctional systems | • need for signal amplification and processing |
| optical sensor | • noncontact detection for mechanical interference | • susceptible to ambient light interference |
| | • immune to electromagnetic interference | • bulky and complex interrogation systems |
| | • fast response and high-spatial temporal resolution | • complex fabrication and high cost |

*5.2.1.2. Touch Sensing.* Touch sensing is one of the fundamental methods for human motion monitoring or recognition, as people often "touch" something to express intent subtly. Tactile input devices detecting light touch, contact, and even pressure or force are used in interactive devices such as XR haptic systems.[530−539] For example, one study demonstrated interactive virtual applications using glove-type devices integrated with tactile sensors (Figure 22a).[464] To enhance force detection sensitivity and range, the authors combined electrodes composed of carbon fabric with a layered microstructure and Ag NW networks with a porous microstructure. In the layered structure, compression expanded the electric contact area, rapidly reducing resistance, while in the porous structure, compression increased the electric contact points, slowly decreasing resistance. Due to the differences in electromechanical characteristics, sensors with a layered structure exhibited high sensitivity but reached signal saturation at a low force of 0.5 N. Conversely, sensors with a porous structure showed less resistance change in response to external force, resulting in lower sensitivity and wider detection range. By combining both structures, the group developed tactile sensors capable of measuring forces up to 6.5 N with high sensitivity. These sensors detected contact and quantified the intensity of touch (Figure 22b). As a result, the authors demonstrated interactive applications using a tactile input device, providing appropriate sound pitch and levels for the virtual piano according to the pressed positions and applied force (Figure 22c).

Pyramid-shaped microstructures can also be applied in tactile sensors because the structures deform under pressure, altering the contact area depending on the degree of compression. Based on this principle, the development of tactile sensors using a magnetic film with pyramid bumps has been reported (Figure 22d).[465] The sensors primarily consisted of a magnetic film with pyramid bumps on one side and a giant magnetoresistive (GMR) film placed at a distance in the direction of the bumps. Notably, this configuration enabled both tactile interaction through direct contact and touchless interaction by detecting changes in the magnetic field caused by approaching objects. As an external magnetic object approached, the magnetic field sensed by the GMR film changed, leading to variations in the output signal. Upon contact, the pyramid bumps touched the GMR film, causing further changes in the output signal due to the deformation of the structures by applied pressure. By classifying these different signal patterns, the authors achieved a tactile sensor capable of both touchless and tactile sensing. They demonstrated an XR interface using the sensors to explore virtual options with touchless swipes and select the option via direct touch (Figure 22e). Another touch input device that measured three-dimensional (3D) information, including position and pressure, using a wavy multiscale structure has been developed (Figure 22f).[466] The bottom electrode of the device was composed of laser-sintered Ag NPs with a laser-induced wavy structure, while the top electrode consisted of Ag NW networks with a porous structure. Owing to the unique structures of these electrodes, the touch sensors could collect both 2D position and depth information, while maintaining transparency. As a result, the wearable touch input device demonstrated its capability to wirelessly transmit shapes drawn on the skin into virtual spaces (Figure 22g).

In analyzing touch motion, it is crucial to measure both static and dynamic tactile signals, which correspond to a wide range of pressure at low frequencies and relatively low pressure at high frequencies, respectively. For example, a wearable


https://doi.org/10.1021/acs.chemrev.4c00966
Chem. Rev. 2025, 125, 11567−11665

Table 10. Summary of Human Motion and Body Monitoring with Various Mechanical Input Devices and Their Characteristics

| | | | | performance | | | | |
|---|---|---|---|---|---|---|---|---|
| type | mechanism | material | stretchability | force (pressure) | strain | frequency | spatial resolution | ref |
| Human Motion Monitoring | | | | | | | | |
| touch | pressure | PU scaffold, Ag NW, carbon fabric | flexible | 6.5 N | | 0.5−4 Hz | 20 mm | 464 |
| | | Py/Cu, Ta, PI films | flexible | 0.24−11.6 kPa | | | 4 mm | 465 |
| | | Ag NW, Ag NP | flexible | 10 kPa | | | 5 mm | 466 |
| | | EGaIn, Ecoflex | stretchable, flexible | 0.8 Pa | | | 7 mm | 467 |
| | vibration | PI, Ti/Au, PVDF-TrFE, PDMS | flexible | 3−80 kPa | | | 1.8 mm | 222 |
| | | rGO, $BaTiO_3$, PDMS | stretchable | 0.1−100 kPa | | 1−1000 Hz | 10 mm | 447 |
| gesture | strain | CFPC, TPU | stretchable | 0−100 kPa | 0−0.12 mm | | 5−20 mm | 544 |
| | | PI, Ag NP | stretchable (15%) | | 0−15% | 40 Hz | 0.4 mm | 542 |
| | | PU, Au, Ag | stretchable (155%) | | 0−10% | 0.2−2 Hz | 1 mm | 559 |
| | | Ag/Au, PU | stretchable | | 0−15% | | | 122 |
| | EMG | PET, Ag ink | flexible | | | 20 Hz | 14.3 mm | 197 |
| | | ecoflex, conductive textile | flexible | | | | 4.2 mm | 553 |
| | pressure | PU, Au, Ag | stretchable (155%) | 1.7−1200 kPa | | | 1 mm | 559 |
| facial expression | strain | PEDOT:PSS, PDMS, AuNP | stretchable (100%) | | 0−100% | 0−300 Hz | 1 cm | 574 |
| | | AlN, PDMS | stretchable | 0−100 kPa | 0.5−15% | 100 Hz | 10 mm | 575 |
| | | PI, Au/Cr, Cu | stretchable (30%) | | 0−30% | | 900 $\mu$m | 568 |

tactile sensing device has been proposed that recognizes both static and dynamic tactile signals in a single device configuration (Figure 22h).[467] The sensors consisted of arch-shaped top electrodes and flat bottom electrodes, which were composed of conductive fabric coated with LM and encapsulated in dielectric elastomer. When slow touch or pressure was applied, the arch-shaped microstructures deformed, altering the distance and contact area between the electrodes, which led to a change in capacitance. This capacitive mechanism was suitable for measuring static tactile distribution. On the other hand, when rapid and repetitive pressure was applied, contact between the elastomers surrounding the electrodes generated output voltage. This triboelectric mechanism was appropriate for detecting dynamic tactile signals. The authors demonstrated the ability to display real-world tactile inputs in virtual spaces (Figure 22i). Furthermore, they successfully distinguished handwriting containing both static and dynamic tactile signals.

Piezoelectric materials are effective for detecting dynamic pressure due to its fast response speed and capability to measure vibrating pressure signals across a wide frequency range.[222] Using poly(vinylidene fluoride-trifluoroethylene) (PVDF-TrFE), the dynamic tactile sensors have been designed, exhibiting a response time of less than 300 $\mu$s, which is shorter than the human tactile response time (Figure 22j). The sensory input devices could detect frequencies ranging from 1 Hz to 1 kHz, allowing for precise detection of tactile stimulation. To enable both static and dynamic pressure detection, pyramid-shaped microstructure electrodes were also integrated into the input devices. The sensor array consisted of microstructure array electrodes for static signal acquisition and dry-etched piezoelectric polymers for dynamic signal detection, enabling accurate interpretation of surface shapes and textures using static and dynamic tactile signals, respectively. The tactile input devices attached to a fingertip collected texture information from various fabrics and spatial information by touching objects of specific shapes, which was then applied to interaction with virtual environments (Figure 22k).

Furthermore, a tactile input device mimicking the human tactile sensing mechanism has also been developed.[447] As discussed above, humans distinguish between static and dynamic tactile information through the skin based on SA and RA receptors, respectively. SA receptors generate output signals in response to sustained pressure stimuli, making them suitable for recognizing static pressure. In contrast, RA receptors produce output signals only at the initial and final points of pressure stimuli, favoring dynamic pressure detection. Inspired by this mechanism, composites that recognized both static and dynamic tactile information were developed by mixing reduced graphene oxide (rGO) microsheets with piezoelectric $BaTiO_3$ ceramic NPs in a polymer matrix (Figure 22l). The piezoresistive rGO sheet-enriched sensors followed percolation theory, where deformation-induced resistance changes were continuously observed, similar to SA receptors. On the other hand, piezoelectric $BaTiO_3$ NP-dominated sensors generated localized voltage through the piezoelectric effect, with minimal resistance changes to overall structural deformations, resembling RA receptors. The integration of both sensors into a single tactile input device facilitated the interpretation of tactile stimuli according to their respective roles. The integrated sensor demonstrated the acquisition of texture information from unknown fabrics, similar to the tactile sensory systems of humans (Figure 22m).

*5.2.1.3. Gesture Recognition.* Gesture recognition is a crucial element of wearable XR devices in facilitating intuitive interactions within virtual environments, as numerous interactions are grounded in physical actions.[540] By leveraging this technology, touchless interfaces can be achieved, enabling users to manipulate virtual objects without physically touching any devices. This allows for more intuitive interaction with


https://doi.org/10.1021/acs.chemrev.4c00966
Chem. Rev. 2025, 125, 11567−11665

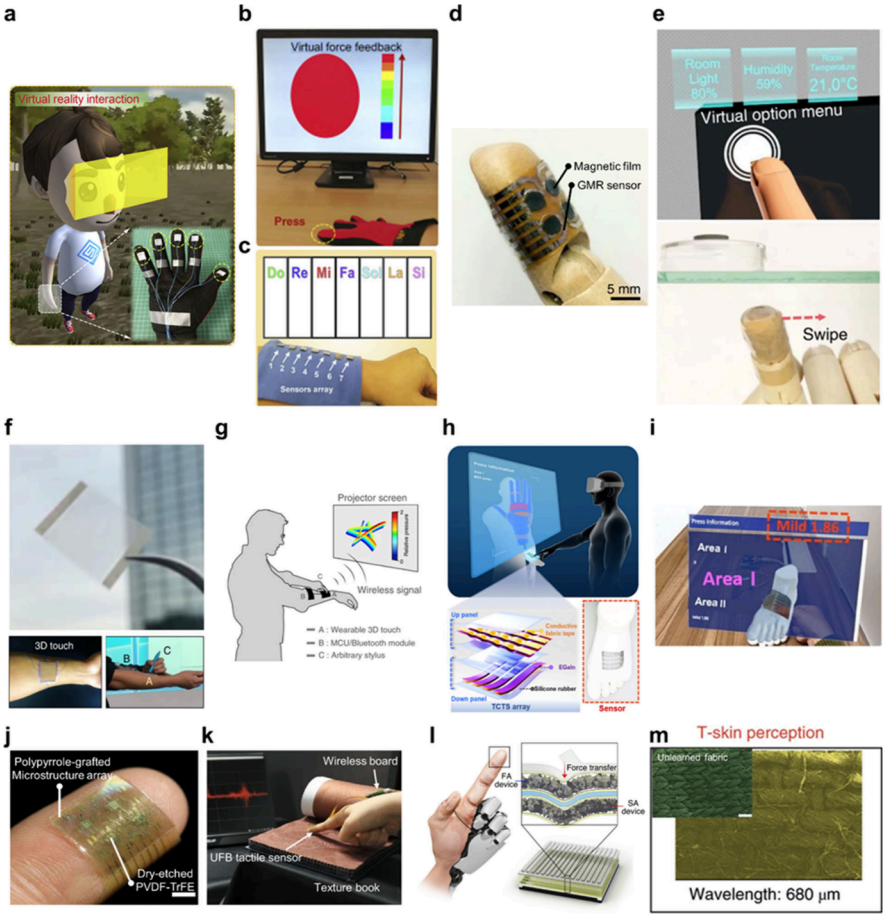


**Figure 22.** Touch sensing devices. (a) Interactive virtual application through a haptic interface integrated with tactile sensors. Inset: the haptic interface worn on the hand. (b) Virtual force feedback represented by color changes according to the detected pressing force. (c) Demonstration of virtual piano that provides sound with varying pitch and levels based on the sensing signals. Reproduced with permission from ref 464. Copyright 2019 Elsevier. (d) Tactile sensors composed of a magnetic film with a bump structure and a GMR film (scale bar: 5 mm). (e) Graphic (top) and optical (bottom) images of an AR scenario where the user explores and selects a virtual option menu. Reproduced with permission from ref 465. Copyright 2019 Springer Nature under CC BY 4.0 license https://creativecommons.org/licenses/by/4.0/. (f) Transparent touch sensor for collecting 3D information (top). Images of the touch sensor attached to the arm (bottom left) and the device being used to draw (bottom right). (g) Schematic illustration showing wireless transmission of shapes drawn on the skin. Reproduced with permission from ref 466. Copyright 2019 Springer Nature under CC BY 4.0 license https://creativecommons.org/licenses/by/4.0/. (h) Bimodal touch sensor that recognizes both static and dynamic tactile signals. (i) Schematic of MR application displaying the pressed area and the pressure intensity. Reproduced with permission from ref 467. Copyright 2024 American Chemical Society under CC BY 4.0 license https://creativecommons.org/licenses/by/4.0/. (j) Tactile sensory system based on resistive and piezoelectric sensors for acquiring static and dynamic pressure information, respectively (scale bar: 2 mm). (k) Digital image of the tactile sensory system collecting texture information from various fabrics. Reproduced with permission from ref 222. Copyright 2022 Springer Nature. (l) Touch sensing device mimicking SA and RA mechanoreceptors. Inset: schematic showing the force sensing mechanism of the device. (m) Classification result of unlearned fabric using texture information obtained through the sensing device. Inset: the image of the unlearned fabric. Reproduced with permission from ref 447. Copyright 2021 Springer Nature.

digital spaces compared to traditional interfaces like a mouse, keyboard, or joystick. In this way, gesture recognition significantly enhances the immersion and user experience in XR environments, offering more seamless and engaging interactions.

The most accessible approach to recognizing various gestures is to capture and analyze strain signals induced by body motions.[529,541−543] For instance, a strain sensor-based gesture recognition system that classified various hand gestures, such as fist clenching, pinching, and palm spreading, has been reported (Figure 23a).[544] The strain sensors were composed of composites in which carbon fiber strands were aligned in one direction within a polymer matrix. Due to the aligned carbon fibers, the composites exhibited low resistance in the horizontal direction and high resistance in the vertical direction on a 2D plane. The authors fabricated these composites into meander patterns with vertical microscale cuts and attached them to a prestrained elastomer substrate. The elastic force of the substrate compressed the meander path, connecting the electrical path horizontally and resulting in overall low resistance. When external force induced stretching, the horizontal contact decreased, increasing the resistance. Based on this mechanism, the strain sensors exhibited high sensitivity with gauge factors exceeding 80,000 and yielded a linear resistance response to stretching. Moreover, they were insensitive to unintended deformations such as bending or twisting. These properties allowed for the clear detection of targeted signals when recognizing discrete and continuous hand gestures. Consequently, the authors demonstrated hand motion-based user interfaces using four


https://doi.org/10.1021/acs.chemrev.4c00966
Chem. Rev. 2025, 125, 11567−11665


**Figure 23.** Gesture recognition systems. (a) Strain-based gesture recognition system that measures muscle deformation to classify various hand gestures. Inset: schematic illustration of the system in operation (left) and magnified image showing a strain sensor of the system (right). Reproduced with permission from ref 544. Copyright 2020 Springer Nature. (b) EMG-based gesture recognition system worn on the forearm with 64-channel soft electrodes. Reproduced with permission from ref 197. Copyright 2020 Springer Nature. (c) Skin-integrated strain sensor based on controlled crack structure (scale bar: 1 mm). (d) Estimation of finger movements based on subtle deformations of wrist skin. Reproduced with permission from ref 542. Copyright 2020 Springer Nature under CC BY 4.0 license https://creativecommons.org/licenses/by/4.0/. (e) Communication scenario where sign language in the real world is converted into text and audio in a VR environment through triboelectric textile sensors. Inset: exploded view of textile sensors detecting strain and touch on the fingers for gesture recognition. (f) VR interaction between a speech-impaired user and a nondisabled user, enabled by real-time sign language recognition and audiovisual translation. Reproduced with permission from ref 553. Copyright 2021 Springer Nature under CC BY 4.0 license https://creativecommons.org/licenses/by/4.0/. (g) Smart gloves integrated with yarn-based sensors measuring the bending angle and grasping pressure of the fingers. (h) Finger movements in the VR


https://doi.org/10.1021/acs.chemrev.4c00966
Chem. Rev. 2025, 125, 11567−11665

**Figure** 23. continued

environment corresponding to real-world grasping actions (inset), showing accurate motion tracking and rendering. Reproduced with permission from ref 559. Copyright 2024 Springer Nature. (i) Soft glove with stretchable lightguide sensors for real-time joint and force sensing. (j) Real-time multijoint bending reconstruction in VR environment via optical sensing. Reproduced with permission from ref 525. Copyright 2020 The American Association for the Advancement of Science. (k) Digital image and schematic illustration of a substrate-less nanomesh sensor used to capture proprioceptive information from the fingers. (l) Demonstration of imaginary keyboard typing with bihand motion detected by nanomesh sensors. (m) Recognition of six objects through hand motion during rubbing using nanomesh sensors and AI technology. Reproduced with permission from ref 122. Copyright 2022 Springer Nature.

sensors attached to the arm to replace the functions of a conventional mouse.

In addition, EMG signals generated by muscle activity are valuable input data for gesture classification.[373,545−547] However, compared to strain or pressure signals, EMG signals require higher sampling rates and are more vulnerable to noise, making it challenging to directly interpret the signals. Because of this, many studies have incorporated AI techniques for EMG-based gesture recognition.[548−550] For example, with the assistance of adaptive learning methods, hand gestures were successfully classified using wearable EMG sensors on the human forearm (Figure 23b).[197] Equipped with computational and wireless communication modules, the soft sensors with 64-channel electrodes wirelessly collected EMG signals for conversion into gestures. The adaptive algorithm enabled real-time learning, inference, and model updates within the compact module, classifying 21 hand gestures, including 12 single-degree, 8 multidegree motions, and a default state.

Increasing the number of sensors is inefficient in terms of data processing when interpreting human motion using raw data. However, it has been shown that machine-learned soft sensors can accurately distinguish hand motions with fewer sensors, enhancing system efficiency.[542] In this study, a laser-induced crack on a sintered Ag NP-based sensor detected extremely subtle deformations by providing highly sensitive performance (Figure 23c). By employing the crack sensor on the wrist, fine deformations of the skin induced by finger movements could be detected. Remarkably, the authors were able to classify multiple motions generated by the movement of all five fingers using only a single sensor (Figure 23d). This approach highlights the potential for rapid and efficient gesture classification using simple sensor input.

Based on gesture recognition techniques, various studies on hand-based sign language prediction have been reported.[551−553] Analyzing the hand motions associated with sign languages is crucial, as they comprise about 40% of daily sign language movements.[554] More than half of hand motions are influenced by finger bending and the rest are affected by wrist movement, fingertip touch, and interaction with the palm. Considering the characteristic motions, a smart glove was developed by integrating triboelectric sensors with a sandwiched nitrile layer between conductive textiles that detected strain and touch in the fingers (Figure 23e).[553] From a deep learning perspective, the authors employed both nonsegmentation and segmentation approaches to classify various words and sentences. While the nonsegmentation method accurately estimated learned data, it struggled with unseen data, whereas the segmentation method allowed for real-time responses to new words and sentences. By combining both approaches, the study achieved barrier-free communication at the sentence level using sign language in a virtual space (Figure 23f).

Similar to the textile sensor, yarn-based sensors are well-suited for integration into conventional clothing or gloves for recognition applications.[555−559] For example, yarn-based sensors composed of an elastic yarn core helically wrapped with metal-coated nanofibers have been integrated into gloves that were compatible with conventional sewing techniques.[559] These gloves enabled the measurement of finger joint angles through bending, while additional sensors sewn at the bottom of the fingertips detected grasp pressure through pressing (Figure 23g). This versatile design enabled the gloves to capture complex hand motions, even facilitating object recognition during interactions (Figure 23h). Its ability to detect multiple types of deformations in a simple configuration supported wearable XR applications that required precise gesture recognition.

Gesture recognition can be achieved by detecting mechanical deformation through optical changes, such as variations in light intensity or RGB signal patterns, using stretchable lightguide-based sensors that can be spatially distributed across multiple regions (Figure 23i).[525] The sensors consist of dual-core elastomeric waveguides with spatially patterned chromatic dyes, where mechanical deformation modulates optical path geometry and absorption, leading to distinguishable changes in RGB signal patterns. A vector-sum model, derived from chromaticity and intensity responses in the CIE color space, was used to decouple and reconstruct individual joint angles across three finger joints using a single sensor. External pressing was independently detected by monitoring the normalized intensity in the clear core, and its location and magnitude were inferred from hue shifts. This integrated system demonstrated real-time and multilocation sensing capabilities, highlighting its suitability for XR interface applications (Figure 23j). Another stretchable optical sensing platform was developed by embedding elastomeric lightguides into a soft fingertip structure, enabling curvature detection through deformation-induced modulation of light transmission.[560] To complement the optical response, ionic liquid-based microfluidic channels were incorporated to measure strain via impedance changes, and piezoresistive composites were used to detect localized pressure through contact resistance variation. These sensing elements were integrated within a layered elastomeric architecture, allowing simultaneous detection of bending, stretching, and pressing in a wearable form factor. This configuration demonstrates the potential of optical sensing as a central mechanism for high-resolution, mechanically adaptive input capture in XR interface applications.

In gesture recognition with soft sensors, conformability with the skin is crucial, as sensors can delaminate with prolonged use due to biological substances such as sweat. The low conformability of the sensor due to the substrate hinders its sensitivity to skin deformation. Therefore, sensors designed with a breathable substrate or a substrate-less configuration


https://doi.org/10.1021/acs.chemrev.4c00966
Chem. Rev. 2025, 125, 11567−11665

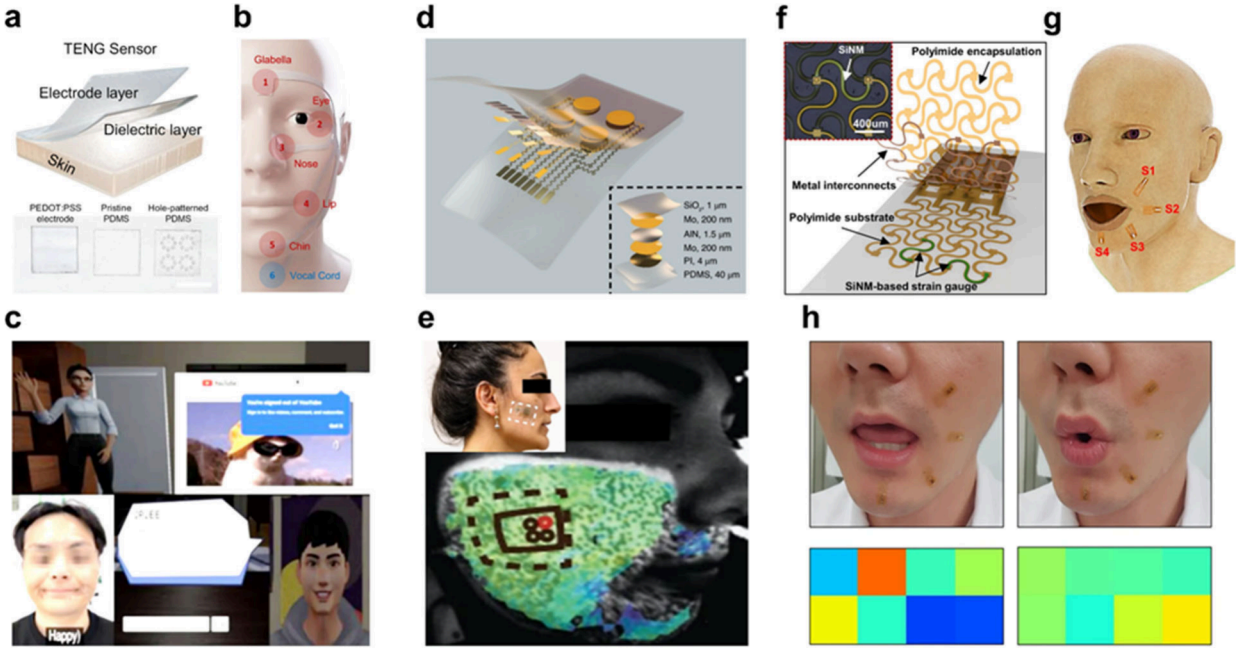


**Figure 24.** Facial expression recognition systems. (a) TENG sensor consisting of electrode and dielectric layers (top), along with corresponding layers such as PEDOT:PSS electrode and two types of dielectric layers for measuring skin strain and vocal vibrations, respectively (bottom). (b) A wearable system consisting of TENG sensors appropriately placed on the face to acquire emotional information. (c) Interactive speech with emotional sharing in XR applications. Reproduced with permission from ref 574. Copyright 2024 Springer Nature under CC BY 4.0 license https://creativecommons.org/licenses/by/4.0/. (d) Schematic illustration of a piezoelectric strain sensor for capturing the dynamic mechanical deformations of facial skin. Inset: exploded illustration of the sensor. (e) Strain distribution map captured by the strain sensors during facial motions. Inset: optical image showing the sensor attached to the face. Reproduced with permission from ref 575. Copyright 2020 Springer Nature. (f) Exploded view of a strain sensor based on SiNMs. Inset: magnified image of the sensor. (g) Schematic showing placement of strain sensors around the mouth to detect facial movements. (h) Optical images (top) and corresponding spatiotemporal features of local strain around the mouth (bottom) during silent speech. Reproduced with permission from ref 568. Copyright 2022 Springer Nature under CC BY 4.0 license https://creativecommons.org/licenses/by/4.0/.

that directly contacts the skin are more suitable.[170,561−563] To address these issues, a substrate-less nanomesh sensor that was printed directly onto the skin has been developed (Figure 23k).[122] This substrate-less configuration of the sensor made direct contact with the skin, allowing it to detect the fine strain occurring in wrinkles caused by finger movements. The sensor was designed as a single pathway extending from the wrist along the index finger with two terminals to detect motion across the entire hand. In this study, a meta-learning technique akin to human cognitive ability was employed to extract gesture information from these aggregated signals. The integration of substrate-less sensors with the advanced AI techniques enabled rapid recognition of various hand tasks based solely on motion patterns, including input through imaginary keyboard typing (Figure 23l) and shape discrimination by analyzing hand movements during rubbing (Figure 23m).

*5.2.1.4. Facial Expression Recognition.* Emotions and moods significantly affect human communication so both verbal and nonverbal expressions are important for natural and immersive interactions. However, these abstract and subtle feelings are difficult to quantify, which complicates the sharing of emotional atmospheres in digital environments. To resolve this challenge, several studies have tried to analyze facial movements and extract emotional information from facial expressions for XR applications. By capturing and interpreting facial movements including vocal vibration,[564−566] mouthing,[563,567−569] and eye movement,[570−573] the approaches aim to enhance emotional communication in virtual spaces, thereby improving user interaction and immersion.

Primarily, emotional information can be extracted from skin strain and vocal vibrations among various facial movements by employing TENG sensors composed of a conductive polymer electrode and a dielectric elastomer film (Figure 24a).[574] The sensors detected strain and vibration by measuring the output voltage produced through the triboelectric effect, with distinct types of dielectric layers responding sensitively to different mechanical stimuli. A dielectric layer with vertically aligned NW structures was sensitive to skin stretching and compression for measuring strain related to facial expressions and mouth movements. Meanwhile, a dielectric layer featuring an array of holes, acting as a sound hole, effectively responded to vibrations for detecting vocal vibrations associated with speech. By strategically placing the sensors on appropriate regions of the face, both verbal and nonverbal expressions could be captured (Figure 24b). This study demonstrated interactive speech in various XR applications, enabling the sharing of emotional atmospheres during human communication (Figure 24c).

For facial expression recognition, it is crucial to quantify the deformations in facial skin caused by muscle contraction and relaxation. Accurate measurement of skin strain and a comprehensive understanding of the mechanisms behind facial deformation facilitate reliable interpretation of facial movements and the extraction of facial expressions. Furthermore, this knowledge serves as a foundation for the development of wearable systems that detect verbal and nonverbal expressions


https://doi.org/10.1021/acs.chemrev.4c00966
Chem. Rev. 2025, 125, 11567−11665

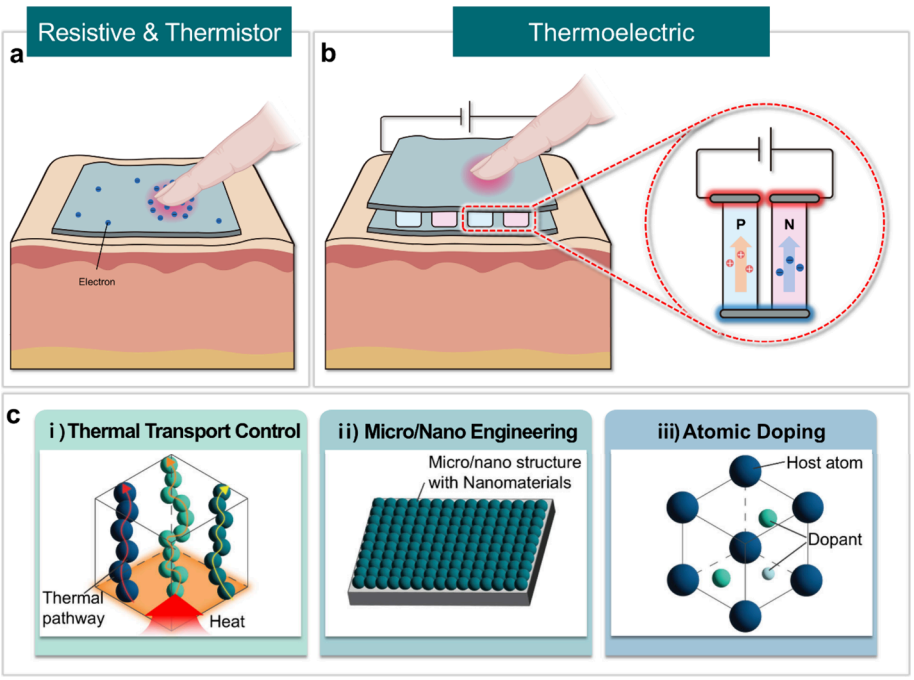


**Figure 25.** Mechanisms for temperature measurement with wearable XR input devices. (a) Resistive-based temperature sensor and thermistor. (b) TE-based temperature sensor using the Seebeck effect. (c) Representative material-based approaches for improving thermal input devices: (i) thermal transport control, (ii) micro/nanoscale engineering, and (iii) atomic doping. Created with BioRender.com.

presented on the face. However, the mechanical deformation of soft tissue is nonlinear and dynamically changes with muscle movements,[575] making the quantitative analysis of skin strain challenging. Regarding this, a piezoelectric strain sensor has been used to analyze the dynamic mechanical interactions between the sensor and the skin on the face (Figure 24d). The sensor consisted of a piezoelectric aluminum nitride (AlN) layer sandwiched between two electrode layers, and measured strain by detecting voltage output in response to surface deformations regardless of direction. The authors utilized 3D reconstruction of the facial model to derive a quantitative correlation between the voltage signals and strain, resulting in a strain distribution map (Figure 24e). The results provide fundamental insights for recognizing various facial motions such as twitching, smiling, and mouthing.

Materials with high Young's modulus, despite their rigidity, can be excellent candidates for detecting the subtle deformations associated with facial movements. Precise measurement of strain around the mouth, without measuring vibration, enabled silent speech interfaces that allow verbal communication without vocalization.[568] The strain sensor designed to capture mouth movements consisted of two vertically arranged silicon nanomembranes (SiNMs) (Figure 24f). The inherently rigid silicon with a single crystalline structure was patterned in a serpentine shape to conform to skin deformations and responded rapidly and sensitively to strain. Moreover, the vertical arrangement allowed for the measurement of the magnitude and direction of local strain. The authors identified the optimal placement of the sensors to classify mouth movements (Figure 24g). By analyzing the spatiotemporal features of local strain around the mouth, the recognition of silently pronounced words was achieved through the developed silent speech interface (Figure 24h). This study demonstrated the promise of rigid materials in decoding fine facial deformations for advanced communication technologies for wearable XR systems.

**5.2.2. Thermal Input Devices.** Temperature is one of the most critical factors for understanding real-world sensations and is an essential element in XR environments. Therefore, accurately conveying temperature changes from the physical environment to the XR environment is crucial, which emphasizes the need for precise detection of temperature variations in the physical world.

*5.2.2.1. Mechanisms and Materials for Thermal Input Devices.* Regarding this, thermo-resistive sensors and thermistors, which operate based on changes in electrical resistance or conductivity with temperature, are widely used for temperature sensing (Figure 25a).[576−579] Thermal resistance temperature sensors and thermistors operate on the principle that the resistance of a conductor changes with temperature, with an increase in resistance referred to as positive temperature coefficient (PTC) and a decrease as negative temperature coefficient (NTC).[580−584]

Typically, pure metallic elements are used as PTC materials, where the resistance increases as the temperature rises due to the increase in the kinetic energy of free electrons, which enhances scattering and reduces electrical conductivity.[585,586] In addition, ceramic-based PTC materials exhibit a sharp increase in resistance near their Curie temperature, driven by phase transitions affecting charge mobility.[587−589] This transition affects the mobility of charge carriers and increases scattering, causing a sharp increase in resistance. Additionally, grain boundaries in the ceramic structure act as barriers to charge transport, and their effectiveness increases with temperature, further amplifying the PTC effect.[590,591] In contrast, in composite materials with conducting polymers or conductive fillers, PTC behavior arises from thermal expansion.[585,592] As the temperature rises, the thermal


https://doi.org/10.1021/acs.chemrev.4c00966
Chem. Rev. 2025, 125, 11567−11665

expansion disrupts conductive pathways formed by filler particles, thereby significantly increasing resistance.

On the other hand, NTC materials are commonly derived from semiconductors such as metal oxides, where electrical resistance is governed by charge carriers.[593,594] In general, NTC thermistors are used due to their high accuracy and fast response times in temperature sensing applications.[595,596] In NTC semiconductors, as the temperature rises, the valence electrons in the semiconductor material become excited to higher energy levels, generating new electron−hole pairs due to thermal excitation. This increase in carrier concentration enhances the conductivity of the semiconductor.[597−599] Similarly, conducting polymers exhibit NTC behavior due to their conjugated $\pi$-electron structures, which enable electron mobility.[600,601] As temperature increases, thermal excitation activates more charge carriers within the conjugated system, while the movement of polarons and bipolarons becomes more dynamic, further boosting conductivity. The electrical properties of conducting polymers are significantly influenced by their doping levels, crystallinity, and temperature. These mechanisms in NTC materials are characterized by their simple structure and fast response, making it suitable for the development of skin-integrated temperature sensory input devices.

Another effective temperature sensing mechanism is TE temperature sensors, which operate based on the Seebeck effect at the contact point (Figure 25b). The Seebeck effect is a physical phenomenon where a voltage difference is generated between two junctions with different temperatures in a closed circuit composed of two dissimilar metals or semiconductors.[602] The TE temperature sensor utilizes the voltage differences, known as TE voltage or Seebeck electromotive force, generated in response to an applied temperature gradient.[603] In contrast to resistance-based temperature sensing, this mechanism has the advantage of minimizing the impact of mechanical deformation on the sensor, as it relies on the voltage difference rather than resistance changes.

To fully leverage the capabilities of wearable thermal input devices, it is essential to ensure efficient delivery of body heat to the sensing interface. This requires careful management of thermal transport from the skin to the sensor, particularly under dynamic conditions such as mechanical deformation, perspiration, and motion (Figure 25c-i). For instance, stretchable thermally conductive elastomers incorporating high-aspect-ratio fillers such as 1D or 2D materials can form interconnected thermal pathways that enable efficient heat transfer.[604] Optimizing the filler geometry, orientation, and spatial distribution further enhances the thermal conductivity without compromising mechanical compliance. In addition, LM-based colloidal materials have shown promise in reducing interfacial thermal resistance through the formation of gradient liquid−solid interfaces.[605,606]

Equally important is the prevention of unintended heat transfer from other components in wearable XR devices, such as computation modules or thermohaptic feedback components, which may inadvertently affect the sensing accuracy or user comfort. To address this, thermal insulation and protection layers have been engineered for skin-interfaced systems. A stretchable thermal protective substrate, composed of PDMS embedded with phase-change microspheres, significantly buffers transient thermal spikes.[607] During operation, the embedded microspheres undergo phase transitions, absorbing significant latent heat and thus limiting the temperature rise at the skin interface. For enhanced passive thermal insulation, gradient-structured aerogel fibers have been reported as high-performance materials.[608] These fibers exhibit radially varying porosity that induces interfacial thermal resistance, drastically reducing thermal conductivity to a value lower than that of air. The gradient design effectively prevents excessive heat flow toward the skin. In addition to thermal isolation and dissipation, precise directional control of heat flow is a promising approach for thermal management in skin-integrated XR systems.[609,610] Thermal metamaterials, designed with engineered spatial anisotropy, enable localized manipulation of heat paths. These systems allow for spatial redistribution of heat around sensitive components or toward desired areas, contributing to both sensing fidelity and overall system efficiency.

To advance the performance of conventional thermistors for skin-interfaced applications, micro- and nanoscale engineering strategies have been widely adopted (Figure 25c-ii). A representative approach involves the nanostructuring of semiconducting materials to achieve seamless integration between the sensing channel and metal electrodes.[595] A flexible NTC thermistor fabricated via laser-induced reductive sintering enables the monolithic formation of metal electrodes and metal oxide sensing channels from a single precursor ink. This intimate interface improves the fidelity of signal transmission, enhancing overall device performance. In parallel, for skin-integrated thermohaptic input systems, it is important to maintain thermal sensing resolution while suppressing deformation-induced signal distortion. One notable study proposed a biomimetic laminated nanostructure inspired by nacre, where MXene nanosheets are hierarchically assembled with poly(vinyl alcohol)/TEMPO-oxidized cellulose nanofibrils.[611] This laminated configuration dissipates in-plane mechanical stress and mitigates strain-induced artifacts. Beyond conventional resistive mechanisms, ionic TE mechanisms have also been explored. An electrolyte-assisted temperature sensor, which mimics a thermocouple structure while utilizing a gel electrolyte to bridge dissimilar metal electrodes, has been demonstrated.[612] The gel electrolyte promotes temperature-dependent redox interactions at the metal−electrolyte interfaces. To further leverage the redox-active interface enabled by the electrolyte, nanohole metasurface electrodes were incorporated, which convert light into localized heat via plasmonic absorption.

Beyond micro- and nanoscale engineering, atomic-level manipulation via defect engineering or doping offers a fundamental route to precisely tailor the intrinsic properties of sensing materials (Figure 25c-iii). This strategy allows for the fine-tuning of the electronic band structure, which directly governs the performance of thermoresistive or TE sensors. In the realm of NTC thermistors, the sensitivity is governed by the activation energy, which is intrinsically linked to the electronic bandgap. Precise control over the bandgap is therefore crucial for enhancing the temperature coefficient of resistance. Representative research involves doping of silicon nanomembranes with gold.[613] Gold acts as a deep-level impurity in silicon, shifting the Fermi level toward the intrinsic level, which dramatically increases the effective activation energy and thereby achieves the high temperature coefficient of resistance. On the other hand, a primary objective of atomic doping in TE sensors is the enhancement of the Seebeck coefficient. Engineering the band structure to achieve the convergence of multiple electronic bands to a single energy


https://doi.org/10.1021/acs.chemrev.4c00966
Chem. Rev. 2025, 125, 11567−11665

level induces high valley degeneracy, which enhances the Seebeck coefficient.[614,615] For example, by mixing selenium into lead telluride, these electron pathways are aligned, which significantly boosts the generation of voltages from heat.[614] This principle also applies to lead selenide doped with gallium antimonide for better performance.[615] Another approach is to create an impurity band, acting as a stepping stone for charge carriers near the primary conduction pathway. Doping silver antimony telluride with tin achieves this, allowing more charges to efficiently contribute to producing electricity and increasing electrical output.[616] In addition, doping can also enhance TE efficiency by modifying the microstructure to obstruct heat transfer, which contributes to higher overall performance.[617]

Table 11 provides a comparative summary of the key advantages and limitations of representative thermal input mechanisms, including resistive/thermistor-based and TE approaches. Table 12 further details the material platforms, sensing ranges, and spatial performance of various temperature sensor implementations applicable to wearable systems. These thermal input technologies play an essential role in enabling XR interfaces to capture nuanced temperature variations across the skin. By providing high sensitivity and conformable thermal sensing, they support real-time, context-aware interactions in immersive environments. As XR devices continue to evolve, the integration of robust and stretchable temperature sensors will be critical to achieving seamless, skin-like input modalities.

**Table 11. Summary of Advantages and Disadvantages of Thermal Input Devices**

| mechanism | advantages | disadvantages |
|---|---|---|
| resistive and thermistor | • high sensitivity to temperature<br>• fast thermal response time<br>• simple, low-cost fabrication | • nonlinear resistance–temperature behavior<br>• affected by humidity or drift<br>• sensitive to material condition changes |
| thermoelectric | • insensitive to mechanical strain<br>• self-powered operation<br>• high thermal sensitivity | • low output voltage<br>• complex material pairing required<br>• sensitive to linearity/reproducibility |

*5.2.2.2. Resistance-Based Thermal Sensing and Input Devices.* As mentioned above, skin conformality is critical for XR interfaces to effectively monitor the physiological information of users in the XR environment. During the motion-based interaction in the XR environment, the XR device must maintain continuous conformal contact to ensure stable and accurate data collection. This attribute is particularly important for skin-interfaced XR devices that measure the temperature on the skin surface, as even a small air gap can cause inaccuracies due to the interfacial thermal resistance.[618−620] Therefore, to meet these requirements, the device must not only be stretchable but also maintain consistent performance under deformation. To address this issue, the stretchable semiconducting SWCNT transistor-based temperature sensor platform has been proposed, achieving high reliability and accuracy through a deformation-suppression circuit (Figure 26a).[621] All transistor components were composed of stretchable materials such as SWCNT, PEDOT:PSS liquid ionic conductor, and block copolymer-based stretchable substrate. By adopting differential readout technology, which combines static voltage readout and dynamic voltage readout, the authors were able to minimize measurement errors within ±1 °C even with 60% strain, without the need for strain engineering (Figure 26b).

In addition, recognizing thermal patterns is essential for XR devices to apply them to the virtual environment in response to real-world interactions and the physical state of users. In this context, a stretchable array-structured temperature sensor can serve as an effective input system for wearable XR devices by detecting thermal patterns of objects in contact with human skin (Figure 26c).[596] Polyaniline nanofiber-based temperature sensors and SWCNT-based thin-film transistors were interconnected using LM to ensure stable performance under

**Table 12. Summary of Thermal Input Devices with Temperature Sensors and Their Characteristics**

| | | | performance | | | |
|---|---|---|---|---|---|---|
| mechanism | material | stretchability | temperature | sensitivity | spatial resolution | ref |
| Temperature Sensor | | | | | | |
| thermo-resistive/ thermistor | SWCNT | stretchable (60%) | sensing range: 15−55 °C | −24.2 mV °C$^{-1}$ | | 621 |
| | SWCNT | stretchable (biaxial 30%) | sensing range: 15−45 °C | 1.0% °C$^{-1}$ | 1 cm | 596 |
| | Au-doped SiNM | stretchable (30%) | sensing range: 25−45 °C | TCR: − 3.73% °C$^{-1}$ | 3 mm | 622 |
| | Ni electrode, NiO NP | flexible | sensing range: 25−70 °C | TCR: − 9.2% °C$^{-1}$ | 8 mm | 595 |
| | $Ag_2S$ | flexible | sensing range: 24−34 °C | TCR: − 4.7% °C$^{-1}$ | 6 mm | 623 |
| | $SnO_2$, SWCNT | flexible | sensing range: 0−40 °C | TCR: − 0.97% °C$^{-1}$ | | 628 |
| | rGO | stretchable (10%) | sensing range: 25−50 °C | TCR: −2.085 °C$^{-1}$ | <6 mm | 629 |
| Seebeck effect | CNT, Ag NW | stretchable (70%) | $\Delta T$: ∼90 °C | Seebeck coeff: 37 $\mu$V °C$^{-1}$ | | 627 |
| | PEDOT:PSS, Ag NP, graphene | stretchable (100%) | $\Delta T$: ∼100 °C | Seebeck coeff: 10 $\mu$V °C$^{-1}$ | 5 mm | 626 |
| | Pt, $In_2O_3$ | flexible | $\Delta T$: ∼100 °C | Seebeck coeff: 76.5 $\mu$V °C$^{-1}$ | | 630 |



https://doi.org/10.1021/acs.chemrev.4c00966
Chem. Rev. 2025, 125, 11567−11665

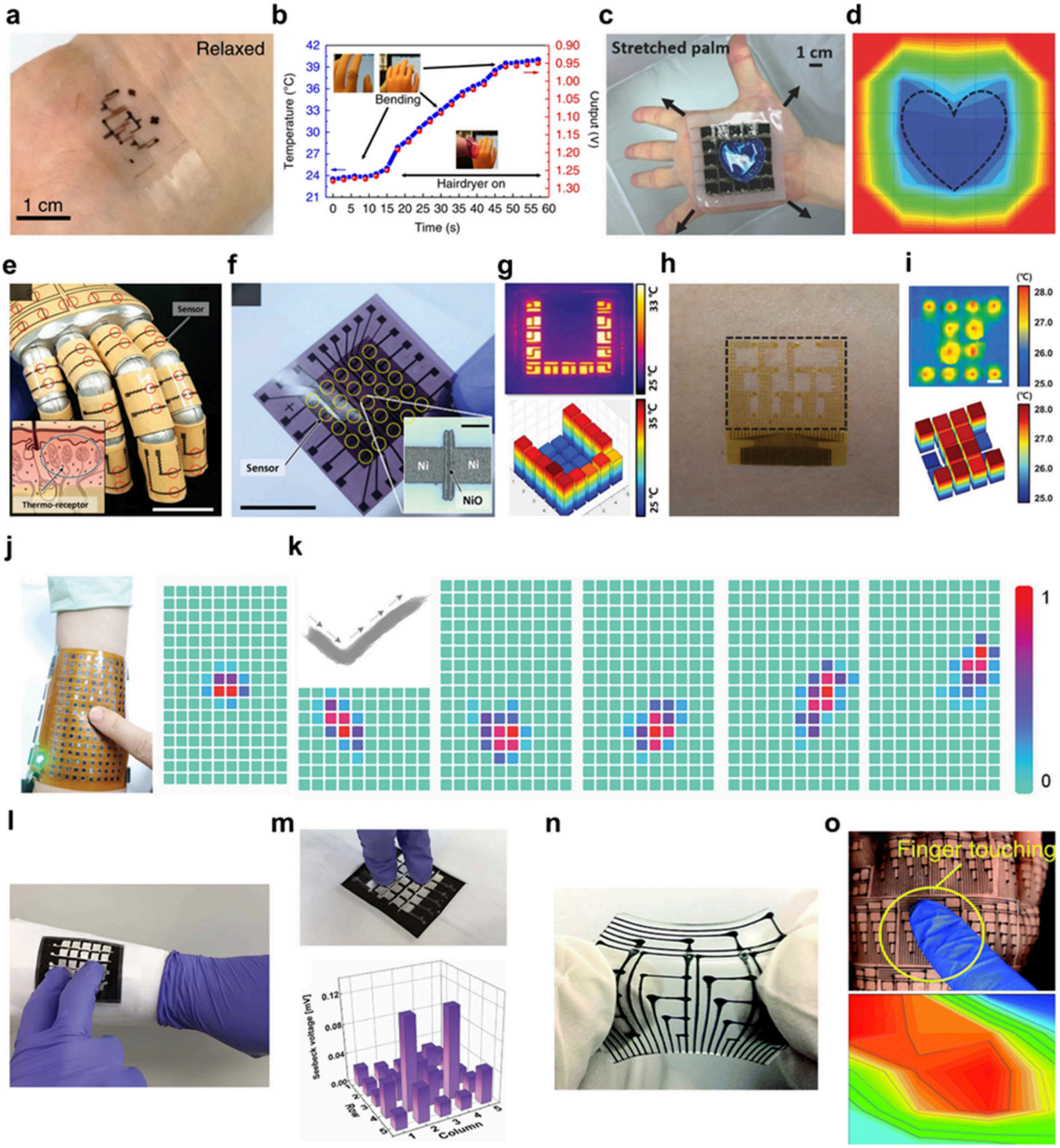


**Figure 26.** Temperature input devices. (a) Stretchable strain-independent circuit integrated temperature sensor (scale bar: 1 cm). (b) Stable sensing performance of the temperature sensor with minimum error under mechanical deformation. Reproduced with permission from ref 621. Copyright 2018 Springer Nature. (c) Polyaniline nanofiber-based stretchable temperature sensor array with heart-shaped water container. (d) Mapping of the corresponding heart-shaped temperature distribution. Reproduced with permission from ref 596. Copyright 2015 Wiley-VCH. (e) NiO-based flexible thermistors on the various parts of the robotic hand. (f) A digital image of a 5 × 5 NiO-based thermistor array (scale bar: 4 cm). Inset: a magnified view of the monolithically integrated Ni electrodes and NiO thermistor (scale bar: 100 $\mu$m). (g) An IR image of the selectively heated thermistor. (Top) and corresponding temperature mapping acquired from the NiO-based temperature thermistor array (bottom). Reproduced with permission from ref 595. Copyright 2020 Wiley-VCH. (h) Stretchable temperature sensing mesh based on Au-doped SiNMs on the human arm. (i) Thermographic image of partially heated Au-doped temperature sensor array (top) and corresponding color heat map of heated Au-doped temperature sensor array. Reproduced with permission from ref 622. Copyright 2022 Wiley-VCH. (j) $Ag_2S$ film-based thermistor array applied to the human arm with a finger interacting with the device (left) and the temperature distribution indicating the location of the finger on the device (right). (k) A digital image of a check symbol demonstrating the detection of dynamic motion using the $Ag_2S$ thin-film thermistor array, along with accompanying images showing temperature distribution changes based on the dynamic motion. Reproduced with permission from ref


https://doi.org/10.1021/acs.chemrev.4c00966
Chem. Rev. 2025, 125, 11567−11665

**Figure** 26. continued

623. Copyright 2022 Wiley-VCH. (l) A photograph of wearable TE-based wearable temperature sensors deposited on the human arm. (m) Finger contact on specific areas of the device (left) and the corresponding TE voltage mapping indicating the location of the contact point and the temperature of the object. Reproduced with permission from ref 626. Copyright 2018 Royal Society of Chemistry under CC BY-NC 3.0 license https://creativecommons.org/licenses/by-nc/3.0/. (n) Highly stretchable temperature sensor based on the Seebeck effect with CNT, Ag NP, and graphene-based printed circuits. (o) Mock-up hand covered with the Seebeck effect-based temperature sensor array showing the finger touch interaction (top) and the resulting temperature distributions of the finger (bottom). Reproduced with permission from ref 627. Copyright 2018 Royal Society of Chemistry under CC BY-NC 3.0 license https://creativecommons.org/licenses/by-nc/3.0/.

biaxial strain of up to 30%. The sensor showed a high resistance sensitivity of 1.0% $°C^{-1}$ within the temperature range of 15−45 °C, along with a rapid response time of 1.8 s. Temperature mapping experiments conducted with the sensor attached to the palm confirmed its capability to accurately detect both the shape and temperature of a heart-shaped aluminum container filled with cold water (Figure 26d).

Spatial resolution is another critical factor in array-based temperature XR devices for detecting and recognizing complex thermal patterns on the skin surface during interactions with objects. Spatial resolution refers to the level of detail in temperature mapping across a given area, with higher resolution enabling more precise detection of temperature gradients and complex thermal patterns. As the sensing elements become smaller, the number of sensors that can be attached to the skin increases, thereby enhancing the detail of the information that can be represented in the XR environment (Figure 26e).

Recently, a high-resolution nickel oxide (NiO)-based thermistor array has been reported, enabling the recognition of thermal patterns (Figure 26f).[595] The laser-based reduction process of nickel NPs facilitated the rapid fabrication of microscale NiO thermistors with a high resolution. By selecting NiO, known for its highly sensitive NTC properties, as the sensing material, the authors developed a precise thermistor array with high sensitivity in the temperature range of 25−70 °C. Consequently, when attached to the philtrum, the thermal input device was capable of detecting even small respiratory temperature changes in real time. Furthermore, the 5 × 5 grid thermistor array accurately identified small temperature variations and recognized letter patterns within an area of approximately 5 $cm^2$ (Figure 26g). Similarly, the ultrasensitive Au-doped SiNM-based wearable sensing device enables precise skin temperature monitoring by conforming closely to the skin (Figure 26h).[622] By adjusting the Au doping concentration, the SiNM exhibited high-temperature sensitivity with NTC properties. Thereby, the wearable thermistor enabled the formation of a thermal map when the sensor array was partially heated, demonstrating its capability to accurately detect temperature changes with high spatial resolution (Figure 26i).

Lastly, the wearable $Ag_2S$ film-based high-performance thermistor array, featuring ultrarapid response and recovery times, enables the development of a wearable thermal touch panel (Figure 26j).[623] The thin-film configuration, with a thickness of 70 $\mu$m, facilitates ultrafast response and recovery times, effectively addressing the low thermal conductivity of the inorganic $Ag_2S$ semiconductor. These characteristics have been experimentally demonstrated to extend beyond merely recognizing the position of contact points, exhibiting the potential for detecting dynamic motion in touch-panel applications (Figure 26k).

*5.2.2.3. TE-Based Thermal Sensing and Input Devices.* On the other hand, the TE mechanism can be effectively arranged in array configurations due to the inherent characteristics of TEDs, which utilize the difference in the Seebeck effect that exists between pairs at contact points. This property has been leveraged in the development of temperature sensors that are highly sensitive to thermal variations while remaining unaffected by stretching or deformation.[624,625] Furthermore, the TE voltage generated by the thermal gradient resulting from the thermal interaction enabled their self-powered nature and efficient energy consumption.

For example, a self-powered wearable temperature sensor can be fabricated using TE fiber (Figure 26l).[626] Unlike conventional TE pallets, the temperature sensor was constructed by stencil-printing TE ink that consists of PEDOT:PSS as the p-type material and Ag NPs and graphene as the n-type materials onto a knitted textile substrate. The sensor generates a voltage in response to temperature differences, producing 1.1 mV with a 100 K temperature gradient, and demonstrates high durability over 800 cycles under 20% strain. Furthermore, it detects real-time temperature changes without a battery by generating voltage based on thermal differences, facilitating both temperature sensing and contact position prediction (Figure 26m). Another example is the development of a highly stretchable temperature sensor utilizing the Seebeck effect with NP-based printed circuits (Figure 26n).[627] This sensor formed a microthermocouple by printing nanomaterial-based inks that consist of CNTs and Ag NWs on a PDMS substrate to create stretchable microthermocouple-based circuits. The sensor demonstrated up to 40% stretchability while maintaining strain-insensitive temperature measurements. It also visualized real-time temperature distribution during finger touch, showing the capability to accurately capture fine temperature patterns on surfaces like skin (Figure 26o).

**5.2.3. Chemical Input Devices.** Human olfaction and gustation are complex sensory processes that rely on the binding of specific chemicals to receptors, which generate electrical signals transmitted to the brain for interpretation.[631] These processes enable the perception of a wide range of smells and tastes, playing a critical role in how humans interact with their environment. Inspired by these biological mechanisms, chemical input devices have been designed to replicate these natural processes, facilitating the detection and differentiation of chemical molecules.[632−635] The implementation of such devices is primarily based on binding affinity, electrochemical reactions, and iontronic mechanisms, each of which contributes to the precise identification of specific compounds within complex mixtures. By emulating the precision and selectivity of human sensory systems, these devices hold


https://doi.org/10.1021/acs.chemrev.4c00966
Chem. Rev. 2025, 125, 11567−11665

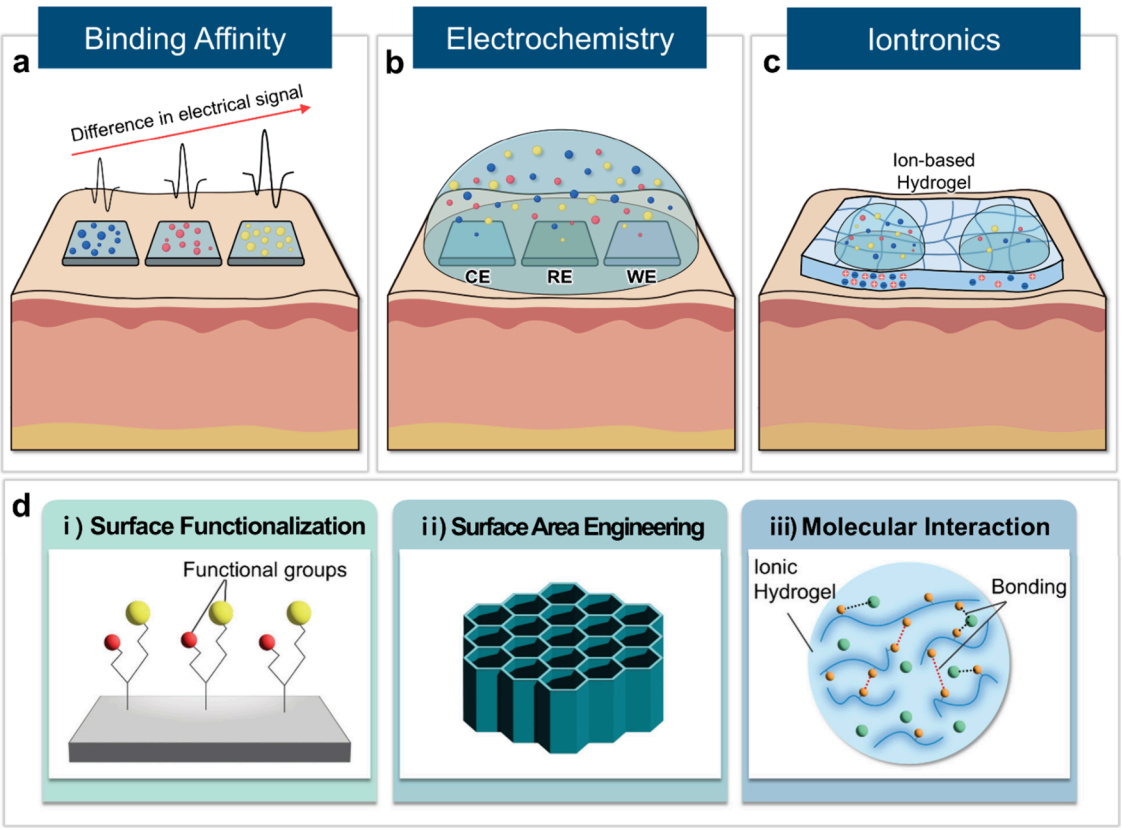


**Figure 27.** Mechanisms for chemical sensing with XR input devices. (a) Chemical sensing mechanism with binding affinity energy. (b) Electrochemical-based sensing mechanism with three-electrode system. (c) Iontronic-based chemical sensing mechanism. (d) Representative material-driven strategies for enhancing chemical input interfaces: (i) surface functionalization, (ii) surface area engineering, and (iii) molecular interaction design. Created with BioRender.com.

considerable potential for XR applications, particularly in detecting and analyzing the surrounding environment.

*5.2.3.1. Mechanisms and Materials for Chemical Input Devices.* The binding affinity mechanism operates similarly to biological receptors, where specific compounds bind to responsive materials on the sensor surface to generate signals (Figure 27a).[636−638] Specifically, binding affinity refers to the ability of a chemical ligand to bind selectively and stably to the binding site of a receptor or sensing surface, defined by selectivity and affinity.[639,640] Selectivity is determined by the structural complementarity and chemical interactions between the ligand and the receptor.[639,641] Structural complementarity describes the precise alignment of the structure of the ligand to the binding site of the receptor. Chemical interactions involve physicochemical forces such as hydrogen bonding, ionic interactions, hydrophobic effects, and van der Waals forces, all of which play a critical role in determining selectivity.[642−644] Affinity, on the other hand, reflects the stability of the interaction between the ligand and the receptor, quantified by the equilibrium dissociation constant.[645] A lower equilibrium dissociation constant value indicates stronger binding, which contributes to stable and reliable signal generation in sensing systems. Together, selectivity and affinity act synergistically in sensor design to ensure high sensitivity and specificity, even in complex environments.

Based on the mechanism, sensory input systems adopt biomolecules such as antibodies,[636,638,646,647] proteins,[648−651] and DNA,[634,652−656] as well as nanomaterials,[632,633,657,658] polymer films,[659−661] and surface-modified electrodes,[662,663] to enhance selectivity and sensitivity toward specific molecules.[664−667] To convert smells or tastes into electrical signals, the systems are integrated with electrodes or transducers composed of nanomaterials such as CNT,[650,668,669] graphene,[670] and conductive polymers.[668] When the analyte binds to the sensor, it induces a change in the properties of sensors, such as mass, charge, or conductivity. By analyzing the signal variations resulting from binding reactions, the concentration and characteristics of the target substance can be determined. While this approach enables precise detection of specific molecules within complex mixtures, it is sensitive to environmental changes.[664,667,671]

In addition, the electrochemical mechanism converts chemical reactions into electrical signals through oxidation-reduction reactions, facilitating the detection of various chemical compounds (Figure 27b).[672−674] Olfactory and gustatory sensors primarily utilize a three-electrode configuration, comprising a working electrode (WE), a counter electrode, and a reference electrode, to investigate redox reactions within the analyte. This configuration enables precise measurement of current and voltage changes between the electrodes, offering high sensitivity and rapid response times for the effective detection of various chemical compounds.[674−676] To analyze the concentration of specific ions, various electrochemical techniques, including chronopotentiometry,[677,678] chronoamperometry,[679,680] and differential pulse voltammetry,[681,682] have been adopted for olfactory and gustatory input devices.


https://doi.org/10.1021/acs.chemrev.4c00966
Chem. Rev. 2025, 125, 11567−11665

In electrochemical mechanisms, the WE serves a pivotal role as the site where chemical reactions are transformed into measurable electrical signals by enabling electron transfer processes and amplify the resulting signals effectively.[674,683,684] It is specifically designed to facilitate and monitor redox reactions, generating electronic responses through surface complementarity and chemical interactions. Unlike binding affinity, which typically involves nonredox molecular recognition, the WE drives electrochemical processes that directly produce quantifiable signals. On its surface, the analyte undergoes oxidation or reduction reactions, which are critical for quantifying chemical concentrations. To optimize performance, the material and surface properties of the electrode are carefully selected and frequently modified.

Surface modification is a key strategy to enhance the chemical selectivity of the WE.[685−687] Functional coatings, such as specific enzymes,[688,689] antibodies,[690−692] or nanomaterials[693−695] are often applied to enable selective interactions with target analytes. These modifications ensure that only specific compounds participate in redox reactions, thereby minimizing interference from nontarget substances. Furthermore, conductive polymers possess unique properties that distinguish them from traditional materials for the WE, such as tunable conductivity through doping and enhanced selectivity.[696,697] Conductive polymers are easily doped due to their conjugated $\pi$-electron system, which allows charge carriers to be introduced efficiently through simple chemical processes. This functionality renders it indispensable in applications requiring real-time detection for olfactory and gustatory sensing.

Lastly, the iontronic mechanism utilizes ionic conductivity and primarily functions based on the movement of ions in response to specific chemical substances (Figure 27c).[698−700] When a chemical substance interacts with the sensor, it alters the concentration or mobility of ions within the system. This system measures the potential difference generated by changes in ion concentration, similar to the physiological signals produced by ion channels in humans. Iontronic sensors achieve high selectivity through the use of selectively responsive materials that interact specifically with target ions, ensuring precise and reliable detection.[699,701] Selectivity is primarily achieved by designing materials with chemical or structural properties specifically tailored to the unique characteristics of the target ion, such as size, charge, or hydration radius.[702,703] These materials selectively allow or facilitate the movement of target ions while effectively blocking or minimizing interference from nontarget species.

For example, ion-selective membranes are specifically engineered to facilitate the transport of target ions while effectively excluding others, relying on differences in their physical and chemical properties.[704−706] These membranes are frequently combined with ion-exchange materials, which further enhance the selective movement of desired ions while suppressing the transport of undesired ones. Similarly, ion gels comprising polymer networks embedded with ionic liquids provide a highly conductive medium tailored for selective ion transport.[707,708] Selectivity in ion gels is achieved through the incorporation of functional groups that promote specific interactions with target ions.[709] Additionally, the cross-linking density of the gel can be adjusted to control pore size, allowing only specific ions to pass based on their hydration radius or charge density.[710,711] Functionalized polymers, designed with ion-specific ligands or binding sites, further enhance selectivity by fostering specific interactions with the target ions, ensuring precision in ion sensing applications.[712−714] In olfactory and gustatory sensors, selectively responsive materials for specific target ions are employed to induce reactions that are subsequently converted into electrical signals. Generally, gel-based iontronic sensors provide exceptional sensitivity and flexibility, rendering them suitable for a variety of environments.[715,716]

To fully realize the potential of the above-mentioned sensing mechanisms, material-level strategies have been actively explored to optimize performance parameters such as sensitivity, selectivity, and stability. Among these strategies, surface functionalization focuses on precisely modifying the chemical properties of a sensing surface to optimize the interaction with specific analytes (Figure 27d-i). This technique imparts sensitivity and selectivity to the sensor while also influencing stability, reproducibility, and suitability for various applications.[717] One representative method involves the functional integration of biological receptors onto electronic platforms.[634] In this context, a chemical linker tailored for dual-affinity, interacting noncovalently with the graphene surface and covalently with amine groups on the receptor proteins, was employed to immobilize human olfactory receptors. This biointerface engineering ensured the stable anchoring and functional orientation of the receptors, enabling distinct signal responses corresponding to the molecular chain length of odorants. In addition to direct chemical functionalization, surface texturing, which is achieved through nanostructuring or material deposition, offers a complementary strategy to further amplify chemical input performance. For instance, a combinational surface functionalization method was implemented by decorating vertically aligned tin oxide nanorods with a range of bimetallic nanocatalysts and transition metal oxides.[718] Such a dual-modification approach not only diversified the catalytic sites but also induced unique redox reaction pathways at each sensing unit. These multidimensional responses enabled highly selective recognition of specific gas species within complex mixtures.

Expanding the accessible surface area directly enhances the interaction between target molecules and sensor surfaces (Figure 27d-ii). One prominent strategy includes 3D porous frameworks, such as aerogels or foams, often composed of hybrid carbon-based materials combined with functional NPs.[719] In this study, the architectures offered exceptionally high surface-to-volume ratios. Furthermore, interconnected pore networks promoted rapid diffusion of chemical species. Tailoring parameters such as filament diameter, pore density, and hierarchical structure enabled control over adsorption dynamics and temporal response. Metal−organic frameworks can also serve as 3D porous components when integrated with highly conductive carbon-based scaffolds, such as laser-induced graphene.[720] This combination yielded hierarchical architecture with coexisting pores, enhancing both molecular access and electronic signal transduction. The high porosity of the frameworks facilitated selective molecular binding via their cavities and surface functionalities, while the underlying scaffold provided mechanical support and rapid signal delivery. In addition, hollow or layered microstructures have been demonstrated to promote interfacial mass transfer.[721] Compared to dense films, these engineered structures minimized boundary layer resistance and accelerated analyte diffusion toward active sensing sites. As a result, chemiresistive


https://doi.org/10.1021/acs.chemrev.4c00966
Chem. Rev. 2025, 125, 11567−11665

sensors built from these films exhibited faster response times and reduced signal degradation even in dynamic environments.

Within iontronic chemical input systems, the dynamic interface formed between ionic liquids and soft matrices is crucial for mediating signal transduction (Figure 27d-iii). Embedding ionic liquids within soft polymeric networks to form ionogels retains ionic mobility and introduces mechanical robustness with leakage resistance. For example, ionogels containing ionic liquids and stretchable semiconducting gels have been reported to create continuous ion conduction pathways across the device.[722] These all-gel configurations enhance ionic transport and electrical transduction, ensuring reliable performance under mechanical deformation. Meanwhile, engineering the hydration behavior of ionic liquid components can control sensor selectivity under varying environmental conditions.[723] Hydrophilic anions tend to strongly coordinate with water molecules, swelling the gel and improving ion mobility in humid conditions. In contrast, less hydrophilic anions reduce water uptake, leading to denser ionogel networks that suppress humidity interference while maintaining permeability to chemical vapors. This molecular-level control has been leveraged to tune the environmental adaptability of iontronic sensing materials. Beyond passive sensing, ionic liquid interfaces can also be utilized for synaptic functionality in neuromorphic chemical devices.[724] In organic electrochemical transistors, the interaction between the ionogels and chemical analytes induces ionic redistribution, modulating the channel conductance like excitatory neurotransmission. The slow relaxation of ions within the polymer matrix leads to prolonged signal retention, which is actively reset by applying electrical pulses. Such ionogel-based gating architectures offer a promising route toward bioinspired chemical sensors that integrate memory, adaptability, and stimulus-specific response.

Table 13 presents the main types of chemical sensing mechanisms, including binding affinity, electrochemistry, and iontronics, along with their respective advantages and disadvantages for olfactory and gustatory input. Furthermore,

**Table 13. Summary of Advantages and Disadvantages of Chemical Input Devices**

| mechanism | advantages | disadvantages |
|---|---|---|
| binding affinity | • high specificity and selectivity | • limited dynamic range due to the equilibrium dissociation constant |
| | • stable and strong binding | • slow dissociation limits real-time use |
| | • compatible with complex environments | • sensitive to environmental changes |
| electrochemistry | • high sensitivity and fast response | • interference from nontargets |
| | • versatile signal amplification | • electrode surface instability |
| | • surface modification for selectivity | • fabrication complexity |
| iontronics | • high ion selectivity | • complex material design |
| | • bioinspired mechanism | • nontarget ion interference |
| | • material-driven precision | • property-sensitive response |

Table 14 provides examples of devices based on these mechanisms, including their materials, sensing targets, and performance characteristics. These chemical input technologies play an important role in extending XR systems to include smell and taste perception. By mimicking the selectivity and responsiveness of the human sensory system, they enhance realism and expand the range of immersive experiences.

*5.2.3.2. Olfactory Input Devices.* As mentioned, various materials such as antibodies,[636,638,646,647] proteins,[648−651] and DNA,[634,652−656] as well as nanomaterials,[632,633,657,658] polymer films,[659−661] and surface-modified electrodes,[662,663] have been utilized as flavor detection materials, with high sensitivity. However, in XR environments, the ability to provide sensory feedback for a wide range of odors is more crucial than merely detecting target substances. From this perspective, diverse sensory input arrays capable of responding to various gaseous molecules are commonly employed in the development of artificial olfactory systems.

Human olfactory input devices generate unique responses to various gaseous molecules through multiple receptor cells. Mimicking the feature of the human olfactory system, artificial olfactory devices use receptor-inspired sensing systems that produce characteristic response patterns to oder molecules.[631] For example, biomimetic sensor arrays (BSA) that incorporate MXene-based nanocomposites capable of detecting odor molecules have been proposed (Figure 28a).[633] During gas adsorption in MXene, electron transfer from gas molecules decreases the carrier hole concentration.[725,726] This phenomenon can be amplified by Schottky barrier structures at the interfaces in the MXene-based nanocomposite, which enhances gas detection performance. By adjusting the MXene ratio in the composite, the authors created chambers with various Schottky barrier structures that generated different signal responses, allowing for the development of a comprehensive library of signal reactions (Figure 28b). Furthermore, an AI algorithm was introduced to detect subtle differences in sensor signals, enabling the detection of odors from human breath and clothing to differentiate individuals. As a result, up to 10 distinct odors were successfully distinguished, achieving a 67.8% success rate in breath detection and 51.1% in clothing detection (Figure 28c).

MXene-based sensor array structures in chambers demonstrated that they are highly effective in detecting various odors. However, advancing wearable olfactory devices requires the development of technology capable of integrating diverse high-performance gas sensors into large-scale arrays on a single chip, similar to how olfactory cells in humans are densely packed within the nasal cavity. Inspired by the human olfactory system, a biomimetic olfactory chip (BOC) integrating up to 10,000 individually addressable sensors has been reported (Figure 28d).[632] A high-density sensor array incorporating vertical metal oxide ($PdO/SnO_2$) nanotubes with a 3D nanoscale structure was fabricated, offering a large, highly structured surface area that enhances effective interaction with gas molecules (Figure 28e). Furthermore, the pixel layer composed of this sensing material was combined with layers of metal oxides with varying compositions, maximizing sensor sensitivity and enabling each pixel to respond to a wide range of gases. The authors employed an AI algorithm to analyze the gas response patterns obtained from the sensors to classify various gases (Figure 28f). As a result, the AI learned the gas response patterns, enabling high-precision predictions with an


https://doi.org/10.1021/acs.chemrev.4c00966
Chem. Rev. 2025, 125, 11567−11665

Table 14. Summary of Olfactory and Gustatory Input Devices with Various Chemical Sensors and Their Characteristics

| | | | performance | | | |
|---|---|---|---|---|---|---|
| mechanism | material | stretchability | odor | taste | spatial resolution | ref |
| Chemical Sensor | | | | | | |
| binding affinity | PdO/$SnO_2$: odor, acetone, CO, ethanol, formaldehyde, $NO_2$, toluene, $H_2$, isobutylene | | 24 smells (camphor-wood, lemon, kiwi fruit...) | | 10−25 $\mu$m | 632 |
| | hORs, graphene, $\alpha$-$MoO_3$, poly(3-hexylthiophene-2,5-diyl) | | 4 short-chain fatty acids | | | 634 |
| | odor: propionic acid, butyric acid, valeric acid, hexanoic acid | | | | | |
| | $Ti_3C_2T_x$, $MAPbBr_3$ | | 10 gases (carvacrol, butyl cinnamate, indole...) | | | 633 |
| | odor: $NH_3$, acetone, EtOH, ether | | | | | |
| electrochemistry | C-based ink | stretchable | | sour, sweet, spice | | 738 |
| | taste: glucose, ascorbic acid, capsaicin | | | | | |
| | trioctylmethylammonium, oleic acid, bis(2-ethylhexyl) phosphate, tetradodecylammonium bromide, 1-hexadecanol, trimeltic acid | flexible | | sour, sweet, salty, astringent | | 737 |
| | taste: KCl, tartaric acid, sucrose, tannic acid | | | | | |
| | L-cysteine, Au NP | | | spicy | | 762 |
| | taste: hydroxy-$\alpha$-sanshool | | | | | |
| | Au NP, zeolitic imidazolate framework-8, $Ti_3C_2$ MXene | | | umami (sweet) | | 763 |
| | taste: inosine 5′-monophosphate, L-glutamic acid monosodium salt hydrate, disodium succinate, beefy meaty peptide | | | | | |
| iontronic | CNT yarn, PEDOT, Taste: $K^+$, $Na^+$, $H^+$ | stretchable (27%) | | four types of water and four types of fruit juice | | 740 |
| | mucin, LiCl | flexible | | astringent | | 168 |
| | taste: tannin | | | | | |
| | mucin, NaCl, Ag/AgCl | | | astringent, bitter | | 755 |
| | taste: tannin/quinine sulfate | | | | | |

accuracy of 99.04%, and was also utilized for predicting gas concentrations in mixed gases.

In addition, the ability to precisely distinguish similar odors is crucial for implementing olfactory information in the XR environment. However, existing olfactory input devices mainly target the detection of individual molecules or compounds with clearly identifiable compositions.[724,727−729] To pave the way for the next generation of XR, it is essential to establish olfactory input devices able to identify subtle distinctions in odor molecules, such as variations in chain length or functional groups.[730] To address this issue, a neuromorphic artificial olfactory system (AOS) utilizing human olfactory receptors (hORs) has been designed to be capable of detecting subtle differences between odors (Figure 28g).[634] This system utilized three unique hORs, each integrated with a lipid membrane for targeted detection, immobilized within nanodiscs on a graphene-extended gate device, forming an olfactory sensory neuron platform. The hOR nanodiscs, coupled with an organic synapse device, detect fine differences between odors based on their binding affinities (Figure 28h). This AOS produced unique patterns for odors and mixtures based on the specific binding affinities between hORs and odorants at the molecular chain length level, followed by learning and recognition by the AI system. As a result, it accurately identified single and mixed odors with over 90% accuracy, particularly distinguishing odors based on molecular chain length for compounds like short-chain fatty acids (Figure 28i).

In addition to directly reading electrical signals, there are methods that detect odors by analyzing color changes induced by compounds.[731,732] However, the color change-based mechanism requires separate processing equipment to analyze the colors, and the intermediary step of color transition may lead to slower response times. Therefore, continued studies to resolve these issues are necessary for the advancement of XR technologies.

*5.2.3.3. Gustatory Input Devices.* Entwined with olfaction, gustation significantly influences daily human experiences and emotions, exerting a profound impact on individual lives. While gustatory information is essential for interaction, current technologies that sense and analyze gustatory information derived from real food encounter significant challenges.[635,733] To address this, several studies have been exploring taste-sensing technologies, including electrochemical methods,[734−738] iontronic analysis,[739−742] triboelectric sensing,[743] and colorimetric analysis,[744−746] paving the way for more natural interactions in XR environments.[737,738,740,744,746]

Electrochemical sensing represents one of the fundamental strategies for the gustatory sensing of liquid or solid foods.[734−738] A wearable glove sensor that utilizes three electrode systems for electrochemical reactions on the fingers to differentiate various foods has been proposed (Figure 29a).[738] The WE for the electrochemical reactions was constructed using carbon and Prussian blue materials. The carbon electrodes were functionalized with ascorbic acid to detect sour flavors and capsaicin molecules to sense spiciness, while the Prussian blue electrodes were utilized for glucose detection to identify sweetness (Figure 29b). This glove distinguished unique electrochemical peaks and signal intensities corresponding to each taste, allowing the detection of sour, sweet, and spicy flavors on different fingers (Figure


https://doi.org/10.1021/acs.chemrev.4c00966
Chem. Rev. 2025, 125, 11567−11665

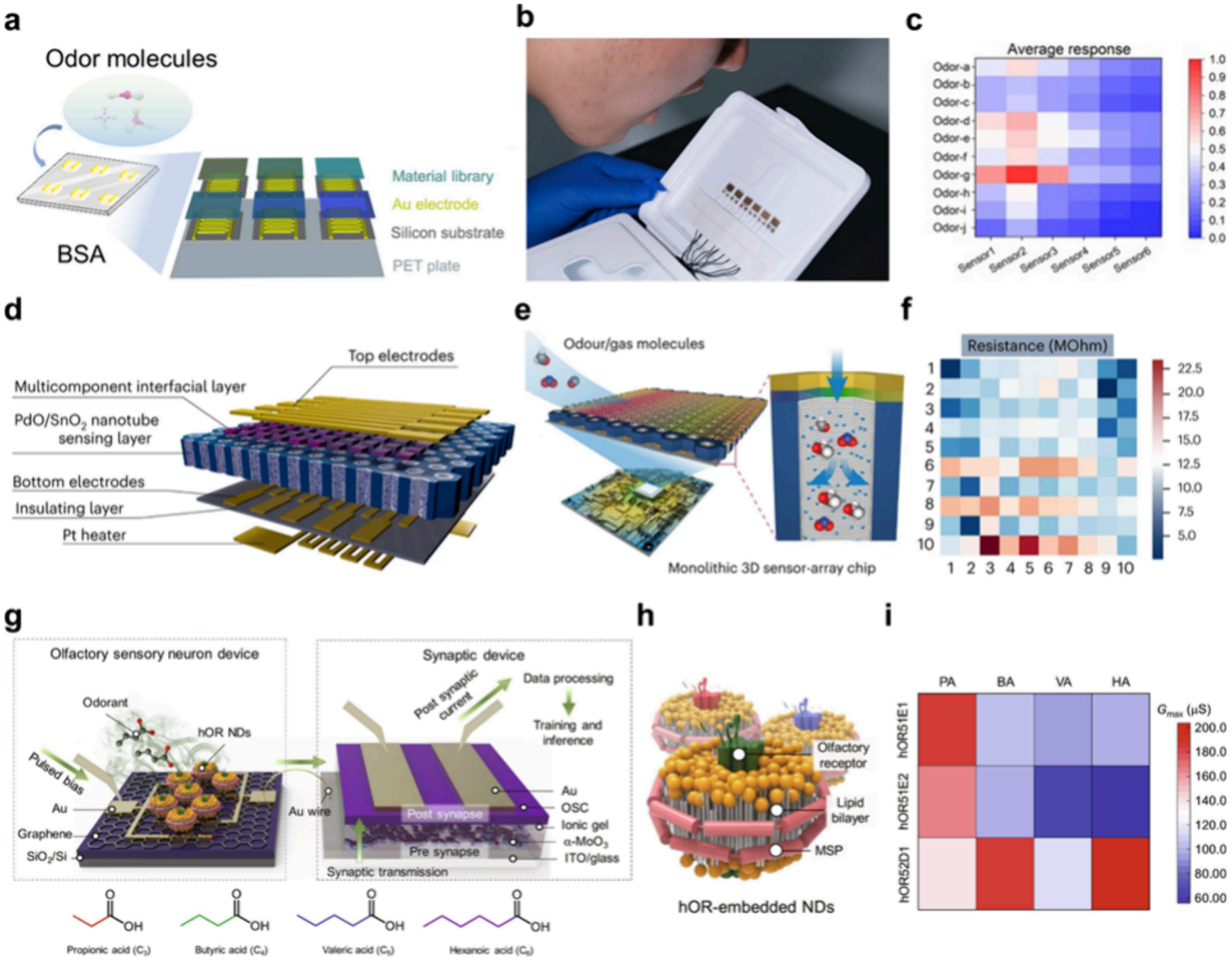


**Figure 28.** Olfactory sensing devices. (a) Schematic of a BSA incorporating MXene-based nanocomposites for the detection of odor molecules. (b) Digital image showing the generation of different signal responses to exhalation using the BSA chambers with various Schottky barrier structures. (c) Classification of 10 different odors using signal processing based on ML. Reproduced with permission from ref 633. Copyright 2023 Elsevier. (d) System design of BOC integrated with up to 10,000 individually addressable sensors. (e) High-density sensor array in the BOC incorporating vertical metal oxide ($PdO/SnO_2$) nanotubes and nanoscale structures for effective interaction with gas molecules. (f) Individual responses of each sensor obtained through the 10 × 10 sensor array chip. Reproduced with permission from ref 632. Copyright 2024 Springer Nature. (g) The main structure of a neuromorphic AOS utilizing hORs. (h) The hOR nanodiscs, combined with an organic synapse device, that detect fine differences between odors based on binding affinities. (i) Patterned channel conductance signals in response to various short-chain fatty acids. Reproduced with permission from ref 634. Copyright 2024 The American Association for the Advancement of Science under CC BY-NC 4.0 license https://creativecommons.org/licenses/by-nc/4.0/.

29c). Additionally, by using conductive gel for contact with food samples, the system could detect the taste of both liquid and solid foods. This system is expected to be beneficial for wearable XR devices, enabling the detection of gustatory elements from various objects in XR environments.

In addition to specific molecules, the presence of specific ions in food is closely linked to taste, making ion-selective sensors suitable for distinguishing distinct tastes.[739−742] For example, salty, sour, and bitter tastes are triggered by $Na^+$, $H^+$, and $K^+$ ions, respectively.[741,747−750] Based on this principle, the electronic tongue has been fabricated using CNT yarn coil-based ion-selective sensors to measure the concentrations of various ions, thereby enabling the differentiation of tastes in beverages and foods (Figure 29d).[740] These coiled CNT yarns, coated with ion-selective membranes, result in ion-selective coiled yarns designed for high sensitivity and selectivity toward specific ions such as $K^+$, $Na^+$, and $H^+$. As a result, the multi-ion potentiometric sensor demonstrated functional sensing performance in real applications, including water-based solutions such as seawater, river water, tap water, and distilled water, as well as fruit juices such as lemon, coconut, pear, and grape juice (Figure 29e). Furthermore, this sensitivity and selectivity were maintained even under 27% stretching and during mechanical deformations such as bending to 180° or tying into knots.

Recent advancements in electronic tongue (E-tongue) systems, designed to distinguish different tastes, have been widely reported. Progress in E-tongue technology has been facilitated by the integration of various materials, including lipid/polymer membranes,[751,752] conjugated polymers,[753,754] hydrogels,[168,755] and human taste cells.[756,757] Despite these advances, the technology still encounters several challenges in


https://doi.org/10.1021/acs.chemrev.4c00966
Chem. Rev. 2025, 125, 11567−11665

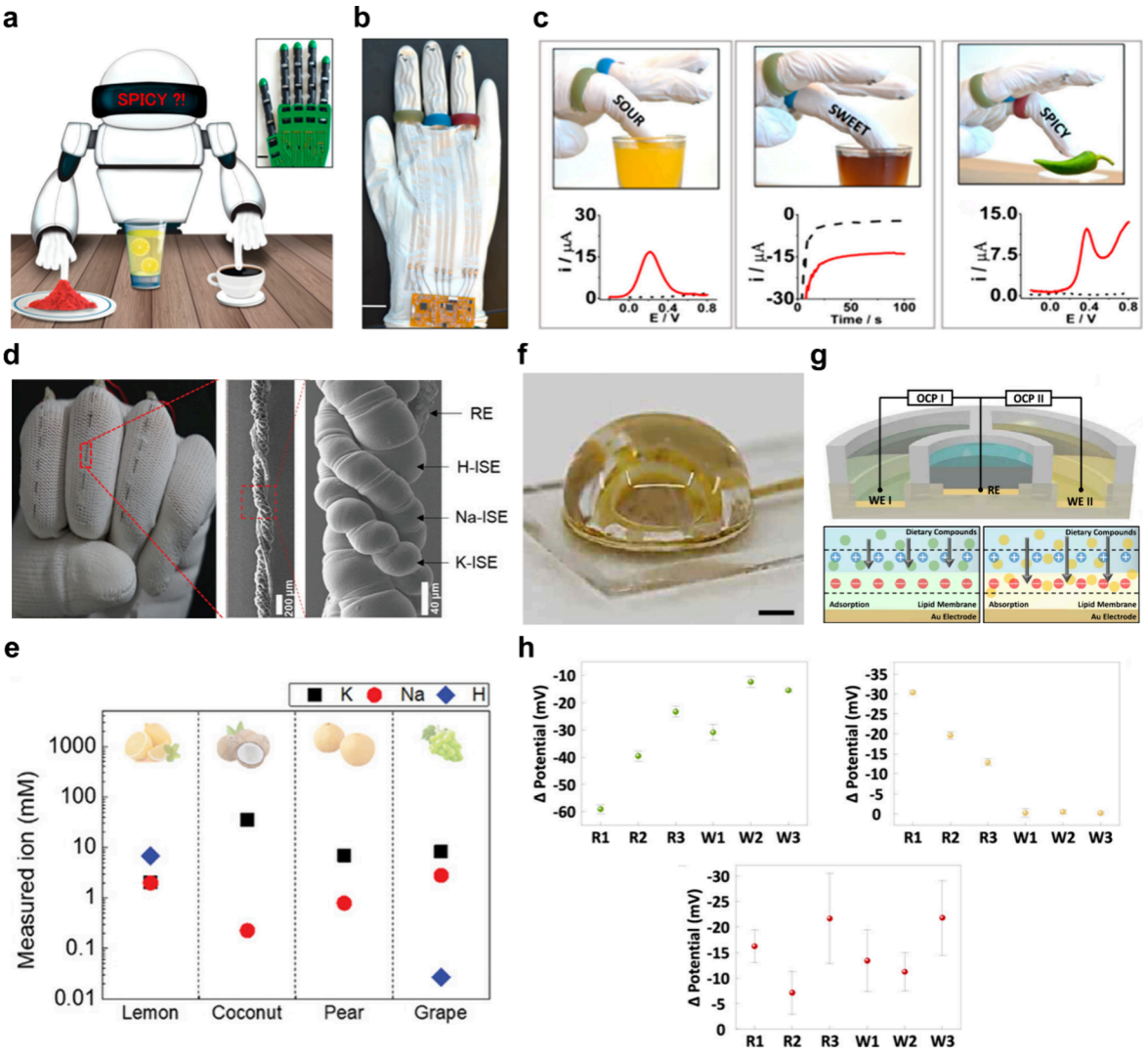


**Figure 29.** Gustatory sensing devices. (a) Electrochemical-based gustatory detection system and its application on the hand of a robot. (b) A glove-type device that differentiates gustatory stimuli through electrochemical reactions occurring at electrodes on the fingers. (c) Gustatory detection via finger touch of the glove and corresponding electrochemical signals: sour (left), sweet (middle), spicy (right). Reproduced with permission from ref 738. Copyright 2024 American Chemical Society. (d) Digital image of gustatory sensing device composed of ion-selective yarn (left). Electron microscopy image (middle) and magnified view (right) of the ion-selective coiled yarns (scale bars: 200 $\mu$m, 40 $\mu$m). (e) Ion concentrations measured by the ion-selective yarn-based sensor in various solutions. Reproduced with permission from ref 740. Copyright 2024 Wiley-VCH. (f) Optical image of the fabricated artificial electronic tongue system with a single drop of dietary compounds in the system. (g) Cross-sectional view of the artificial electronic tongue system illustrating the mechanism of sensing various dietary compounds with one system. (h) High accuracy of E-tongue system with different electrochemical potential in classifying six samples (wines). Reproduced with permission from ref 737. Copyright 2023 American Chemical Society.

accurately evaluating real taste profiles resulting from the interactions of taste elements, such as amplifying and masking effects. Furthermore, ensuring consistent and reliable performance under dynamic testing conditions, particularly with high variability, remains a critical issue.[758] To address this, an electronic tongue system has been proposed, mimicking human taste buds and employing a specialized deep-learning algorithm for gustatory analysis (Figure 29f).[737] This system integrated four working WEs into a single device that mimics taste buds, with each WE utilizing specific lipid membranes to selectively detect distinct taste qualities such as sourness, saltiness, sweetness, and astringency (Figure 29g). The obtained electrochemical signals from the multichannel gustatory sensor were analyzed and interpreted through deep neural networks. As a result, the artificial electronic tongue system accomplished approximately 95% accuracy in classifying six varieties of wine while maintaining close to 90% accuracy (Figure 29h).

Taste-sensing devices utilizing triboelectric,[743,759] and colorimetric[745,760,761] methods can also be used for gustatory feedback. However, triboelectric-based devices could only sense substances in the form of falling droplets, and colorimetric devices required separate processing tasks and equipment for color analysis. Therefore, further studies are needed to improve the versatility and miniaturization of sensing technologies for XR gustatory devices.

**5.2.4. Multimodal Sensory Input Devices.** As discussed above, for a wearable XR input device to simultaneously perceive various types of sensory information, a multimodal strategy is essential.[764] This can be achieved either by


https://doi.org/10.1021/acs.chemrev.4c00966
Chem. Rev. 2025, 125, 11567−11665


**Figure 30.** Multimodal sensory input devices. (a) Schematic illustration of a multimodal sensory input device with vertically integrated pressure sensor and temperature sensor. (b) Illustration of 64 body-mounted sensors for simultaneous pressure and temperature sensing, enabling detailed spatial mapping of tactile and thermal stimuli. Reproduced with permission from ref 196. Copyright 2018 The American Association for the Advancement of Science. (c) Diagram of the iontronic-based sensory input device and its mechanism for detecting both mechanical and gustatory stimuli. Reproduced with permission from ref 700. Copyright 2023 American Chemical Society. (d) Schematic image of the core component of the multimodal sensory device and its working mechanism, detecting temperature (left) through the Seebeck effect and pressure (right) through the piezoresistive effect. (e) A photograph of a multimodal sensory array attached to a prosthetic hand, grasping a human hand. (f) Mapping images showing the corresponding sensed temperature (top) and pressure (bottom) data resulting from grasping a human hand. Reproduced with permission from ref 178. Copyright 2015 Springer Nature under CC BY 4.0 license https://creativecommons.org/licenses/by/4.0/. (g) A photograph of multimodal sensory input device for mechanical and thermal sensing on the mock-up hand (left). A schematic diagram of the multimodal device with ion-conductor (top right) and its working mechanism (bottom right). (h) Changes in parameters of ion-conductor depending on the mechanical stimuli and thermal stimuli. (i) Demonstration of the decoupling of mechanical and thermal stimuli using ion-conductor-based sensory input device. Reproduced with permission from ref.179. Copyright 2020 The American Association for the Advancement of Science.

integrating multiple sensors within a single device[176,196,765] or by employing a novel mechanism that differentiates between distinct signals.[178,179,766] Consequently, developing such a device necessitates advanced manufacturing techniques, material science, and engineering expertise, as well as sophisticated signal processing methods, which greatly exceed the requirements of single-input devices.[767−769] This chapter provides a detailed exploration of various soft multimodal input devices.

The most accessible strategy involves integrating multiple individual sensors into a single device, typically combining the detection of mechanical and thermal stimuli.[176,196,770] For instance, a wearable device with a miniaturized array of sensors capable of precisely measuring localized pressure and temper-


https://doi.org/10.1021/acs.chemrev.4c00966
Chem. Rev. 2025, 125, 11567−11665

ature has been presented (Figure 30a).[196] This device interfaces with one or more large loop antennas connected to RF power and data collection electronics, enabling multiplexed operation over several tens of centimeters. The simultaneous wireless operation of 65 sensors positioned on the limbs, torso, neck, and head demonstrates the feasibility of pressure throughout the body and temperature monitoring during daily activities. (Figure 30b). These multiple wireless skin-like devices are mounted on human skin to measure two parameters in real time. The time-dependent data captured can be represented as spatiotemporal color plots mapped onto the body form. This approach allows for the comprehensive acquisition of motion and physiological data, with the resulting mapping serving as a valuable method for transmitting real-world information into XR environments.

Another approach could involve decoupling a single electrical signal that responds to two stimuli within the material. Recently, an iontronic sensor capable of detecting both pressure and taste was developed using the dielectric properties of conductive hydrogel (Figure 30c).[700] Mechanical pressure changes the contact area of the electrodes with a hierarchical structure, resulting in variations in the capacitance of the iontronic sensor. In contrast, chemical stimuli modify the mechanical properties of the hydrogel-based dielectric layer through the Hofmeister effect. When mechanical and chemical stimuli occur simultaneously, the capacitance response to mechanical stimuli changes due to the altered mechanical properties of the hydrogel caused by ion concentration. As a result, a single capacitance signal is influenced by both stimuli, and AI techniques are employed to distinguish between pressure and taste. The iontronic sensor, utilizing a hierarchical structure, demonstrated high mechanical sensing capabilities, differentiating between 15 chemical cosolvents and identifying 5 types of commercial beverages in response to chemical stimuli. This demonstrates the feasibility of separating two stimuli using a single sensor, mimicking the functionality of the human tongue.

Alternatively, devices can be designed by combining materials with two different mechanisms. Wearable multimodal sensory input devices have been designed that utilize organic TE materials supported by a microstructured frame to convert external pressure and temperature into distinct electrical signals.[178,771,772] For example, the independent Seebeck and piezoresistive effects were integrated into a single device structure, with the active layers formed by depositing organic TE materials onto a flexible microstructured frame to enable simultaneous sensing of temperature and pressure (Figure 30d).[178] When the device interacts with an object that applies combined temperature and pressure, the TE materials detect the temperature difference through the Seebeck effect, enabling the temperature of the object to be measured within 2 s. Simultaneously, the microstructured frame experiences mechanical deformation, resulting in a change in resistance proportional to the applied pressure in 2 ms. Utilizing screen printing technology, the author developed a spatially high-resolution microstructured TE array consisting of 1350 pixels (0.25 $mm^2$ per pixel) on a fabric frame to meet the requirements of wearable XR systems. This array can be integrated into prosthetic limbs, capturing detailed temperature and pressure images (Figure 30e). The collected data, monitored via the reconstructed map, corresponded closely with the pixel colors in the distribution maps (Figure 30f).

Lastly, the most efficient and ideal approach involves extracting distinct electrical signals for different stimuli within a single material, which generates electrical signals with varying slope and response times.[773,774] However, it is challenging to distinguish the response from each external stimulus without the assistance of AI technology. Regarding this issue, a recent study has proposed an ion-conducting sensor to independently distinguish strain and temperature (Figure 30g).[179] The sensor leverages the inherent physical properties of the ion-conductor to separately measure the effects of mechanical stimuli and thermal stimuli. The electrical properties of the ion-conductor were changed in response to variations in both strain and temperature, enabling the sensor to clearly identify the response to each stimulus (Figure 30h). In detail, the charge relaxation time ($\tau$) serves as an intrinsic variable for temperature measurement, remaining constant regardless of strain. In contrast, normalized capacitance ($C/C_0$) acts as an extrinsic variable sensitive to strain changes. By normalizing capacitance against a reference value, the influence of temperature can be mitigated, thereby facilitating effective strain detection. Thus, the sensor array with the ion-conductor demonstrates the potential to effectively collect two types of stimulus information, enabling the decoupling of temperature and strain distributions at contact points through mapping techniques (Figure 30i).

In this way, when external stimuli are applied to the skin, multiple sensations are transmitted simultaneously. These multimodal input devices exhibit promise for wearable XR technology by enabling the simultaneous collection of multiple types of information from a single device, effectively mimicking human sensory capabilities. Advanced design capabilities and a thorough understanding of the underlying mechanisms of materials are essential for multimodal input devices to accurately and simultaneously detect various physiological signals from the body.

### 5.3. Integrated Sensory Feedback and Input Devices

While individual feedback or input technologies are important, as discussed above, integrated sensory feedback and input systems are essential for immersive XR applications. By combining feedback and input functions, it is possible to create closed-loop systems that provide precise stimulation and sensing simultaneously.[156,238] These systems detect the user response to specific haptic stimuli, enabling the delivery of more accurate and tailored feedback signals. Furthermore, the feedback itself helps users adjust their actions, allowing them to fine-tune their behavior for better manipulation of the device.[177] Most importantly, the integration of sensory feedback and input functions within a single device is indispensable for effective communication among multiple individuals in XR applications. In the process where user actions are detected, processed, and transmitted as feedback to others, the feedback and input functions must operate seamlessly. For comprehensive understanding, this chapter provides an overview of integrated sensory feedback and input devices, emphasizing their importance in enhancing interaction and communication in XR environments.

To combine sensory feedback and input functions, the most common strategy is to integrate individual feedback and sensing modules into a single device. For example, a wearable system could be integrated with multiple sensors and feedback actuators to recognize hand motions and provide mechanical stimuli.[221] The system utilized a triboelectric mechanism to


https://doi.org/10.1021/acs.chemrev.4c00966
Chem. Rev. 2025, 125, 11567−11665

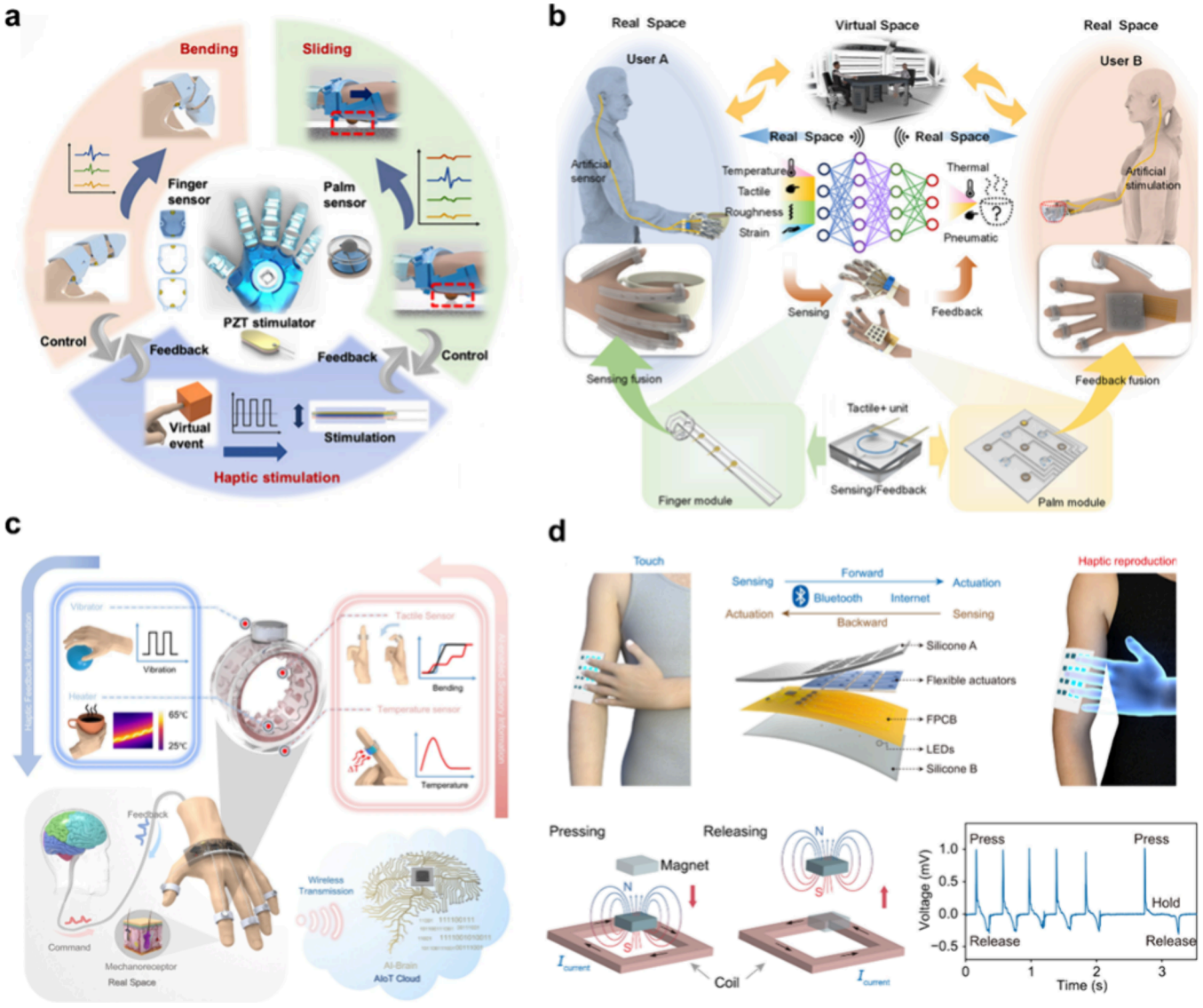


**Figure 31.** Integrated sensory feedback and input devices. (a) Wearable system integrated with vibrational feedback actuators and multiple sensors that measure bending and sliding motions. Reproduced with permission from ref 221. Copyright 2020 The American Association for the Advancement of Science under CC BY-NC 4.0 license https://creativecommons.org/licenses/by-nc/4.0/. (b) Haptic interface employing TENG-based units with feedback and sensing functions for immersive somatosensory sensations. Reproduced with permission from ref 238. Copyright 2022 American Chemical Society. (c) Ring-type integrated feedback and input device for mechanical and thermal sensations. Reproduced with permission from ref 253. Copyright 2022 Springer Nature under CC BY 4.0 license https://creativecommons.org/licenses/by/4.0/. (d) Schematic illustration of wireless touch transmission through mechanohaptic interface with feedback and input features based on electromagnetic mechanism. Reproduced with permission from ref 156. Copyright 2022 The American Association for the Advancement of Science under CC BY 4.0 license https://creativecommons.org/licenses/by/4.0/.

measure the bending and sliding motions of the hand (Figure 31a). A curved triboelectric sensor captured finger bending through the electric signals generated by contact and separation between the sensor and the finger, while a hemispherical sensor with four contact points detected lateral interactions of the palm. For mechanical feedback, the system employed piezoelectric materials. PZT actuators generating vibrations provided mechanical feedback corresponding to specific VR scenarios. As a result, the integration of hand movement recognition and vibrational feedback enabled precise motion control and immersive interaction in VR environments. This system was successfully demonstrated in an interactive VR baseball application, highlighting its potential for enhancing user experience.

Wearable XR interfaces can be designed to provide multimodal feedback and sensing functions for realizing immersive somatosensory sensations. One study has proposed a wearable device that simultaneously collected mechanical and thermal information while providing mechano- and thermo-haptic feedback.[238] In this study, the developed TENG-based single unit with feedback and sensing capabilities could be customized and integrated according to specific purposes and target body parts, resulting in a compact and multifunctional device (Figure 31b). The electrical signals generated by the TENG enabled various motion sensing, such as strain, pressure, and vibration from the user and the external environment. Notably, it also sensed the actuation of the device, allowing for precise control without additional sensors.


https://doi.org/10.1021/acs.chemrev.4c00966
Chem. Rev. 2025, 125, 11567−11665

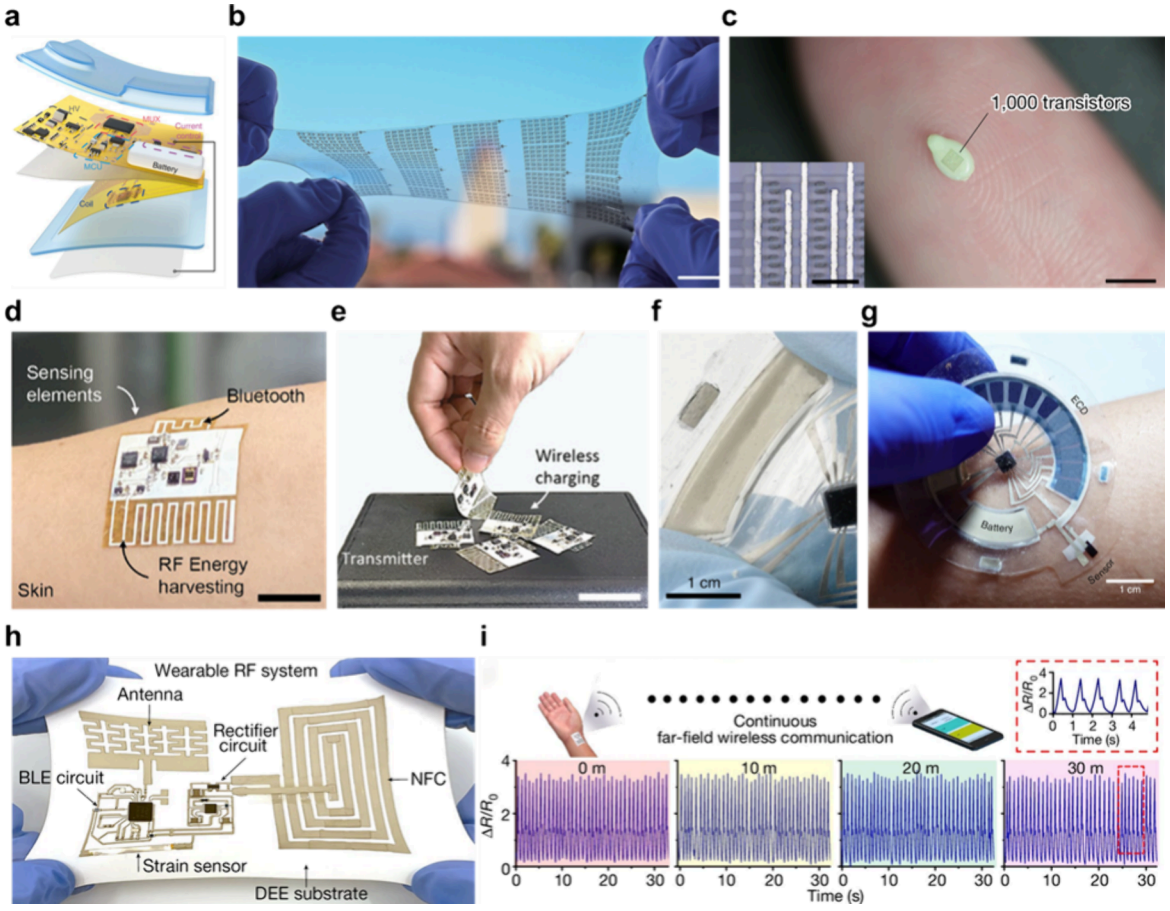


**Figure 32.** System-level integration for untethered soft wearable XR devices. (a) Electronic system including various components based on commercial f-PCB technology. Reproduced with permission from ref 242. Copyright 2022 Springer Nature. (b) Optical image of intrinsically stretchable transistors (scale bar: 3 cm). (c) Digital image of stretchable transistors with high integration density on a tiny object (scale bar: 3 mm). Inset: optical microscope image of the transistor array (scale bar: 50 $\mu$m). Reproduced with permission from ref 778. Copyright 2024 Springer Nature. (d) Skin-integrated electronics equipped with a thin-film antenna for wireless charging (scale bar: 15 mm). (e) Wireless charging through a radio frequency wave transmitter (scale bar: 20 mm). Reproduced with permission from ref 193. Copyright 2021 Wiley-VCH. (f) A stretchable battery composed of soft and ink-based materials under large deformation (scale bar: 1 cm). (g) An on-skin electronic device integrated with a stretchable battery (scale bar: 1 cm). Reproduced with permission from ref 792. Copyright 2022 Springer Nature. (h) Strain-invariant stretchable electronic device including various wireless communication components. (i) Demonstration of stable wireless communication of the device during body movements. Inset: magnified view of the collected signals. Reproduced with permission from ref 776. Copyright 2024 Springer Nature.

Moreover, a thermistor embedded in the unit measured the temperature of contacted objects in the real world. From a feedback perspective, air chambers embedded in certain positions provided pressure and kinesthetic feedback based on pneumatic actuation, while resistive heaters delivered thermohaptic feedback. This approach, utilizing a single unit with both feedback and sensing functions, facilitated a compact form factor and seamless fusion of the two functionalities.

Similarly, another study reported a ring-type integrated feedback and input device for mechanical and thermal sensations (Figure 31c).[253] The authors integrated pyramid-structured triboelectric sensors on the inner surface of the ring to collect tactile signals generated by finger movements and embedded pyroelectric sensors on the outer surface to measure the temperature of external objects. Both sensors, employing triboelectric and pyroelectric effects, operated through a self-powered mechanism, significantly reducing power requirements and enhancing usability. Furthermore, gesture and object recognition were achieved by processing tactile signals via voltage integration and ML techniques. In addition, the integration of a vibration motor and a resistive heater in the device allowed for the provision of multimodal feedback, such as vibrational and thermal stimulation. As a result, the miniaturized ring-type device, with combined multimodal feedback and sensing features, enabled the transmission of mechanical and thermal information from real objects interacted with by the user to VR environments, allowing others to experience these sensations.

The most ideal approach to integrating sensory feedback and input features is to design a component that simultaneously performs actuation and sensing through a single mechanism. For instance, an actuator has been developed that incorporates both mechanical feedback and sensing functions.[156] This actuator, composed of an elastomeric frame integrated with a magnet and a conductive coil, utilized an electromagnetic mechanism to achieve vibrational actuation and tactile sensing simultaneously. In detail, when current was applied to the coil, the generated alternating magnetic field induced vibrational motions of the magnet, resulting in mechanohaptic feedback. Conversely, when external forces deformed the actuator, the movement of the magnet induced a current in the coil, allowing for the detection of touch or contact as a tactile


https://doi.org/10.1021/acs.chemrev.4c00966
Chem. Rev. 2025, 125, 11567−11665

sensor. Since these feedback and input features originated from electromagnetic induction, the device could be designed with a simple structure and a single operating mechanism. The authors integrated the actuators into an array to fabricate a haptic interface for wireless touch transmission, which successfully demonstrated the sharing of tactile sensations between two users (Figure 31d).

These integrated sensory feedback and input devices can collect various sensory information from the user and deliver it to other users, enabling realistic experiences and effective interactions in XR applications. For the advancement of wearable XR technology, the integration is crucial and requires a comprehensive understanding of materials and mechanisms, as well as careful consideration of system design.

## 6. SYSTEM-LEVEL INTEGRATION FOR UNTETHERED SOFT WEARABLE XR DEVICES

The evolution of XR technologies has driven a growing demand for highly immersive and real-time interaction environments. Achieving this goal requires seamless system-level integration, particularly in wearable devices that offer untethered and wireless operation without compromising performance or user experience. For soft wearable haptic XR interfaces, the devices must be lightweight, imperceptible, and comfortable to wear for long-term use while maintaining robust functionality. However, the process of collecting diverse signals via sensory input components, processing them using computational units, generating feedback through actuators, and wirelessly transmitting or displaying information, necessitates numerous components. Therefore, system-level integration focuses on combining the various subsystems, such as actuators, sensors, electronic circuits, power management units, and wireless communication modules, into a compact device. The overarching goal is to balance these components to minimize bulk while maximizing functionality and efficiency. The complexity arises from the need for simultaneous attention to both hardware and software, addressing how signals are processed, how power is delivered, and how information is transmitted wirelessly without latency. Additionally, integrating these components on a soft and flexible substrate requires careful consideration of material properties, stretchability, and mechanical resilience.

### 6.1. Electronic System Design

The design of electronic systems for soft wearable XR devices demands a multidisciplinary approach, combining advances in microelectronics, materials engineering, and embedded systems. The electronic system needs to be capable of acquiring data from various sensing components, processing the data in real time, and providing the necessary output through actuators that generate haptic feedback. At the core of the system is a processing unit, typically an MCU or more advanced system-on-chip, that coordinates signal processing, power management, and wireless communication. The operation of the processing unit requires additional electronic components, such as resistors, capacitors, transistors, and integrated circuit (IC) chips. The system design to integrate these components into soft form factors for wearable devices is essential because most electronic components are rigid.

One representative approach is to incorporate electronic elements into rigid island structures on flexible or stretchable substrates. This method, based on commercial f-PCB technology, allows for the rapid and cost-effective integration of advanced semiconductor technologies with soft sensors and actuators. The electronic system, designed for wireless tactile sensing and feedback, should include various modules such as an MCU, a power driver module, a battery, and a wireless charging coil (Figure 32a).[242] Despite diverse electronic modules, the system remained compact, lightweight, and flexible. To further improve wearability, the thickness of the substrate can be reduced. For instance, ultrathin electronic systems integrated with f-PCBs under 10 $\mu$m in thickness have been reported for biosignal sensing applications.[775] In addition, by utilizing a stretchable substrate, it was possible to construct systems where the overall structure was stretchable, despite the individual components being rigid.[776]

However, significant challenges persist as most electronic components remain rigid and thicker than the substrate, highlighting the inherent limitations of merely improving the substrate. Therefore, developing stretchable components is inevitable, particularly focusing on fabricating the stretchable transistor as the foundation of ICs. For instance, a stretchable transistor array was developed, where the semiconductor, dielectric, and conductor were all composed of intrinsically stretchable materials.[777] Through significant advancements in materials engineering and process scalability, the authors developed an intrinsically stretchable IC with a high density of 100,000 transistors per square centimeter.[778] The stretchable transistor array maintained stable operation even under large deformation (Figure 32b). Additionally, the high integration density was achieved by placing transistors on a tiny object (Figure 32c). Based on the stretchable transistors, the group fabricated ICs with switching frequencies in the MHz range, demonstrating the potential for high-frequency signal acquisition and on-skin computing. Further advancements in the integration of stretchable transistors will be critical for the future development of soft wearable devices. Such innovations could lead to new applications in high-performance computing directly on the skin, enabling seamless and immersive interaction with digital environments.

### 6.2. Power Management

Achieving untethered operation of skin-integrated XR interfaces requires a wearable, efficient, and robust power supply to support the electronic systems. In most wearable electronics, DC power is preferred due to its compatibility with electronic systems including microprocessors, sensors, and displays. DC power is easily regulated and can be efficiently supplied via compact battery systems. However, AC power is also necessary for specific components, such as vibration-generating actuators, thermal management devices controlled by pulse-width modulation, and wireless communication modules. Therefore, system-level integration for power management needs to be flexible, allowing conversion between DC and AC power sources based on the specific requirements of XR systems. Additionally, these power management systems should be designed with energy harvesting and storage elements in mind to maximize efficiency and sustainability in wearable applications.

Energy harvesting devices offer a promising solution for extending the operational time of skin-integrated XR systems, reducing dependence on bulky batteries. These devices capture ambient energy from the environment and convert it into usable electrical power. Several energy harvesting techniques have been explored for wearable devices, including TE,[779,780] piezoelectric,[781−783] triboelectric,[784−786] and photovol-


https://doi.org/10.1021/acs.chemrev.4c00966
Chem. Rev. 2025, 125, 11567−11665

taic[787,788] methods. These approaches generate electrical power from environmental sources such as temperature gradients, mechanical deformations, body movements, or solar energy, thus enhancing the versatility of wearable devices. However, power management systems must be carefully designed based on whether the generated power is DC or AC. For instance, energy harvesters utilizing piezoelectric or triboelectric techniques generate AC power, requiring converters to rectify the AC voltage into DC voltage for most electronic applications.

Another wireless, battery-independent method involves radio frequency identification (RFID) technology. Typically used for tracking and identification, RFID enables both power and data transfer through inductive coupling between two conductors. Specifically, near-field communication (NFC), a type of RFID, operates at a high-frequency band of 13.56 MHz and facilitates bidirectional communication within a short distance of 4 cm. Although continuous power supply is challenging due to the short distance, NFC can activate sensors and collect data when the power source, such as a mobile phone or NFC reader, approaches the device. Another method of achieving an untethered system involves integrating a wirelessly chargeable.[193] An on-skin device equipped with a thin-film antenna and an AC/DC conversion module could be wirelessly charged using radio frequency energy (Figure 32d). Near a 915 MHz transmitter, operational energy was retained via wireless charging techniques (Figure 32e).

Energy storage devices are also fundamental components for untethered wearable XR interfaces. Traditional Li-ion and Li-polymer batteries are widely used in wearable electronics due to their high energy density and relatively small form factor. However, when integrated into skin-integrated systems, these batteries face challenges such as rigid form factors, safety concerns, and limited lifespan. To address these limitations, research has increasingly focused on supercapacitors,[789−791] and stretchable batteries.[203,792,793] A stretchable battery was developed by applying a segmented design that positioned active cell arrays on a stretchable substrate with stretchable electronic circuits based on Li-ion battery technology, resulting in high areal capacity and mechanical stretchability.[203]

Another approach involves intrinsically stretchable materials to fabricate batteries for skin-integrated electronic systems. A stretchable battery was developed with all key components such as current collector, anode, cathode, and separator, made from soft, ink-based materials.[792] This battery was encapsulated in a soft elastomeric layer, enabling it to withstand significant deformation while maintaining stable performance (Figure 32f). Due to its stretchability and electromechanical stability, this battery was well-suited for integration into wearable electronic systems (Figure 32g). These advancements point to the future of stretchable and durable energy solutions for skin-integrated devices.

### 6.3. Wireless Communication

Wearable XR systems typically incorporate wireless communication modules. For an immersive and seamless user experience, integrating technologies including wireless fidelity (WiFi), Bluetooth low energy (BLE), and NFC is important to enable wireless data transmission without cumbersome wires. These communication technologies must be carefully selected and optimized according to factors such as power consumption, data transmission speed, range, and system flexibility. Effective wireless communication allows wearable XR devices to interact with external systems, synchronize with digital platforms, and maintain real-time data exchange. Each technology presents distinct advantages and limitations, making their optimal integration crucial for enhancing the overall user experience in XR systems.

WiFi is one of the most widely used wireless communication technologies, providing high data transmission rates and long-range connectivity. Operating on several frequency bands, including 2.4 and 5 GHz, WiFi supports data-intensive applications in XR environments. In skin-integrated XR systems, WiFi enables real-time data synchronization with external servers, cloud platforms, and other connected devices. However, WiFi typically consumes more power than other technologies, making it less ideal for energy-constrained wearable devices. Balancing power consumption with performance remains a significant design challenge, despite the high-bandwidth capacity and communication speed of WiFi.

BLE, on the other hand, is widely used in wearable electronic systems due to its low power consumption and relatively long communication range of up to 100 m. Operating in the 2.4 GHz band, BLE supports low-latency communication for skin-integrated devices, which need to conserve power while maintaining continuous connections with external devices such as smartphones or computing devices. This technology enables real-time communication between wearable sensory input devices and other systems that offer immediate data display or processing capability for data sets.

NFC operates at 13.56 MHz and supports communication over short distances, typically just a few centimeters. While NFC is not designed for continuous data transmission like WiFi or BLE, it offers unique advantages for wearable XR systems. NFC can operate using minimal power provided by an NFC reader, making battery-free systems feasible. Despite its limitations in communication range and data rate, NFC can complement other wireless technologies by providing on-demand interactions in wearable systems.

Another important component in wireless communication is the antenna, which must be designed with the appropriate resonance frequency based on the frequency band of the signal. However, in stretchable devices, dynamic deformations of the skin can cause frequency shifts, compromising communication quality and efficiency. To resolve this issue, strain-invariant stretchable electronics have been developed to maintain their original radio frequency characteristics even under deformation (Figure 32h).[776] The stretchable antenna was fabricated on a substrate consisting of dielectro-elastic materials with variable permittivity, preventing frequency shifts when stretched. Additionally, this technology could be easily integrated with existing stretchable technologies, such as stretchable circuits and wearable sensory input devices. The strain-invariant property enabled stable wireless communication at distances longer than 30 m, even with wrist movements (Figure 32i). As a result, these advancements enabled the system-level integration of wireless communication technologies in soft wearable XR systems, and it is essential to understand the characteristics of each technology and apply them according to the specific needs of the XR devices.

## 7. AI TECHNIQUES FOR SOFT WEARABLE XR DEVICES

AI techniques play a pivotal role in the functionality of wearable devices by converting large quantities of raw sensory input data into actionable and meaningful insights. This


https://doi.org/10.1021/acs.chemrev.4c00966
Chem. Rev. 2025, 125, 11567−11665

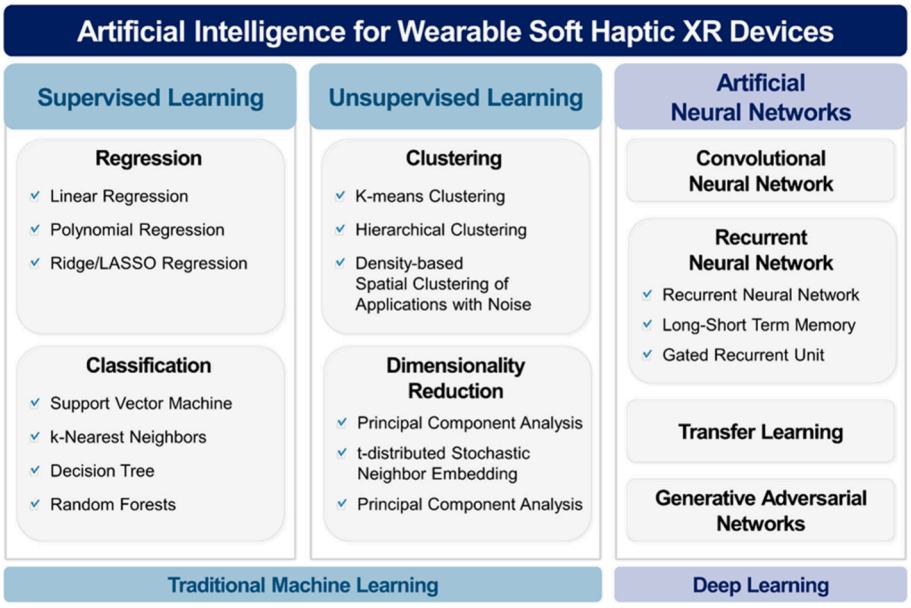


**Figure 33.** Overview of AI technologies for soft haptic XR devices. Various algorithms for supervised and unsupervised learning in traditional ML and diverse artificial neural networks for deep learning.

conversion is crucial in a range of applications such as health monitoring systems, medical devices, and entertainment applications using interactive XR environments. To enhance both the functionality and the user experience, the rapid and accurate interpretation of sensory input data should be accomplished. We explore various advanced techniques in signal processing, traditional ML technologies, and neural network-based deep learning, effectively managing complex data from physiological and environmental sensors (Figure 33). These methods not only improve the adaptability and responsiveness of wearable haptic devices but also enable them to tailor their responses based on individual user behavior patterns.

### 7.1. Feature Extraction and ML Technologies

Signal processing is the initial stage of handling data in wearable haptic devices for extracting usable components from input signals and generating realistic feedback signals. Fourier and Wavelet transforms can be utilized for this purpose, providing a means to analyze complex time series data streams such as ECG, EEG, EOG, or EMG signals based on their constituent frequencies. These methods enhance the detection and analysis of user intention for wearable haptic devices requiring continuous monitoring and immediate feedback. The ability to accurately process and analyze these signals in real time is necessary for haptic XR applications, such as adjusting user experiences according to intentions detected through physiological changes and providing immersive feedback based on environmental interactions.

Statistical methods are applied for further refinement and interpretation of data. These methods offer useful insights into the underlying trends of data, facilitating predictive analysis. For example, regression analysis helps identify relationships between input and output data, allowing for the prediction of outcomes based on input data. Hypothesis testing evaluates the significance of observed patterns, ensuring that detected trends are not due to random chance. These techniques help in understanding the fundamental relationships in data produced in XR environments. While traditional statistical approaches provide basic insights, the complex and massive data generated by wearable XR interfaces necessitate more advanced analytical methods for deeper interpretation.

ML methods offer a transformative approach to making decisions based on input data and identifying patterns that are not easily detectable through traditional statistical methods. These methods, represented by supervised and unsupervised learning, are being utilized to process and interpret the data generated by wearable XR devices, depending on the distinct advantages of each approach.

Supervised learning, a primary ML method, trains a model using labeled data, pairing each input with a corresponding label to teach the model how to accurately map inputs to expected outputs. For instance, support vector machines (SVMs) are algorithms that determine the ideal hyperplane for partitioning data points into various classes with the maximum margin. This ability makes SVMs particularly effective for classification such as distinguishing between different physical activities or identifying spoken sentences using subtle throat movements without voice signals.[567] The flexibility of SVMs, by using kernel functions, enables them to handle linear and nonlinear data, making them versatile for various types of signals, which originate from user interactions in XR environments. However, SVMs can demand significant computational resources, particularly when dealing with large data sets, and necessitate precise hyperparameter tuning and appropriate kernel selection for best results.

Another ML method is k-nearest neighbors (kNN) for supervised learning. This nonparametric approach determines the class of data points by considering the majority class from their "k" nearest neighbors within the feature space. This simplicity makes kNN a promising tool for wearable XR interfaces where quick and straightforward classification is required, such as real-time motion and gesture recognition. For instance, the kNN algorithm was integrated with soft sensory foams to classify various deformation types and predict the magnitude of the types.[794] This technique facilitated recognizing different gestures based on mechanical deformation induced by movements, enabling intuitive control of XR


https://doi.org/10.1021/acs.chemrev.4c00966
Chem. Rev. 2025, 125, 11567−11665

devices. One of the notable advantages of kNN is that it requires no prior assumptions about how the data is distributed, which allows it to be flexible and effective in various scenarios. Nevertheless, the performance of kNN can be affected by the choice of "k" and it can become computationally expensive as the size of the data set increases. In addition, this algorithm is sensitive to imbalanced data, where the majority class can dominate the classification process, leading to biased results.

Random forests algorithm, an ensemble learning method, combines multiple decision trees to enhance classification accuracy and mitigate overfitting. Each tree within the forest is trained on a randomly selected subset of data, and the aggregate of all tree predictions constitutes the desired output. This methodology strengthens the robustness and precision of the learning model, making random forests particularly suitable for complex data from various sensory input devices. For example, random forests can be utilized for activity recognition to accurately classify user activities, such as analyzing sleep–wake stages using data from the movement of the wrist.[795] Nonetheless, despite their ability to reduce overfitting compared to single decision trees, interpreting the results from a large ensemble of trees can be challenging, complicating the understanding of the decision-making process of the model.

Unsupervised learning differs from supervised learning by handling unlabeled data. The goal is to find hidden patterns or intrinsic characteristics in data without predefined labels. Since only input data without labels is needed, unsupervised learning is particularly useful in exploratory data analysis and situations where labeled data is scarce or expensive to obtain. With wearable electronics, unsupervised learning methods are widely utilized for dimensionality reduction and clustering.

Principal component analysis (PCA), one of the unsupervised learning techniques, is employed for dimensionality reduction to simplify intricate data. Through this algorithm, the data is transformed into a new coordinate system, with the first coordinate, or first principal component, capturing the highest variance, followed by the second coordinate with the next largest variance, and so on. This dimensionality reduction facilitates refining data, reducing noise, and highlighting the most important features. Because of this, PCA can be used to preprocess data before implementing other ML algorithms and deep learning algorithms that are explored in the next section.[796] By retaining only the most significant components, PCA helps in improving the efficiency and accuracy of the subsequent learning models. However, PCA assumes linearity in the data and may not capture nonlinear relationships effectively.

Beyond PCA, clustering algorithms such as K-means and hierarchical clustering are fundamental approaches in unsupervised learning. K-means clustering partitions data into K-distinct clusters based on distance measures, typically utilizing Euclidean distance. Each data point is mapped to the nearest cluster center, and the centers are repeatedly adjusted until they converge. This approach is applicable for analyzing chemical information obtained from wearable interfaces and for detecting anomalies within data clusters.[797,798] Despite its simplicity and efficiency, this method requires the a priori specification of the number of clusters, which may pose a limitation in applications where the optimal number of clusters is unknown.

Hierarchical clustering constructs a clusters tree through either an agglomerative (bottom-up) or divisive (top-down) strategy. Hierarchical clustering, unlike K-means clustering, operates without requiring the number of clusters to be specified beforehand. This flexibility makes it particularly advantageous for exploratory data analysis, as it naturally organizes data into a hierarchy. For example, it can be used to analyze accelerometer activity profiles as biomarkers to evaluate health conditions.[799] However, hierarchical clustering is computationally intensive, typically with a complexity of $O(n^3)$, making it less suitable for large data sets. Therefore, this approach often needs to be combined with efficient data structures, heuristic methods, and other optimizations or approximations to improve its scalability and performance.

Furthermore, the integration of feature extraction and ML techniques can result in the development of more robust and accurate models. For instance, unsupervised methods such as PCA and clustering can be employed to preprocess data, thereby reducing its complexity before data is delivered to other learning algorithms.[197] This preprocessing step enhances the performance of the models by emphasizing the most relevant features and minimizing noise. In the context of XR haptic interfaces, this enables more accurate detection of user actions, improved prediction of intention, and more efficient operation of the devices, providing users with reliable feedback and recommendations.

The incorporation of these ML techniques paves the way for deep learning, which is explored in the next chapter. This section delves into the utilization of deep neural networks to further enhance the capabilities of wearable XR interfaces.

### 7.2. Deep Learning

Deep learning is a subset of ML, especially leveraging neural networks with a large number of layers to model complex patterns in data. This technique is beneficial for wearable XR interfaces, where data can be high-dimensional and intricate. Deep learning models, including convolutional neural networks (CNNs) and recurrent neural networks (RNNs), have proven highly effective in managing the complex and dynamic data streams generated by wearable interfaces.

CNNs are highly effective at managing spatial data, making them particularly well-suited for applications involving image or video inputs. Convolutional layers within these networks facilitate the automatic and adaptive learning of spatial feature hierarchies, enhancing the efficacy of the model in tasks such as gesture recognition and facial expression analysis. CNNs can process raw sensor data from cameras or other vision systems to detect and interpret user movements, improving the interactivity and functionality of XR interfaces. Although the use of CNNs in skin-interfaced wearable devices is less prevalent, primarily due to the difficulty in obtaining image or video data from these devices, recent research suggests their significant potential in this area. For instance, a skin-integrated facial interface was developed based on CNN models, which converted facial strain signals and vocal vibrational signals into personalized emotional context information.[574]

RNNs, including long short-term memory (LSTM) networks, are designed to process sequential data, which is prevalent in wearable devices that continuously monitor user activities over time. Due to the ability to learn temporal dependencies, these models are suitable for activity recognition, health monitoring, and real-time feedback systems. However, traditional RNNs encounter difficulties with long-


https://doi.org/10.1021/acs.chemrev.4c00966
Chem. Rev. 2025, 125, 11567−11665

term dependencies because of the vanishing gradient problem. LSTMs mitigate this issue through a unique cell structure that enables the retention of information over extended periods. The advent of LSTMs has facilitated the analysis of time-series data, making it more effective and insightful. For example, LSTMs have been employed to identify complex motion patterns from a single skin sensor in real time, demonstrating their capability to handle dynamic and sequential data efficiently.[542] The models can also be utilized to analyze patterns in various types of data, including time-series vibrational signals, temperature variation, and chemical information.

Generative adversarial networks (GANs) offer a promising approach to deep learning. GANs consist of a generator and a discriminator, two neural networks in opposition, that collaborate through competition to create data that becomes progressively more lifelike. Despite significant advancements in generating realistic data, the application of GANs in skin-interfaced XR devices remains relatively underexplored. It is postulated that their potential in wearable XR interfaces lies in their ability to enhance data augmentation, simulate realistic sensory input data, and improve the robustness of models against diverse environmental conditions. However, several challenges hinder their widespread adoption in this domain. The integration of GANs with skin-interfaced devices requires sophisticated algorithms to interpret and generate multimodal data captured by these systems. Unlike traditional image data, skin-interfaced wearable sensory input devices collect various types of data, including electrical, mechanical, and biochemical information. Additionally, the paucity of large, high-quality data sets specifically tailored for wearable devices limits the effective learning of GANs. Despite these constraints, the future integration of GANs with skin-interfaced XR devices holds significant promise, potentially revolutionizing the field by enabling more sophisticated, accurate, and adaptive user interactions.

Transfer learning is another impactful technique in deep learning that enables models to use knowledge from one task to enhance learning and performance in another task. This method is particularly beneficial in contexts with limited labeled data, such as wearable XR interfaces, where data can be complex and insufficient. Transfer learning facilitates the fine-tuning of pretrained models on extensive data sets to achieve specific goals like gesture recognition[122] or health monitoring,[800] using data from wearable sensory input devices. This approach not only reduces the need for large amounts of labeled data but also enables fast learning and better generalization to unseen data. For example, research on developing skin-integrated devices with unsupervised learning schemes for hand task recognition exemplified the potential of transfer learning. The research demonstrated rapid adaptation to arbitrary tasks using various hand motions by translating skin stretches into proprioceptive signals.[122] This approach highlights the transformative capability of transfer learning in advancing the functionalities of wearable XR interfaces.

Integrating deep learning into skin-interfaced XR devices improves accuracy and reliability, enabling sophisticated user interactions. By utilizing powerful pattern recognition capabilities, these devices provide intuitive feedback, enhancing engagement and satisfaction in diverse fields such as healthcare, education, and entertainment. Deep learning also facilitates the development of personalized systems that adapt to individual user preferences, delivering customized feedback. Overall, deep learning advances soft wearable XR devices, leading to intelligent, adaptive, and user-centric technologies that enrich daily life.

### 7.3. Real-time Feedback and Recognition

Real-time feedback and recognition are critical components of interactive devices such as soft wearable XR interfaces. The ability to process and respond to user inputs instantaneously is essential for providing immersive user experiences. High latency, especially when it exceeds human neural reaction time typically around 150−250 ms, can lead to delays in response, causing discomfort or disorientation during interactions with VR environments.[801] Excessive latency can result in a break in the sense of presence, making the VR environment feel less real and engaging. Real-time processing is also important for adaptive systems, where the device needs to adjust its responses based on user action and environmental context. Without this capability, the device may fail to provide appropriate assistance or feedback, diminishing its utility and user satisfaction. To address these challenges, data processing techniques, including ML and deep learning algorithms, need to be optimized for latency reduction.

Optimizing the algorithms for low latency is an important strategy for wearable XR devices with limited computing resources. Optimization involves designing and fine-tuning learning models to ensure they operate rapidly without compromising accuracy. A key optimization technique is model pruning, which systematically removes redundant parameters from neural networks to enhance efficiency. By eliminating unnecessary elements, computational resources are conserved, resulting in faster data processing. Another significant method is quantization, which reduces the precision of numerical values in calculations, typically converting 32-bit floating-point numbers to 8-bit integers. This reduction in precision facilitates efficient data processing and decreases memory usage, as lower precision numbers require less storage and processing resources. However, it is crucial to maintain accuracy levels appropriate for the specific application, ensuring that the reduced precision does not adversely affect the performance of the device.

Therefore, these techniques for lightweight architectures are specifically designed to balance speed, accuracy, and resource efficiency, making them suitable for real-time applications on devices with constrained processing power and battery life. One example was highlighted in the study of wearable silent speech interfaces utilizing textile strain sensors integrated into a smart choker. The group introduced an ultrasensitive strain sensor capturing subtle throat movements for decoding silent speech. To process the data generated by high-sensitivity sensors, they developed a lightweight 1D CNN with residual blocks. The blocks included pairs of convolutional layers that were finely tuned to handle the high information density of the speech signals. This approach ensured that essential temporal features could be captured while the computational demands were minimized. As a result, the neural network model was optimized for real-time speech recognition, reducing the computational load by 90% while maintaining a high accuracy of 95% in speech decoding.[802]

Real-time operation is indispensable for the effectiveness of soft wearable XR interfaces, as it ensures seamless and immersive user interactions. The development of advanced optimization techniques will further enhance user experiences. Additionally, the emergence of hardware with high-perform-


https://doi.org/10.1021/acs.chemrev.4c00966
Chem. Rev. 2025, 125, 11567−11665

ance processing capabilities will facilitate the real-time operation of XR devices in a compact form. These advancements will overcome latency challenges, providing users with seamless experiences that fully exploit the potential of wearable technology.

## 8. APPLICATIONS WITH SOFT WEARABLE XR DEVICES

Recent advancements in wearable XR devices and the integration of AI have led to a wide range of XR-based applications, driving innovative changes across multiple sectors. XR technologies provide users with immersive virtual experiences without the constraints of physical space, allowing for the simulation of various situations that may be dangerous, rare, or impossible to encounter in the physical world. Thereby, these attributes make XR applications particularly suitable for work assistance,[206,803−807] training,[808] education,[221,412,414,809−812] medical devices,[208,813−818] and entertainment.[209,221,412,414,819−825] This chapter explores the potential of XR technology through experimental demonstrations highlighting its practical applications across various fields. Particularly, this chapter will examine potential practical applications of wearable XR devices, which are currently being developed in simplified forms at the laboratory level, in conjunction with visual devices. Table 15 summarizes AI-assisted wearable XR systems along with the practical applications in which these integrated systems are being actively explored.

### 8.1. Work Assistance

As previously discussed, soft wearable XR devices can be applied to different areas of the human skin, providing multiple forms of feedback. When integrated with devices such as VR glasses that deliver high-resolution visual information, they can produce a synergistic effect (Figure 34a).[206] For example, teleoperation is a technology that allows operators to remotely interact with equipment located in distant or physically inaccessible and hazardous areas (Figure 34b).[209,820] This technology enables operators to perform tasks in real-time while remaining in a safe location, making it particularly valuable in high-risk environments such as offshore sites, space, and nuclear power plants. Robotic equipment can mirror human movements in remote or virtual environments using wearable input devices or sensors, while feedback systems provide real-time information such as the forces applied in the virtual environment or the outcomes from the actions of robots. This allows users to intuitively understand how their inputs are translated and reflected in the remote environment. The integration of VR glasses and skin-interfaced wearable XR devices greatly enhances user immersion and accuracy in remote tasks by delivering real-time visual and tactile information, enabling precise tasks such as medical sample collection in VR environments or the manipulation of robotic arms.

Similarly, a robotic arm system for remotely controlling industrial manipulators has been developed through visual and haptic feedback devices to improve operator efficiency (Figure 34c).[805] This system provided various forms of haptic feedback, including virtual guiding forces, virtual resistance, and real-time interaction forces, which significantly reduced operator workload while enhancing accuracy and efficiency in complex task environments. In particular, the system offered a realistic remote control environment using VR devices. Experiments involving grab-and-place tasks demonstrated that the system can significantly reduce task duration and operator fatigue. Furthermore, the haptic feedback minimized errors during tasks and thereby enhanced productivity by providing proper feedback to the operator. This integrated visual and haptic feedback system is expected to make a substantial contribution to improving productivity and safety in remote operation tasks.

Moreover, an intuitive remote robotic welding system has been proposed using MR technology (Figure 34d).[804] This MR-based technology was particularly useful in fields such as surgery, repair, and manufacturing, as it allows workers to instantly access necessary information and guidance, thereby improving both efficiency and precision. The proposed system was able to reflect the hand movements of users in the actions of the welding robot, allowing the center point of the tool to be controlled based on spatial velocity. Introducing MR-based fixtures, the system provided visual and haptic guidance to the user and prevented collisions during welding. Experiments conducted with unskilled welders demonstrated a performance improvement of over 56% compared to cases without the MR-based fixture. The system reduced the time required for torch alignment while enhancing task precision and stability. Additionally, the remote robotic welding system enables unskilled users to perform professional welding tasks, showing promise in reducing training costs and duration.

Meanwhile, remote surgical mentoring systems that utilize AR platforms are also highly beneficial in enhancing surgical efficiency.[826,827] Given that medical professionals responsible for patient care often lack adequate opportunities for practice, there is a critical need for technologies that can help minimize errors. In this regard, AR systems enabled medical professionals to wear headsets that provide a real-time first-person view of the surgical site, allowing remote experts to overlay 3D surgical guidance that the local medical team can visually follow (Figure 34e).[803] This facilitates real-time visualization of the position of surgical instruments and target areas during surgeries. In particular, this system proves invaluable during emergency procedures such as tracheotomies, where a remote mentor can correct the tool usage of operators or incision locations in real-time and clearly indicate critical anatomical structures. This system enables safer and more efficient surgical procedures, even in urgent situations. In extreme cases, these technologies empower laypersons to administer first aid in critical situations, serving as a vital tool to help ensure that emergency patients do not miss the golden hour when immediate transportation to a hospital is not possible.

### 8.2. Education

Education is also one of the important areas that can be realized through wearable XR devices. In the field of education, while hands-on experience is invaluable, many educational activities are frequently confined to audiovisual materials due to time and environmental constraints. However, the XR technologies enable the virtual reproduction of situations that are difficult to experience physically, providing learners with deeper and more vivid educational experiences.[809,810,828] For instance, virtual scenarios immerse learners in realistic contexts, enabling active thinking and problem-solving through experiential learning, rather than passively receiving information. Thereby, these immersive environments significantly enhance the focus and motivation of learners by effectively stimulating their senses, fostering a deeper understanding of


https://doi.org/10.1021/acs.chemrev.4c00966
Chem. Rev. 2025, 125, 11567−11665

Table 15. Summary of Soft Wearable XR Devices-Based Applications Assisted with AI Technologies

| applications | actuating/sensing part | data modality | algorithms | classification accuracy | ref |
|---|---|---|---|---|---|
| hand motion-based application: teleoperation | mechanical input: forearm | motion sensing: EMG | CNN | 99% | 850 |
| hand motion-based VR application | mechanical input: wrist | strain sensing: piezoresistive | LSTM | 96.2% | 542 |
| hand motion-based VR application: entertainment | mechanical input: hand | strain sensing: piezoresistive | meta-learning | 85% | 122 |
| hand motion-based VR application: entertainment | mechanical and thermal feedback and input: finger | mechanical feedback: ERM motor<br>thermal feedback: Joule heating<br>bending sensing: triboelectric<br>temperature sensing: pyroelectric | SVM | 94% | 253 |
| tactile information-based VR application: entertainment | mechanical and thermal feedback and input: hand | mechanical feedback: pneumatic<br>thermal feedback: Joule heating<br>tactile sensing: triboelectric<br>temperature sensing: thermistor | CNN | 96% | 238 |
| motion-based VR application: teleoperation | mechanical feedback and input: whole body | vibrotactile: electromagnetic<br>bending/pressure: piezoresistive | | | 206 |
| motion-based AR application: medical devices (rehabilitation) | mechanical input: hand | motion sensing: EMG | | | 813 |
| thermal VR application: medical devices (rehabilitation) | thermal feedback: hand | temperature feedback: Peltier | | | 335 |
| object recognition-based VR application: training/ entertainment | mechanical input: finger | pressure sensing: triboelectric | CNN | 96.88% | 221 |
| | | | SVM | 96.41% | |
| hand motion-based VR/AR applications: entertainment | mechanical input: finger | bending sensing: triboelectric | CNN | 96.7−98.3% | 820 |
| hand motion-based application: teleoperation/entertainment | tactile feedback and input: finger | vibrotactile feedback: electromagnetic<br>pressure sensing: piezoresistive | adaptive learning | 94% | 209 |
| olfactory MR application: olfactory entertainment/education | olfactory feedback: nose | chemical molecule: cartridge | reinforcement learning: list-wise recommendation framework | low latency, olfactory enhancement | 414 |
| olfactory application | olfactory input | chemical detection: electrical resistance | deep learning: classification and regression tree algorithm | 68.2% | 633 |
| olfactory application | olfactory input | chemical detection: gas adsorption | SVM | 99.04% | 632 |
| olfactory application | olfactory input | chemical detection: binding affinity | artificial neural network | 94.67% | 150 |
| gustatory application | gustatory input: finger | chemical detection: electrochemical | deep learning: bootstrap algorithm | 95% | 737 |

the situation presented. This approach is particularly effective for understanding complex concepts and visualizing abstract content, especially when combined with VR devices that primarily engage visual and auditory stimuli, as well as wearable XR devices that recognize user actions and reflect them in the virtual environment while providing feedback to users.

First, XR educational environment will enable students to engage in a more vivid and effective botany class, moving beyond the traditional reliance on illustrations and photographs (Figure 35a).[412] The use of olfactory feedback devices mounted on the faces of students, in conjunction with VR glasses, enables them to experience the distinct aromas of various plants. Furthermore, the motion capture system allows


https://doi.org/10.1021/acs.chemrev.4c00966
Chem. Rev. 2025, 125, 11567−11665

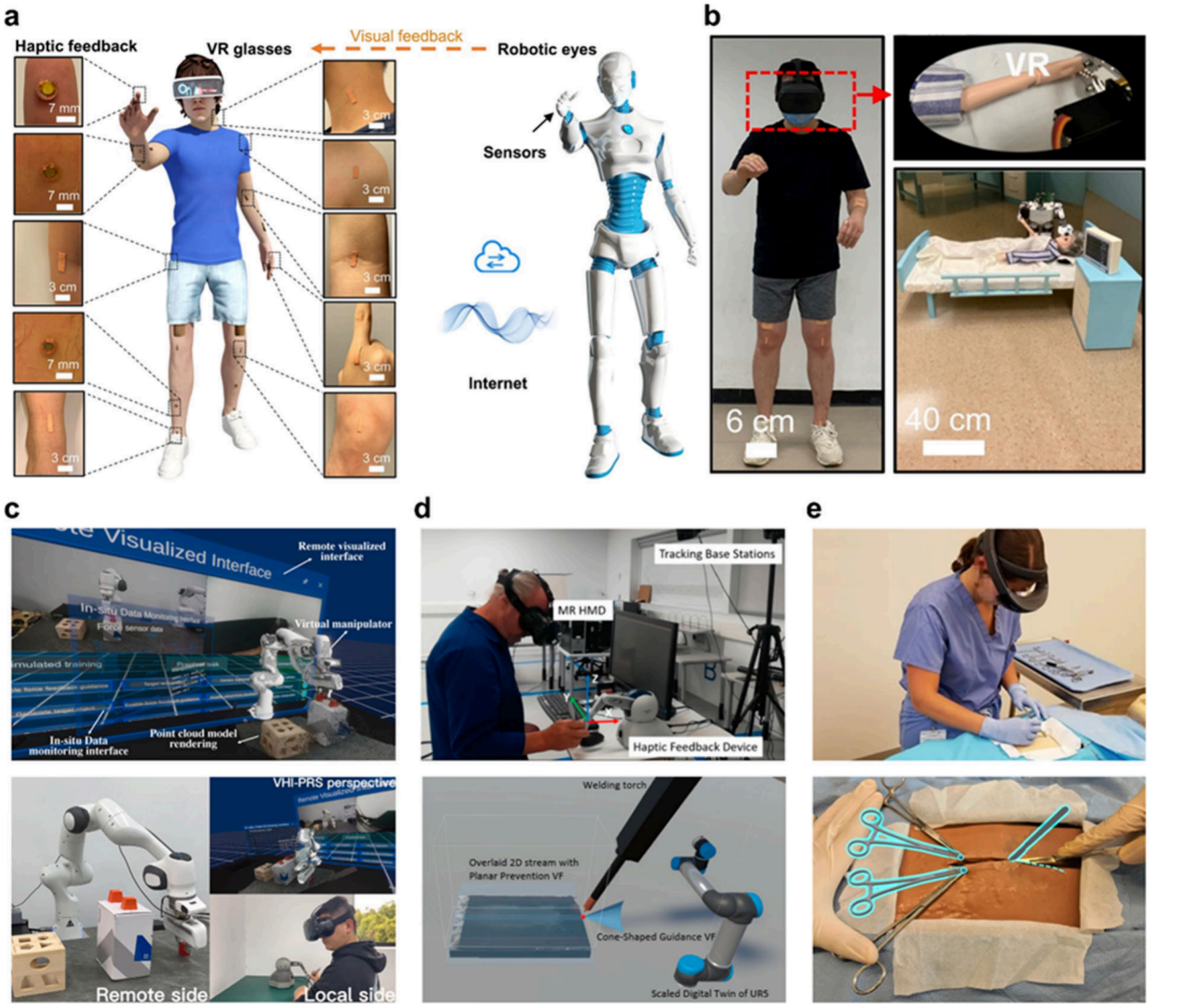


**Figure 34.** Application of wearable XR devices for work assistance. (a) Soft wearable XR devices integrated with haptic actuators and high-resolution VR glasses to provide multiple forms of feedback. A user remotely controlling a robot through glasses and feedback devices (left). A robot being remotely controlled by the user (right). (b) Application of teleoperation technology that enables remote interaction with equipment located in distant or physically inaccessible areas. User controlling remotely (left), view through VR glasses (top right), and remote patient care using a robot (bottom right) (scale bars: 6 cm, 40 cm). Reproduced with permission from ref 206. Copyright 2022 The American Association for the Advancement of Science. (c) Robotic arm system for remotely controlling industrial manipulators through visual and haptic feedback devices. Images of the system in the VR environment (top), robotic arm on the remote side (bottom left), and user operating the system (bottom right). Reproduced with permission from ref 805. Copyright 2024 Elsevier. (d) Intuitive remote welding robot with MR devices (top) and welding operation in MR interface (bottom). Reproduced with permission from ref 804. Copyright 2021 Multidisciplinary Digital Publishing Institute under CC BY 4.0 license https://creativecommons.org/licenses/by/4.0/. (e) AR Surgical telementoring. Medical professionals wearing VR headsets (top) and first-person view of medical professionals wearing VR headsets and 3D surgical guidance from remote experts (bottom). Reproduced with permission from ref 803. Copyright 2020 Springer Nature under CC BY 4.0 license https://creativecommons.org/licenses/by/4.0/.

for real-time detection of movements, enabling them to manipulate and smell the plants within the VR classroom. Consequently, learners can engage in a multidimensional educational experience that transcends simple visual and auditory information by incorporating olfactory sensations as well.

Likewise, in an MR-based simulation environment for emergency fire response and construction facilities, users are placed in a space where virtual and physical objects are combined, allowing them to practice making correct decisions (Figure 35b).[812,829] When a fire occurs in a virtual office, users can practice the necessary steps to extinguish the fire using virtual extinguishers. The MR-based system creates corresponding situations based on the reactions of users by tracking their actions in real-time. The system provides feedback based on these actions and simulates potential consequences for not following the correct procedures. This interactive approach allows learners to experience realistic fire response training in a safe environment. Furthermore, by employing wearable XR devices, prospective parents can acquire essential caregiving skills prior to the arrival of their child. Smart prosthetic skin, which incorporates mechanical and thermal input arrays,


https://doi.org/10.1021/acs.chemrev.4c00966
Chem. Rev. 2025, 125, 11567−11665

humidity sensors, and electroresistive heaters, can simulate scenarios such as detecting a wet diaper or identifying areas that require care when the baby is unwell (Figure 35c).[811] This innovative technology serves as an effective tool for instructing parents on the appropriate actions to take in various caregiving situations.

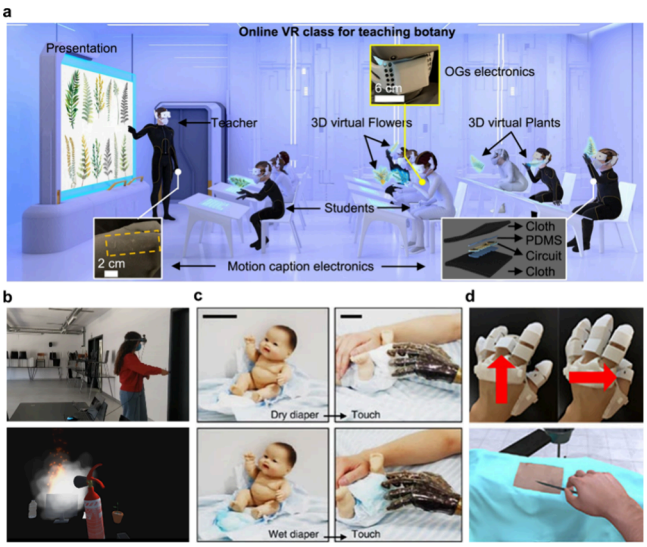


**Figure 35.** Application of wearable XR devices for education. (a) Online VR class with olfactory feedback device for teaching botany. Reproduced with permission from ref 412. Copyright 2023 Springer Nature under CC BY 4.0 license https://creativecommons.org/licenses/by/4.0/. (b) MR-based simulation environment for emergency fire response. A user wearing VR equipment and performing an emergency fire response scenario (top) and view from the user perspective (bottom). Reproduced with permission from ref 812. Copyright 2022 Multidisciplinary Digital Publishing Institute under CC BY 4.0 license https://creativecommons.org/licenses/by/4.0/. (c) Acquiring caregiving skills for prospective parents through smart prosthetic skin and simulations (scale bar: 10 cm). Reproduced with permission from ref 811. Copyright 2014 Springer Nature. (d) Soft wearable gloves replicating hand movements in a VR surgical environment. Optical images of surgical skills and movement control using the gloves (top) and a VR image of corresponding movements in the virtual environment (bottom). Reproduced with permission from ref 221. Copyright 2022 The American Association for the Advancement of Science.

Most importantly, in tasks where mistakes are not permissible, such as medical procedures, simulators are highly beneficial, providing learners with a safe environment free from risks, where they can practice repeatedly. These real-time feedback systems allow learners to instantly recognize and correct their errors, helping them to make better decisions. For instance, soft wearable gloves equipped with feedback and input devices can accurately replicate the hand movements of users in a VR surgical environment while they are holding surgical tools in real-time (Figure 35d).[221] Such feedback mechanisms are crucial for helping learners practice their skills repeatedly and reduce errors. Additionally, various studies in medical education have shown that VR simulators are highly effective in safely replicating real situations while improving the surgical abilities of unskilled doctors.[830] Virtual laparoscopic training systems simulate surgical procedures with great precision, allowing physicians to experience deep cognitive immersion and refine their skills while maintaining a low cognitive load.[831,832]

### 8.3. Rehabilitation and Sensory Substitution

In addition to surgical mentoring and simulation, wearable XR devices offer a diverse array of applications in the medical field, especially in rehabilitation.[814−816,833] XR-based rehabilitation systems offer a broader range of training environments than traditional methods, greatly enhancing patient motivation and the quality of training. This is particularly important in rehabilitation processes where repetitive movements and intensive training are essential. Furthermore, the use of a VR environment enables the swift creation of scenarios that demand agility through the integration of virtual objects, thereby offering an effective approach to rehabilitation. One of the key advantages of these technologies is that XR environments offer real-time feedback, enabling patients to immediately correct their movement patterns, thus leading to more efficient recovery. Another major benefit is the ability to perform remote training, overcoming the constraints of time and medical facilities, making it particularly useful.

In the field of physical rehabilitation, exoskeletons have served as powerful tools to provide mechanical assistance and real-time feedback to patients, enabling effective motor training in both clinical and remote settings. Integrated with XR technologies, the hybrid upper-arm exoskeleton system has been developed, which leverages an anatomical digital twin to simulate realistic torque feedback in VR and MR environments (Figure 36a).[834] By incorporating quasi-direct drive actuators and EMG-based motion analysis, these systems delivered precise resistance tailored to individual rehabilitation. The exoskeleton synchronized with the upper-limb movements and augmented them with programmable torque outputs, allowing for repetitive yet adaptive training exercises. Furthermore, the use of a digital twin enabled clinicians to monitor muscle activity and joint kinematics remotely, enhancing the personalization of therapy and enabling data-driven intervention. Such integration of mechanical support with XR interfaces not only enhanced patient engagement but also improved recovery outcomes by providing immersive, guided rehabilitation that bridges the gap between virtual and real-world experiences. Likewise, an MR-based rehabilitation system designed to help patients train their arm strength and balance has been proposed (Figure 36b).[813] Motion trackers and EMG sensors attached to the arm capture the movements of patients, which are visualized in real-time within the VR environment. This visual feedback enables patients to monitor their actions as they engage in exercises according to the programmed procedures. Moreover, the collected EMG data can measure muscle activity, serving as an effective means to monitor the rehabilitation status of patients. Furthermore, the system encouraged autonomous training, reducing the inconvenience of hospital visits and enabling continuous rehabilitation. With the assistance of AI technology, XR-based rehabilitation systems have been further advanced through the integration of real-time EEG sensing and deep-learning-based cognitive state recognition (Figure 36c).[835] The system incorporates a biomechanically accurate exoskeleton that replicates the structure of the human arm and synchronizes with the musculoskeletal profile of the user to apply individualized torque patterns during training. EEG signals are collected to monitor cognitive states including attention, fatigue, and emotional engagement. These signals are processed using a


https://doi.org/10.1021/acs.chemrev.4c00966
Chem. Rev. 2025, 125, 11567−11665

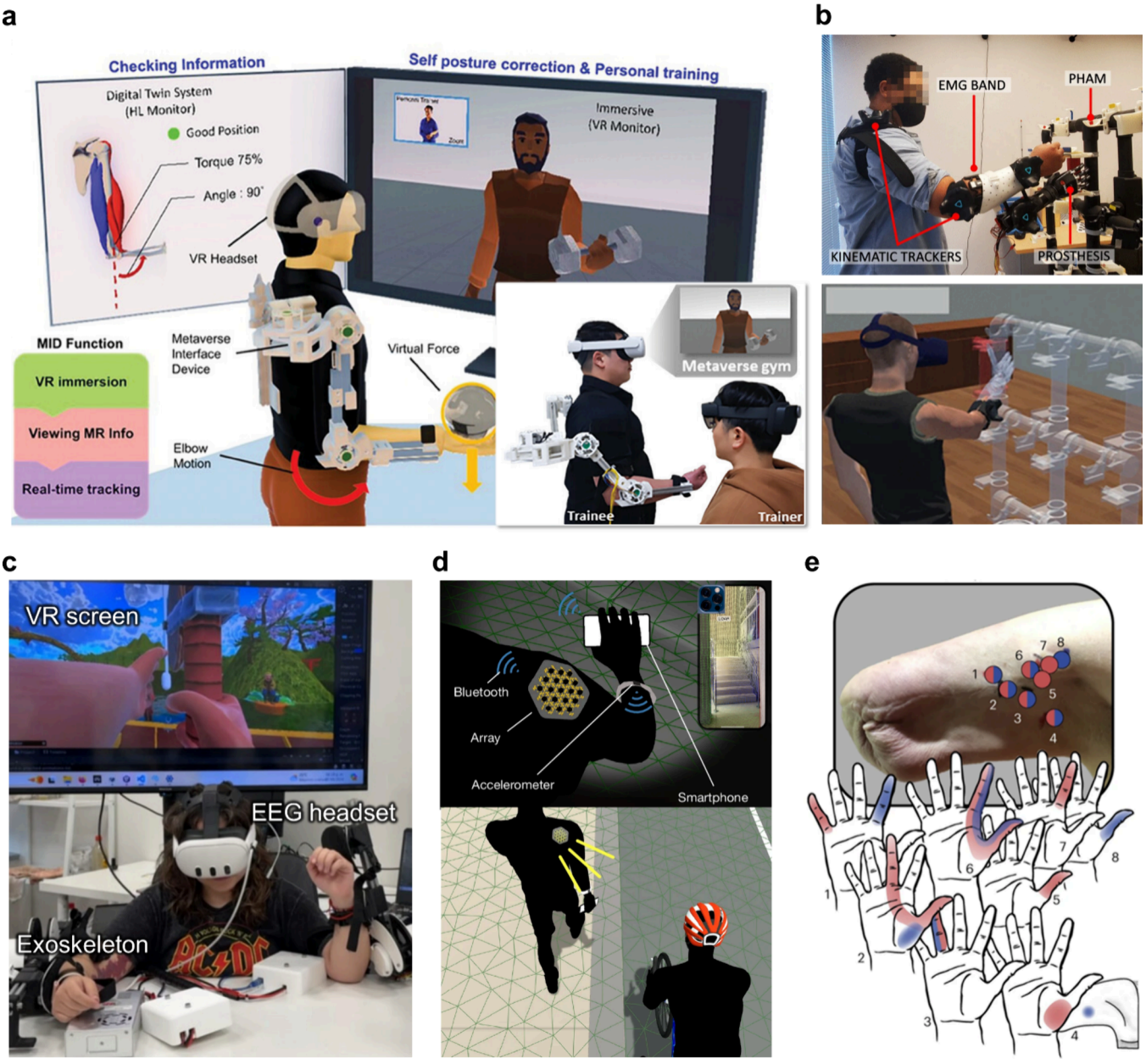


**Figure 36.** Application of wearable XR devices for rehabilitation and sensory substitution. (a) Hybrid upper-arm exoskeleton system integrated with an anatomical digital twin, enabling immersive rehabilitation. Inset: the scenario enables the trainer and trainee to interact using extended reality. Reproduced with permission from ref 834. Copyright 2023 Wiley-VCH. (b) MR-based rehabilitation system assisting patients in training arm strength and balance control. Optical image of patient undergoing rehabilitation with equipment in the real world (top) and corresponding VR image (bottom). Reproduced with permission from ref 813. Copyright 2023 Springer Nature under CC BY 4.0 license https://creativecommons.org/licenses/by/4.0/. (c) Real-time integration of EEG headset, upper-limb exoskeleton, and VR interface for cognitive−motor rehabilitation using motor imagery-based control. Reproduced with permission from ref 835. Copyright 2025 MDPI under CC BY 4.0 license https://creativecommons.org/licenses/by/4.0/. (d) Skin-integrated haptic system designed for sensory substitution, delivering structured feedback to assist perception and motor control in users with sensory impairments. Reproduced with permission from ref 199. Copyright 2024 Springer Nature. (e) Wearable thermal feedback TED for neurological rehabilitation. Reproduced with permission from ref 335. Copyright 2023 Springer Nature.

combination of CNN and LSTM models, and the output is used to adjust exercise parameters in real time. By aligning mechanical assistance with the cognitive condition of the user, the system enhances engagement and promotes more effective motor learning.

In addition, sensory substitution represents a key component of XR-based rehabilitation, enabling the brain to reinterpret feedback delivered through alternative sensory channels. By mapping sensory cues such as vibration, thermal feedback, or visual input onto lost or impaired modalities, XR systems can restore functional perception and promote neuroplasticity during motor or sensory rehabilitation through alternative channels.[836,837] In XR-based rehabilitation, where direct physical interaction is often limited, sensory substitution plays a critical role in providing perceptual cues for motor control and spatial awareness.[838,839] It supports rehabilitation by reinforcing sensorimotor integration, reducing cognitive load, and enhancing learning in repetitive tasks. Moreover,


https://doi.org/10.1021/acs.chemrev.4c00966
Chem. Rev. 2025, 125, 11567−11665

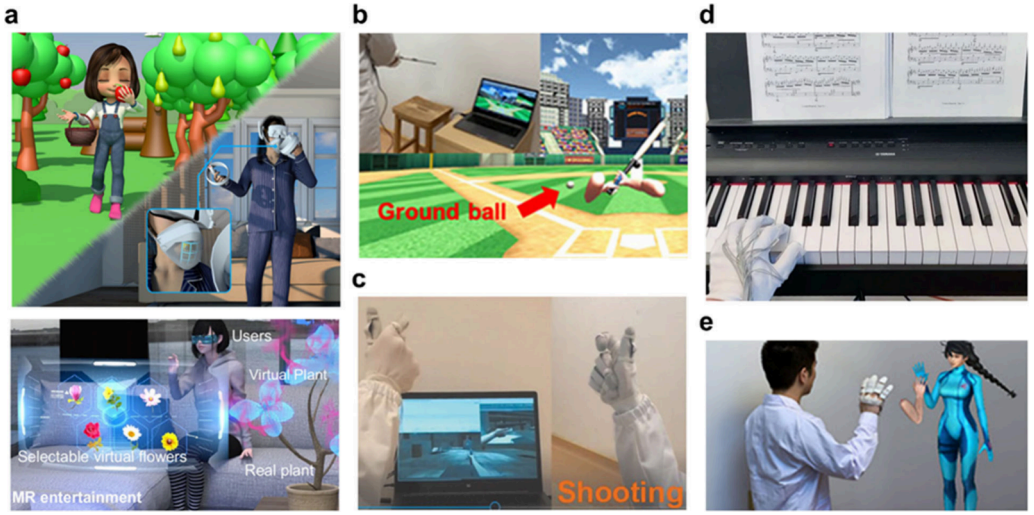


**Figure 37.** Application of wearable XR devices for entertainment. (a) Olfaction-based XR system offering a more emotional and realistic experience by enabling users to smell apples in a virtual orchard (top) or care for plants at home (bottom) while experiencing the connected scents of virtual plants. Reproduced with permission from ref 412. Copyright 2023 Springer Nature under CC BY 4.0 license https://creativecommons.org/licenses/by/4.0/. Reproduced with permission from ref 414. Copyright 2024 Springer Nature under CC BY 4.0 license https://creativecommons.org/licenses/by/4.0/. (b) User hitting a virtual baseball with a bat in an XR environment using a haptic smart glove with feedback and input devices. Reproduced with permission from ref 221. Copyright 2022 The American Association for the Advancement of Science. (c) Digital image of a user performing a trigger-pulling motion in a virtual shooting game using triboelectric textile-based sensory input devices. Reproduced with permission from ref 820. Copyright 2020 Wiley-VCH under CC BY 4.0 license https://creativecommons.org/licenses/by/4.0/. (d) Smart glove that detects finger movements when the user plays a digital piano and provides tactile feedback simulating the sensation of piano keys. Reproduced with permission from ref 811. Copyright 2024 Springer Nature under CC BY 4.0 license https://creativecommons.org/licenses/by/4.0/. (e) Interaction with others without physical constraints through virtual avatars in a shared VR space. Reproduced with permission from ref 221. Copyright 2022 The American Association for the Advancement of Science.

sensory substitution can strengthen the sense of embodiment by allowing users to experience artificial stimuli as if they were interacting with real physical objects, thereby improving both task performance and therapeutic engagement.[840] By facilitating cross-modal processing and adaptability, sensory substitution contributes to more immersive, effective, and personalized rehabilitation experiences.

Skin-integrated haptic systems have been developed to deliver spatially patterned vibratory stimuli as perceptual feedback for individuals with sensory deficits. A soft, wireless device incorporating an array of miniaturized actuators and embedded motion sensors has been proposed, which detects body movement and transmits coordinated tactile cues to the skin (Figure 36d).[199] The system operates in conjunction with a smartphone, which integrates environmental data from LiDAR sensors and other modules to generate real-time alerts. Through this connected interface, users can perceive spatial information such as the approach of surrounding objects or changes in the environment via substitute tactile signals. By aligning vibratory feedback with user motion and orientation, the device facilitates intuitive motor responses and improves situational awareness. Its skin-conformal design supports unobtrusive wearability and long-term adaptation, offering an effective solution for sensory substitution in wearable assistive technologies. Wearable XR feedback devices can also support communication by substituting visual information with vibrotactile cues, offering alternative interaction pathways for individuals with sensory or physical impairments.[841−843] For example, fingertip-mounted actuator arrays have been designed to convey spatial patterns representing Braille characters, enabling visually impaired users to perceive text through touch.[208] Such systems can also be integrated into prosthetic hands to deliver passive tactile information, helping amputees regain a sense of contact and environmental awareness. These approaches highlight the potential of vibrotactile substitution for enhancing accessible communication in wearable platforms.

Focusing specifically on rehabilitation, wearable thermal feedback devices can serve as powerful tool for sensory substitution, particularly for patients experiencing phantom pain after limb amputation.[844,845] Phantom pain refers to the phenomenon where patients feel pain in a limb that no longer physically exists, often resistant to conventional drug or physical therapy. In this respect, artificial thermal feedback generated by wearable TEDs has been shown to effectively support neurological rehabilitation and sensory recovery in upper-limb amputees (Figure 36e).[335] During training, upper-limb amputees performed virtual object identification tasks while receiving spatiotemporally mapped thermal cues via thin-film TEDs attached to the residual limb. The thermal feedback improved the perception of contact and grasping actions during prosthetic use, thereby facilitating a more natural interaction with virtual objects. By substituting lost tactile input with artificial thermal signals, the system acts as a form of sensory substitution, enhancing the embodiment and functional integration of the prosthetic limb.

### 8.4. Entertainment

In the field of entertainment, XR technology has become an essential component, offering immersive and interactive experiences that are revolutionizing user engagement across various types of content. Entertainment has evolved beyond mere enjoyment to emerge as an important element in alleviating human stress and providing emotional relief.[846] In this regard, as multisensory stimulation continues to advance, XR technology provides increasingly rich and realistic experiences for entertainment applications. For instance, the


https://doi.org/10.1021/acs.chemrev.4c00966
Chem. Rev. 2025, 125, 11567−11665

olfaction-based XR system offers a more emotional and realistic experience, allowing users to pick apples in a virtual orchard and smell the real scent of apples, or they can tend to plants in their home while experiencing the connected scents of both real and virtual plants (Figure 37a).[412,414] Furthermore, the use of an MR environment enables individuals to cultivate personalized orchards within their homes, allowing for the flexible transformation of their living spaces according to personal preferences. Additionally, olfactory feedback can elicit emotional responses, thereby enhancing user immersion and highlighting the potential of XR technologies to enrich and deepen user experiences.

In addition, traditional gaming environments have relied on traditional input devices such as keyboard, mouse and flat visual experiences, but XR enhances spatial interaction and immersion, allowing users to become fully absorbed in the game world.[824,847,848] The integration of XR technology eliminates physical constraints, fostering more creative gameplay and enabling personalized experiences for users. In sports games, XR devices allow users to train with immediate feedback derived from their physical data, resulting in more delicate and realistic gaming experiences.[849] For instance, users can hit a virtual baseball with a bat in an XR environment using a haptic smart glove with feedback and input devices (Figure 37b).[221] This smart glove detects hand movements and reflects them in real-time in the virtual space, capturing subtle movements and finger bends. Players can swing the virtual bat just like they would a real bat, enhancing the realism of the gameplay. As users swing their hands to hit the ball, they receive tactile feedback, further heightening the sense of realism. Furthermore, triboelectric textile-based wearable input devices accurately recognize figure gestures, and they reflect these gestures in the virtual shooting game, such as when a user performs a trigger-pulling motion to fire a gun in the game (Figure 37c).[820] This capability facilitates more intuitive control, allowing users to engage in gameplay with heightened immersion and realism. Similarly, the smart glove was able to detect finger movements when the user plays a digital piano, providing tactile feedback that simulates the sensation of piano keys (Figure 37d).[209] This creates a highly realistic experience of playing a physical piano within the XR environment.

Social interaction is a crucial element of entertainment, and XR technology provides innovative interactions that bridge the physical and digital worlds, enhancing user engagement in social networks. This immersion extends beyond text-based communication to more intuitive and emotional forms of interaction. For example, interacting with others through virtual avatars in a shared VR space allows for emotional exchanges without physical constraints (Figure 37e).[221] The hand gestures of users can be synchronized with the virtual character, facilitating natural emotional exchanges. With wearable XR technology, interactions transcend simple visual information to encompass tactile and motion recognition, facilitating comprehensive engagement. This enables users to access information through multiple channels, engage directly, and interact in a more meaningful manner, thereby transforming traditional communication methods into novel forms of emotional expression and interaction within social networks.

In this way, wearable feedback and input XR devices are driving new possibilities in the realms of work assistance, education, medical devices, and entertainment. The future of XR technology based on wearable devices is expected to become increasingly sophisticated, facilitating personalized user experiences and maximizing their potential beyond physical limitations. This evolution will not only represent a technological advancement but also fundamentally transform how individuals live and work, marking a significant turning point in society as XR technology becomes more deeply integrated into daily life.

## 9. CHALLENGES AND OUTLOOK

The realization of a seamless integration between physical and virtual worlds in the futuristic trajectory relies significantly on the advancement of soft wearable XR interfaces. Over recent decades, notable progress has been observed in immersive XR environments facilitated by soft electronic devices. Furthermore, the utilization of advanced AI algorithms has not only improved the performance of wearable XR devices but also introduced new functionalities. The integration of these innovative and powerful technologies is facilitating the emergence of unprecedented applications through soft wearable XR devices, thereby enhancing the creativity and overall well-being of human life.

### 9.1. Challenges

Despite these advancements, contemporary soft wearable XR devices face numerous ethical and technical issues that need to be resolved to guarantee the effective development and implementation of innovative XR applications. In this section, we will deal with the various technical issues that XR devices encounter in the formation and detection of sensory experiences.

**9.1.1. Technical Issues in Soft Wearable XR Devices.** First, this subsection will discuss the challenges that soft wearable XR devices must overcome to provide more realistic and effective stimulation and perception. This discussion will focus on key areas that require enhancement, including mechanical, thermal, olfactory, and gustatory feedback, as well as input devices.

*9.1.1.1. Absence of Powerful and Precise Mechanical Systems.* Traditional rigid wearable XR devices have generally been bulky but are capable of exerting significant forces on users without causing harm. However, as soft wearable XR devices have evolved to become lighter and more compact, challenges have emerged in applying sufficient force. While technologies such as electrotactile systems can instantaneously simulate high forces through electrical stimulation, safety concerns regarding the application of electricity on the skin cannot be ignored. As a result, there are pressing issues related to the development of mechanical systems that can deliver higher power. Furthermore, challenges persist with multimodal actuators. Although there is ongoing development of multimodal soft XR devices that incorporate both mechanical and electrotactile mechanisms, actuators capable of simultaneously providing shear stress and normal force remain largely undeveloped. Furthermore, the implementation of technologies such as variable stiffness, which can convey sensations of texture and hardness for both dynamic and static stimuli, is essential for creating a more immersive and realistic XR environment. As discussed in previous chapters, accurately mimicking stimuli is essential for effectively activating the receptors in our skin. Therefore, there is a critical need for devices that can implement more specific mechanical stimuli within soft wearable XR systems.

*9.1.1.2. Issue of Residual Heat in the Thermohaptic Devices.* Due to the inherent characteristics of soft wearable


https://doi.org/10.1021/acs.chemrev.4c00966
Chem. Rev. 2025, 125, 11567−11665

XR devices, the device surface is often in continuous contact with the skin. In the physical world, when we hold a hot object and subsequently release it, the temperature of the skin decreases rapidly. However, in the context of thermal sensation reconstruction using XR devices, the sustained contact between the device surface and the skin may not accurately reflect real-world conditions, potentially leading to safety concerns such as burns due to residual heat. Although feedback systems employing Peltier devices have partially mitigated this issue, the challenge of heat sinks resulting from prolonged use remains inadequately addressed. Therefore, there is a critical need for additional devices capable of managing heat output and modulating contact with the skin to effectively control residual heat.

*9.1.1.3. Issues of Olfactory and Gustatory Feedback Devices.* Currently, wearable XR devices predominantly focus on the development of visual, auditory, and haptic feedback. In contrast, creating devices for olfactory and gustatory feedback presents significant challenges due to the underlying mechanisms and the anatomical locations of the sensory organs, which complicate the delivery of a highly immersive sensory experience. Olfactory receptors in the nasal cavity and gustatory receptors are primarily activated by chemical substances, necessitating the transfer of these substances to elicit a response. However, wearable XR devices struggle to contain the chemical substances required for effective odor and taste representation. Even when such substances can be stored, their variety and quantity remain limited, thereby constraining the range of aromas and flavors that can be accurately reproduced. The olfactory feedback device discussed in this paper demonstrates the capability to express specific scents in a programmable yet limited context. Conversely, research on gustatory feedback devices is sparse, primarily because it is impractical for users to consume chemical substances directly. Furthermore, while it is feasible to stimulate receptors through electrical impulses, achieving a highly immersive experience remains challenging, as this would require electrodes to be positioned directly in the nasal and oral cavities. Unless highly miniaturized, film-like devices can be effectively integrated into the body, the development of a comprehensive XR environment utilizing olfactory and gustatory feedback devices is likely to require substantial time and further innovation.

*9.1.1.4. Transformation of Information Required for XR Environments Through Input Devices.* Over the past several decades, soft sensors based on soft electronics have achieved significant advancements, demonstrating high accuracy and sensitivity in response to simple mechanical, thermal, and chemical stimuli. Presently, these sensors have progressed to a level where they can analyze complex stimuli through integration with advanced AI technologies. However, although the intricate and random data sets generated by these sensors can be interpreted with high accuracy by AI, questions arise regarding the ability of these systems to classify environments in the same manner as humans. For soft wearable XR devices to be effectively implemented in XR environments, they must be capable of recognizing and translating a range of human actions and states, such as movements, gestures, and physiological states, even in dynamic and unpredictable situations, and subsequently relay this information to the XR environment. Achieving this goal necessitates careful consideration of various factors, including the number of sensors, the size of the data sets, the efficiency of the AI, and the development of innovative AI models. Furthermore, unresolved challenges remain concerning the storage of this data and the methods of its transmission.

**9.1.2. Ethics in Soft Wearable XR Devices.** The development of novel wearable XR devices and their applications is propelling the evolution of innovative technologies. However, beyond technical challenges, these advancements also present unprecedented ethical concerns, particularly in relation to personal privacy and data protection, as XR environments increasingly incorporate personal information and social interactions.[851] In addition, although virtual reality is not a physical entity, it serves as a social space, which raises ethical issues due to the lack of established regulatory frameworks and legal protections. Additionally, as the boundaries between the real world and virtual reality become increasingly blurred, issues such as VR syndrome and a lack of interactions in the physical world are becoming more prominent.

*9.1.2.1. Privacy and Data Protection Issues.* The development of wearable XR devices extends beyond providing highly immersive experiences for entertainment purposes. These devices have the potential to facilitate more intuitive and seamless interactions with individuals over long distances. If remote interactions can be efficiently supported, this could enhance social interactions, enable remote medical services, and even contribute to the realization of a new cyber world, often referred to as the Metaverse.

However, the intrinsic nature of wearable XR devices is that they are personal, perceptual tools, inherently processing and storing private information about users. For these devices to interact with others, they must connect to networks such as the Internet, which increases the likelihood of personal data being stored or exposed. As such, concerns surrounding privacy and data protection are becoming increasingly significant. The volume of data collected through XR devices is growing, raising the risk of data breaches and misuse. Although wearable XR devices explicitly designed for remote communication are not yet commercially available, the current development trajectory suggests that such technologies will soon become a reality. To prepare for this, it is crucial to establish appropriate regulations and legal frameworks to protect user privacy and ensure data security.

*9.1.2.2. Psychological and Social Implications.* XR technology facilitated by wearable devices is advancing rapidly. Visual and auditory devices, in particular, have reached a level suitable for commercialization, offering immersive experiences through high-resolution graphics and 3D audio. However, the high level of immersion these technologies provide can negatively influence the perceptions and behaviors of users in real life as they become more deeply absorbed in VR environments.[852] For instance, users may experience a blurring of boundaries between reality and the virtual world, or there may be a decline in social interactions. Such changes could disproportionately affect certain groups, like the younger generation.

Additionally, it is crucial for companies and researchers to uphold their responsibility in ensuring that users have safe and ethical experiences. While certain actions are restricted or prohibited by regulations in the physical world, such restrictions may not apply in XR environments, raising concerns about user safety and rights. Therefore, establishing ethical standards and guidelines is essential to protect users, ensure the long-term success of XR technology, and mitigate potential harms.


https://doi.org/10.1021/acs.chemrev.4c00966
Chem. Rev. 2025, 125, 11567−11665

### 9.2. Outlook

Future XR systems are expected to evolve toward encompassing multiple senses beyond just vision and hearing, moving beyond conventional interfaces to provide more immersive and interactive experiences. Despite the various technological, ethical, and regulatory challenges surrounding wearable XR devices, continuous advancements in innovation and research on materials and mechanisms will offer the potential to overcome these barriers. Successfully addressing issues such as the development of feedback mechanisms, the integration of feedback and input devices for sensory transmission, and the synchronization of sensory feedback between the real world and the virtual world via closed-loop systems will be essential for establishing more immersive and interactive XR environments.

Moreover, if the technologies currently being realized at the laboratory level become commercialized and are used in everyday life, limitless technologies and applications that will benefit humanity, including entertainment, job training and simulation, work assistance, telemedicine platforms, and teleoperation will be developed and bring significant societal impact. These advancements, particularly when combined with ML, hold great potential to redefine the HMI and revolutionize immersive XR experiences through wearable XR devices. In addition, recent research on next-generation XR technologies, though still in its early stages, has explored sensory transmission techniques that directly stimulate nerves rather than relying on receptors.

Future research directions will include brain-machine interfaces (BMIs), which open up new possibilities for integrating neural input and feedback pathways into XR systems. Particularly, noninvasive BMI technologies are gaining attention as a safer alternative and represent a feasible goal for wearable XR devices, since they eliminate the need for surgical procedures and can be safely and comfortably used in daily life.[853,854] For example, wearable EEG-based BMIs enable hands-free control of virtual environments by decoding user intentions from brain signals, while emerging neurostimulation technologies offer the potential to deliver artificial sensory experiences through direct brain or nerve stimulation. Recent studies demonstrate that wearable EEG devices can decode user intention with high accuracy through reactive paradigms, allowing users to manipulate virtual objects or navigate interfaces using only their gaze or cognitive attention.[855,856] These approaches have been successfully integrated with AR and VR headsets, forming lightweight, user-friendly systems suitable for extended use.

On the XR feedback side, emerging neurostimulation technologies offer the potential to deliver artificial sensory experiences by directly modulating peripheral or central neural pathways. Peripheral nerve functionalization, for instance, involves modifying the structural or functional characteristics of peripheral nerves to regulate and utilize neural activity.[857] Optogenetic functionalization, as an example, employs light to stimulate or inhibit peripheral nerve activity.[858−860] This technique enables selective neural activation and independent control of multiple neural groups through wavelength-specific stimulation, offering the potential to replicate diverse sensations with single actuation.[858,859,861−864] Furthermore, peripheral nerve stimulation through miniature electrical actuators can elicit haptic illusions that replicate tactile sensations without mechanical contact. Likewise, transcranial magnetic or electrical stimulation methods have been used to induce visual or vestibular perceptions by activating specific regions of the brain, offering a new channel for multisensory XR feedback.[865]

By directly stimulating the brain or nerves without engaging receptor pathways, BMIs provide rapid response times and the ability to replicate diverse sensations with a single stimulus, facilitating device miniaturization, simplification, and energy efficiency.[866−870] Notably, BMI-based interfaces may provide access to novel feedback modalities such as chemohaptic stimulation, enabling the perception of chemical senses or hybrid sensations that are otherwise difficult to generate using conventional physical feedback devices alone. In addition, advanced BMIs will require neural signal interpretation techniques and intelligent signal processing algorithms to enable real-time interaction to effectively bridge human brain and XR devices. Although still in an early stage, the integration of noninvasive BMIs with XR systems demonstrates great promise as future XR interfaces. As BMI technologies evolve to interact directly with the human brain, issues related to safety, data privacy, and neuroethics will need to be addressed alongside technical challenges.

In conclusion, the technologies discussed in this paper have made substantial progress and form a foundation for advancing the next generation of XR-based applications. While several challenges remain, combining an in-depth understanding of materials and mechanisms with creative engineering approaches can facilitate the development of technologies that offer highly immersive experiences and increasingly blur the boundaries between the real and virtual worlds. As XR technologies mature, they will fundamentally reshape the nature of human−machine interaction. The diminishing boundary between the real world and the digital world will trigger paradigm shifts across education, work, entertainment, and healthcare, while also raising important ethical and societal questions as these systems move toward broader commercialization.

## AUTHOR INFORMATION

### Corresponding Authors

**Seung Hwan Ko** − *Department of Mechanical Engineering, Seoul National University, Seoul 08826, Republic of Korea; Institute of Advanced Machinery and Design (SNU-IAMD), Institute of Engineering Research, and Interdisciplinary Program in Bioengineering, Seoul National University, Seoul 08826, Republic of Korea;* orcid.org/0000-0002-7477-0820; Email: maxko@snu.ac.kr

**John A. Rogers** − *Querrey Simpson Institute for Bioelectronics, Northwestern University, Evanston, Illinois 60208, United States; Department of Materials Science and Engineering, Department of Mechanical Engineering, and Department of Biomedical Engineering, Northwestern University, Evanston, Illinois 60208, United States; Department of Neurological Surgery, Northwestern University Feinberg School of Medicine, Chicago, Illinois 60611, United States; Department of Pediatrics, Feinberg School of Medicine, Northwestern University, Chicago, Illinois 60611, United States;* orcid.org/0000-0002-2980-3961; Email: jrogers@northwestern.edu

**Deog-Gyu Seo** − *Department of Conservative Dentistry and Dental Research Institute, School of Dentistry, Seoul National University, Seoul 03080, Republic of Korea*; Email: dgseo@snu.ac.kr



https://doi.org/10.1021/acs.chemrev.4c00966
Chem. Rev. 2025, 125, 11567−11665

## Authors

**Kyung Rok Pyun** − *Department of Mechanical Engineering, Seoul National University, Seoul 08826, Republic of Korea; Querrey Simpson Institute for Bioelectronics, Northwestern University, Evanston, Illinois 60208, United States*

**Jung Jae Park** − *Department of Mechanical Engineering, Seoul National University, Seoul 08826, Republic of Korea;* orcid.org/0009-0008-1098-3457

**Jiyong Ahn** − *Department of Mechanical Engineering, Seoul National University, Seoul 08826, Republic of Korea*

**Yoon Seon Lee** − *Department of Conservative Dentistry and Dental Research Institute, School of Dentistry, Seoul National University, Seoul 03080, Republic of Korea*

**Hongchan Kim** − *Department of Mechanical Engineering, Seoul National University, Seoul 08826, Republic of Korea*

**Jinsol Kim** − *Department of Mechanical Engineering, Seoul National University, Seoul 08826, Republic of Korea*

**Sangjin Yoon** − *Department of Mechanical Engineering, Seoul National University, Seoul 08826, Republic of Korea*

**Kyoung-Ho Ha** − *Querrey Simpson Institute for Bioelectronics, Northwestern University, Evanston, Illinois 60208, United States*

Complete contact information is available at: https://pubs.acs.org/10.1021/acs.chemrev.4c00966

## Author Contributions

**Kyung Rok Pyun**, **Jung Jae Park**, and **Jiyong Ahn** contributed equally to this work. CRediT: **Kyung Rok Pyun** conceptualization, investigation, original draft, writing-review and editing; **Jung Jae Park** conceptualization, investigation, original draft, writing-review and editing; **Jiyong Ahn** conceptualization, investigation, original draft, writing-review and editing; **Yoon Seon Lee** writing-original draft, writing-review and editing; **Hongchan Kim** writing-original draft, writing-review and editing; **Jinsol Kim** writing-original draft, writing-review and editing; **Sangjin Yoon** writing-original draft, writing-review and editing; **Kyoung-Ho Ha** writing-original draft, writing-review and editing; **Deog-Gyu Seo** conceptualization, funding acquisition, project administration, supervision, writing-original draft, writing-review and editing; **John A. Rogers** conceptualization, funding acquisition, project administration, supervision, writing-original draft, writing-review and editing; **Seung Hwan Ko** conceptualization, funding acquisition, project administration, supervision, writing-original draft, writing-review and editing.

## Notes

The authors declare no competing financial interest.

## Biographies

Kyung Rok Pyun is currently a Postdoctoral Fellow at Querrey Simpson Institute for Bioelectronics at Northwestern University. He received his B.S. degree in the Department of Mechanical Engineering from Sungkyunkwan University in 2016. He earned M.S. and Ph.D. degrees in the Department of Mechanical and Aerospace Engineering from Seoul National University in 2018 and 2024, respectively. His research primarily focuses on the integration of soft sensors with AI technology for proprioceptive soft robots and wearable electronics based on biocompatible materials.

Jung Jae Park is currently a Ph.D. candidate in the Department of Mechanical Engineering at Seoul National University. He received his B.S. and M.S. degrees in Mechanical and Aerospace Engineering from Seoul National University in 2017 and 2019, respectively. His research focuses on stretchable electronics based on soft materials and advanced fabrication processes for human−machine interface and soft robotics, combined with artificial intelligence.

Jiyong Ahn is currently a Ph.D. candidate in the Department of Mechanical Engineering at Seoul National University. He earned his B.S. degree in the Department of Mechanical Engineering from Kyung Hee University in 2019. His research focuses on molecular dynamics simulation and advanced fabrication processes for conducting polymer-based wearable electronics and bioelectronics.

Yoon Seon Lee is currently a third-year Postdoctoral resident in the Department of Conservative Dentistry at Seoul National University. She received her B.S degree from New York University in 2013, D.D.S. and Ph.D. degrees from the School of Dentistry at Seoul National University in 2021. Her research focuses on molecular mechanisms of odontoblast differentiation, clinically on dentin hypersensitivity and dentin repair.

Hongchan Kim is currently a Ph.D. candidate in the Department of Mechanical Engineering at Seoul National University. He received his B.S. degree in the Department of Mechanical Engineering from Konkuk University in 2022. His current research focuses on wearable electronics for haptic interfaces.

Jinsol Kim is currently a Ph.D. candidate in the Department of Mechanical Engineering at Seoul National University. She received her B.S. degree in the Department of Mechanical Engineering from Sungkyunkwan University in 2022. Her current research focuses on the AI technology for wearable bioelectronics.

Sangjin Yoon is currently a Ph.D. candidate in the Department of Mechanical Engineering at Seoul National University. He earned his B.S. degree in the Department of Mechanical Engineering and Forest Environment Science from Seoul National University in 2023. His current research focuses on wearable sensors for artificial electronic skin.

Kyoung-Ho Ha is currently a Postdoctoral Fellow at the Querrey Simpson Institute for Bioelectronics at Northwestern University. He received his B.S. and M.S. degrees in Mechanical and Aerospace Engineering from Seoul National University in 2013 and 2015, respectively, and his Ph.D. in Mechanical Engineering from the University of Texas at Austin in 2022. His research interests include miniaturized skin-integrated actuators and soft pressure sensors for advanced haptic interfaces.

Deog-Gyu Seo is currently a tenured professor of the Department of Conservative Dentistry at Seoul National University. He received his B.S. and D.D.S. (Doctor of Dental Surgery) degrees from the School of Dentistry at Yonsei University in 2001, followed by an M.S. degree in Conservative Dentistry from Yonsei University in 2004, along with a specialist board certification from the Ministry of Health and Welfare. He then earned his Ph.D. in Conservative Dentistry from Yonsei University in 2009. His research focuses on biomimetic materials such as bioremineralization with calcium silicate and catechol-based primers inspired by sea mussels, as well as bonding mechanics analysis involving zirconia, ceramics, 3D printing resins, and composite adhesion. His clinical research includes cracked tooth analysis, dentin hypersensitivity, laser canal disinfection, and the development of machine learning devices for the diagnosis of root canal orifices and dental caries.

John A. Rogers obtained B.A. and B.S. degrees in Chemistry and in Physics from the University of Texas−Austin, in 1989. From MIT, he received S.M. degrees in Physics and in Chemistry in 1992 and his Ph.D. degree in Physical Chemistry in 1995. From 1995 to 1997,



https://doi.org/10.1021/acs.chemrev.4c00966
Chem. Rev. 2025, 125, 11567−11665

Rogers was a Junior Fellow in the Harvard University Society of Fellows. He joined Bell Laboratories as a member of technical staff in the Condensed Matter Physics Research Department in 1997 and served as director of this department from the end of 2000 to 2002. He then spent 13 years on the faculty at University of Illinois, most recently as the Swanlund Chair Professor and Director of the Seitz Materials Research Laboratory. In 2016, he joined Northwestern University as the Louis Simpson and Kimberly Querrey Professor of Materials Science and Engineering, Biomedical Engineering, and Medicine, with affiliate appointments in Mechanical Engineering, Electrical and Computer Engineering, and Chemistry, where he is also Director of the Querrey Simpson Institute for Bioelectronics.

Seung Hwan Ko is currently a Professor of Mechanical Engineering at Seoul National University, where he serves as the Principal Investigator of the ANTS Laboratory (http://ants.snu.ac.kr). He received his B.S. degree in the Department of Mechanical Engineering from Yonsei University in 2000 and his M.S. degree in the Department of Mechanical Engineering from Seoul National University in 2002. Then, he earned his Ph.D. degree in the Department of Mechanical Engineering at the University of California, Berkeley in 2006. Under his supervision, the ANTS Laboratory focuses on pioneering research in soft materials, innovative fabrication process developing soft materials, fabrication processes, and the development of wearable and bioelectronic devices to overcome existing challenges within current research fields. Currently, the primary research endeavor is the development of advanced soft wearable electronic devices, specifically designed to enhance AR/VR applications.

## ACKNOWLEDGMENTS

This research was supported by the National Research Foundation of Korea (NRF) funded by the Ministry of Science and ICT (RS-2025-11092968, RS-2022-NR068144, RS-2025-02223634) and by Basic Science Research Program through the NRF funded by the Ministry of Education (RS-2024-00412962).

## REFERENCES

(1) Rauschnabel, P. A.; Felix, R.; Hinsch, C.; Shahab, H.; Alt, F. What is XR? Towards a framework for augmented and virtual reality. *Comput. Hum. Behav.* **2022**, *133*, 107289.
(2) Pyun, K. R.; Rogers, J. A.; Ko, S. H. Materials and devices for immersive virtual reality. *Nat. Rev. Mater.* **2022**, *7* (11), 841−843.
(3) Xi, N.; Chen, J.; Gama, F.; Riar, M.; Hamari, J. The challenges of entering the metaverse: An experiment on the effect of extended reality on workload. *Inf. Syst. Front.* **2022**, *25*, 659−680.
(4) Nilsson, N. C.; Nordahl, R.; Serafin, S. Immersion revisited: A review of existing definitions of immersion and their relation to different theories of presence. *Hum. Technol.* **2016**, *12* (2), 108−134.
(5) Li, X.; Yi, W.; Chi, H.-L.; Wang, X.; Chan, A. P. A critical review of virtual and augmented reality (VR/AR) applications in construction safety. *Autom. Constr.* **2018**, *86*, 150−162.
(6) Kim, H.; Kwon, Y. T.; Lim, H. R.; Kim, J. H.; Kim, Y. S.; Yeo, W. H. Recent advances in wearable sensors and integrated functional devices for virtual and augmented reality applications. *Adv. Funct. Mater.* **2021**, *31* (39), 2005692.
(7) Park, J.; Lee, Y.; Cho, S.; Choe, A.; Yeom, J.; Ro, Y. G.; Kim, J.; Kang, D.-h.; Lee, S.; Ko, H. Soft Sensors and Actuators for Wearable Human-Machine Interfaces. *Chem. Rev.* **2024**, *124* (4), 1464−1534.
(8) Jung, Y. H.; Kim, J. H.; Rogers, J. A. Skin-integrated vibrohaptic interfaces for virtual and augmented reality. *Adv. Funct. Mater.* **2021**, *31* (39), 2008805.
(9) Lee, J.; Kim, D.; Sul, H.; Ko, S. H. Thermo-haptic materials and devices for wearable virtual and augmented reality. *Adv. Funct. Mater.* **2021**, *31* (39), 2007376.
(10) Kourtesis, P.; Argelaguet, F.; Vizcay, S.; Marchal, M.; Pacchierotti, C. Electrotactile feedback applications for hand and arm interactions: A systematic review, meta-analysis, and future directions. *IEEE Trans. Haptics* **2022**, *15* (3), 479−496.
(11) Yin, R.; Wang, D.; Zhao, S.; Lou, Z.; Shen, G. Wearable sensors-enabled human-machine interaction systems: from design to application. *Adv. Funct. Mater.* **2021**, *31* (11), 2008936.
(12) Ko, S. H.; Rogers, J. Functional materials and devices for XR (VR/AR/MR) applications. *Adv. Funct. Mater.* **2021**, *31* (39), 2106546.
(13) Bang, J.; Choi, S. H.; Pyun, K. R.; Jung, Y.; Hong, S.; Kim, D.; Lee, Y.; Won, D.; Jeong, S.; Shin, W.; et al. Bioinspired electronics for intelligent soft robots. *Nat. Rev. Electr. Eng.* **2024**, *1*, 597−613.
(14) Won, D.; Bang, J.; Choi, S. H.; Pyun, K. R.; Jeong, S.; Lee, Y.; Ko, S. H. Transparent electronics for wearable electronics application. *Chem. Rev.* **2023**, *123* (16), 9982−10078.
(15) Hale, K. S.; Stanney, K. M. Deriving haptic design guidelines from human physiological, psychophysical, and neurological foundations. *IEEE Comput. Graph. Appl.* **2004**, *24* (2), 33−39.
(16) Kim, D.; Kim, S.-H.; Kim, T.; Kang, B. B.; Lee, M.; Park, W.; Ku, S.; Kim, D.; Kwon, J.; Lee, H.; et al. Review of machine learning methods in soft robotics. *PLoS One* **2021**, *16* (2), No. e0246102.
(17) Hunt, S. D. Theory status, inductive realism, and approximate truth: No miracles, no charades. *Int. Stud. Philos. Sci.* **2011**, *25* (2), 159−178.
(18) Benford, S.; Giannachi, G. *Performing mixed reality*; MIT press, 2011.
(19) Craig, A. B. *Understanding Augmented Reality: Concepts and Applications*; Morgan Kaufmann, 2013.
(20) Carmigniani, J.; Furht, B.; Anisetti, M.; Ceravolo, P.; Damiani, E.; Ivkovic, M. Augmented reality technologies, systems and applications. *Multimed. Tools Appl.* **2011**, *51*, 341−377.
(21) Jerald, J. *The VR Book: Human-Centered Design for Virtual Reality*; Morgan & Claypool, 2015.
(22) Speicher, M.; Hall, B. D.; Nebeling, M. What is mixed reality? In *Proceedings of the 2019 CHI Conference on Human Factors in Computing Systems*, 2019; pp 1−15.
(23) Bekele, M. K.; Pierdicca, R.; Frontoni, E.; Malinverni, E. S.; Gain, J. A survey of augmented, virtual, and mixed reality for cultural heritage. *J. Comput. Cult. Herit.* **2018**, *11* (2), 1−36.
(24) Rosenberg, L. B. Virtual fixtures: Perceptual tools for telerobotic manipulation. In *Proceedings of IEEE Virtual Reality Annual International Symposium*; IEEE, 1993; pp 76−82.
(25) Feiner, S.; MacIntyre, B.; Höllerer, T.; Webster, A. A touring machine: Prototyping 3D mobile augmented reality systems for exploring the urban environment. *Pers. Technol.* **1997**, *1*, 208−217.
(26) Jack, D.; Boian, R.; Merians, A. S.; Tremaine, M.; Burdea, G. C.; Adamovich, S. V.; Recce, M.; Poizner, H. Virtual reality-enhanced stroke rehabilitation. *IEEE Trans. Neural Syst. Rehabil. Eng.* **2001**, *9* (3), 308−318.
(27) Mistry, P.; Maes, P. SixthSense: a wearable gestural interface. In *ACM Siggraph Asia 2009 Sketches*; Association for Computing Machinery, 2009.
(28) Lingley, A. R.; Ali, M.; Liao, Y.; Mirjalili, R.; Klonner, M.; Sopanen, M.; Suihkonen, S.; Shen, T.; Otis, B. P.; Lipsanen, H.; et al. A single-pixel wireless contact lens display. *J. Micromech. Microeng.* **2011**, *21* (12), 125014.
(29) Lopes, P.; Ion, A.; Baudisch, P. Impacto: Simulating physical impact by combining tactile stimulation with electrical muscle stimulation. In *Proceedings of the 28th Annual ACM Symposium on User Interface Software & Technology*, 2015; pp 11−19.
(30) Choi, I.; Hawkes, E. W.; Christensen, D. L.; Ploch, C. J.; Follmer, S. Wolverine: A wearable haptic interface for grasping in virtual reality. In *2016 IEEE/RSJ International Conference on Intelligent Robots and Systems (IROS)*; IEEE, 2016; pp 986−993.


https://doi.org/10.1021/acs.chemrev.4c00966
*Chem. Rev.* 2025, 125, 11567−11665

(31) Yu, X.; Xie, Z.; Yu, Y.; Lee, J.; Vazquez-Guardado, A.; Luan, H.; Ruban, J.; Ning, X.; Akhtar, A.; Li, D.; et al. Skin-integrated wireless haptic interfaces for virtual and augmented reality. *Nature* **2019**, *575* (7783), 473−479.
(32) Lee, J.; Sul, H.; Lee, W.; Pyun, K. R.; Ha, I.; Kim, D.; Park, H.; Eom, H.; Yoon, Y.; Jung, J.; Lee, D.; Ko, S. H. Stretchable skin-like cooling/heating device for reconstruction of artificial thermal sensation in virtual reality. *Adv. Funct. Mater.* **2020**, *30* (29), 1909171.
(33) Huang, Y.; Zhou, J.; Ke, P.; Guo, X.; Yiu, C. K.; Yao, K.; Cai, S.; Li, D.; Zhou, Y.; Li, J.; Wong, T. H.; Liu, Y.; Li, L.; Gao, Y.; Huang, X.; Li, H.; Li, J.; Zhang, B.; Chen, Z.; Zheng, H.; Yang, X.; Gao, H.; Zhao, Z.; Guo, X.; Song, E.; Wu, H.; Wang, Z.; Xie, Z.; Zhu, K.; Yu, X. A skin-integrated multimodal haptic interface for immersive tactile feedback. *Nat. Electron.* **2023**, *6* (12), 1020−1031.
(34) Ha, K.-H.; Yoo, J.; Li, S.; Mao, Y.; Xu, S.; Qi, H.; Wu, H.; Fan, C.; Yuan, H.; Kim, J.-T.; et al. Full freedom-of-motion actuators as advanced haptic interfaces. *Science* **2025**, *387* (6741), 1383−1390.
(35) Parsons, T. D.; Gaggioli, A.; Riva, G. Virtual reality for research in social neuroscience. *Brain Sci.* **2017**, *7* (4), 42.
(36) Hayward, V.; Astley, O. R. Performance measures for haptic interfaces. In *Robotics Research: The Seventh International Symposium*; Springer, 1996; pp 195−206.
(37) Doerner, R.; Steinicke, F. Perceptual aspects of VR. In *Virtual and Augmented Reality (VR/AR) Foundations and Methods of Extended Realities (XR)*; Springer, 2022; pp 39−70.
(38) Boff, K. R.; Kaufman, L.; Thomas, J. P. *Handbook of Perception and Human Performance*; Wiley: New York, 1986.
(39) Dargahi, J.; Najarian, S. Human tactile perception as a standard for artificial tactile sensing—a review. *Int. J. Med. Robot. Comput. Assist. Surg.* **2004**, *1* (1), 23−35.
(40) Schepers, R. J.; Ringkamp, M. Thermoreceptors and thermosensitive afferents. *Neurosci. Biobehav. Rev.* **2010**, *34* (2), 177−184.
(41) Mombaerts, P. Genes and ligands for odorant, vomeronasal and taste receptors. *Nat. Rev. Neurosci.* **2004**, *5* (4), 263−278.
(42) Woolf, C. J.; Ma, Q. Nociceptors—noxious stimulus detectors. *Neuron* **2007**, *55* (3), 353−364.
(43) Wicher, D. Design principles of sensory receptors. *Front. Cell. Neurosci.* **2010**, *4*, 2099.
(44) Zahorik, P.; Brungart, D. S.; Bronkhorst, A. W. Auditory distance perception in humans: A summary of past and present research. *Acta Acust. United Acust.* **2005**, *91* (3), 409−420.
(45) Tuthill, J. C.; Azim, E. Proprioception. *Curr. Biol.* **2018**, *28* (5), R194−R203.
(46) Kanitakis, J. Anatomy, histology and immunohistochemistry of normal human skin. *Eur. J. Dermatol.* **2002**, *12* (4), 390−401.
(47) Kolarsick, P. A.; Kolarsick, M. A.; Goodwin, C. Anatomy and physiology of the skin. *J. Dermat. Nurses Assoc.* **2011**, *3* (4), 203−213.
(48) Roudaut, Y.; Lonigro, A.; Coste, B.; Hao, J.; Delmas, P.; Crest, M. Touch sense: functional organization and molecular determinants of mechanosensitive receptors. *Channels* **2012**, *6* (4), 234−245.
(49) Macefield, V. G. Physiological characteristics of low-threshold mechanoreceptors in joints, muscle and skin in human subjects. *Clin. Exp. Pharmacol. Physiol.* **2005**, *32* (1−2), 135−144.
(50) Hao, J.; Bonnet, C.; Amsalem, M.; Ruel, J.; Delmas, P. Transduction and encoding sensory information by skin mechanoreceptors. *Pflügers Archiv-European Journal of Physiology* **2015**, *467*, 109−119.
(51) Handler, A.; Ginty, D. D. The mechanosensory neurons of touch and their mechanisms of activation. *Nat. Rev. Neurosci.* **2021**, *22* (9), 521−537.
(52) Hu, J.; Milenkovic, N.; Lewin, G. R. The high threshold mechanotransducer: a status report. *Pain* **2006**, *120* (1−2), 3−7.
(53) Li, L.; Rutlin, M.; Abraira, V. E.; Cassidy, C.; Kus, L.; Gong, S.; Jankowski, M. P.; Luo, W.; Heintz, N.; Koerber, H. R.; et al. The functional organization of cutaneous low-threshold mechanosensory neurons. *Cell* **2011**, *147* (7), 1615−1627.
(54) Kandel, E. R.; Schwartz, J. H.; Jessell, T. M.; Siegelbaum, S.; Hudspeth, A. J.; Mack, S. *Principles of Neural Science*; McGraw-Hill: New York, 2000.
(55) Cavanaugh, D. J.; Lee, H.; Lo, L.; Shields, S. D.; Zylka, M. J.; Basbaum, A. I.; Anderson, D. J. Distinct subsets of unmyelinated primary sensory fibers mediate behavioral responses to noxious thermal and mechanical stimuli. *Proc. Natl. Acad. Sci. U. S. A.* **2009**, *106* (22), 9075−9080.
(56) Koziol, L. F.; Budding, D. E.; Chidekel, D. Sensory integration, sensory processing, and sensory modulation disorders: Putative functional neuroanatomic underpinnings. *Cerebellum* **2011**, *10* (4), 770−792.
(57) Katta, S.; Krieg, M.; Goodman, M. B. Feeling force: physical and physiological principles enabling sensory mechanotransduction. *Annu. Rev. Cell Dev. Biol.* **2015**, *31* (1), 347−371.
(58) Olausson, H.; Wessberg, J.; Morrison, I.; McGlone, F.; Vallbo, A. The neurophysiology of unmyelinated tactile afferents. *Neurosci. Biobehav. Rev.* **2010**, *34* (2), 185−191.
(59) Abraira, V. E.; Ginty, D. D. The sensory neurons of touch. *Neuron* **2013**, *79* (4), 618−639.
(60) Basbaum, A. I.; Bautista, D. M.; Scherrer, G.; Julius, D. Cellular and molecular mechanisms of pain. *Cell* **2009**, *139* (2), 267−284.
(61) Hao, J.; Delmas, P. Multiple desensitization mechanisms of mechanotransducer channels shape firing of mechanosensory neurons. *J. Neurosci.* **2010**, *30* (40), 13384−13395.
(62) Iggo, A.; Ogawa, H. Correlative physiological and morphological studies of rapidly adapting mechanoreceptors in cat's glabrous skin. *J. Physiol.* **1977**, *266* (2), 275−296.
(63) Johansson, R. S. Tactile sensibility in the human hand: receptive field characteristics of mechanoreceptive units in the glabrous skin area. *J. Physiol.* **1978**, *281* (1), 101−125.
(64) Delmas, P.; Hao, J.; Rodat-Despoix, L. Molecular mechanisms of mechanotransduction in mammalian sensory neurons. *Nat. Rev. Neurosci.* **2011**, *12* (3), 139−153.
(65) Sato, M. Response of Pacinian corpuscles to sinusoidal vibration. *J. Physiol.* **1961**, *159* (3), 391.
(66) Munger, B. L.; Idez, C. The structure and function of cutaneous sensory receptors. *Arch. Histol. Cytol.* **1988**, *51* (1), 1−34.
(67) Vallbo, A. B.; Johansson, R. S. Properties of cutaneous mechanoreceptors in the human hand related to touch sensation. *Hum. Neurobiol.* **1984**, *3* (1), 3−14.
(68) Iggo, A.; Muir, A. R. The structure and function of a slowly adapting touch corpuscle in hairy skin. *J. Physiol.* **1969**, *200* (3), 763.
(69) Woodbury, C. J.; Koerber, H. R. Central and peripheral anatomy of slowly adapting type I low-threshold mechanoreceptors innervating trunk skin of neonatal mice. *J. Comp. Neurol.* **2007**, *505* (5), 547−561.
(70) Chambers, M. R.; Andres, K.; Duering, M. v.; Iggo, A. The structure and function of the slowly adapting type II mechanoreceptor in hairy skin. *Exp. Physiol.* **1972**, *57* (4), 417−445.
(71) Purves, D.; Augustine, G. J.; Fitzpatrick, D.; Hall, W.; LaMantia, A.-S.; White, L. *Neurosciences*; De Boeck Supérieur, 2019.
(72) Cauna, N. Nerve supply and nerve endings in Meissner's corpuscles. *Am. J. Anat.* **1956**, *99* (2), 315−350.
(73) Loewenstein, W.; Skalak, R. Mechanical transmission in a Pacinian corpuscle. An analysis and a theory. *J. Physiol.* **1966**, *182* (2), 346−378.
(74) Zimmerman, A.; Bai, L.; Ginty, D. D. The gentle touch receptors of mammalian skin. *Science* **2014**, *346* (6212), 950−954.
(75) McGlone, F.; Olausson, H.; Boyle, J. A.; Jones-Gotman, M.; Dancer, C.; Guest, S.; Essick, G. Touching and feeling: differences in pleasant touch processing between glabrous and hairy skin in humans. *Eur. J. Neurosci.* **2012**, *35* (11), 1782−1788.
(76) Ackerley, R.; Saar, K.; McGlone, F.; Backlund Wasling, H. Quantifying the sensory and emotional perception of touch: differences between glabrous and hairy skin. *Front. Behav. Neurosci.* **2014**, *8*, 34.


https://doi.org/10.1021/acs.chemrev.4c00966
*Chem. Rev.* 2025, 125, 11567−11665

(77) Patapoutian, A.; Peier, A. M.; Story, G. M.; Viswanath, V. ThermoTRP channels and beyond: mechanisms of temperature sensation. *Nat. Rev. Neurosci.* **2003**, *4* (7), 529−539.
(78) Chéry-Croze, S. Relationship between noxious cold stimuli and the magnitude of pain sensation in man. *Pain* **1983**, *15* (1−4), 265−269.
(79) Dubin, A. E.; Patapoutian, A. Nociceptors: the sensors of the pain pathway. *J. Clin. Invest.* **2010**, *120* (11), 3760−3772.
(80) Campero, M.; Serra, J.; Ochoa, J. L. C-polymodal nociceptors activated by noxious low temperature in human skin. *J. Physiol.* **1996**, *497* (2), 565−572.
(81) Willis, W. D., Jr.; Coggeshall, R. E. *Sensory Mechanisms of the Spinal Cord: Vol. 1 Primary Afferent Neurons and the Spinal Dorsal Horn*; Springer Science & Business Media, 2012.
(82) Araki, I.; Du, S.; Kobayashi, H.; Sawada, N.; Mochizuki, T.; Zakoji, H.; Takeda, M. Roles of mechanosensitive ion channels in bladder sensory transduction and overactive bladder. *Int. J. Urol.* **2008**, *15* (8), 681−687.
(83) Coste, B.; Mathur, J.; Schmidt, M.; Earley, T. J.; Ranade, S.; Petrus, M. J.; Dubin, A. E.; Patapoutian, A. Piezo1 and Piezo2 are essential components of distinct mechanically activated cation channels. *Science* **2010**, *330* (6000), 55−60.
(84) Lingueglia, E. Acid-sensing ion channels in sensory perception. *J. Biol. Chem.* **2007**, *282* (24), 17325−17329.
(85) Damann, N.; Voets, T.; Nilius, B. TRPs in our senses. *Curr. Biol.* **2008**, *18* (18), R880−R889.
(86) McKemy, D. D.; Neuhausser, W. M.; Julius, D. Identification of a cold receptor reveals a general role for TRP channels in thermosensation. *Nature* **2002**, *416* (6876), 52−58.
(87) Vaidehi, N.; Floriano, W. B.; Trabanino, R.; Hall, S. E.; Freddolino, P.; Choi, E. J.; Zamanakos, G.; Goddard, W. A., III Prediction of structure and function of G protein-coupled receptors. *Proc. Natl. Acad. Sci. U. S. A.* **2002**, *99* (20), 12622−12627.
(88) Maßberg, D.; Hatt, H. Human olfactory receptors: novel cellular functions outside of the nose. *Physiol. Rev.* **2018**, *98* (3), 1739−1763.
(89) Amoore, J. E.; Hautala, E. Odor as an ald to chemical safety: Odor thresholds compared with threshold limit values and volatilities for 214 industrial chemicals in air and water dilution. *J. Appl. Toxicol.* **1983**, *3* (6), 272−290.
(90) Gaillard, I.; Rouquier, S.; Giorgi, D. Olfactory receptors. *Cell. Mol. Life Sci.* **2004**, *61*, 456−469.
(91) Paik, S. I.; Lehman, M. N.; Seiden, A. M.; Duncan, H. J.; Smith, D. V. Human olfactory biopsy: the influence of age and receptor distribution. *Archives of Otolaryngology-Head & Neck Surgery* **1992**, *118* (7), 731−738.
(92) Silverthorn, D. U. *Human Physiology*; Jones & Bartlett Publishers, 2015.
(93) Buck, L. B. The molecular architecture of odor and pheromone sensing in mammals. *Cell* **2000**, *100* (6), 611−618.
(94) Breer, H. Olfactory receptors: molecular basis for recognition and discrimination of odors. *Anal. Bioanal. Chem.* **2003**, *377*, 427−433.
(95) Sharma, A.; Kumar, R.; Aier, I.; Semwal, R.; Tyagi, P.; Varadwaj, P. Sense of smell: structural, functional, mechanistic advancements and challenges in human olfactory research. *Curr. Neuropharmacol.* **2019**, *17* (9), 891−911.
(96) Zarzo, M. The sense of smell: molecular basis of odorant recognition. *Biol. Rev.* **2007**, *82* (3), 455−479.
(97) Jones, D. T.; Reed, R. R. Golf: an olfactory neuron specific-G protein involved in odorant signal transduction. *Science* **1989**, *244* (4906), 790−795.
(98) Billig, G. M.; Pál, B.; Fidzinski, P.; Jentsch, T. J. Ca2+-activated Cl- currents are dispensable for olfaction. *Nat. Neurosci.* **2011**, *14* (6), 763−769.
(99) Schild, D.; Restrepo, D. Transduction mechanisms in vertebrate olfactory receptor cells. *Physiol. Rev.* **1998**, *78* (2), 429−466.
(100) Kurahashi, T.; Menini, A. Mechanism of odorant adaptation in the olfactory receptor cell. *Nature* **1997**, *385* (6618), 725−729.
(101) Spehr, M.; Munger, S. D. Olfactory receptors: G protein-coupled receptors and beyond. *J. Neurochem.* **2009**, *109* (6), 1570−1583.
(102) Buck, L. B.; Bargmann, C. Smell and taste: The chemical senses. *Princ. Neural. Sci.* **2000**, *4*, 625−647.
(103) Lindemann, B. Receptors and transduction in taste. *Nature* **2001**, *413* (6852), 219−225.
(104) Lindemann, B. Taste reception. *Physiol. Rev.* **1996**, *76* (3), 719−766.
(105) Chaudhari, N.; Landin, A. M.; Roper, S. D. A metabotropic glutamate receptor variant functions as a taste receptor. *Nat. Neurosci.* **2000**, *3* (2), 113−119.
(106) Adler, E.; Hoon, M. A.; Mueller, K. L.; Chandrashekar, J.; Ryba, N. J.; Zuker, C. S. A novel family of mammalian taste receptors. *Cell* **2000**, *100* (6), 693−702.
(107) Margolskee, R. F. Molecular mechanisms of bitter and sweet taste transduction. *J. Biol. Chem.* **2002**, *277* (1), 1−4.
(108) Nelson, G.; Hoon, M. A.; Chandrashekar, J.; Zhang, Y.; Ryba, N. J.; Zuker, C. S. Mammalian sweet taste receptors. *Cell* **2001**, *106* (3), 381−390.
(109) Huang, A. L.; Chen, X.; Hoon, M. A.; Chandrashekar, J.; Guo, W.; Tränkner, D.; Ryba, N. J.; Zuker, C. S. The cells and logic for mammalian sour taste detection. *Nature* **2006**, *442* (7105), 934−938.
(110) Kim, K. K.; Suh, Y.; Ko, S. H. Smart stretchable electronics for advanced human-machine interface. *Adv. Intell. Syst.* **2021**, *3* (2), 2000157.
(111) Kim, J. J.; Wang, Y.; Wang, H.; Lee, S.; Yokota, T.; Someya, T. Skin electronics: next-generation device platform for virtual and augmented reality. *Adv. Funct. Mater.* **2021**, *31* (39), 2009602.
(112) Yin, J.; Hinchet, R.; Shea, H.; Majidi, C. Wearable soft technologies for haptic sensing and feedback. *Adv. Funct. Mater.* **2021**, *31* (39), 2007428.
(113) Jeong, J.-W.; Yeo, W.-H.; Akhtar, A.; Norton, J. J.; Kwack, Y.-J.; Li, S.; Jung, S.-Y.; Su, Y.; Lee, W.; Xia, J.; et al. Materials and optimized designs for human-machine interfaces via epidermal electronics. *Adv. Mater.* **2013**, *25* (47), 6839−6846.
(114) Rogers, J. A.; Someya, T.; Huang, Y. Materials and mechanics for stretchable electronics. *Science* **2010**, *327* (5973), 1603−1607.
(115) Mazzotta, A.; Carlotti, M.; Mattoli, V. Conformable on-skin devices for thermo-electro-tactile stimulation: Materials, design, and fabrication. *Mater. Adv.* **2021**, *2* (6), 1787−1820.
(116) Wu, H.; Tian, Y.; Luo, H.; Zhu, H.; Duan, Y.; Huang, Y. Fabrication techniques for curved electronics on arbitrary surfaces. *Adv. Mater. Technol.* **2020**, *5* (8), 2000093.
(117) Yuk, H.; Wu, J.; Zhao, X. Hydrogel interfaces for merging humans and machines. *Nat. Rev. Mater.* **2022**, *7* (12), 935−952.
(118) Yuk, H.; Lu, B.; Zhao, X. Hydrogel bioelectronics. *Chem. Soc. Rev.* **2019**, *48* (6), 1642−1667.
(119) Ershad, F.; Thukral, A.; Yue, J.; Comeaux, P.; Lu, Y.; Shim, H.; Sim, K.; Kim, N.-I.; Rao, Z.; Guevara, R.; Contreras, L.; Pan, F.; Zhang, Y.; Guan, Y.-S.; Yang, P.; Wang, X.; Wang, P.; Wu, X.; Yu, C. Ultra-conformal drawn-on-skin electronics for multifunctional motion artifact-free sensing and point-of-care treatment. *Nat. Commun.* **2020**, *11* (1), 3823.
(120) Miyamoto, A.; Lee, S.; Cooray, N. F.; Lee, S.; Mori, M.; Matsuhisa, N.; Jin, H.; Yoda, L.; Yokota, T.; Itoh, A.; et al. Inflammation-free, gas-permeable, lightweight, stretchable on-skin electronics with nanomeshes. *Nat. Nanotechnol.* **2017**, *12* (9), 907−913.
(121) Lee, S.; Franklin, S.; Hassani, F. A.; Yokota, T.; Nayeem, M. O. G.; Wang, Y.; Leib, R.; Cheng, G.; Franklin, D. W.; Someya, T. Nanomesh pressure sensor for monitoring finger manipulation without sensory interference. *Science* **2020**, *370* (6519), 966−970.
(122) Kim, K. K.; Kim, M.; Pyun, K.; Kim, J.; Min, J.; Koh, S.; Root, S. E.; Kim, J.; Nguyen, B.-N. T.; Nishio, Y.; Han, S.; Choi, J.; Kim, C-Y.; Tok, J. B.-H.; Jo, S.; Ko, S. H.; Bao, Z. A substrate-less nanomesh receptor with meta-learning for rapid hand task recognition. *Nat. Electron.* **2022**, *6*, 64−75.


https://doi.org/10.1021/acs.chemrev.4c00966
*Chem. Rev.* 2025, 125, 11567−11665

(123) Kim, D.-H.; Lu, N.; Ma, R.; Kim, Y.-S.; Kim, R.-H.; Wang, S.; Wu, J.; Won, S. M.; Tao, H.; Islam, A.; et al. Epidermal electronics. *Science* **2011**, *333* (6044), 838−843.
(124) Kim, J.; Lee, J.; Son, D.; Choi, M. K.; Kim, D.-H. Deformable devices with integrated functional nanomaterials for wearable electronics. *Nano Converg.* **2016**, *3*, 4.
(125) Chortos, A.; Bao, Z. Skin-inspired electronic devices. *Mater. Today* **2014**, *17* (7), 321−331.
(126) Song, S.; Kim, K. Y.; Lee, S. H.; Kim, K. K.; Lee, K.; Lee, W.; Jeon, H.; Ko, S. H. Recent advances in 1D nanomaterial-based bioelectronics for healthcare applications. *Adv. NanoBiomed Res.* **2022**, *2* (3), 2100111.
(127) Gong, S.; Cheng, W. One-dimensional nanomaterials for soft electronics. *Adv. Electron. Mater.* **2017**, *3* (3), 1600314.
(128) Kim, S. J.; Choi, K.; Lee, B.; Kim, Y.; Hong, B. H. Materials for flexible, stretchable electronics: graphene and 2D materials. *Annu. Rev. Mater. Res.* **2015**, *45* (1), 63−84.
(129) Chen, J.; Yu, Q.; Cui, X.; Dong, M.; Zhang, J.; Wang, C.; Fan, J.; Zhu, Y.; Guo, Z. An overview of stretchable strain sensors from conductive polymer nanocomposites. *J. Mater. Chem. C* **2019**, *7* (38), 11710−11730.
(130) Kayser, L. V.; Lipomi, D. J. Stretchable conductive polymers and composites based on PEDOT and PEDOT: PSS. *Adv. Mater.* **2019**, *31* (10), 1806133.
(131) Kim, T.; Cho, M.; Yu, K. J. Flexible and stretchable bio-integrated electronics based on carbon nanotube and graphene. *Materials* **2018**, *11* (7), 1163.
(132) Liu, G.; Zhang, Z.; Li, Z.; Guo, L.; Ning, L. 0D to 2D carbon-based materials in flexible strain sensors: recent advances and perspectives. *2D Mater.* **2023**, *10* (2), 022002.
(133) Dickey, M. D. Stretchable and soft electronics using liquid metals. *Adv. Mater.* **2017**, *29* (27), 1606425.
(134) Kim, M.; Lim, H.; Ko, S. H. Liquid metal patterning and unique properties for next-generation soft electronics. *Adv. Sci.* **2023**, *10* (6), 2205795.
(135) Lee, H. R.; Kim, C. C.; Sun, J. Y. Stretchable ionics-a promising candidate for upcoming wearable devices. *Adv. Mater.* **2018**, *30* (42), 1704403.
(136) Wang, H.; Wang, Z.; Yang, J.; Xu, C.; Zhang, Q.; Peng, Z. Ionic gels and their applications in stretchable electronics. *Macromol. Rapid Commun.* **2018**, *39* (16), 1800246.
(137) Yoon, Y.; Truong, P. L.; Lee, D.; Ko, S. H. Metal-oxide nanomaterials synthesis and applications in flexible and wearable sensors. *ACS Nanosci. Au* **2022**, *2* (2), 64−92.
(138) Joo, H.; Jung, D.; Sunwoo, S. H.; Koo, J. H.; Kim, D. H. Material design and fabrication strategies for stretchable metallic nanocomposites. *Small* **2020**, *16* (11), 1906270.
(139) Matsuhisa, N.; Chen, X.; Bao, Z.; Someya, T. Materials and structural designs of stretchable conductors. *Chem. Soc. Rev.* **2019**, *48* (11), 2946−2966.
(140) Hua, Q.; Shen, G. Low-dimensional nanostructures for monolithic 3D-integrated flexible and stretchable electronics. *Chem. Soc. Rev.* **2024**, *53* (3), 1316−1353.
(141) Xue, Z.; Song, H.; Rogers, J. A.; Zhang, Y.; Huang, Y. Mechanically-guided structural designs in stretchable inorganic electronics. *Adv. Mater.* **2020**, *32* (15), 1902254.
(142) Lee, G.; Zarei, M.; Wei, Q.; Zhu, Y.; Lee, S. G. Surface wrinkling for flexible and stretchable sensors. *Small* **2022**, *18* (42), 2203491.
(143) Gong, M.; Zhang, L.; Wan, P. Polymer nanocomposite meshes for flexible electronic devices. *Prog. Polym. Sci.* **2020**, *107*, 101279.
(144) Park, J. J.; Won, P.; Ko, S. H. A review on hierarchical origami and kirigami structure for engineering applications. *INT. J. PRECIS. ENG. MAN-GT.* **2019**, *6*, 147−161.
(145) Luo, Y.; Abidian, M. R.; Ahn, J.-H.; Akinwande, D.; Andrews, A. M.; Antonietti, M.; Bao, Z.; Berggren, M.; Berkey, C. A.; Bettinger, C. J.; et al. Technology roadmap for flexible sensors. *ACS Nano* **2023**, *17* (6), 5211−5295.
(146) Choi, S.; Han, S. I.; Jung, D.; Hwang, H. J.; Lim, C.; Bae, S.; Park, O. K.; Tschabrunn, C. M.; Lee, M.; Bae, S. Y.; et al. Highly conductive, stretchable and biocompatible Ag-Au core-sheath nanowire composite for wearable and implantable bioelectronics. *Nat. Nanotechnol.* **2018**, *13* (11), 1048−1056.
(147) Jung, Y.; Kim, M.; Kim, T.; Ahn, J.; Lee, J.; Ko, S. H. Functional materials and innovative strategies for wearable thermal management applications. *Nano-Micro Lett.* **2023**, *15*, 160.
(148) Chen, F.; Huang, Q.; Zheng, Z. Permeable conductors for wearable and on-skin electronics. *Small Struct.* **2022**, *3* (1), 2100135.
(149) McShan, D.; Ray, P. C.; Yu, H. Molecular toxicity mechanism of nanosilver. *J. Food Drug Anal.* **2014**, *22* (1), 116−127.
(150) Won, D.; Kim, J.; Choi, J.; Kim, H.; Han, S.; Ha, I.; Bang, J.; Kim, K. K.; Lee, Y.; Kim, T.-S.; Park, J.-H.; Kim, C-Y.; Ko, S. H. Digital selective transformation and patterning of highly conductive hydrogel bioelectronics by laser-induced phase separation. *Sci. Adv.* **2022**, *8* (23), No. eabo3209.
(151) Lu, B.; Yuk, H.; Lin, S.; Jian, N.; Qu, K.; Xu, J.; Zhao, X. Pure Pedot:Pss hydrogels. *Nat. Commun.* **2019**, *10*, 1043.
(152) Won, D.; Kim, H.; Kim, J.; Kim, H.; Kim, M. W.; Ahn, J.; Min, K.; Lee, Y.; Hong, S.; Choi, J.; et al. Laser-induced wet stability and adhesion of pure conducting polymer hydrogels. *Nat. Electron.* **2024**, *7*, 475−486.
(153) Li, K.; Cheng, X.; Zhu, F.; Li, L.; Xie, Z.; Luan, H.; Wang, Z.; Ji, Z.; Wang, H.; Liu, F.; Xue, Y.; Jiang, C.; Feng, X.; Li, L.; Rogers, J. A.; Huang, Y.; Zhang, Y. A generic soft encapsulation strategy for stretchable electronics. *Adv. Funct. Mater.* **2019**, *29* (8), 1806630.
(154) Liu, H.; Qing, H.; Li, Z.; Han, Y. L.; Lin, M.; Yang, H.; Li, A.; Lu, T. J.; Li, F.; Xu, F. A promising material for human-friendly functional wearable electronics. *Mater. Sci. Eng. R Rep.* **2017**, *112*, 1−22.
(155) Larson, C.; Peele, B.; Li, S.; Robinson, S.; Totaro, M.; Beccai, L.; Mazzolai, B.; Shepherd, R. Highly stretchable electroluminescent skin for optical signaling and tactile sensing. *Science* **2016**, *351* (6277), 1071−1074.
(156) Li, D.; Zhou, J.; Yao, K.; Liu, S.; He, J.; Su, J.; Qu, Q. a.; Gao, Y.; Song, Z.; Yiu, C.; Sha, C.; Sun, Z.; Zhang, B.; Li, J.; Huang, L.; Xu, C.; Wong, T. H.; Huang, X.; Li, J.; Ye, R.; Wei, L.; Zhang, Z.; Guo, X.; Dai, Y.; Xie, Z.; Yu, X. Touch IoT enabled by wireless self-sensing and haptic-reproducing electronic skin. *Sci. Adv.* **2022**, *8* (51), No. eade2450.
(157) Arwani, R. T.; Tan, S. C. L.; Sundarapandi, A.; Goh, W. P.; Liu, Y.; Leong, F. Y.; Yang, W.; Zheng, X. T.; Yu, Y.; Jiang, C.; et al. Stretchable ionic-electronic bilayer hydrogel electronics enable in situ detection of solid-state epidermal biomarkers. *Nat. Mater.* **2024**, *23*, 1115−1122.
(158) Song, E.; Lee, Y. K.; Li, R.; Li, J.; Jin, X.; Yu, K. J.; Xie, Z.; Fang, H.; Zhong, Y.; Du, H.; Zhang, J.; Fang, G.; Kim, Y.; Yoon, Y.; Alam, M. A.; Mei, Y.; Huang, Y.; Rogers, J. A. Transferred, ultrathin oxide bilayers as biofluid barriers for flexible electronic implants. *Adv. Funct. Mater.* **2018**, *28* (12), 1702284.
(159) Lim, C.; Hong, Y. J.; Jung, J.; Shin, Y.; Sunwoo, S.-H.; Baik, S.; Park, O. K.; Choi, S. H.; Hyeon, T.; Kim, J. H.; Lee, S.; Kim, D.-H. Tissue-like skin-device interface for wearable bioelectronics by using ultrasoft, mass-permeable, and low-impedance hydrogels. *Sci. Adv.* **2021**, *7* (19), No. eabd3716.
(160) Yang, J.; Zhang, Z.; Zhou, P.; Zhang, Y.; Liu, Y.; Xu, Y.; Gu, Y.; Qin, S.; Haick, H.; Wang, Y. Toward a new generation of permeable skin electronics. *Nanoscale* **2023**, *15* (7), 3051−3078.
(161) Yao, K.; Zhuang, Q.; Zhang, Q.; Zhou, J.; Yiu, C. K.; Zhang, J.; Ye, D.; Yang, Y.; Wong, K. W.; Chow, L.; Huang, T.; Qiu, Y.; Jia, S.; Li, Z.; Zhao, G.; Zhang, H.; Zhu, J.; Huang, X.; Li, J.; Gao, Y.; Wang, H.; Li, J.; Huang, Y.; Li, D.; Zhang, B.; Wang, J.; Chen, Z.; Guo, G.; Zheng, Z.; Yu, X. A fully integrated breathable haptic textile. *Sci. Adv.* **2024**, *10* (42), No. eadq9575.
(162) Ma, Z.; Huang, Q.; Xu, Q.; Zhuang, Q.; Zhao, X.; Yang, Y.; Qiu, H.; Yang, Z.; Wang, C.; Chai, Y.; et al. Permeable superelastic liquid-metal fibre mat enables biocompatible and monolithic stretchable electronics. *Nat. Mater.* **2021**, *20* (6), 859−868.


https://doi.org/10.1021/acs.chemrev.4c00966
*Chem. Rev.* 2025, 125, 11567−11665

(163) Zhuang, Q.; Yao, K.; Zhang, C.; Song, X.; Zhou, J.; Zhang, Y.; Huang, Q.; Zhou, Y.; Yu, X.; Zheng, Z. Permeable, three-dimensional integrated electronic skins with stretchable hybrid liquid metal solders. *Nat. Electron.* **2024**, *7* (7), 598−609.
(164) Min, J.; Tu, J.; Xu, C.; Lukas, H.; Shin, S.; Yang, Y.; Solomon, S. A.; Mukasa, D.; Gao, W. Skin-interfaced wearable sweat sensors for precision medicine. *Chem. Rev.* **2023**, *123* (8), 5049−5138.
(165) Zhang, B.; Li, J.; Zhou, J.; Chow, L.; Zhao, G.; Huang, Y.; Ma, Z.; Zhang, Q.; Yang, Y.; Yiu, C. K.; et al. A three-dimensional liquid diode for soft, integrated permeable electronics. *Nature* **2024**, *628* (8006), 84−92.
(166) Li, W.; Lu, L.; Kottapalli, A. G. P.; Pei, Y. Bioinspired sweat-resistant wearable triboelectric nanogenerator for movement monitoring during exercise. *Nano Energy* **2022**, *95*, 107018.
(167) Yang, X.; Wang, S.; Liu, M.; Li, L.; Zhao, Y.; Wang, Y.; Bai, Y.; Lu, Q.; Xiong, Z.; Feng, S.; Zhang, T. All-nanofiber-based Janus epidermal electrode with directional sweat permeability for artifact-free biopotential monitoring. *Small* **2022**, *18* (12), 2106477.
(168) Yeom, J.; Choe, A.; Lim, S.; Lee, Y.; Na, S.; Ko, H. Soft and ion-conducting hydrogel artificial tongue for astringency perception. *Sci. Adv.* **2020**, *6* (23), No. eaba5785.
(169) Celebi, K.; Buchheim, J.; Wyss, R. M.; Droudian, A.; Gasser, P.; Shorubalko, I.; Kye, J.-I.; Lee, C.; Park, H. G. Ultimate permeation across atomically thin porous graphene. *Science* **2014**, *344* (6181), 289−292.
(170) Jiang, Z.; Chen, N.; Yi, Z.; Zhong, J.; Zhang, F.; Ji, S.; Liao, R.; Wang, Y.; Li, H.; Liu, Z.; et al. A 1.3-micrometre-thick elastic conductor for seamless on-skin and implantable sensors. *Nat. Electron.* **2022**, *5* (11), 784−793.
(171) Yoon, H.; Choi, J.; Kim, J.; Kim, J.; Min, J.; Kim, D.; Jeong, S.; Lee, J. G.; Bang, J.; Choi, S. H.; Jeong, Y.; Kim, C-Y.; Ko, S. H. Adaptive epidermal bioelectronics by highly breathable and stretchable metal nanowire bioelectrodes on electrospun nanofiber membrane. *Adv. Funct. Mater.* **2024**, *34* (22), 2313504.
(172) Pyun, K. R.; Jeong, S.; Yoo, M. J.; Choi, S. H.; Baik, G.; Lee, M.; Song, J.; Ko, S. H. Tunable Radiative Cooling by Mechanochromic Electrospun Micro-Nanofiber Matrix. *Small* **2024**, *20* (20), 2308572.
(173) Huang, Y.; Yao, K.; Li, J.; Li, D.; Jia, H.; Liu, Y.; Yiu, C. K.; Park, W.; Yu, X. Recent advances in multi-mode haptic feedback technologies towards wearable interfaces. *Mater. Today Phys.* **2022**, *22*, 100602.
(174) Shih, B.; Shah, D.; Li, J.; Thuruthel, T. G.; Park, Y.-L.; Iida, F.; Bao, Z.; Kramer-Bottiglio, R.; Tolley, M. T. Electronic skins and machine learning for intelligent soft robots. *Sci. Robot.* **2020**, *5* (41), No. eaaz9239.
(175) Lee, D.; Bae, J. Soft Multimodal Sensors with Decoupled Multimodality and Minimal Wiring for Wearable Systems. *Adv. Funct. Mater.* **2024**, *34*, 2409841.
(176) Ho, D. H.; Sun, Q.; Kim, S. Y.; Han, J. T.; Kim, D. H.; Cho, J. H. Stretchable and multimodal all graphene electronic skin. *Adv. Mater.* **2016**, *28* (13), 2601−2608.
(177) Xu, B.; Akhtar, A.; Liu, Y.; Chen, H.; Yeo, W.-H.; Park, S. I.; Boyce, B.; Kim, H.; Yu, J.; Lai, H.-Y.; Jung, S.; Zhou, Y.; Kim, J.; Cho, S.; Huang, Y.; Bretl, T.; Rogers, J. A. An epidermal stimulation and sensing platform for sensorimotor prosthetic control, management of lower back exertion, and electrical muscle activation. *Adv. Mater.* **2016**, *28* (22), 4462.
(178) Zhang, F.; Zang, Y.; Huang, D.; Di, C.-a.; Zhu, D. Flexible and self-powered temperature-pressure dual-parameter sensors using microstructure-frame-supported organic thermoelectric materials. *Nat. Commun.* **2015**, *6* (1), 8356.
(179) You, I.; Mackanic, D. G.; Matsuhisa, N.; Kang, J.; Kwon, J.; Beker, L.; Mun, J.; Suh, W.; Kim, T. Y.; Tok, J. B.-H.; et al. Artificial multimodal receptors based on ion relaxation dynamics. *Science* **2020**, *370* (6519), 961−965.
(180) Yao, D. R.; Kim, I.; Yin, S.; Gao, W. Multimodal soft robotic actuation and locomotion. *Adv. Mater.* **2024**, *36*, 2308829.
(181) Zhu, M.; Memar, A. H.; Gupta, A.; Samad, M.; Agarwal, P.; Visell, Y.; Keller, S. J.; Colonnese, N. Pneusleeve: In-fabric multimodal actuation and sensing in a soft, compact, and expressive haptic sleeve. In *Proceedings of the 2020 CHI Conference on Human Factors in Computing Systems*, 2020; pp 1−12.
(182) Wang, T.; Jin, T.; Lin, W.; Lin, Y.; Liu, H.; Yue, T.; Tian, Y.; Li, L.; Zhang, Q.; Lee, C. Multimodal sensors enabled autonomous soft robotic system with self-adaptive manipulation. *ACS Nano* **2024**, *18* (14), 9980−9996.
(183) Zhou, S.; Li, Y.; Wang, Q.; Lyu, Z. Integrated Actuation and Sensing: Toward Intelligent Soft Robots. *Cyborg Bionic Syst.* **2024**, *5*, 0105.
(184) Yu, M.; Cheng, X.; Peng, S.; Cao, Y.; Lu, Y.; Li, B.; Feng, X.; Zhang, Y.; Wang, H.; Jiao, Z.; et al. A self-sensing soft pneumatic actuator with closed-Loop control for haptic feedback wearable devices. *Mater. Des.* **2022**, *223*, 111149.
(185) Zeng, W.; Shu, L.; Li, Q.; Chen, S.; Wang, F.; Tao, X. M. Fiber-based wearable electronics: a review of materials, fabrication, devices, and applications. *Adv. Mater.* **2014**, *26* (31), 5310−5336.
(186) Jung, J.; Kim, K. K.; Suh, Y. D.; Hong, S.; Yeo, J.; Ko, S. H. Recent progress in controlled nano/micro cracking as an alternative nano-patterning method for functional applications. *Nanoscale Horiz.* **2020**, *5* (7), 1036−1049.
(187) Rogers, J. A.; Nuzzo, R. G. Recent progress in soft lithography. *Mater. Today* **2005**, *8* (2), 50−56.
(188) Zhang, Y.; Zhang, F.; Yan, Z.; Ma, Q.; Li, X.; Huang, Y.; Rogers, J. A. Printing, folding and assembly methods for forming 3D mesostructures in advanced materials. *Nat. Rev. Mater.* **2017**, *2* (4), 17019.
(189) Park, H.; Park, J. J.; Bui, P. D.; Yoon, H.; Grigoropoulos, C. P.; Lee, D.; Ko, S. H. Laser-Based Selective Material Processing for Next-Generation Additive Manufacturing. *Adv. Mater.* **2024**, *36*, 2307586.
(190) Saadi, M.; Maguire, A.; Pottackal, N. T.; Thakur, M. S. H.; Ikram, M. M.; Hart, A. J.; Ajayan, P. M.; Rahman, M. M. Direct ink writing: a 3D printing technology for diverse materials. *Adv. Mater.* **2022**, *34* (28), 2108855.
(191) Zhu, Z.; Ng, D. W. H.; Park, H. S.; McAlpine, M. C. 3D-printed multifunctional materials enabled by artificial-intelligence-assisted fabrication technologies. *Nat. Rev. Mater.* **2021**, *6* (1), 27−47.
(192) Ren, Z.; Yang, J.; Kim, S.; Hsiao, Y.-H.; Lang, J.; Chen, Y. A lightweight high-voltage boost circuit for soft-actuated micro-aerial-robots. In *2023 IEEE International Conference on Robotics and Automation (ICRA)*; IEEE, 2023; pp 3397−3403.
(193) Kim, K. K.; Choi, J.; Kim, J. H.; Nam, S.; Ko, S. H. Evolvable skin electronics by in situ and in operando adaptation. *Adv. Funct. Mater.* **2022**, *32* (4), 2106329.
(194) Kim, Y.; Suh, J. M.; Shin, J.; Liu, Y.; Yeon, H.; Qiao, K.; Kum, H. S.; Kim, C.; Lee, H. E.; Choi, C.; et al. Chip-less wireless electronic skins by remote epitaxial freestanding compound semiconductors. *Science* **2022**, *377* (6608), 859−864.
(195) Someya, T.; Bao, Z.; Malliaras, G. G. The rise of plastic bioelectronics. *Nature* **2016**, *540* (7633), 379−385.
(196) Han, S.; Kim, J.; Won, S. M.; Ma, Y.; Kang, D.; Xie, Z.; Lee, K.-T.; Chung, H. U.; Banks, A.; Min, S.; Heo, S. Y.; Davies, C. R.; Lee, J. W.; Lee, C.-H.; Kim, B. H.; Li, K.; Zhou, Y.; Wei, C.; Feng, X.; Huang, Y.; Rogers, J. A. Battery-free, wireless sensors for full-body pressure and temperature mapping. *Sci. Transl. Med.* **2018**, *10* (435), No. eaan4950.
(197) Moin, A.; Zhou, A.; Rahimi, A.; Menon, A.; Benatti, S.; Alexandrov, G.; Tamakloe, S.; Ting, J.; Yamamoto, N.; Khan, Y.; et al. A wearable biosensing system with in-sensor adaptive machine learning for hand gesture recognition. *Nat. Electron.* **2021**, *4* (1), 54−63.
(198) Sundaram, S.; Kellnhofer, P.; Li, Y.; Zhu, J.-Y.; Torralba, A.; Matusik, W. Learning the signatures of the human grasp using a scalable tactile glove. *Nature* **2019**, *569* (7758), 698−702.
(199) Flavin, M. T.; Ha, K.-H.; Guo, Z.; Li, S.; Kim, J.-T.; Saxena, T.; Simatos, D.; Al-Najjar, F.; Mao, Y.; Bandapalli, S.; et al. Bioelastic


https://doi.org/10.1021/acs.chemrev.4c00966
*Chem. Rev.* 2025, 125, 11567−11665

state recovery for haptic sensory substitution. *Nature* **2024**, *635*, 345−352.
(200) Zavanelli, N.; Yeo, W.-H. Advances in screen printing of conductive nanomaterials for stretchable electronics. *ACS Omega* **2021**, *6* (14), 9344−9351.
(201) Sun, B.; Long, Y.-Z.; Chen, Z.-J.; Liu, S.-L.; Zhang, H.-D.; Zhang, J.-C.; Han, W.-P. Recent advances in flexible and stretchable electronic devices via electrospinning. *J. Mater. Chem. C* **2014**, *2* (7), 1209−1219.
(202) Abbel, R.; Galagan, Y.; Groen, P. Roll-to-roll fabrication of solution processed electronics. *Adv. Eng. Mater.* **2018**, *20* (8), 1701190.
(203) Xu, S.; Zhang, Y.; Cho, J.; Lee, J.; Huang, X.; Jia, L.; Fan, J. A.; Su, Y.; Su, J.; Zhang, H.; Cheng, H.; Lu, B.; Yu, C.; Chuang, C.; Kim, T.-i.; Song, T.; Shigeta, K.; Kang, S.; Dagdeviren, C.; Petrov, I.; Braun, P. V.; Huang, Y.; Paik, U.; Rogers, J. A. Stretchable batteries with self-similar serpentine interconnects and integrated wireless recharging systems. *Nat. Commun.* **2013**, *4* (1), 1543.
(204) Lim, D.; Hong, I.; Park, S. U.; Chae, J. W.; Lee, S.; Baac, H. W.; Shin, C.; Lee, J.; Roh, Y.; Im, C.; Park, Y.; Lee, G.; Kim, U.; Koh, J.-S.; Kang, D.; Han, S.; Won, S. M. Functional Encapsulating Structure for Wireless and Immediate Monitoring of the Fluid Penetration. *Adv. Funct. Mater.* **2022**, *32* (31), 2201854.
(205) Vural, M.; Mohammadi, M.; Seufert, L.; Han, S.; Crispin, X.; Fridberger, A.; Berggren, M.; Tybrandt, K. Soft electromagnetic vibrotactile actuators with integrated vibration amplitude sensing. *ACS Appl. Mater. Interfaces* **2023**, *15* (25), 30653−30662.
(206) Liu, Y.; Yiu, C.; Song, Z.; Huang, Y.; Yao, K.; Wong, T.; Zhou, J.; Zhao, L.; Huang, X.; Nejad, S. K.; Wu, M.; Li, D.; He, J.; Guo, X.; Yu, J.; Feng, X.; Xie, Z.; Yu, X. Electronic skin as wireless human-machine interfaces for robotic VR. *Sci. Adv.* **2022**, *8* (2), No. eabl6700.
(207) Dong, Z.; Wang, Y.; Wen, J.; Li, F.; Du, Q.; Zhang, Y.; Zhao, X. NdFeB/PDMS Flexible Electromagnetic Actuator with Vibration and Nonvibration Dual Modes Based on Three-Dimensional Coils. *ACS Appl. Electron. Mater.* **2024**, *6* (1), 310−318.
(208) Li, D.; He, J.; Song, Z.; Yao, K.; Wu, M.; Fu, H.; Liu, Y.; Gao, Z.; Zhou, J.; Wei, L.; Zhang, Z.; Dai, Y.; Xie, Z.; Yu, X. Miniaturization of mechanical actuators in skin-integrated electronics for haptic interfaces. *Microsyst. Nanoeng.* **2021**, *7* (1), 85.
(209) Luo, Y.; Liu, C.; Lee, Y. J.; DelPreto, J.; Wu, K.; Foshey, M.; Rus, D.; Palacios, T.; Li, Y.; Torralba, A.; Matusik, W. Adaptive tactile interaction transfer via digitally embroidered smart gloves. *Nat. Commun.* **2024**, *15*, 868.
(210) Lim, K.; Lee, J.; Kim, S.; Oh, M.; Koh, C. S.; Seo, H.; Hong, Y.-M.; Chung, W. G.; Jang, J.; Lim, J. A.; Jung, H. H.; Park, J.-U. Interference haptic stimulation and consistent quantitative tactility in transparent electrotactile screen with pressure-sensitive transistors. *Nat. Commun.* **2024**, *15*, 7147.
(211) Akhtar, A.; Sombeck, J.; Boyce, B.; Bretl, T. Controlling sensation intensity for electrotactile stimulation in human-machine interfaces. *Sci. Robot.* **2018**, *3* (17), No. eaap9770.
(212) Ying, M.; Bonifas, A. P.; Lu, N.; Su, Y.; Li, R.; Cheng, H.; Ameen, A.; Huang, Y.; Rogers, J. A. Silicon nanomembranes for fingertip electronics. *Nanotechnology* **2012**, *23* (34), 344004.
(213) Schaffner, M.; Faber, J. A.; Pianegonda, L.; Rühs, P. A.; Coulter, F.; Studart, A. R. 3D printing of robotic soft actuators with programmable bioinspired architectures. *Nat. Commun.* **2018**, *9*, 878.
(214) Song, K.; Kim, S. H.; Jin, S.; Kim, S.; Lee, S.; Kim, J.-S.; Park, J.-M.; Cha, Y. Pneumatic actuator and flexible piezoelectric sensor for soft virtual reality glove system. *Sci. Rep.* **2019**, *9*, 8988.
(215) Frediani, G.; Carpi, F. Tactile display of softness on fingertip. *Sci. Rep.* **2020**, *10*, 20491.
(216) Wang, R.; Jiang, L.; Li, J.; Dai, Z.; Liu, M.; Lv, P.; Li, X.; Zhu, M. Tactile and Kinesthetic Communication Glove with Fusion of Triboelectric Sensing and Pneumatic Actuation. *Nano Energy* **2024**, *131*, 110273.
(217) Sun, L.; Okada, Y. Vibrotactile piezoelectric stimulation system with precise and versatile timing control for somatosensory research. *J. Neurosci. Methods* **2019**, *317*, 29−36.
(218) Sone, J. Fingertip tactile sensation via piezoelectric micromachined ultrasonic transducers with an amplified interface. *Sci. Rep.* **2024**, *14*, 2629.
(219) Shouji, Y.; Sekine, T.; Ito, K.; Ito, N.; Yasuda, T.; Wang, Y.-F.; Takeda, Y.; Kumaki, D.; Santos, F. D. D.; Miyabo, A.; Tokito, S. Fast Response, High-Power Tunable Ultrathin Soft Actuator by Functional Piezoelectric Material Composite for Haptic Device Application. *Adv. Electron. Mater.* **2023**, *9* (9), 2201040.
(220) Ozaki, T.; Ohta, N.; Jimbo, T.; Hamaguchi, K. A wireless radiofrequency-powered insect-scale flapping-wing aerial vehicle. *Nat. Electron.* **2021**, *4* (11), 845−852.
(221) Zhu, M.; Sun, Z.; Zhang, Z.; Shi, Q.; He, T.; Liu, H.; Chen, T.; Lee, C. Haptic-feedback smart glove as a creative human-machine interface (HMI) for virtual/augmented reality applications. *Sci. Adv.* **2020**, *6* (19), No. eaaz8693.
(222) Jin, H.; Kim, Y.; Youm, W.; Min, Y.; Seo, S.; Lim, C.; Hong, C.-H.; Kwon, S.; Park, G.; Park, S.; Kim, H. J. Highly pixelated, untethered tactile interfaces for an ultra-flexible on-skin telehaptic system. *npj Flex. Electron.* **2022**, *6*, 82.
(223) Lay, R.; Deijs, G. S.; Malmström, J. The intrinsic piezoelectric properties of materials-a review with a focus on biological materials. *RSC Adv.* **2021**, *11* (49), 30657−30673.
(224) Yang, M.-M.; Zhu, T.-Y.; Renz, A. B.; Sun, H.-M.; Liu, S.; Gammon, P. M.; Alexe, M. Auxetic piezoelectric effect in heterostructures. *Nat. Mater.* **2024**, *23* (1), 95−100.
(225) Park, S.-H.; Chuang, S.-L. Crystal-orientation effects on the piezoelectric field and electronic properties of strained wurtzite semiconductors. *Phys. Rev. B* **1999**, *59* (7), 4725.
(226) Hao, J.; Li, W.; Zhai, J.; Chen, H. Progress in high-strain perovskite piezoelectric ceramics. *Mater. Sci. Eng. R Rep.* **2019**, *135*, 1−57.
(227) Su, Y.; Li, W.; Cheng, X.; Zhou, Y.; Yang, S.; Zhang, X.; Chen, C.; Yang, T.; Pan, H.; Xie, G.; Chen, G.; Zhao, X.; Xiao, X.; Li, B.; Tai, H.; Jiang, Y.; Chen, L.-Q.; Li, F.; Chen, J. High-performance piezoelectric composites via $\beta$ phase programming. *Nat. Commun.* **2022**, *13*, 4867.
(228) Szewczyk, P. K.; Gradys, A.; Kim, S. K.; Persano, L.; Marzec, M.; Kryshtal, A.; Busolo, T.; Toncelli, A.; Pisignano, D.; Bernasik, A.; et al. Enhanced piezoelectricity of electrospun polyvinylidene fluoride fibers for energy harvesting. *ACS Appl. Mater. Interfaces* **2020**, *12* (11), 13575−13583.
(229) Mandal, D.; Henkel, K.; Schmeißer, D. The electroactive $\beta$-phase formation in poly (vinylidene fluoride) by gold nanoparticles doping. *Mater. Lett.* **2012**, *73*, 123−125.
(230) Acosta, M.; Novak, N.; Rojas, V.; Patel, S.; Vaish, R.; Koruza, J.; Rossetti, G.; Rödel, J. BaTiO3-based piezoelectrics: Fundamentals, current status, and perspectives. *Appl. Phys. Rev.* **2017**, *4* (4), 041305.
(231) Maurya, D.; Pramanick, A.; An, K.; Priya, S. Enhanced piezoelectricity and nature of electric-field induced structural phase transformation in textured lead-free piezoelectric Na0. 5Bi0. 5TiO3-BaTiO3 ceramics. *Appl. Phys. Lett.* **2012**, *100* (17), 172906.
(232) Jaykhedkar, N.; Tripathy, N.; Shah, V.; Pujari, B.; Premkumar, S. A comprehensive study of pressure dependent phase transitions in ferroelectric PbTiO3, PbZrO3 and BaTiO3. *Mater. Chem. Phys.* **2020**, *254*, 123545.
(233) Xavier, M. S.; Tawk, C. D.; Zolfagharian, A.; Pinskier, J.; Howard, D.; Young, T.; Lai, J.; Harrison, S. M.; Yong, Y. K.; Bodaghi, M.; et al. Soft pneumatic actuators: A review of design, fabrication, modeling, sensing, control and applications. *IEEE Access* **2022**, *10*, 59442−59485.
(234) Zhao, H.; O'brien, K.; Li, S.; Shepherd, R. F. Optoelectronically innervated soft prosthetic hand via stretchable optical waveguides. *Sci. Robot.* **2016**, *1* (1), No. eaai7529.
(235) Thuruthel, T. G.; Shih, B.; Laschi, C.; Tolley, M. T. Soft robot perception using embedded soft sensors and recurrent neural networks. *Sci. Robot.* **2019**, *4* (26), No. eaav1488.
(236) Justus, K. B.; Hellebrekers, T.; Lewis, D. D.; Wood, A.; Ingham, C.; Majidi, C.; LeDuc, P. R.; Tan, C. A biosensing soft robot:

Autonomous parsing of chemical signals through integrated organic and inorganic interfaces. *Sci. Robot.* **2019**, *4* (31), No. eaax0765.
(237) Terryn, S.; Brancart, J.; Lefeber, D.; Van Assche, G.; Vanderborght, B. Self-healing soft pneumatic robots. *Sci. Robot.* **2017**, *2* (9), No. eaan4268.
(238) Zhu, M.; Sun, Z.; Lee, C. Soft modular glove with multimodal sensing and augmented haptic feedback enabled by materials' multifunctionalities. *ACS Nano* **2022**, *16* (9), 14097−14110.
(239) Wang, Y.; Liang, J.; Yu, J.; Shan, Y.; Huang, X.; Lin, W.; Pan, Q.; Zhang, T.; Zhang, Z.; Gao, Y.; et al. Multiscale haptic interfaces for metaverse. *Device* **2024**, *2* (6), 100326.
(240) Gao, Y.; Yao, K.; Jia, S.; Huang, Y.; Zhao, G.; Zhang, B.; Liu, Y.; Yu, X. Advances in materials for haptic skin electronics. *Matter* **2024**, *7* (9), 2826−2845.
(241) Gu, G.; Zhang, N.; Xu, H.; Lin, S.; Yu, Y.; Chai, G.; Ge, L.; Yang, H.; Shao, Q.; Sheng, X.; et al. A soft neuroprosthetic hand providing simultaneous myoelectric control and tactile feedback. *Nat. Biomed. Eng.* **2023**, *7* (4), 589−598.
(242) Yao, K.; Zhou, J.; Huang, Q.; Wu, M.; Yiu, C. K.; Li, J.; Huang, X.; Li, D.; Su, J.; Hou, S.; et al. Encoding of tactile information in hand via skin-integrated wireless haptic interface. *Nat. Mach. Intell.* **2022**, *4* (10), 893−903.
(243) Keef, C. V.; Kayser, L. V.; Tronboll, S.; Carpenter, C. W.; Root, N. B.; Finn, M.; O'Connor, T. F.; Abuhamdieh, S. N.; Davies, D. M.; Runser, R.; Meng, Y. S.; Ramachandran, V. S.; Lipomi, D. J. Virtual texture generated using elastomeric conductive block copolymer in a wireless multimodal haptic glove. *Adv. Intell. Syst.* **2020**, *2* (4), 2000018.
(244) Shaner, S. W.; Islam, M.; Kristoffersen, M. B.; Azmi, R.; Heissler, S.; Ortiz-Catalan, M.; Korvink, J. G.; Asplund, M. Skin stimulation and recording: Moving towards metal-free electrodes. *Biosens. Bioelectron. X* **2022**, *11*, 100143.
(245) Shahrim, N. A. A.; Ahmad, Z.; Wong Azman, A.; Fachmi Buys, Y.; Sarifuddin, N. Mechanisms for doped PEDOT: PSS electrical conductivity improvement. *Mater. Adv.* **2021**, *2* (22), 7118−7138.
(246) Pyo, D.; Ryu, S.; Kyung, K.-U.; Yun, S.; Kwon, D.-S. High-pressure endurable flexible tactile actuator based on microstructured dielectric elastomer. *Appl. Phys. Lett.* **2018**, *112* (6), 061902.
(247) Song, E.; Xie, Z.; Bai, W.; Luan, H.; Ji, B.; Ning, X.; Xia, Y.; Baek, J. M.; Lee, Y.; Avila, R.; et al. Miniaturized electromechanical devices for the characterization of the biomechanics of deep tissue. *Nat. Biomed. Eng.* **2021**, *5* (7), 759−771.
(248) Qiu, W.; Li, Z.; Wang, G.; Peng, Y.; Zhang, M.; Wang, X.; Zhong, J.; Lin, L. A Moisture-Resistant Soft Actuator with Low Driving Voltages for Haptic Stimulations in Virtual Games. *ACS Appl. Mater. Interfaces* **2022**, *14* (27), 31257−31266.
(249) Hwang, I.; Kim, H. J.; Mun, S.; Yun, S.; Kang, T. J. A light-driven vibrotactile actuator with a polymer bimorph film for localized haptic rendering. *ACS Appl. Mater. Interfaces* **2021**, *13* (5), 6597−6605.
(250) Abad, S.-A.; Herzig, N.; Raitt, D.; Koltzenburg, M.; Wurdemann, H. Bioinspired adaptable multiplanar mechano-vibrotactile haptic system. *Nat. Commun.* **2024**, *15*, 7631.
(251) LaMotte, R. H.; Mountcastle, V. B. Capacities of humans and monkeys to discriminate vibratory stimuli of different frequency and amplitude: a correlation between neural events and psychological measurements. *J. Neurophysiol.* **1975**, *38* (3), 539−559.
(252) Talbot, W. H.; Darian-Smith, I.; Kornhuber, H. H.; Mountcastle, V. B. The sense of flutter-vibration: comparison of the human capacity with response patterns of mechanoreceptive afferents from the monkey hand. *J. Neurophysiol.* **1968**, *31* (2), 301−334.
(253) Sun, Z.; Zhu, M.; Shan, X.; Lee, C. Augmented tactile-perception and haptic-feedback rings as human-machine interfaces aiming for immersive interactions. *Nat. Commun.* **2022**, *13*, 5224.
(254) Jung, Y. H.; Yoo, J.-Y.; Vázquez-Guardado, A.; Kim, J.-H.; Kim, J.-T.; Luan, H.; Park, M.; Lim, J.; Shin, H.-S.; Su, C.-J.; et al. A wireless haptic interface for programmable patterns of touch across large areas of the skin. *Nat. Electron.* **2022**, *5* (6), 374−385.
(255) Grasso, G.; Rosset, S.; Shea, H. Fully 3D-printed, stretchable, and conformable haptic interfaces. *Adv. Funct. Mater.* **2023**, *33* (20), 2213821.
(256) Chen, Y.; Wu, H.; Wang, X.; Qiu, P.; Wan, H.; Jiao, J.; Wang, D.; Zhang, Z. Wireless programmable patterns of electro-hydraulic haptic electronic skins able to create surface morphology. *Chem. Eng. J.* **2024**, *500*, 156612.
(257) Jang, S.-Y.; Cho, M.; Kim, H.; Choi, M.; Mun, S.; Youn, J.-H.; Park, J.; Hwang, G.; Hwang, I.; Yun, S.; Kyung, K.-U. Dynamically reconfigurable shape-morphing and tactile display via hydraulically coupled mergeable and splittable PVC gel actuator. *Sci. Adv.* **2024**, *10* (39), No. eadq2024.
(258) Acome, E.; Mitchell, S. K.; Morrissey, T.; Emmett, M.; Benjamin, C.; King, M.; Radakovitz, M.; Keplinger, C. Hydraulically amplified self-healing electrostatic actuators with muscle-like performance. *Science* **2018**, *359* (6371), 61−65.
(259) Lendlein, A.; Kelch, S. Shape-memory polymers. *Angew. Chem.-Int. Ed.* **2002**, *41* (12), 2034−2057.
(260) Besse, N.; Rosset, S.; Zarate, J. J.; Shea, H. Flexible active skin: large reconfigurable arrays of individually addressed shape memory polymer actuators. *Adv. Mater. Technol.* **2017**, *2* (10), 1700102.
(261) Lendlein, A.; Gould, O. E. Reprogrammable recovery and actuation behaviour of shape-memory polymers. *Nat. Rev. Mater.* **2019**, *4* (2), 116−133.
(262) Pelrine, R.; Kornbluh, R.; Pei, Q.; Joseph, J. High-speed electrically actuated elastomers with strain greater than 100%. *Science* **2000**, *287* (5454), 836−839.
(263) Pu, J.; Meng, Y.; Xie, Z.; Peng, Z.; Wu, J.; Shi, Y.; Plamthottam, R.; Yang, W.; Pei, Q. A unimorph nanocomposite dielectric elastomer for large out-of-plane actuation. *Sci. Adv.* **2022**, *8* (9), No. eabm6200.
(264) Kim, E.; Lai, J.-C.; Michalek, L.; Wang, W.; Xu, C.; Lyu, H.; Yu, W.; Park, H.; Tomo, Y.; Root, S. E.; Lee, B.; Park, J.; Park, B.; Wei, S.; Zhao, C.; Bao, Z. A Transparent, Patternable, and Stretchable Conducting Polymer Solid Electrode for Dielectric Elastomer Actuators. *Adv. Funct. Mater.* **2025**, *35*, 2411880.
(265) Duduta, M.; Wood, R. J.; Clarke, D. R. Multilayer dielectric elastomers for fast, programmable actuation without prestretch. *Adv. Mater.* **2016**, *28* (36), 8058−8063.
(266) Leroy, E.; Hinchet, R.; Shea, H. Multimode hydraulically amplified electrostatic actuators for wearable haptics. *Adv. Mater.* **2020**, *32* (36), 2002564.
(267) Chen, S.; Chen, Y.; Yang, J.; Han, T.; Yao, S. Skin-integrated stretchable actuators toward skin-compatible haptic feedback and closed-loop human-machine interactions. *npj Flex. Electron.* **2023**, *7*, 1.
(268) Ni, C.; Chen, D.; Yin, Y.; Wen, X.; Chen, X.; Yang, C.; Chen, G.; Sun, Z.; Wen, J.; Jiao, Y.; et al. Shape memory polymer with programmable recovery onset. *Nature* **2023**, *622* (7984), 748−753.
(269) Huang, J.; Jiang, Y.; Chen, Q.; Xie, H.; Zhou, S. Bioinspired thermadapt shape-memory polymer with light-induced reversible fluorescence for rewritable 2D/3D-encoding information carriers. *Nat. Commun.* **2023**, *14*, 7131.
(270) Zhao, Q.; Zou, W.; Luo, Y.; Xie, T. Shape memory polymer network with thermally distinct elasticity and plasticity. *Sci. Adv.* **2016**, *2*, No. e1501297.
(271) Jin, B.; Song, H.; Jiang, R.; Song, J.; Zhao, Q.; Xie, T. Programming a crystalline shape memory polymer network with thermo-and photo-reversible bonds toward a single-component soft robot. *Sci. Adv.* **2018**, *4*, No. eaao3865.
(272) Lendlein, A.; Jiang, H.; Jünger, O.; Langer, R. Light-induced shape-memory polymers. *Nature* **2005**, *434* (7035), 879−882.
(273) Shou, Q.; Uto, K.; Iwanaga, M.; Ebara, M.; Aoyagi, T. Near-infrared light-responsive shape-memory poly (ε-caprolactone) films that actuate in physiological temperature range. *Polym. J.* **2014**, *46* (8), 492−498.
(274) Kim, M. S.; Lee, H. S.; Cho, Y.; Heo, J. K.; Quan, Y. J.; Lee, S. W.; Pahk, H. J.; Ahn, S. H. Surface nanopatterned shape memory alloy (SMA)-based photosensitive artificial muscle. *Adv. Opt. Mater.* **2022**, *10* (5), 2102024.


https://doi.org/10.1021/acs.chemrev.4c00966
*Chem. Rev.* 2025, 125, 11567−11665

(275) Liu, Y.; Lv, H.; Lan, X.; Leng, J.; Du, S. Review of electro-active shape-memory polymer composite. *Compos. Sci. Technol.* **2009**, *69* (13), 2064−2068.
(276) Huang, X.; Ford, M.; Patterson, Z. J.; Zarepoor, M.; Pan, C.; Majidi, C. Shape memory materials for electrically-powered soft machines. *J. Mater. Chem. B* **2020**, *8* (21), 4539−4551.
(277) Liu, Q.; Wang, W.; Reynolds, M. F.; Cao, M. C.; Miskin, M. Z.; Arias, T. A.; Muller, D. A.; McEuen, P. L.; Cohen, I. Micrometer-sized electrically programmable shape-memory actuators for low-power microrobotics. *Sci. Robot.* **2021**, *6* (52), No. eabe6663.
(278) Kim, D.; Kim, B.; Shin, B.; Shin, D.; Lee, C.-K.; Chung, J.-S.; Seo, J.; Kim, Y.-T.; Sung, G.; Seo, W.; Kim, S.; Hong, S.; Hwang, S.; Han, S.; Kang, D.; Lee, H.-S.; Koh, J.-S. Actuating compact wearable augmented reality devices by multifunctional artificial muscle. *Nat. Commun.* **2022**, *13*, 4155.
(279) Ji, X.; Liu, X.; Cacucciolo, V.; Civet, Y.; El Haitami, A.; Cantin, S.; Perriard, Y.; Shea, H. Untethered feel-through haptics using 18-$\mu$m thick dielectric elastomer actuators. *Adv. Funct. Mater.* **2021**, *31* (39), 2006639.
(280) Wang, D.; Song, M.; Naqash, A.; Zheng, Y.; Xu, W.; Zhang, Y. Toward whole-hand kinesthetic feedback: A survey of force feedback gloves. *IEEE Trans. Haptics* **2019**, *12* (2), 189−204.
(281) Chen, X.; Gong, L.; Wei, L.; Yeh, S.-C.; Da Xu, L.; Zheng, L.; Zou, Z. A wearable hand rehabilitation system with soft gloves. *IEEE Trans. Ind. Inform.* **2021**, *17* (2), 943−952.
(282) Kang, B. B.; Choi, H.; Lee, H.; Cho, K.-J. Exo-glove poly II: A polymer-based soft wearable robot for the hand with a tendon-driven actuation system. *Soft Robot.* **2019**, *6* (2), 214−227.
(283) Polygerinos, P.; Wang, Z.; Galloway, K. C.; Wood, R. J.; Walsh, C. J. Soft robotic glove for combined assistance and at-home rehabilitation. *Robot. Auton. Syst.* **2015**, *73*, 135−143.
(284) Jiang, Z.-C.; Liu, Q.; Xiao, Y.-Y.; Zhao, Y. Liquid Crystal Elastomers for Actuation: A Perspective on Structure-Property-Function Relation. *Prog. Polym. Sci.* **2024**, *153*, 101829.
(285) Choi, S. H.; Kim, J. H.; Ahn, J.; Kim, T.; Jung, Y.; Won, D.; Bang, J.; Pyun, K. R.; Jeong, S.; Kim, H.; et al. Phase patterning of liquid crystal elastomers by laser-induced dynamic crosslinking. *Nat. Mater.* **2024**, *23* (6), 834−843.
(286) Pei, Z.; Yang, Y.; Chen, Q.; Terentjev, E. M.; Wei, Y.; Ji, Y. Mouldable liquid-crystalline elastomer actuators with exchangeable covalent bonds. *Nat. Mater.* **2014**, *13* (1), 36−41.
(287) Maurin, V.; Chang, Y.; Ze, Q.; Leanza, S.; Wang, J.; Zhao, R. R. Liquid crystal elastomer-liquid metal composite: ultrafast, untethered, and programmable actuation by induction heating. *Adv. Mater.* **2024**, *36* (34), 2302765.
(288) Kim, H.; Lee, J. A.; Ambulo, C. P.; Lee, H. B.; Kim, S. H.; Naik, V. V.; Haines, C. S.; Aliev, A. E.; Ovalle-Robles, R.; Baughman, R. H.; Ware, T. H. Intelligently actuating liquid crystal elastomer-carbon nanotube composites. *Adv. Funct. Mater.* **2019**, *29* (48), 1905063.
(289) Kotikian, A.; Morales, J. M.; Lu, A.; Mueller, J.; Davidson, Z. S.; Boley, J. W.; Lewis, J. A. Innervated, self-sensing liquid crystal elastomer actuators with closed loop control. *Adv. Mater.* **2021**, *33* (27), 2101814.
(290) Camargo, C. J.; Campanella, H.; Marshall, J. E.; Torras, N.; Zinoviev, K.; Terentjev, E. M.; Esteve, J. Localised actuation in composites containing carbon nanotubes and liquid crystalline elastomers. *Macromol. Rapid Commun.* **2011**, *32* (24), 1953−1959.
(291) Torras, N.; Zinoviev, K.; Camargo, C.; Campo, E. M.; Campanella, H.; Esteve, J.; Marshall, J.; Terentjev, E.; Omastová, M.; Krupa, I.; et al. Tactile device based on opto-mechanical actuation of liquid crystal elastomers. *Sens. Actuator A-Phys.* **2014**, *208*, 104−112.
(292) Zeng, H.; Wani, O. M.; Wasylczyk, P.; Kaczmarek, R.; Priimagi, A. Self-regulating iris based on light-actuated liquid crystal elastomer. *Adv. Mater.* **2017**, *29* (30), 1701814.
(293) Finkelmann, H.; Nishikawa, E.; Pereira, G.; Warner, M. A new opto-mechanical effect in solids. *Phys. Rev. Lett.* **2001**, *87* (1), 015501.
(294) Fowler, H. E.; Rothemund, P.; Keplinger, C.; White, T. J. Liquid crystal elastomers with enhanced directional actuation to electric fields. *Adv. Mater.* **2021**, *33* (43), 2103806.
(295) He, Q.; Wang, Z.; Wang, Y.; Minori, A.; Tolley, M. T.; Cai, S. Electrically controlled liquid crystal elastomer-based soft tubular actuator with multimodal actuation. *Sci. Adv.* **2019**, *5* (10), No. eaax5746.
(296) Spillmann, C. M.; Naciri, J.; Ratna, B.; Selinger, R. L.; Selinger, J. V. Electrically induced twist in smectic liquid-crystalline elastomers. *J. Phys. Chem. B* **2016**, *120* (26), 6368−6372.
(297) Zhai, Y.; Wang, Z.; Kwon, K. S.; Cai, S.; Lipomi, D. J.; Ng, T. N. Printing multi-material organic haptic actuators. *Adv. Mater.* **2021**, *33* (19), 2002541.
(298) Zhao, H.; Jalving, J.; Huang, R.; Knepper, R.; Ruina, A.; Shepherd, R. A helping hand: Soft orthosis with integrated optical strain sensors and EMG control. *IEEE Robot. Autom. Mag.* **2016**, *23* (3), 55−64.
(299) Kim, D.; Kang, B. B.; Kim, K. B.; Choi, H.; Ha, J.; Cho, K.-J.; Jo, S. Eyes are faster than hands: A soft wearable robot learns user intention from the egocentric view. *Sci. Robot.* **2019**, *4* (26), No. eaav2949.
(300) Tezuka, M.; Ishimaru, K.; Miki, N. Electrotactile display composed of two-dimensionally and densely distributed microneedle electrodes. *Sens. Actuator A-Phys.* **2017**, *258*, 32−38.
(301) Lin, W.; Zhang, D.; Lee, W. W.; Li, X.; Hong, Y.; Pan, Q.; Zhang, R.; Peng, G.; Tan, H. Z.; Zhang, Z.; Wei, L.; Yang, Z. Super-resolution wearable electrotactile rendering system. *Sci. Adv.* **2022**, *8* (36), No. eabp8738.
(302) Shi, Y.; Wang, F.; Tian, J.; Li, S.; Fu, E.; Nie, J.; Lei, R.; Ding, Y.; Chen, X.; Wang, Z. L. Self-powered electro-tactile system for virtual tactile experiences. *Sci. Adv.* **2021**, *7* (6), No. eabe2943.
(303) Yeo, W.-H.; Kim, Y.-S.; Lee, J.; Ameen, A.; Shi, L.; Li, M.; Wang, S.; Ma, R.; Jin, S. H.; Kang, Z.; et al. Multifunctional epidermal electronics printed directly onto the skin. *Adv. Mater.* **2013**, *25* (20), 2773−2778.
(304) Lim, S.; Son, D.; Kim, J.; Lee, Y. B.; Song, J. K.; Choi, S.; Lee, D. J.; Kim, J. H.; Lee, M.; Hyeon, T.; et al. Transparent and stretchable interactive human machine interface based on patterned graphene heterostructures. *Adv. Funct. Mater.* **2015**, *25* (3), 375−383.
(305) Rakkolainen, I.; Farooq, A.; Kangas, J.; Hakulinen, J.; Rantala, J.; Turunen, M.; Raisamo, R. Technologies for multimodal interaction in extended reality—a scoping review. *Multimodal Technol. Interaction* **2021**, *5* (12), 81.
(306) Min, X.; Sun, S.; Qi, Y. XR CUBE: Multi-sensory Intelligent Interaction Device for Extended Reality Application. *IEEE Access* **2024**, *12*, 78058−78073.
(307) Park, M.; Yoo, J.-Y.; Yang, T.; Jung, Y. H.; Vazquez-Guardado, A.; Li, S.; Kim, J.-H.; Shin, J.; Maeng, W.-Y.; Lee, G.; Yoo, S.; Luan, H.; Kim, J.-T.; Shin, H.-S.; Flavin, M. T.; Yoon, H.-J.; Miljkovic, N.; Huang, Y.; King, W. P.; Rogers, J. A. Skin-integrated systems for power efficient, programmable thermal sensations across large body areas. *Proc. Natl. Acad. Sci. U. S. A.* **2023**, *120* (6), No. e2217828120.
(308) Kim, D.; Bang, J.; Lee, W.; Ha, I.; Lee, J.; Eom, H.; Kim, M.; Park, J.; Choi, J.; Kwon, J.; et al. Highly stretchable and oxidation-resistive Cu nanowire heater for replication of the feeling of heat in a virtual world. *J. Mater. Chem. A* **2020**, *8* (17), 8281−8291.
(309) Wang, B.; Yang, K.; Cheng, H.; Ye, T.; Wang, C. A hydrophobic conductive strip with outstanding one-dimensional stretchability for wearable heater and strain sensor. *Chem. Eng. J.* **2021**, *404*, 126393.
(310) Oh, J.; Kim, S.; Lee, S.; Jeong, S.; Ko, S. H.; Bae, J. A liquid metal based multimodal sensor and haptic feedback device for thermal and tactile sensation generation in virtual reality. *Adv. Funct. Mater.* **2021**, *31* (39), 2007772.
(311) Wang, Q. W.; Zhang, H. B.; Liu, J.; Zhao, S.; Xie, X.; Liu, L.; Yang, R.; Koratkar, N.; Yu, Z. Z. Multifunctional and water-resistant MXene-decorated polyester textiles with outstanding electromagnetic interference shielding and joule heating performances. *Adv. Funct. Mater.* **2019**, *29* (7), 1806819.


https://doi.org/10.1021/acs.chemrev.4c00966
*Chem. Rev.* 2025, 125, 11567−11665

(312) Li, K.; Chang, T. H.; Li, Z.; Yang, H.; Fu, F.; Li, T.; Ho, J. S.; Chen, P. Y. Biomimetic MXene textures with enhanced light-to-heat conversion for solar steam generation and wearable thermal management. *Adv. Energy Mater.* **2019**, *9* (34), 1901687.
(313) Ma, C.; Yuan, Q.; Du, H.; Ma, M.-G.; Si, C.; Wan, P. Multiresponsive MXene (Ti3C2T x)-decorated textiles for wearable thermal management and human motion monitoring. *ACS Appl. Mater. Interfaces* **2020**, *12* (30), 34226−34234.
(314) Jia, X.; Shen, B.; Zhang, L.; Zheng, W. Waterproof MXene-decorated wood-pulp fabrics for high-efficiency electromagnetic interference shielding and Joule heating. *Compos. Pt. B-Eng.* **2020**, *198*, 108250.
(315) Yao, S.; Cui, J.; Cui, Z.; Zhu, Y. Soft electrothermal actuators using silver nanowire heaters. *Nanoscale* **2017**, *9* (11), 3797−3805.
(316) Cui, Z.; Han, Y.; Huang, Q.; Dong, J.; Zhu, Y. Electrohydrodynamic printing of silver nanowires for flexible and stretchable electronics. *Nanoscale* **2018**, *10* (15), 6806−6811.
(317) Tian, B.; Liu, Q.; Luo, C.; Feng, Y.; Wu, W. Multifunctional ultrastretchable printed soft electronic devices for wearable applications. *Adv. Electron. Mater.* **2020**, *6* (2), 1900922.
(318) Lan, W.; Chen, Y.; Yang, Z.; Han, W.; Zhou, J.; Zhang, Y.; Wang, J.; Tang, G.; Wei, Y.; Dou, W.; et al. Ultraflexible transparent film heater made of Ag nanowire/PVA composite for rapid-response thermotherapy pads. *ACS Appl. Mater. Interfaces* **2017**, *9* (7), 6644−6651.
(319) Kim, Y. I.; An, S.; Kim, M.-W.; Jo, H.-S.; Kim, T.-G.; Swihart, M. T.; Yarin, A. L.; Yoon, S. S. Highly transparent, conducting, body-attachable metallized fibers as a flexible and stretchable film. *J. Alloy. Compd.* **2019**, *790*, 1127−1136.
(320) Huang, J.; Xu, Z.; Qiu, W.; Chen, F.; Meng, Z.; Hou, C.; Guo, W.; Liu, X. Y. Stretchable and heat-resistant protein-based electronic skin for human thermoregulation. *Adv. Funct. Mater.* **2020**, *30* (13), 1910547.
(321) Kim, T.; Kim, Y. W.; Lee, H. S.; Kim, H.; Yang, W. S.; Suh, K. S. Uniformly interconnected silver-nanowire networks for transparent film heaters. *Adv. Funct. Mater.* **2013**, *23* (10), 1250−1255.
(322) Huang, J.; Li, Y.; Xu, Z.; Li, W.; Xu, B.; Meng, H.; Liu, X.; Guo, W. An integrated smart heating control system based on sandwich-structural textiles. *Nanotechnology* **2019**, *30* (32), 325203.
(323) Zhao, M.; Li, D.; Huang, J.; Wang, D.; Mensah, A.; Wei, Q. A multifunctional and highly stretchable electronic device based on silver nanowire/wrap yarn composite for a wearable strain sensor and heater. *J. Mater. Chem. C* **2019**, *7* (43), 13468−13476.
(324) Cheng, Y.; Zhang, H.; Wang, R.; Wang, X.; Zhai, H.; Wang, T.; Jin, Q.; Sun, J. Highly stretchable and conductive copper nanowire based fibers with hierarchical structure for wearable heaters. *ACS Appl. Mater. Interfaces* **2016**, *8* (48), 32925−32933.
(325) Hsu, P.-C.; Liu, X.; Liu, C.; Xie, X.; Lee, H. R.; Welch, A. J.; Zhao, T.; Cui, Y. Personal thermal management by metallic nanowire-coated textile. *Nano Lett.* **2015**, *15* (1), 365−371.
(326) Hong, S.; Lee, H.; Lee, J.; Kwon, J.; Han, S.; Suh, Y. D.; Cho, H.; Shin, J.; Yeo, J.; Ko, S. H. Highly stretchable and transparent metal nanowire heater for wearable electronics applications. *Adv. Mater.* **2015**, *27* (32), 4744−4751.
(327) Yan, S.; Yuan, Q.; Wu, J.; Jia, Z. A free-standing, phase-change liquid metal mold for 3D flexible microfluidics. *Front. Bioeng. Biotechnol.* **2022**, *10*, 1094294.
(328) Smith, M.; Cacucciolo, V.; Shea, H. Fiber pumps for wearable fluidic systems. *Science* **2023**, *379* (6639), 1327−1332.
(329) Reeder, J. T.; Xie, Z.; Yang, Q.; Seo, M.-H.; Yan, Y.; Deng, Y.; Jinkins, K. R.; Krishnan, S. R.; Liu, C.; McKay, S.; et al. Soft, bioresorbable coolers for reversible conduction block of peripheral nerves. *Science* **2022**, *377* (6601), 109−115.
(330) Kotagama, P.; Phadnis, A.; Manning, K. C.; Rykaczewski, K. Rational design of soft, thermally conductive composite liquid-cooled tubes for enhanced personal, robotics, and wearable electronics cooling. *Adv. Mater. Technol.* **2019**, *4* (7), 1800690.
(331) Cai, S.; Ke, P.; Narumi, T.; Zhu, K. Thermairglove: A pneumatic glove for thermal perception and material identification in virtual reality. In *2020 IEEE Conference on Virtual Reality and 3D User Interfaces (VR)*; IEEE, 2020; pp 248−257.
(332) Bartkowiak, G.; Dabrowska, A.; Marszalek, A. Assessment of an active liquid cooling garment intended for use in a hot environment. *Appl. Ergon.* **2017**, *58*, 182−189.
(333) Lee, D.; Park, H.; Park, G.; Kim, J.; Kim, H.; Cho, H.; Han, S.; Kim, W. Liquid-metal-electrode-based compact, flexible, and high-power thermoelectric device. *Energy* **2019**, *188*, 116019.
(334) Hong, S.; Gu, Y.; Seo, J. K.; Wang, J.; Liu, P.; Meng, Y. S.; Xu, S.; Chen, R. Wearable thermoelectrics for personalized thermoregulation. *Sci. Adv.* **2019**, *5* (5), No. eaaw0536.
(335) Osborn, L. E.; Venkatasubramanian, R.; Himmtann, M.; Moran, C. W.; Pierce, J. M.; Gajendiran, P.; Wormley, J. M.; Ung, R. J.; Nguyen, H. H.; Crego, A. C. G.; et al. Evoking natural thermal perceptions using a thin-film thermoelectric device with high cooling power density and speed. *Nat. Biomed. Eng.* **2024**, *8* (8), 1004−1017.
(336) Kim, S.-W.; Kim, S. H.; Kim, C. S.; Yi, K.; Kim, J.-S.; Cho, B. J.; Cha, Y. Thermal display glove for interacting with virtual reality. *Sci. Rep.* **2020**, *10*, 11403.
(337) Ye, C.; Zhao, L.; Yang, S.; Li, X. Recent Research on Preparation and Application of Smart Joule Heating Fabrics. *Small* **2024**, *20* (18), 2309027.
(338) Zheng, L.; Ambrosetti, M.; Tronconi, E. Joule-heated catalytic reactors toward decarbonization and process intensification: a review. *ACS Eng. Au* **2024**, *4* (1), 4−21.
(339) Choi, S.; Han, S. I.; Kim, D.; Hyeon, T.; Kim, D.-H. High-performance stretchable conductive nanocomposites: materials, processes, and device applications. *Chem. Soc. Rev.* **2019**, *48* (6), 1566−1595.
(340) Kim, D. C.; Shim, H. J.; Lee, W.; Koo, J. H.; Kim, D. H. Material-based approaches for the fabrication of stretchable electronics. *Adv. Mater.* **2020**, *32* (15), 1902743.
(341) Kim, K.; Park, Y. G.; Hyun, B. G.; Choi, M.; Park, J. U. Recent advances in transparent electronics with stretchable forms. *Adv. Mater.* **2019**, *31* (20), 1804690.
(342) Catenacci, M. J.; Reyes, C.; Cruz, M. A.; Wiley, B. J. Stretchable conductive composites from Cu-Ag nanowire felt. *ACS Nano* **2018**, *12* (4), 3689−3698.
(343) Song, T.-B.; Chen, Y.; Chung, C.-H.; Yang, Y.; Bob, B.; Duan, H.-S.; Li, G.; Tu, K.-N.; Huang, Y.; Yang, Y. Nanoscale joule heating and electromigration enhanced ripening of silver nanowire contacts. *ACS Nano* **2014**, *8* (3), 2804−2811.
(344) Fang, R.; Yao, B.; Chen, T.; Xu, X.; Xue, D.; Hong, W.; Wang, H.; Wang, Q.; Zhang, S. 3D Highly Stretchable Liquid Metal/Elastomer Composites with Strain-Enhanced Conductivity. *Adv. Funct. Mater.* **2024**, *34* (31), 2310225.
(345) Zhu, S.; So, J. H.; Mays, R.; Desai, S.; Barnes, W. R.; Pourdeyhimi, B.; Dickey, M. D. Ultrastretchable fibers with metallic conductivity using a liquid metal alloy core. *Adv. Funct. Mater.* **2013**, *23* (18), 2308−2314.
(346) Bhuyan, P.; Wei, Y.; Sin, D.; Yu, J.; Nah, C.; Jeong, K.-U.; Dickey, M. D.; Park, S. Soft and stretchable liquid metal composites with shape memory and healable conductivity. *ACS Appl. Mater. Interfaces* **2021**, *13* (24), 28916−28924.
(347) Yamagishi, K.; Ching, T.; Chian, N.; Tan, M.; Zhou, W.; Huang, S. Y.; Hashimoto, M. Flexible and stretchable liquid-metal microfluidic electronics using directly printed 3D microchannel networks. *Adv. Funct. Mater.* **2024**, *34* (31), 2311219.
(348) Parida, K.; Bark, H.; Lee, P. S. Emerging thermal technology enabled augmented reality. *Adv. Funct. Mater.* **2021**, *31* (39), 2007952.
(349) Baranowski, L. L.; Jeffrey Snyder, G.; Toberer, E. S. Effective thermal conductivity in thermoelectric materials. *J. Appl. Phys.* **2013**, *113* (20), 204904.
(350) Yoshihama, H.; Kaneko, H. Design of thermoelectric materials with high electrical conductivity, high Seebeck coefficient, and low thermal conductivity. *Anal. Sci. Adv.* **2021**, *2* (5−6), 289−294.


https://doi.org/10.1021/acs.chemrev.4c00966
*Chem. Rev.* 2025, 125, 11567−11665

(351) Li, J.-F.; Liu, W.-S.; Zhao, L.-D.; Zhou, M. High-performance nanostructured thermoelectric materials. *NPG Asia Mater.* **2010**, *2* (4), 152−158.
(352) Poudel, B.; Hao, Q.; Ma, Y.; Lan, Y.; Minnich, A.; Yu, B.; Yan, X.; Wang, D.; Muto, A.; Vashaee, D.; et al. High-thermoelectric performance of nanostructured bismuth antimony telluride bulk alloys. *Science* **2008**, *320* (5876), 634−638.
(353) He, J.; Sootsman, J. R.; Girard, S. N.; Zheng, J.-C.; Wen, J.; Zhu, Y.; Kanatzidis, M. G.; Dravid, V. P. On the origin of increased phonon scattering in nanostructured PbTe based thermoelectric materials. *J. Am. Chem. Soc.* **2010**, *132* (25), 8669−8675.
(354) Nielsch, K.; Bachmann, J.; Kimling, J.; Böttner, H. Thermoelectric nanostructures: from physical model systems towards nanograined composites. *Adv. Energy Mater.* **2011**, *1* (5), 713−731.
(355) Xia, J.; Yang, J.; Sun, K.; Mao, D.; Wang, X.; Li, H.-F.; He, J. Balancing electron and phonon scatterings while tailoring carrier concentration in SnTe for enhancing thermoelectric performance. *J. Eur. Ceram. Soc.* **2023**, *43* (11), 4791−4798.
(356) Xiong, Q.; Han, G.; Wang, G.; Lu, X.; Zhou, X. The Doping Strategies for Modulation of Transport Properties in Thermoelectric Materials. *Adv. Funct. Mater.* **2024**, *34*, 2411304.
(357) Moshwan, R.; Liu, W.-D.; Shi, X.-L.; Wang, Y.-P.; Zou, J.; Chen, Z.-G. Realizing high thermoelectric properties of SnTe via synergistic band engineering and structure engineering. *Nano Energy* **2019**, *65*, 104056.
(358) Pei, Y.; Wang, H.; Snyder, G. J. Band engineering of thermoelectric materials. *Adv. Mater.* **2012**, *24* (46), 6125−6135.
(359) Kim, J.-H.; Vazquez-Guardado, A.; Luan, H.; Kim, J.-T.; Yang, D. S.; Zhang, H.; Chang, J.-K.; Yoo, S.; Park, C.; Wei, Y.; Christiansen, Z.; Kim, S.; Avila, R.; Kim, J. U.; Lee, Y. J.; Shin, H.-S.; Zhou, M.; Jeon, S. W.; Baek, J. M.; Lee, Y.; Kim, S. Y.; Lim, J.; Park, M.; Jeong, H.; Won, S. M.; Chen, R.; Huang, Y.; Jung, Y. H.; Yoo, J.-Y.; Rogers, J. A. A wirelessly programmable, skin-integrated thermo-haptic stimulator system for virtual reality. *Proc. Natl. Acad. Sci. U. S. A.* **2024**, *121* (22), No. e2404007121.
(360) Hu, C.; Kiene, M.; Ho, P. S. Thermal conductivity and interfacial thermal resistance of polymeric low k films. *Appl. Phys. Lett.* **2001**, *79* (25), 4121−4123.
(361) Huang, C.; Qian, X.; Yang, R. Thermal conductivity of polymers and polymer nanocomposites. *Mater. Sci. Eng. R Rep.* **2018**, *132*, 1−22.
(362) Xie, X.; Yang, K.; Li, D.; Tsai, T.-H.; Shin, J.; Braun, P. V.; Cahill, D. G. High and low thermal conductivity of amorphous macromolecules. *Phys. Rev. B* **2017**, *95* (3), 035406.
(363) Jasmee, S.; Omar, G.; Othaman, S. S. C.; Masripan, N. A.; Hamid, H. A. Interface thermal resistance and thermal conductivity of polymer composites at different types, shapes, and sizes of fillers: A review. *Polym. Compos.* **2021**, *42* (6), 2629−2652.
(364) Ngo, I.-L.; Byon, C. A review on enhancing thermal conductivity of transparent and flexible polymer composites. *Sci. Adv. Mater.* **2016**, *8* (2), 257−266.
(365) Xiao, M.; Du, B. X. Review of high thermal conductivity polymer dielectrics for electrical insulation. *High Volt.* **2016**, *1* (1), 34−42.
(366) Xu, S.; Liu, J.; Wang, X. Thermal conductivity enhancement of polymers via structure tailoring. *J. Enhanc. Heat Transfer* **2020**, *27* (5), 463−489.
(367) Dudchenko, A. V.; Chen, C.; Cardenas, A.; Rolf, J.; Jassby, D. Frequency-dependent stability of CNT Joule heaters in ionizable media and desalination processes. *Nat. Nanotechnol.* **2017**, *12* (6), 557−563.
(368) Zhou, B.; Han, X.; Li, L.; Feng, Y.; Fang, T.; Zheng, G.; Wang, B.; Dai, K.; Liu, C.; Shen, C. Ultrathin, flexible transparent Joule heater with fast response time based on single-walled carbon nanotubes/poly (vinyl alcohol) film. *Compos. Sci. Technol.* **2019**, *183*, 107796.
(369) Zhang, D.; Yin, R.; Zheng, Y.; Li, Q.; Liu, H.; Liu, C.; Shen, C. Multifunctional MXene/CNTs based flexible electronic textile with excellent strain sensing, electromagnetic interference shielding and Joule heating performances. *Chem. Eng. J.* **2022**, *438*, 135587.
(370) Jeong, S.; Oh, J.; Kim, H.; Bae, J.; Ko, S. H. Pattern design of a liquid metal-based wearable heater for constant heat generation under biaxial strain. *iScience* **2023**, *26* (7), 107008.
(371) Kim, S.; Saito, M.; Wei, Y.; Bhuyan, P.; Choe, M.; Fujie, T.; Mondal, K.; Park, S. Stretchable and wearable polymeric heaters and strain sensors fabricated using liquid metals. *Sens. Actuator A-Phys.* **2023**, *355*, 114317.
(372) Liu, P.; Li, Y.; Xu, Y.; Bao, L.; Wang, L.; Pan, J.; Zhang, Z.; Sun, X.; Peng, H. Stretchable and energy-efficient heating carbon nanotube fiber by designing a hierarchically helical structure. *Small* **2018**, *14* (4), 1702926.
(373) Won, P.; Park, J. J.; Lee, T.; Ha, I.; Han, S.; Choi, M.; Lee, J.; Hong, S.; Cho, K.-J.; Ko, S. H. Stretchable and transparent kirigami conductor of nanowire percolation network for electronic skin applications. *Nano Lett.* **2019**, *19* (9), 6087−6096.
(374) Lin, Y.; Genzer, J.; Dickey, M. D. Attributes, fabrication, and applications of gallium-based liquid metal particles. *Adv. Sci.* **2020**, *7* (12), 2000192.
(375) Jung, Y.; Ha, I.; Kim, M.; Ahn, J.; Lee, J.; Ko, S. H. High heat storing and thermally diffusive artificial skin for wearable thermal management. *Nano Energy* **2023**, *105*, 107979.
(376) Ren, S.; Zhang, M.; Ye, S.; Wu, K.; Sun, Z.; Du, Y.; Fang, J. Highly efficient multi-layer flexible heatsink for wearable thermoelectric cooling. *Chem. Eng. J.* **2024**, *499*, 155914.
(377) Chua, K. J.; Chou, S. K.; Yang, W.; Yan, J. Achieving better energy-efficient air conditioning-a review of technologies and strategies. *Appl. Energy* **2013**, *104*, 87−104.
(378) Angell, C.; Sichina, W.; Oguni, M. Heat capacity of water at extremes of supercooling and superheating. *J. Phys. Chem.* **1982**, *86* (6), 998−1002.
(379) Cheng, S.; Wu, Z. Microfluidic electronics. *Lab Chip* **2012**, *12* (16), 2782−2791.
(380) Zhang, B.; Dong, Q.; Korman, C. E.; Li, Z.; Zaghloul, M. E. Flexible packaging of solid-state integrated circuit chips with elastomeric microfluidics. *Sci. Rep.* **2013**, *3*, 1098.
(381) Zhao, J.; Luo, W.; Kim, J.-K.; Yang, J. Graphene oxide aerogel beads filled with phase change material for latent heat storage and release. *ACS Appl. Energy Mater.* **2019**, *2* (5), 3657−3664.
(382) Wan, X.; Wang, F.; Udayraj. Numerical analysis of cooling effect of hybrid cooling clothing incorporated with phase change material (PCM) packs and air ventilation fans. *Int. J. Heat Mass Transfer* **2018**, *126*, 636−648.
(383) Hou, J.; Yang, Z.; Xu, P.; Huang, G. Design and performance evaluation of novel personal cooling garment. *Appl. Therm. Eng.* **2019**, *154*, 131−139.
(384) Wang, W.; Cai, Y.; Du, M.; Hou, X.; Liu, J.; Ke, H.; Wei, Q. Ultralight and flexible carbon foam-based phase change composites with high latent-heat capacity and photothermal conversion capability. *ACS Appl. Mater. Interfaces* **2019**, *11* (35), 31997−32007.
(385) Tong, J. K.; Huang, X.; Boriskina, S. V.; Loomis, J.; Xu, Y.; Chen, G. Infrared-transparent visible-opaque fabrics for wearable personal thermal management. *ACS Photonics* **2015**, *2* (6), 769−778.
(386) Jing, J.-h.; Wu, H.-y.; Shao, Y.-w.; Qi, X.-d.; Yang, J.-h.; Wang, Y. Melamine foam-supported form-stable phase change materials with simultaneous thermal energy storage and shape memory properties for thermal management of electronic devices. *ACS Appl. Mater. Interfaces* **2019**, *11* (21), 19252−19259.
(387) Zhang, G.; Zhang, X.; Huang, H.; Wang, J.; Li, Q.; Chen, L.-Q.; Wang, Q. Toward Wearable Cooling Devices: Highly Flexible Electrocaloric Ba0. 67 Sr0. 33 TiO3 Nanowire Arrays. *Adv. Mater.* **2016**, *28* (24), 4811−4816.
(388) Ma, R.; Zhang, Z.; Tong, K.; Huber, D.; Kornbluh, R.; Ju, Y. S.; Pei, Q. Highly efficient electrocaloric cooling with electrostatic actuation. *Science* **2017**, *357* (6356), 1130−1134.
(389) Wang, D.; Chen, X.; Yuan, G.; Jia, Y.; Wang, Y.; Mumtaz, A.; Wang, Y.; Liu, J.-M. Toward artificial intelligent self-cooling electronic

skins: Large electrocaloric effect in all-inorganic flexible thin films at room temperature. *J. Materiomics* **2019**, *5* (1), 66−72.
(390) Yang, C.; Han, Y.; Feng, C.; Lin, X.; Huang, S.; Cheng, X.; Cheng, Z. Toward multifunctional electronics: flexible NBT-based film with a large electrocaloric effect and high energy storage property. *ACS Appl. Mater. Interfaces* **2020**, *12* (5), 6082−6089.
(391) Cao, T.; Shi, X.-L.; Chen, Z.-G. Advances in the design and assembly of flexible thermoelectric device. *Prog. Mater. Sci.* **2023**, *131*, 101003.
(392) Wei, J.; Yang, L.; Ma, Z.; Song, P.; Zhang, M.; Ma, J.; Yang, F.; Wang, X. Review of current high-ZT thermoelectric materials. *J. Mater. Sci.* **2020**, *55*, 12642−12704.
(393) Birkholz, U.; Fettig, R.; Rosenzweig, J. Fast semiconductor thermoelectric devices. *Sens. Actuator* **1987**, *12* (2), 179−184.
(394) Morgan, K.; Zeimpekis, I.; Feng, Z.; Hewak, D. Enhancing thermoelectric properties of bismuth telluride and germanium telluride thin films for wearable energy harvesting. *Thin Solid Films* **2022**, *741*, 139015.
(395) Goncalves, L.; Alpuim, P.; Rolo, A.; Correia, J. Thermal co-evaporation of Sb2Te3 thin-films optimized for thermoelectric applications. *Thin Solid Films* **2011**, *519* (13), 4152−4157.
(396) Abt, M.; Wolf, M.; Feldhoff, A.; Overmeyer, L. Combined spray-coating and laser structuring of thermoelectric ceramics. *J. Mater. Process. Technol.* **2020**, *275*, 116319.
(397) Sharma, P. K.; Senguttuvan, T.; Sharma, V. K.; Chaudhary, S. Revisiting the thermoelectric properties of lead telluride. *Mater. Today Energy* **2021**, *21*, 100713.
(398) Dughaish, Z. Lead telluride as a thermoelectric material for thermoelectric power generation. *Physica B* **2002**, *322* (1−2), 205−223.
(399) Hu, L.; Gao, H.; Liu, X.; Xie, H.; Shen, J.; Zhu, T.; Zhao, X. Enhancement in thermoelectric performance of bismuth telluride based alloys by multi-scale microstructural effects. *J. Mater. Chem.* **2012**, *22* (32), 16484−16490.
(400) Zhuang, H. L.; Yu, J.; Li, J. F. Nanocomposite Strategy toward Enhanced Thermoelectric Performance in Bismuth Telluride. *Small Sci.* **2025**, *5*, 2400284.
(401) Park, K.; Ahn, K.; Cha, J.; Lee, S.; Chae, S. I.; Cho, S.-P.; Ryee, S.; Im, J.; Lee, J.; Park, S.-D.; et al. Extraordinary off-stoichiometric bismuth telluride for enhanced n-type thermoelectric power factor. *J. Am. Chem. Soc.* **2016**, *138* (43), 14458−14468.
(402) Francioso, L.; De Pascali, C.; Sglavo, V.; Grazioli, A.; Masieri, M.; Siciliano, P. Modelling, fabrication and experimental testing of an heat sink free wearable thermoelectric generator. *Energy Conv. Manag.* **2017**, *145*, 204−213.
(403) Lee, G.; Kim, C. S.; Kim, S.; Kim, Y. J.; Choi, H.; Cho, B. J. Flexible heatsink based on a phase-change material for a wearable thermoelectric generator. *Energy* **2019**, *179*, 12−18.
(404) Soudry, Y.; Lemogne, C.; Malinvaud, D.; Consoli, S.-M.; Bonfils, P. Olfactory system and emotion: common substrates. *Eur. Ann. Otorhinolaryngol.-Head Neck Dis.* **2011**, *128* (1), 18−23.
(405) Aiken, M. P.; Berry, M. J. Posttraumatic stress disorder: possibilities for olfaction and virtual reality exposure therapy. *Virtual Real.* **2015**, *19*, 95−109.
(406) Kerruish, E. Arranging sensations: smell and taste in augmented and virtual reality. *Senses Soc.* **2019**, *14* (1), 31−45.
(407) Kadohisa, M. Effects of odor on emotion, with implications. *Front. Syst. Neurosci.* **2013**, *7*, 66.
(408) Rochet, M.; El-Hage, W.; Richa, S.; Kazour, F.; Atanasova, B. Depression, olfaction, and quality of life: a mutual relationship. *Brain Sci.* **2018**, *8* (5), 80.
(409) Kontaris, I.; East, B. S.; Wilson, D. A. Behavioral and neurobiological convergence of odor, mood and emotion: A review. *Front. Behav. Neurosci.* **2020**, *14*, 35.
(410) Lach, G.; Schellekens, H.; Dinan, T. G.; Cryan, J. F. Anxiety, depression, and the microbiome: a role for gut peptides. *Neurotherapeutics* **2018**, *15* (1), 36−59.
(411) Komori, T.; Fujiwara, R.; Tanida, M.; Nomura, J.; Yokoyama, M. M. Effects of citrus fragrance on immune function and depressive states. *Neuroimmunomodulation* **2004**, *2* (3), 174−180.
(412) Liu, Y.; Yiu, C. K.; Zhao, Z.; Park, W.; Shi, R.; Huang, X.; Zeng, Y.; Wang, K.; Wong, T. H.; Jia, S.; Zhou, J.; Gao, Z.; Zhao, L.; Yao, K.; Li, J.; Sha, C.; Gao, Y.; Zhao, G.; Huang, Y.; Li, D.; Guo, Q.; Li, Y.; Yu, X. Soft, miniaturized, wireless olfactory interface for virtual reality. *Nat. Commun.* **2023**, *14*, 2297.
(413) Ranasinghe, N.; Nguyen, T. N. T.; Liangkun, Y.; Lin, L.-Y.; Tolley, D.; Do, E. Y.-L. Vocktail: A virtual cocktail for pairing digital taste, smell, and color sensations. In *Proceedings of the 25th ACM International Conference on Multimedia*, 2017; pp 1139−1147.
(414) Liu, Y.; Jia, S.; Yiu, C. K.; Park, W.; Chen, Z.; Nan, J.; Huang, X.; Chen, H.; Li, W.; Gao, Y.; Song, W.; Yokota, T.; Someya, T.; Zhao, Z.; Li, Y.; Yu, X. Intelligent wearable olfactory interface for latency-free mixed reality and fast olfactory enhancement. *Nat. Commun.* **2024**, *15*, 4474.
(415) Radvansky, B. A.; Dombeck, D. A. An olfactory virtual reality system for mice. *Nat. Commun.* **2018**, *9*, 839.
(416) Bahremand, A.; Manetta, M.; Lai, J.; Lahey, B.; Spackman, C.; Smith, B. H.; Gerkin, R. C.; LiKamWa, R. The Smell Engine: A system for artificial odor synthesis in virtual environments. In *2022 IEEE Conference on Virtual Reality and 3D User Interfaces (VR)*; IEEE, 2022; pp 241−249.
(417) Ranasinghe, N.; Cheok, A. D.; Fernando, O. N. N.; Nii, H.; Gopalakrishnakone, P. Digital taste: electronic stimulation of taste sensations. In *Ambient Intelligence: Second International Joint Conference on AmI 2011, Amsterdam, The Netherlands, November 16−18, 2011. Proceedings 2*; Springer, 2011; pp 345−349.
(418) Karunanayaka, K.; Cheok, A. D.; Vedadi, S. Digital smell: toward electrically reproducing artificial smell sensations. *IEEE Access* **2023**, *11*, 50659−50670.
(419) Ranasinghe, N.; Tolley, D.; Nguyen, T. N. T.; Yan, L.; Chew, B.; Do, E. Y.-L. Augmented flavours: Modulation of flavour experiences through electric taste augmentation. *Food Res. Int.* **2019**, *117*, 60−68.
(420) Ranasinghe, N.; Cheok, A.; Nakatsu, R.; Do, E. Y.-L. Simulating the sensation of taste for immersive experiences. In *Proceedings of the 2013 ACM International Workshop on Immersive Media Experiences*; Association for Computing Machinery, 2013; pp 29−34.
(421) Ranasinghe, N.; Lee, K.-Y.; Suthokumar, G.; Do, E. Y.-L. Taste+ digitally enhancing taste sensations of food and beverages. In *Proceedings of the 22nd ACM International Conference on Multimedia*, 2014; pp 737−738.
(422) Holbrook, E. H.; Puram, S. V.; See, R. B.; Tripp, A. G.; Nair, D. G. Induction of smell through transethmoid electrical stimulation of the olfactory bulb. In *International Forum of Allergy & Rhinology*; Wiley Online Library, 2019; Vol. *9*, pp 158−164.
(423) Weiss, T.; Shushan, S.; Ravia, A.; Hahamy, A.; Secundo, L.; Weissbrod, A.; Ben-Yakov, A.; Holtzman, Y.; Cohen-Atsmoni, S.; Roth, Y.; et al. From nose to brain: Un-sensed electrical currents applied in the nose alter activity in deep brain structures. *Cereb. Cortex* **2016**, *26* (11), 4180−4191.
(424) Amores, J.; Dotan, M.; Maes, P. Development and study of ezzence: a modular scent wearable to improve wellbeing in home sleep environments. *Front. Psychol.* **2022**, *13*, 791768.
(425) Yang, P.; Shi, Y.; Tao, X.; Liu, Z.; Li, S.; Chen, X.; Wang, Z. L. Self-powered virtual olfactory generation system based on bionic fibrous membrane and electrostatic field accelerated evaporation. *EcoMat* **2023**, *5* (2), No. e12298.
(426) de Paiva Guimarães, M.; Martins, J. M.; Dias, D. R. C.; Guimarães, R. d. F. R.; Gnecco, B. B. An olfactory display for virtual reality glasses. *Multimedia Syst.* **2022**, *28* (5), 1573−1583.
(427) Nakamoto, T.; Ito, S.; Kato, S.; Qi, G. P. Multicomponent olfactory display using solenoid valves and SAW atomizer and its blending-capability evaluation. *IEEE Sens. J.* **2018**, *18* (13), 5213−5218.


https://doi.org/10.1021/acs.chemrev.4c00966
*Chem. Rev.* 2025, 125, 11567−11665

(428) Uziel, A. Stimulation of human olfactory neuro-epithelium by long-term continuous electrical currents. *J. Physiol.* **1973**, *66* (4), 409−422.
(429) Sato, M.; Kodama, N.; Sasaki, T.; Ohta, M. Olfactory evoked potentials: experimental and clinical studies. *J. Neurosurg.* **1996**, *85* (6), 1122−1126.
(430) Miyashita, H. Norimaki synthesizer: Taste display using ion electrophoresis in five gels. In *Extended Abstracts of the 2020 CHI Conference on Human Factors in Computing Systems*, 2020; pp 1−6.
(431) Yan, L.; Chew, B.; Sun, J.; Chiu, L.-A.; Ranasinghe, N.; Do, E. Y.-L. Multimodal Digital Taste Experience with D'Licious Vessel. In *Virtual, Augmented and Mixed Reality: 7th International Conference, VAMR 2015, Held as Part of HCI International 2015, Los Angeles, CA, USA, August 2−7, 2015, Proceedings 7*; Springer, 2015; pp 409−418.
(432) Ranasinghe, N.; Lee, K.-Y.; Suthokumar, G.; Do, E. Y.-L. Virtual ingredients for food and beverages to create immersive taste experiences: The sensation of taste as an electronic media. *Multimed. Tools Appl.* **2016**, *75*, 12291−12309.
(433) Ranasinghe, N.; Suthokumar, G.; Lee, K.-Y.; Do, E. Y.-L. Digital flavor: towards digitally simulating virtual flavors. In *Proceedings of the 2015 ACM on International Conference on Multimodal Interaction*; ACM, 2015; pp 139−146.
(434) Niijima, A.; Ogawa, T. Study on control method of virtual food texture by electrical muscle stimulation. In *Adjunct Proceedings of the 29th Annual ACM Symposium on User Interface Software and Technology*; ACM, 2016; pp 199−200.
(435) Auvray, M.; Spence, C. The multisensory perception of flavor. *Conscious. Cogn.* **2008**, *17* (3), 1016−1031.
(436) Shankar, M. U.; Levitan, C. A.; Prescott, J.; Spence, C. The influence of color and label information on flavor perception. *Chemosens. Percept.* **2009**, *2*, 53−58.
(437) Liu, Y.; Park, W.; Yiu, C. K.; Huang, X.; Jia, S.; Chen, Y.; Zhang, H.; Chen, H.; Wu, P.; Wu, M.; Liu, Z.; Gao, Y.; Zhu, K.; Zhao, Z.; Li, Y.; Yokota, T.; Someya, T.; Yu, X. Miniaturized, portable gustation interfaces for VR/AR/MR. *Proc. Natl. Acad. Sci. U. S. A.* **2024**, *121* (49), No. e2412116121.
(438) Wang, D.; Ohnishi, K.; Xu, W. Multimodal haptic display for virtual reality: A survey. *IEEE Trans. Ind. Electron.* **2020**, *67* (1), 610−623.
(439) Lee, J.; Choi, S. Multimodal Haptic Feedback for Virtual Collisions Combining Vibrotactile and Electrical Muscle Stimulation. *IEEE Trans. Haptics* **2024**, *17* (1), 33−38.
(440) Yem, V.; Kajimoto, H. Wearable tactile device using mechanical and electrical stimulation for fingertip interaction with virtual world. In *2017 IEEE Virtual Reality (VR)*; IEEE, 2017; pp 99−104.
(441) Fan, L.; Song, A.; Zhang, H. Development of an integrated haptic sensor system for multimodal human-computer interaction using ultrasonic Array and cable robot. *IEEE Sens. J.* **2022**, *22* (5), 4634−4643.
(442) Akshita; Alagarai Sampath, H.; Indurkhya, B.; Lee, E.; Bae, Y. Towards multimodal affective feedback: Interaction between visual and haptic modalities. In *Proceedings of the 33rd Annual ACM Conference on Human Factors in Computing Systems*; ACM, 2015; pp 2043−2052.
(443) Burdea, G.; Richard, P.; Coiffet, P. Multimodal virtual reality: Input-output devices, system integration, and human factors. *International Journal of Human-Computer Interaction* **1996**, *8* (1), 5−24.
(444) Yang, T. H.; Kim, J. R.; Jin, H.; Gil, H.; Koo, J. H.; Kim, H. J. Recent advances and opportunities of active materials for haptic technologies in virtual and augmented reality. *Adv. Funct. Mater.* **2021**, *31* (39), 2008831.
(445) Abad, A. C.; Ormazabal, M.; Reid, D.; Ranasinghe, A. An untethered multimodal haptic hand wearable. In *2021 IEEE Sensors*; IEEE, 2021; pp 1−4.
(446) Tsai, D.-R.; Hsu, W. A new type of a large-area multi-touch tactile device operated by electrotactile stimulation. In *2019 IEEE World Haptics Conference (WHC)*; IEEE, 2019; pp 313−318.
(447) Chun, S.; Kim, J.-S.; Yoo, Y.; Choi, Y.; Jung, S. J.; Jang, D.; Lee, G.; Song, K.-I.; Nam, K. S.; Youn, I.; et al. An artificial neural tactile sensing system. *Nat. Electron.* **2021**, *4* (6), 429−438.
(448) Gong, S.; Schwalb, W.; Wang, Y.; Chen, Y.; Tang, Y.; Si, J.; Shirinzadeh, B.; Cheng, W. A wearable and highly sensitive pressure sensor with ultrathin gold nanowires. *Nat. Commun.* **2014**, *5* (1), 3132.
(449) Han, S.; Liu, C.; Xu, H.; Yao, D.; Yan, K.; Zheng, H.; Chen, H.-J.; Gui, X.; Chu, S.; Liu, C. Multiscale nanowire-microfluidic hybrid strain sensors with high sensitivity and stretchability. *npj Flex. Electron.* **2018**, *2*, 16.
(450) Tang, N.; Zhou, C.; Qu, D.; Fang, Y.; Zheng, Y.; Hu, W.; Jin, K.; Wu, W.; Duan, X.; Haick, H. A highly aligned nanowire-based strain sensor for ultrasensitive monitoring of subtle human motion. *Small* **2020**, *16* (24), 2001363.
(451) Pang, C.; Lee, G.-Y.; Kim, T.-i.; Kim, S. M.; Kim, H. N.; Ahn, S.-H.; Suh, K.-Y. A flexible and highly sensitive strain-gauge sensor using reversible interlocking of nanofibres. *Nat. Mater.* **2012**, *11* (9), 795−801.
(452) Kim, K. K.; Hong, S.; Cho, H. M.; Lee, J.; Suh, Y. D.; Ham, J.; Ko, S. H. Highly sensitive and stretchable multidimensional strain sensor with prestrained anisotropic metal nanowire percolation networks. *Nano Lett.* **2015**, *15* (8), 5240−5247.
(453) Li, G.; Zhang, M.; Liu, S.; Yuan, M.; Wu, J.; Yu, M.; Teng, L.; Xu, Z.; Guo, J.; Li, G.; et al. Three-dimensional flexible electronics using solidified liquid metal with regulated plasticity. *Nat. Electron.* **2023**, *6* (2), 154−163.
(454) Chen, B.; Cao, Y.; Li, Q.; Yan, Z.; Liu, R.; Zhao, Y.; Zhang, X.; Wu, M.; Qin, Y.; Sun, C.; Yao, W.; Cao, Z.; Ajayan, P. M.; Chee, M. O. L.; Dong, P.; Li, Z.; Shen, J.; Ye, M. Liquid metal-tailored gluten network for protein-based e-skin. *Nat. Commun.* **2022**, *13*, 1206.
(455) Peng, H.; Xin, Y.; Xu, J.; Liu, H.; Zhang, J. Ultra-stretchable hydrogels with reactive liquid metals as asymmetric force-sensors. *Mater. Horizons* **2019**, *6* (3), 618−625.
(456) Wu, Y.; Zhou, Y.; Asghar, W.; Liu, Y.; Li, F.; Sun, D.; Hu, C.; Wu, Z.; Shang, J.; Yu, Z.; Li, R.-W.; Yang, H. Liquid Metal-Based Strain Sensor with Ultralow Detection Limit for Human-Machine Interface Applications. *Adv. Intell. Syst.* **2021**, *3* (10), 2000235.
(457) Shi, C.; Zou, Z.; Lei, Z.; Zhu, P.; Nie, G.; Zhang, W.; Xiao, J. Stretchable, rehealable, recyclable, and reconfigurable integrated strain sensor for joint motion and respiration monitoring. *Research* **2021**, *2021*, 9846036.
(458) Rahman, M. S.; Huddy, J. E.; Hamlin, A. B.; Scheideler, W. J. Broadband mechanoresponsive liquid metal sensors. *npj Flex. Electron.* **2022**, *6*, 71.
(459) Li, H.; Lin, J.; Lin, S.; Zhong, H.; Jiang, B.; Liu, X.; Wu, W.; Li, W.; Iranmanesh, E.; Zhou, Z.; Li, W.; Wang, K. A bioinspired tactile scanner for computer haptics. *Nat. Commun.* **2024**, *15*, 7632.
(460) Lin, L.; Park, S.; Kim, Y.; Bae, M.; Lee, J.; Zhang, W.; Gao, J.; Paek, S. H.; Piao, Y. Wearable and stretchable conductive polymer composites for strain sensors: How to design a superior one? *Nano Mater. Sci.* **2023**, *5* (4), 392−403.
(461) Lu, Y.; Liu, Z.; Yan, H.; Peng, Q.; Wang, R.; Barkey, M. E.; Jeon, J.-W.; Wujcik, E. K. Ultrastretchable conductive polymer complex as a strain sensor with a repeatable autonomous self-healing ability. *ACS Appl. Mater. Interfaces* **2019**, *11* (22), 20453−20464.
(462) Pan, L.; Chortos, A.; Yu, G.; Wang, Y.; Isaacson, S.; Allen, R.; Shi, Y.; Dauskardt, R.; Bao, Z. An ultra-sensitive resistive pressure sensor based on hollow-sphere microstructure induced elasticity in conducting polymer film. *Nat. Commun.* **2014**, *5* (1), 3002.
(463) Su, Q.; Zou, Q.; Li, Y.; Chen, Y.; Teng, S.-Y.; Kelleher, J. T.; Nith, R.; Cheng, P.; Li, N.; Liu, W.; Dai, S.; Liu, Y.; Mazursky, A.; Xu, J.; Jin, L.; Lopes, P.; Wang, S. A stretchable and strain-unperturbed pressure sensor for motion interference-free tactile monitoring on skins. *Sci. Adv.* **2021**, *7* (48), No. eabi4563.
(464) Liao, X.; Song, W.; Zhang, X.; Zhan, H.; Liu, Y.; Wang, Y.; Zheng, Y. Hetero-contact microstructure to program discerning tactile interactions for virtual reality. *Nano Energy* **2019**, *60*, 127−136.


https://doi.org/10.1021/acs.chemrev.4c00966
*Chem. Rev.* 2025, 125, 11567−11665

(465) Ge, J.; Wang, X.; Drack, M.; Volkov, O.; Liang, M.; Canon Bermudez, G. S.; Illing, R.; Wang, C.; Zhou, S.; Fassbender, J.; Kaltenbrunner, M.; Makarov, D. A bimodal soft electronic skin for tactile and touchless interaction in real time. *Nat. Commun.* **2019**, *10*, 4405.
(466) Kim, K. K.; Ha, I.; Won, P.; Seo, D.-G.; Cho, K.-J.; Ko, S. H. Transparent wearable three-dimensional touch by self-generated multiscale structure. *Nat. Commun.* **2019**, *10*, 2582.
(467) Xie, X.; Wang, Q.; Zhao, C.; Sun, Q.; Gu, H.; Li, J.; Tu, X.; Nie, B.; Sun, X.; Liu, Y.; et al. Neuromorphic Computing-Assisted Triboelectric Capacitive-Coupled Tactile Sensor Array for Wireless Mixed Reality Interaction. *ACS Nano* **2024**, *18* (26), 17041−17052.
(468) Tian, L.; Zimmerman, B.; Akhtar, A.; Yu, K. J.; Moore, M.; Wu, J.; Larsen, R. J.; Lee, J. W.; Li, J.; Liu, Y.; et al. Large-area MRI-compatible epidermal electronic interfaces for prosthetic control and cognitive monitoring. *Nat. Biomed. Eng.* **2019**, *3* (3), 194−205.
(469) Tan, P.; Wang, H.; Xiao, F.; Lu, X.; Shang, W.; Deng, X.; Song, H.; Xu, Z.; Cao, J.; Gan, T.; Wang, B.; Zhou, X. Solution-processable, soft, self-adhesive, and conductive polymer composites for soft electronics. *Nat. Commun.* **2022**, *13*, 358.
(470) Shar, A.; Glass, P.; Park, S. H.; Joung, D. 3D Printable One-Part Carbon Nanotube-Elastomer Ink for Health Monitoring Applications. *Adv. Funct. Mater.* **2023**, *33* (5), 2211079.
(471) Jung, D.; Lim, C.; Shim, H. J.; Kim, Y.; Park, C.; Jung, J.; Han, S. I.; Sunwoo, S.-H.; Cho, K. W.; Cha, G. D.; Kim, D. C.; Koo, J. H.; Kim, J. H.; Hyeon, T.; Kim, D.-H. Dae-Hyeong. Highly conductive and elastic nanomembrane for skin electronics. *Science* **2021**, *373* (6558), 1022−1026.
(472) Stankovich, S.; Dikin, D. A.; Dommett, G. H.; Kohlhaas, K. M.; Zimney, E. J.; Stach, E. A.; Piner, R. D.; Nguyen, S. T.; Ruoff, R. S. Graphene-based composite materials. *Nature* **2006**, *442* (7100), 282−286.
(473) Liu, N.; Chortos, A.; Lei, T.; Jin, L.; Kim, T. R.; Bae, W.-G.; Zhu, C.; Wang, S.; Pfattner, R.; Chen, X.; Sinclair, R.; Bao, Z. Ultratransparent and stretchable graphene electrodes. *Sci. Adv.* **2017**, *3* (9), No. e1700159.
(474) Zhou, J.; Long, X.; Huang, J.; Jiang, C.; Zhuo, F.; Guo, C.; Li, H.; Fu, Y.; Duan, H. Multiscale and hierarchical wrinkle enhanced graphene/Ecoflex sensors integrated with human-machine interfaces and cloud-platform. *npj Flex. Electron.* **2022**, *6*, 55.
(475) Zhang, Y.-Z.; Lee, K. H.; Anjum, D. H.; Sougrat, R.; Jiang, Q.; Kim, H.; Alshareef, H. N. MXenes stretch hydrogel sensor performance to new limits. *Sci. Adv.* **2018**, *4* (6), No. eaat0098.
(476) Liu, Y.; Xu, Z.; Ji, X.; Xu, X.; Chen, F.; Pan, X.; Fu, Z.; Chen, Y.; Zhang, Z.; Liu, H.; Cheng, B.; Liang, J. Ag-thiolate interactions to enable an ultrasensitive and stretchable MXene strain sensor with high temporospatial resolution. *Nat. Commun.* **2024**, *15*, 5354.
(477) Kang, D.; Pikhitsa, P. V.; Choi, Y. W.; Lee, C.; Shin, S. S.; Piao, L.; Park, B.; Suh, K.-Y.; Kim, T.-i.; Choi, M. Ultrasensitive mechanical crack-based sensor inspired by the spider sensory system. *Nature* **2014**, *516* (7530), 222−226.
(478) Kim, T.; Hong, I.; Kim, M.; Im, S.; Roh, Y.; Kim, C.; Lim, J.; Kim, D.; Park, J.; Lee, S.; Lim, D.; Cho, J.; Huh, S.; Jo, S.-U.; Kim, C.; Koh, J.-S.; Han, S.; Kang, D. Ultra-stable and tough bioinspired crack-based tactile sensor for small legged robots. *npj Flex. Electron.* **2023**, *7*, 22.
(479) Lee, J.-H.; Kim, Y.-N.; Lee, J.; Jeon, J.; Bae, J.-Y.; Lee, J.-Y.; Kim, K.-S.; Chae, M.; Park, H.; Kim, J.-h.; Lee, K.-S.; Kim, J.; Hyun, J. K.; Kang, D.; Kang, S.-K. Hypersensitive meta-crack strain sensor for real-time biomedical monitoring. *Sci. Adv.* **2024**, *10* (51), No. eads9258.
(480) Boutry, C. M.; Negre, M.; Jorda, M.; Vardoulis, O.; Chortos, A.; Khatib, O.; Bao, Z. A hierarchically patterned, bioinspired e-skin able to detect the direction of applied pressure for robotics. *Sci. Robot.* **2018**, *3* (24), No. eaau6914.
(481) Chen, X.; Luo, Y.; Chen, Y.; Li, S.; Deng, S.; Wang, B.; Zhang, Q.; Li, X.; Li, X.; Wang, C.; He, J.; Tian, H.; Shao, J. Biomimetic Contact Behavior Inspired Tactile Sensing Array with Programmable Microdomes Pattern by Scalable and Consistent Fabrication. *Adv. Sci.* **2024**, *11* (43), 2408082.
(482) Niu, H.; Li, H.; Li, N.; Kan, H.; Liu, J.; Wang, C.; Gao, S.; Li, Y.; Xu, X. Intelligent Robotic Sensory System with Epidermis-Dermis Bionic Electronic Skin for Autonomous Hardness/Softness-Based Material Perception. *Adv. Funct. Mater.* **2025**, *35*, 2500511.
(483) Yang, R.; Dutta, A.; Li, B.; Tiwari, N.; Zhang, W.; Niu, Z.; Gao, Y.; Erdely, D.; Xin, X.; Li, T.; Cheng, H. Iontronic pressure sensor with high sensitivity over ultra-broad linear range enabled by laser-induced gradient micro-pyramids. *Nat. Commun.* **2023**, *14*, 2907.
(484) Mannsfeld, S. C. B.; Tee, B. C. K.; Stoltenberg, R. M.; Chen, C. V. H. H.; Barman, S.; Muir, B. V. O.; Sokolov, A. N.; Reese, C.; Bao, Z. Highly sensitive flexible pressure sensors with microstructured rubber dielectric layers. *Nat. Mater.* **2010**, *9* (10), 859−864.
(485) Cho, J.-Y.; Kim, S. E.; Beak, C.-J.; Lee, J.; Suh, W.; Lee, B.-Y.; Lee, S.-H. Tactile near-sensor computing systems incorporating hourglass-shaped microstructured capacitive sensors for bio-realistic energy efficiency. *npj Flex. Electron.* **2025**, *9*, 34.
(486) Zhang, Y.; Lu, Q.; He, J.; Huo, Z.; Zhou, R.; Han, X.; Jia, M.; Pan, C.; Wang, Z. L.; Zhai, J. Localizing strain via micro-cage structure for stretchable pressure sensor arrays with ultralow spatial crosstalk. *Nat. Commun.* **2023**, *14*, 1252.
(487) Khang, D.-Y.; Jiang, H.; Huang, Y.; Rogers, J. A. A stretchable form of single-crystal silicon for high-performance electronics on rubber substrates. *Science* **2006**, *311* (5758), 208−212.
(488) Kim, D.-H.; Ahn, J.-H.; Choi, W. M.; Kim, H.-S.; Kim, T.-H.; Song, J.; Huang, Y. Y.; Liu, Z.; Lu, C.; Rogers, J. A. Stretchable and foldable silicon integrated circuits. *Science* **2008**, *320* (5875), 507−511.
(489) Blees, M. K.; Barnard, A. W.; Rose, P. A.; Roberts, S. P.; McGill, K. L.; Huang, P. Y.; Ruyack, A. R.; Kevek, J. W.; Kobrin, B.; Muller, D. A.; et al. Graphene kirigami. *Nature* **2015**, *524* (7564), 204−207.
(490) Shyu, T. C.; Damasceno, P. F.; Dodd, P. M.; Lamoureux, A.; Xu, L.; Shlian, M.; Shtein, M.; Glotzer, S. C.; Kotov, N. A. A kirigami approach to engineering elasticity in nanocomposites through patterned defects. *Nat. Mater.* **2015**, *14* (8), 785−789.
(491) Rafsanjani, A.; Zhang, Y.; Liu, B.; Rubinstein, S. M.; Bertoldi, K. Kirigami skins make a simple soft actuator crawl. *Sci. Robot.* **2018**, *3* (15), No. eaar7555.
(492) Fan, J. A.; Yeo, W.-H.; Su, Y.; Hattori, Y.; Lee, W.; Jung, S.-Y.; Zhang, Y.; Liu, Z.; Cheng, H.; Falgout, L.; et al. Fractal design concepts for stretchable electronics. *Nat. Commun.* **2014**, *5* (1), 3266.
(493) Wang, Y.; Zhu, C.; Pfattner, R.; Yan, H.; Jin, L.; Chen, S.; Molina-Lopez, F.; Lissel, F.; Liu, J.; Rabiah, N. I.; Chen, Z.; Chung, J. W.; Linder, C.; Toney, M. F.; Murmann, B.; Bao, Z. A highly stretchable, transparent, and conductive polymer. *Sci. Adv.* **2017**, *3* (3), No. e1602076.
(494) Nevrela, J.; Micjan, M.; Novota, M.; Kovacova, S.; Pavuk, M.; Juhasz, P.; Kovac, J., Jr; Jakabovic, J.; Weis, M. Secondary doping in poly (3, 4-ethylenedioxythiophene): Poly (4-styrenesulfonate) thin films. *J. Polym. Sci. Pt. B-Polym. Phys.* **2015**, *53* (16), 1139−1146.
(495) Kwon, S.-J.; Han, T.-H.; Ko, T. Y.; Li, N.; Kim, Y.; Kim, D. J.; Bae, S.-H.; Yang, Y.; Hong, B. H.; Kim, K. S.; Ryu, S.; Lee, T.-W. Extremely stable graphene electrodes doped with macromolecular acid. *Nat. Commun.* **2018**, *9*, 2037.
(496) Kaur, B.; Kumar, S.; Kaushik, B. K. Novel wearable optical sensors for vital health monitoring systems—a review. *Biosensors* **2023**, *13* (2), 181.
(497) Jha, R.; Mishra, P.; Kumar, S. Advancements in optical fiber-based wearable sensors for smart health monitoring. *Biosens. Bioelectron.* **2024**, *254*, 116232.
(498) Chen, J.; Liu, B.; Zhang, H. Review of fiber Bragg grating sensor technology. *Front. Optoelectron. China* **2011**, *4*, 204−212.
(499) Ghosh, B.; Mandal, S. Fiber Bragg grating-based optical filters for high-resolution sensing: A comprehensive analysis. *Results Opt.* **2023**, *12*, 100441.


https://doi.org/10.1021/acs.chemrev.4c00966
*Chem. Rev.* 2025, 125, 11567−11665

(500) Guo, G.; Zhang, D.; Duan, Y.; Zhang, G.; Chai, J. Strain-sensing mechanism and axial stress response characterization of bolt based on fiber bragg grating sensing. *Energies* **2022**, *15* (17), 6384.
(501) Guo, J.; Zhou, B.; Zong, R.; Pan, L.; Li, X.; Yu, X.; Yang, C.; Kong, L.; Dai, Q. Stretchable and highly sensitive optical strain sensors for human-activity monitoring and healthcare. *ACS Appl. Mater. Interfaces* **2019**, *11* (37), 33589−33598.
(502) Jiang, J.; Zhang, N.; Min, R.; Cheng, X.; Qu, H.; Hu, X. Recent achievements on grating fabrications in polymer optical fibers with photosensitive dopants: a review. *Polymers* **2022**, *14* (2), 273.
(503) Tan, W.; Shi, Z.-Y.; Smith, S.; Birnbaum, D.; Kopelman, R. Submicrometer intracellular chemical optical fiber sensors. *Science* **1992**, *258* (5083), 778−781.
(504) Lee, B. H.; Kim, Y. H.; Park, K. S.; Eom, J. B.; Kim, M. J.; Rho, B. S.; Choi, H. Y. Interferometric fiber optic sensors. *Sensors* **2012**, *12* (3), 2467−2486.
(505) Marra, G.; Fairweather, D. M.; Kamalov, V.; Gaynor, P.; Cantono, M.; Mulholland, S.; Baptie, B.; Castellanos, J. C.; Vagenas, G.; Gaudron, J.-O.; et al. Optical interferometry-based array of seafloor environmental sensors using a transoceanic submarine cable. *Science* **2022**, *376* (6595), 874−879.
(506) Flores-Bravo, J. A.; Illarramendi, M. A.; Zubia, J.; Villatoro, J. Optical fiber interferometer for temperature-independent refractive index measuring over a broad range. *Opt. Laser Technol.* **2021**, *139*, 106977.
(507) Zhou, J.; Wang, Y.; Liao, C.; Sun, B.; He, J.; Yin, G.; Liu, S.; Li, Z.; Wang, G.; Zhong, X.; et al. Intensity modulated refractive index sensor based on optical fiber Michelson interferometer. *Sens. Actuator B-Chem.* **2015**, *208*, 315−319.
(508) Creath, K. V phase-measurement interferometry techniques. In *Progress in Optics*; Elsevier, 1988; Vol. *26*, pp 349−393.
(509) Lam, B.; Guo, C. Complete characterization of ultrashort optical pulses with a phase-shifting wedged reversal shearing interferometer. *Light: Science & Applications* **2018**, *7*, 30.
(510) Al-Hayali, S. K.; Salman, A. M.; Al-Janabi, A. H. High sensitivity balloon-like interferometric optical fiber humidity sensor based on tuning gold nanoparticles coating thickness. *Measurement* **2021**, *170*, 108703.
(511) Li, H.; Li, H.; Lou, X.; Meng, F.; Zhu, L. Soft optical fiber curvature sensor for finger joint angle proprioception. *Optik* **2019**, *179*, 298−304.
(512) Mishra, P.; Chatterjee, K.; Kumar, H.; Jha, R. Flexible and wearable photonic-crystal fiber interferometer for physiological monitoring and healthcare. *ACS Appl. Opt. Mater.* **2023**, *1* (2), 569−577.
(513) Zhuang, Y.; Xie, R. J. Mechanoluminescence rebrightening the prospects of stress sensing: a review. *Adv. Mater.* **2021**, *33* (50), 2005925.
(514) Huang, Z.; Li, X.; Liang, T.; Ren, B.; Zhang, X.; Zheng, Y.; Zhang, Q. a.; Fang, Z.; Wu, M.; Zulfiqar, M.; Jing, L.; Qu, S.; Chen, B.; Gan, J.; Peng, D. Smart mechanoluminescent phosphors: A review of zinc sulfide-based materials for advanced mechano-optical applications. *Responsive Materials* **2024**, *2* (3), No. e20240019.
(515) Qasem, A.; Xiong, P.; Ma, Z.; Peng, M.; Yang, Z. Recent advances in mechanoluminescence of doped zinc sulfides. *Laser & Photonics Reviews* **2021**, *15* (12), 2100276.
(516) Bai, G.; Tsang, M. K.; Hao, J. Tuning the luminescence of phosphors: beyond conventional chemical method. *Adv. Opt. Mater.* **2015**, *3* (4), 431−462.
(517) Hirai, Y. On Sense and Deform: Molecular Luminescence for Mechanoscience. *ACS Appl. Opt. Mater.* **2024**, *2* (6), 1025−1045.
(518) Liang, H.; He, Y.; Chen, M.; Jiang, L.; Zhang, Z.; Heng, X.; Yang, L.; Hao, Y.; Wei, X.; Gan, J.; Yang, Z. Self-powered stretchable mechanoluminescent optical fiber strain sensor. *Adv. Intell. Syst.* **2021**, *3* (9), 2100035.
(519) Xomalis, A.; Demirtzioglou, I.; Plum, E.; Jung, Y.; Nalla, V.; Lacava, C.; MacDonald, K. F.; Petropoulos, P.; Richardson, D. J.; Zheludev, N. I. Fibre-optic metadevice for all-optical signal modulation based on coherent absorption. *Nat. Commun.* **2018**, *9* (1), 182.
(520) Gu, Z.; Shi, Y.; Zhu, Z.; Li, Z.; Zou, M.; Yang, C.; Liu, Y.; Yu, Y.; Zhang, X. All-integrated multidimensional optical sensing with a photonic neuromorphic processor. *Sci. Adv.* **2025**, *11* (22), No. eadu7277.
(521) Anwar Zawawi, M.; O'Keffe, S.; Lewis, E. Intensity-modulated fiber optic sensor for health monitoring applications: a comparative review. *Sens. Rev.* **2013**, *33* (1), 57−67.
(522) Sabri, N.; Aljunid, S. A.; Salim, M. S.; Fouad, S. Fiber optic sensors: short review and applications. *Recent trends in physics of material science and technology* **2015**, *204*, 299−311.
(523) Polygerinos, P.; Seneviratne, L. D.; Althoefer, K. Modeling of light intensity-modulated fiber-optic displacement sensors. *IEEE Trans. Instrum. Meas.* **2011**, *60* (4), 1408−1415.
(524) Choi, M.; Humar, M.; Kim, M. S.; Yun, S.-H. Step-index optical fiber made of biocompatible hydrogels. *Adv. Mater.* **2015**, *27* (27), 4081.
(525) Bai, H.; Li, S.; Barreiros, J.; Tu, Y.; Pollock, C. R.; Shepherd, R. F. Stretchable distributed fiber-optic sensors. *Science* **2020**, *370* (6518), 848−852.
(526) Liu, Z.; Hu, X.; Bo, R.; Yang, Y.; Cheng, X.; Pang, W.; Liu, Q.; Wang, Y.; Wang, S.; Xu, S.; et al. A three-dimensionally architected electronic skin mimicking human mechanosensation. *Science* **2024**, *384* (6699), 987−994.
(527) Wang, S.; Yao, Y.; Deng, W.; Chu, X.; Yang, T.; Tian, G.; Ao, Y.; Sun, Y.; Lan, B.; Ren, X.; et al. Mass-Produced Skin-Inspired Piezoresistive Sensing Array with Interlocking Interface for Object Recognition. *ACS Nano* **2024**, *18* (17), 11183−11192.
(528) Qiu, Y.; Wang, F.; Zhang, Z.; Shi, K.; Song, Y.; Lu, J.; Xu, M.; Qian, M.; Zhang, W.; Wu, J.; Zhang, Z.; Chai, H.; Liu, A.; Jiang, H.; Wu, H. Quantitative softness and texture bimodal haptic sensors for robotic clinical feature identification and intelligent picking. *Sci. Adv.* **2024**, *10* (30), No. eadp0348.
(529) Wang, M.; Yan, Z.; Wang, T.; Cai, P.; Gao, S.; Zeng, Y.; Wan, C.; Wang, H.; Pan, L.; Yu, J.; et al. Gesture recognition using a bioinspired learning architecture that integrates visual data with somatosensory data from stretchable sensors. *Nat. Electron.* **2020**, *3* (9), 563−570.
(530) Wang, S.; Fan, X.; Zhang, Z.; Su, Z.; Ding, Y.; Yang, H.; Zhang, X.; Wang, J.; Zhang, J.; Hu, P. A Skin-Inspired High-Performance Tactile Sensor for Accurate Recognition of Object Softness. *ACS Nano* **2024**, *18* (26), 17175−17184.
(531) Lee, S. W.; Yun, S. Y.; Han, J. K.; Nho, Y. H.; Jeon, S. B.; Choi, Y. K. Spike-Based Neuromorphic Hardware for Dynamic Tactile Perception with a Self-Powered Mechanoreceptor Array. *Adv. Sci.* **2024**, *11*, 2402175.
(532) Corzo, D.; Alexandre, E. B.; Alshareef, Y.; Bokhari, F.; Xin, Y.; Zhang, Y.; Kosel, J.; Bryant, D.; Lubineau, G.; Baran, D. Cure-on-demand 3D printing of complex geometries for enhanced tactile sensing in soft robotics and extended reality. *Mater. Today* **2024**, *78*, 20−31.
(533) Hao, S.; Wang, W.; Ma, C.; Li, X.; Liu, X.; Wang, Y.; Xue, Z.; Xu, F.; Yang, J. A Laminated Strategy Enabled Sustainable Tactile Array with Ultra-Stable Sensory Augmentation. *Adv. Funct. Mater.* **2024**, *34*, 2410360.
(534) Kim, K.; Hong, J.-H.; Bae, K.; Lee, K.; Lee, D. J.; Park, J.; Zhang, H.; Sang, M.; Ju, J. E.; Cho, Y. U.; Kang, K.; Park, W.; Jung, S.; Lee, J. W.; Xu, B.; Kim, J.; Yu, K. J. Extremely durable electrical impedance tomography-based soft and ultrathin wearable e-skin for three-dimensional tactile interfaces. *Sci. Adv.* **2024**, *10* (38), No. eadr1099.
(535) Sultan, M. J.; Bag, A.; Hong, S. J.; Wang, G.; Kumar, S.; Chouhdry, H. H.; Lee, N.-E. Tactile sensory synapse based on organic electrochemical transistors with ionogel triboelectric layer. *Nano Energy* **2024**, *131*, 110202.
(536) Chiu, Y.-S.; Rinawati, M.; Chang, Y.-H.; Aulia, S.; Chang, C.-C.; Chang, L.-Y.; Hung, W.-S.; Mizuguchi, H.; Haw, S.-C.; Yeh, M.-H. Enhancing self-induced polarization of PVDF-based triboelectric film


https://doi.org/10.1021/acs.chemrev.4c00966
*Chem. Rev.* 2025, 125, 11567−11665

by P-doped g-C3N4 for ultrasensitive triboelectric pressure sensors. *Nano Energy* **2024**, *131*, 110207.
(537) Chen, P.; Qin, L.; Ma, Z.; Zeng, T.; Xie, Y.; Zhang, C.; Luo, T.; Zhou, W.; Zhang, J. A hybrid tactile sensor enabling full-bandwidth and ultra high-sensitivity sensing using a stress regulator. *Nano Energy* **2024**, *131*, 110264.
(538) Jin, T.; Sun, Z.; Li, L.; Zhang, Q.; Zhu, M.; Zhang, Z.; Yuan, G.; Chen, T.; Tian, Y.; Hou, X.; Lee, C. Triboelectric nanogenerator sensors for soft robotics aiming at digital twin applications. *Nat. Commun.* **2020**, *11* (1), 5381.
(539) Zhou, Y.; Zhao, X.; Xu, J.; Chen, G.; Tat, T.; Li, J.; Chen, J. A multimodal magnetoelastic artificial skin for underwater haptic sensing. *Sci. Adv.* **2024**, *10*, No. eadj8567.
(540) Pyun, K. R.; Kwon, K.; Yoo, M. J.; Kim, K. K.; Gong, D.; Yeo, W.-H.; Han, S.; Ko, S. H. Machine-learned wearable sensors for real-time hand-motion recognition: toward practical applications. *Natl. Sci. Rev.* **2024**, *11* (2), nwad298.
(541) Sim, K.; Rao, Z.; Zou, Z.; Ershad, F.; Lei, J.; Thukral, A.; Chen, J.; Huang, Q.-A.; Xiao, J.; Yu, C. Metal oxide semiconductor nanomembrane-based soft unnoticeable multifunctional electronics for wearable human-machine interfaces. *Sci. Adv.* **2019**, *5* (8), No. eaav9653.
(542) Kim, K. K.; Ha, I.; Kim, M.; Choi, J.; Won, P.; Jo, S.; Ko, S. H. A deep-learned skin sensor decoding the epicentral human motions. *Nat. Commun.* **2020**, *11*, 2149.
(543) Huang, Y.; Gao, L.; Zhao, Y.; Guo, X.; Liu, C.; Liu, P. Highly flexible fabric strain sensor based on graphene nanoplatelet-polyaniline nanocomposites for human gesture recognition. *J. Appl. Polym. Sci.* **2017**, *134* (39), 45340.
(544) Araromi, O. A.; Graule, M. A.; Dorsey, K. L.; Castellanos, S.; Foster, J. R.; Hsu, W.-H.; Passy, A. E.; Vlassak, J. J.; Weaver, J. C.; Walsh, C. J.; et al. Ultra-sensitive and resilient compliant strain gauges for soft machines. *Nature* **2020**, *587* (7833), 219−224.
(545) Jiang, Y.; Ji, S.; Sun, J.; Huang, J.; Li, Y.; Zou, G.; Salim, T.; Wang, C.; Li, W.; Jin, H.; et al. A universal interface for plug-and-play assembly of stretchable devices. *Nature* **2023**, *614* (7948), 456−462.
(546) Geng, W.; Du, Y.; Jin, W.; Wei, W.; Hu, Y.; Li, J. Gesture recognition by instantaneous surface EMG images. *Sci. Rep.* **2016**, *6*, 36571.
(547) Sultana, A.; Ahmed, F.; Alam, M. S. A systematic review on surface electromyography-based classification system for identifying hand and finger movements. *Healthc. Anal.* **2023**, *3*, 100126.
(548) Wei, W.; Dai, Q.; Wong, Y.; Hu, Y.; Kankanhalli, M.; Geng, W. Surface-electromyography-based gesture recognition by multi-view deep learning. *IEEE Trans. Biomed. Eng.* **2019**, *66* (10), 2964−2973.
(549) Lee, H.; Lee, S.; Kim, J.; Jung, H.; Yoon, K. J.; Gandla, S.; Park, H.; Kim, S. Stretchable array electromyography sensor with graph neural network for static and dynamic gestures recognition system. *npj Flex. Electron.* **2023**, *7*, 20.
(550) Emayavaramban, G.; Divyapriya, S.; Mansoor, V.M.; Amudha, A.; Siva Ramkumar, M.; Nagaveni, P.; SivaramKrishnan, M. SEMG based classification of hand gestures using artificial neural network. *Mater. Today* **2021**, *37*, 2591−2598.
(551) Zhou, Z.; Chen, K.; Li, X.; Zhang, S.; Wu, Y.; Zhou, Y.; Meng, K.; Sun, C.; He, Q.; Fan, W.; et al. Sign-to-speech translation using machine-learning-assisted stretchable sensor arrays. *Nat. Electron.* **2020**, *3* (9), 571−578.
(552) Shan, L.; Liu, Y.; Zhang, X.; Li, E.; Yu, R.; Lian, Q.; Chen, X.; Chen, H.; Guo, T. Bioinspired kinesthetic system for human-machine interaction. *Nano Energy* **2021**, *88*, 106283.
(553) Wen, F.; Zhang, Z.; He, T.; Lee, C. AI enabled sign language recognition and VR space bidirectional communication using triboelectric smart glove. *Nat. Commun.* **2021**, *12*, 5378.
(554) Liddell, S. K. *Grammar, Gesture, And Meaning in American Sign Language*; Cambridge University Press, 2003.
(555) Jang, Y.; Kim, S. M.; Spinks, G. M.; Kim, S. J. Carbon nanotube yarn for fiber-shaped electrical sensors, actuators, and energy storage for smart systems. *Adv. Mater.* **2020**, *32* (5), 1902670.
(556) Lu, H.; Zhang, Y.; Zhu, M.; Li, S.; Liang, H.; Bi, P.; Wang, S.; Wang, H.; Gan, L.; Wu, X.-E.; Zhang, Y. Intelligent perceptual textiles based on ionic-conductive and strong silk fibers. *Nat. Commun.* **2024**, *15*, 3289.
(557) Tian, X.; Lee, P. M.; Tan, Y. J.; Wu, T. L. Y.; Yao, H.; Zhang, M.; Li, Z.; Ng, K. A.; Tee, B. C. K.; Ho, J. S. Wireless body sensor networks based on metamaterial textiles. *Nat. Electron.* **2019**, *2* (6), 243−251.
(558) Wang, L.; Qi, X.; Li, C.; Wang, Y. Multifunctional Tactile Sensors for Object Recognition. *Adv. Funct. Mater.* **2024**, *34*, 2409358.
(559) Tashakori, A.; Jiang, Z.; Servati, A.; Soltanian, S.; Narayana, H.; Le, K.; Nakayama, C.; Yang, C.-l.; Wang, Z. J.; Eng, J. J.; et al. Capturing complex hand movements and object interactions using machine learning-powered stretchable smart textile gloves. *Nat. Mach. Intell.* **2024**, *6* (1), 106−118.
(560) Kim, T.; Lee, S.; Hong, T.; Shin, G.; Kim, T.; Park, Y.-L. Heterogeneous sensing in a multifunctional soft sensor for human-robot interfaces. *Sci. Robot.* **2020**, *5* (49), No. eabc6878.
(561) Zhang, Z.; Yang, J.; Wang, H.; Wang, C.; Gu, Y.; Xu, Y.; Lee, S.; Yokota, T.; Haick, H.; Someya, T.; Wang, Y. A 10-micrometer-thick nanomesh-reinforced gas-permeable hydrogel skin sensor for long-term electrophysiological monitoring. *Sci. Adv.* **2024**, *10* (2), No. eadj5389.
(562) Jeong, W.; Lee, S.; Choi, H.; Bae, J.; Lee, S.-H.; Ma, Y.; Yoo, S.; Ha, J.-H.; Hong, J.-I.; Park, S.; et al. Washable, stretchable, and reusable core-shell metal nanowire network-based electronics on a breathable polymer nanomesh substrate. *Mater. Today* **2022**, *61*, 30−39.
(563) Wang, Y.; Lee, S.; Yokota, T.; Wang, H.; Jiang, Z.; Wang, J.; Koizumi, M.; Someya, T. A durable nanomesh on-skin strain gauge for natural skin motion monitoring with minimum mechanical constraints. *Sci. Adv.* **2020**, *6* (33), No. eabb7043.
(564) Yang, Q.; Jin, W.; Zhang, Q.; Wei, Y.; Guo, Z.; Li, X.; Yang, Y.; Luo, Q.; Tian, H.; Ren, T.-L. Mixed-modality speech recognition and interaction using a wearable artificial throat. *Nat. Mach. Intell.* **2023**, *5* (2), 169−180.
(565) Lee, S.; Kim, J.; Yun, I.; Bae, G. Y.; Kim, D.; Park, S.; Yi, I.-M.; Moon, W.; Chung, Y.; Cho, K. An ultrathin conformable vibration-responsive electronic skin for quantitative vocal recognition. *Nat. Commun.* **2019**, *10*, 2468.
(566) Zhao, X.; Zhou, Y.; Li, A.; Xu, J.; Karjagi, S.; Hahm, E.; Rulloda, L.; Li, J.; Hollister, J.; Kavehpour, P.; et al. A self-filtering liquid acoustic sensor for voice recognition. *Nat. Electron.* **2024**, *7* (10), 924−932.
(567) Che, Z.; Wan, X.; Xu, J.; Duan, C.; Zheng, T.; Chen, J. Speaking without vocal folds using a machine-learning-assisted wearable sensing-actuation system. *Nat. Commun.* **2024**, *15*, 1873.
(568) Kim, T.; Shin, Y.; Kang, K.; Kim, K.; Kim, G.; Byeon, Y.; Kim, H.; Gao, Y.; Lee, J. R.; Son, G.; Kim, T.; Jun, Y.; Kim, J.; Lee, J.; Um, S.; Kwon, Y.; Son, B. G.; Cho, M.; Sang, M.; Shin, J.; Kim, K.; Suh, J.; Choi, H.; Hong, S.; Cheng, H.; Kang, H.-G.; Hwang, D.; Yu, K. J. Ultrathin crystalline-silicon-based strain gauges with deep learning algorithms for silent speech interfaces. *Nat. Commun.* **2022**, *13*, 5815.
(569) Wang, Y.; Tang, T.; Xu, Y.; Bai, Y.; Yin, L.; Li, G.; Zhang, H.; Liu, H.; Huang, Y. All-weather, natural silent speech recognition via machine-learning-assisted tattoo-like electronics. *npj Flex. Electron.* **2021**, *5*, 20.
(570) Shi, Y.; Yang, P.; Lei, R.; Liu, Z.; Dong, X.; Tao, X.; Chu, X.; Wang, Z. L.; Chen, X. Eye tracking and eye expression decoding based on transparent, flexible and ultra-persistent electrostatic interface. *Nat. Commun.* **2023**, *14*, 3315.
(571) Ameri, S. K.; Kim, M.; Kuang, I. A.; Perera, W. K.; Alshiekh, M.; Jeong, H.; Topcu, U.; Akinwande, D.; Lu, N. Imperceptible electrooculography graphene sensor system for human-robot interface. *npj 2D Mater. Appl.* **2018**, *2*, 19.
(572) Lee, J. H.; Kim, H.; Hwang, J.-Y.; Chung, J.; Jang, T.-M.; Seo, D. G.; Gao, Y.; Lee, J.; Park, H.; Lee, S.; et al. 3D printed, customizable, and multifunctional smart electronic eyeglasses for


https://doi.org/10.1021/acs.chemrev.4c00966
*Chem. Rev.* 2025, 125, 11567−11665

wearable healthcare systems and human-machine interfaces. *ACS Appl. Mater. Interfaces* **2020**, *12* (19), 21424−21432.
(573) Zhu, H.; Yang, H.; Xu, S.; Ma, Y.; Zhu, S.; Mao, Z.; Chen, W.; Hu, Z.; Pan, R.; Xu, Y.; Xiong, Y.; Chen, Y.; Lu, Y.; Ning, X.; Jiang, D.; Yuan, S.; Xu, F. Frequency-encoded eye tracking smart contact lens for human-machine interaction. *Nat. Commun.* **2024**, *15*, 3588.
(574) Lee, J. P.; Jang, H.; Jang, Y.; Song, H.; Lee, S.; Lee, P. S.; Kim, J. Encoding of multi-modal emotional information via personalized skin-integrated wireless facial interface. *Nat. Commun.* **2024**, *15*, 530.
(575) Sun, T.; Tasnim, F.; McIntosh, R. T.; Amiri, N.; Solav, D.; Anbarani, M. T.; Sadat, D.; Zhang, L.; Gu, Y.; Karami, M. A.; et al. Decoding of facial strains via conformable piezoelectric interfaces. *Nat. Biomed. Eng.* **2020**, *4* (10), 954−972.
(576) Li, Q.; Zhang, L. N.; Tao, X. M.; Ding, X. Review of flexible temperature sensing networks for wearable physiological monitoring. *Adv. Healthc. Mater.* **2017**, *6* (12), 1601371.
(577) Kuzubasoglu, B. A.; Bahadir, S. K. Flexible temperature sensors: A review. *Sens. Actuator A-Phys.* **2020**, *315*, 112282.
(578) Su, Y.; Ma, C.; Chen, J.; Wu, H.; Luo, W.; Peng, Y.; Luo, Z.; Li, L.; Tan, Y.; Omisore, O. M.; Zhu, Z.; Wang, L.; Li, H. Printable, highly sensitive flexible temperature sensors for human body temperature monitoring: a review. *Nanoscale Res. Lett.* **2020**, *15*, 200.
(579) Cai, J.; Du, M.; Li, Z. Flexible temperature sensors constructed with fiber materials. *Adv. Mater. Technol.* **2022**, *7* (7), 2101182.
(580) Ukil, A.; Braendle, H.; Krippner, P. Distributed temperature sensing: Review of technology and applications. *IEEE Sens. J.* **2012**, *12* (5), 885−892.
(581) Zha, J.-W.; Wu, D.-H.; Yang, Y.; Wu, Y.-H.; Li, R. K.; Dang, Z.-M. Enhanced positive temperature coefficient behavior of the high-density polyethylene composites with multi-dimensional carbon fillers and their use for temperature-sensing resistors. *RSC Adv.* **2017**, *7* (19), 11338−11344.
(582) Bali, C.; Brandlmaier, A.; Ganster, A.; Raab, O.; Zapf, J.; Hübler, A. Fully inkjet-printed flexible temperature sensors based on carbon and PEDOT: PSS. *Mater. Today* **2016**, *3* (3), 739−745.
(583) Turkani, V. S.; Maddipatla, D.; Narakathu, B. B.; Bazuin, B. J.; Atashbar, M. Z. A carbon nanotube based NTC thermistor using additive print manufacturing processes. *Sens. Actuator A-Phys.* **2018**, *279*, 1−9.
(584) Lee, M.; Yoo, M. Detectivity of thin-film NTC thermal sensors. *Sens. Actuator A-Phys.* **2002**, *96* (2−3), 97−104.
(585) Xu, H.; Wu, Y.; Yang, D.; Wang, J.; Xie, H. Study on theories and influence factors of PTC property in polymer-based conductive composites. *Rev. Adv. Mater. Sci.* **2011**, *27* (2), 173−183.
(586) Wang, M.; Jiang, X.; Yuan, Y.; Zhou, F.; Li, T. Study on the low Curie point positive temperature coefficient (PTC) material based on the conductive model. *Mater. Chem. Phys.* **2024**, *312*, 128676.
(587) Kumari, S.; Kumar, A.; Kumar, A.; Kumar, V.; Thakur, V. N.; Kumar, A.; Goyal, P.; Gaur, A.; Arya, A.; Sharma, A. Enhanced Curie temperature and superior temperature stability by site selected doping in BCZT based lead-free ceramics. *Ceram. Int.* **2022**, *48* (10), 13780−13793.
(588) Lee, S.; Bock, J. A.; Trolier-McKinstry, S.; Randall, C. A. Ferroelectric-thermoelectricity and Mott transition of ferroelectric oxides with high electronic conductivity. *J. Eur. Ceram. Soc.* **2012**, *32* (16), 3971−3988.
(589) Preis, W.; Sitte, W. Electrical properties of grain boundaries in interfacially controlled functional ceramics. *J. Electroceram.* **2015**, *34* (2), 185−206.
(590) Vollman, M.; Waser, R. Grain boundary defect chemistry of acceptor-doped titanates: space charge layer width. *J. Am. Ceram. Soc.* **1994**, *77* (1), 235−243.
(591) Waser, R.; Hagenbeck, R. Grain boundaries in dielectric and mixed-conducting ceramics. *Acta Mater.* **2000**, *48* (4), 797−825.
(592) Yi, X.-S.; Shen, L.; Pan, Y. Thermal volume expansion in polymeric PTC composites: a theoretical approach. *Compos. Sci. Technol.* **2001**, *61* (7), 949−956.
(593) Poncé, S.; Li, W.; Reichardt, S.; Giustino, F. First-principles calculations of charge carrier mobility and conductivity in bulk semiconductors and two-dimensional materials. *Rep. Prog. Phys.* **2020**, *83* (3), 036501.
(594) Karl, N. Charge carrier transport in organic semiconductors. *Synth. Met.* **2003**, *133*, 649−657.
(595) Shin, J.; Jeong, B.; Kim, J.; Nam, V. B.; Yoon, Y.; Jung, J.; Hong, S.; Lee, H.; Eom, H.; Yeo, J.; Choi, J.; Lee, D.; Ko, S. H. Sensitive wearable temperature sensor with seamless monolithic integration. *Adv. Mater.* **2020**, *32* (2), 1905527.
(596) Hong, S. Y.; Lee, Y. H.; Park, H.; Jin, S. W.; Jeong, Y. R.; Yun, J.; You, I.; Zi, G.; Ha, J. S. Stretchable active matrix temperature sensor array of polyaniline nanofibers for electronic skin. *Adv. Mater.* **2016**, *28* (5), 930−935.
(597) Feteira, A.; Reichmann, K. NTC ceramics: past, present and future. *Adv. Sci. Technol.* **2011**, *67*, 124−133.
(598) Fritsch, S.; Sarrias, J.; Brieu, M.; Couderc, J.; Baudour, J.; Snoeck, E.; Rousset, A. Correlation between the structure, the microstructure and the electrical properties of nickel Manganite negative temperature coefficient (NTC) thermistors. *Solid State Ion.* **1998**, *109* (3−4), 229−237.
(599) Yan, M.-H.; Zhang, Z.-F.; Huang, H.-H.; Li, Z.-L.; Li, P.; Hao, J.-G.; Li, W.; Du, J.; Joshi, M. K.; Fu, P. Multi-scale structural regulation of negative temperature coefficient effect and electrical conduction mechanism of xSm2O3-(1-x) CaCu3Ti4O12 ceramics. *Ceram. Int.* **2024**, *50* (24), 54390−54400.
(600) John, A. T.; Narayanasamy, A.; George, D.; Hariharan, M. The effect of single-atom substitution on structure and band gap in organic semiconductors. *Cryst. Growth Des.* **2022**, *22* (2), 1237−1243.
(601) Sun, L.; Zhu, W.; Yang, F.; Li, B.; Ren, X.; Zhang, X.; Hu, W. Molecular cocrystals: design, charge-transfer and optoelectronic functionality. *Phys. Chem. Chem. Phys.* **2018**, *20* (9), 6009−6023.
(602) Boyer, A.; Cisse, E. Properties of thin film thermoelectric materials: application to sensors using the Seebeck effect. *Mater. Sci. Eng., B* **1992**, *13* (2), 103−111.
(603) Van Herwaarden, A.; Sarro, P. Thermal sensors based on the Seebeck effect. *Sens. Actuator* **1986**, *10* (3−4), 321−346.
(604) Sun, B.; Huang, X. Seeking advanced thermal management for stretchable electronics. *npj Flex. Electron.* **2021**, *5*, 12.
(605) Wu, K.; Dou, Z.; Deng, S.; Wu, D.; Zhang, B.; Yang, H.; Li, R.; Lei, C.; Zhang, Y.; Fu, Q.; Yu, G. Mechanochemistry-mediated colloidal liquid metals for electronic device cooling at kilowatt levels. *Nat. Nanotechnol.* **2025**, *20*, 104−111.
(606) Park, J. J.; Ko, S. H. Nanoscale gradient interface for efficient heat transfer. *Nat. Nanotechnol.* **2025**, *20* (1), 8−9.
(607) Nie, S.; Cai, M.; Yang, H.; Shen, L.; Wang, S.; Zhu, Y.; Song, J. Soft, stretchable thermal protective substrates for wearable electronics. *npj Flex. Electron.* **2022**, *6*, 36.
(608) Fu, X.; Si, L.; Zhang, Z.; Yang, T.; Feng, Q.; Song, J.; Zhu, S.; Ye, D. Gradient all-nanostructured aerogel fibers for enhanced thermal insulation and mechanical properties. *Nat. Commun.* **2025**, *16*, 2357.
(609) Sha, W.; Xiao, M.; Zhang, J.; Ren, X.; Zhu, Z.; Zhang, Y.; Xu, G.; Li, H.; Liu, X.; Chen, X.; Gao, L.; Qiu, C.-W.; Hu, R. Robustly printable freeform thermal metamaterials. *Nat. Commun.* **2021**, *12*, 7228.
(610) Li, W.; Sigmund, O.; Zhang, X. S. Analytical realization of complex thermal meta-devices. *Nat. Commun.* **2024**, *15*, 5527.
(611) Hao, S.; Fu, Q.; Meng, L.; Xu, F.; Yang, J. A biomimetic laminated strategy enabled strain-interference free and durable flexible thermistor electronics. *Nat. Commun.* **2022**, *13*, 6472.
(612) Shiran Chaharsoughi, M.; Edberg, J.; Andersson Ersman, P.; Crispin, X.; Zhao, D.; Jonsson, M. P. Ultrasensitive electrolyte-assisted temperature sensor. *npj Flex. Electron.* **2020**, *4*, 23.
(613) Sang, M.; Kang, K.; Zhang, Y.; Zhang, H.; Kim, K.; Cho, M.; Shin, J.; Hong, J.-H.; Kim, T.; Lee, S. K.; Yeo, W.-H.; Lee, J. W.; Lee, T.; Xu, B.; Yu, K. J. Ki Jun. Ultrahigh sensitive Au-doped silicon nanomembrane based wearable sensor arrays for continuous skin

temperature monitoring with high precision. *Adv. Mater.* **2022**, *34* (4), 2105865.
(614) Pei, Y.; Shi, X.; LaLonde, A.; Wang, H.; Chen, L.; Snyder, G. J. Convergence of electronic bands for high performance bulk thermoelectrics. *Nature* **2011**, *473* (7345), 66−69.
(615) Zhou, J.; Cui, H.-H.; Liu, Y.; Ming, H.; Yu, Y.; Dravid, V. P.; Luo, Z.-Z.; Yan, Q.; Zou, Z.; Kanatzidis, M. G. Conduction band convergence and local structure distortion for superior thermoelectric performance of GaSb-doped n-type PbSe thermoelectrics. *Nat. Commun.* **2025**, *16*, 5749.
(616) Zhang, Y.; Xing, C.; Wang, D.; Genc, A.; Lee, S. H.; Chang, C.; Li, Z.; Zheng, L.; Lim, K. H.; Zhu, H.; Smriti, R. B.; Liu, Y.; Cheng, S.; Hong, M.; Fan, X.; Mao, Z.; Zhao, L.-D.; Cabot, A.; Zhu, T.; Poudel, B. Realizing high power factor and thermoelectric performance in band engineered AgSbTe2. *Nat. Commun.* **2025**, *16*, 22.
(617) Wang, L.; Zhang, W.; Back, S. Y.; Kawamoto, N.; Nguyen, D. H.; Mori, T. High-performance Mg3Sb2-based thermoelectrics with reduced structural disorder and microstructure evolution. *Nat. Commun.* **2024**, *15*, 6800.
(618) Lor, W.-B.; Chu, H.-S. Effect of interface thermal resistance on heat transfer in a composite medium using the thermal wave model. *Int. J. Heat Mass Transfer* **2000**, *43* (5), 653−663.
(619) Kim, T.; Kim, S.; Kim, E.; Kim, T.; Cho, J.; Song, C.; Baik, S. High-temperature skin softening materials overcoming the trade-off between thermal conductivity and thermal contact resistance. *Small* **2021**, *17* (38), 2102128.
(620) Saggin, B.; Tarabini, M.; Lanfranchi, G. A device for the skin-contact thermal resistance measurement. *IEEE Trans. Instrum. Meas.* **2012**, *61* (2), 489−495.
(621) Zhu, C.; Chortos, A.; Wang, Y.; Pfattner, R.; Lei, T.; Hinckley, A. C.; Pochorovski, I.; Yan, X.; To, J. W.-F.; Oh, J. Y.; et al. Stretchable temperature-sensing circuits with strain suppression based on carbon nanotube transistors. *Nat. Electron.* **2018**, *1* (3), 183−190.
(622) Sang, M.; Kang, K.; Zhang, Y.; Zhang, H.; Kim, K.; Cho, M.; Shin, J.; Hong, J.-H.; Kim, T.; Lee, S. K.; Yeo, W.-H.; Lee, J. W.; Lee, T.; Xu, B.; Yu, K. J. Ultrahigh sensitive Au-doped silicon nanomembrane based wearable sensor arrays for continuous skin temperature monitoring with high precision. *Adv. Mater.* **2022**, *34* (4), 2105865.
(623) Zhao, X.-F.; Yang, S.-Q.; Wen, X.-H.; Huang, Q.-W.; Qiu, P.-F.; Wei, T.-R.; Zhang, H.; Wang, J.-C.; Zhang, D. W.; Shi, X.; Lu, H.-L. A fully flexible intelligent thermal touch panel based on intrinsically plastic Ag2S semiconductor. *Adv. Mater.* **2022**, *34* (13), 2107479.
(624) Wen, N.; Guan, X.; Fan, Z.; Guo, Y.; Cong, T.; Huang, H.; Li, C.; Zhang, J.; Lei, B.; Yang, R.; et al. A highly stretchable and breathable self-powered dual-parameter sensor for decoupled temperature and strain sensing. *Org. Electron.* **2023**, *113*, 106723.
(625) Wang, F.; Chen, J.; Cui, X.; Liu, X.; Chang, X.; Zhu, Y. Wearable ionogel-based fibers for strain sensors with ultrawide linear response and temperature sensors insensitive to strain. *ACS Appl. Mater. Interfaces* **2022**, *14* (26), 30268−30278.
(626) Jung, M.; Jeon, S.; Bae, J. Scalable and facile synthesis of stretchable thermoelectric fabric for wearable self-powered temperature sensors. *RSC Adv.* **2018**, *8* (70), 39992−39999.
(627) Xin, Y.; Zhou, J.; Lubineau, G. A highly stretchable strain-insensitive temperature sensor exploits the Seebeck effect in nanoparticle-based printed circuits. *J. Mater. Chem. A* **2019**, *7* (42), 24493−24501.
(628) Xu, K.; Lu, Y.; Yamaguchi, T.; Arie, T.; Akita, S.; Takei, K. Highly precise multifunctional thermal management-based flexible sensing sheets. *ACS Nano* **2019**, *13* (12), 14348−14356.
(629) Shin, Y.; Kim, Y. W.; Kang, H. J.; Lee, J. H.; Byun, J. E.; Yang, J.-Y.; Lee, J. W. Stretchable and skin-mountable temperature sensor array using reduction-controlled graphene oxide for dermatological thermography. *Nano Lett.* **2023**, *23* (11), 5391−5398.
(630) Liu, Z.; Tian, B.; Zhang, B.; Liu, J.; Zhang, Z.; Wang, S.; Luo, Y.; Zhao, L.; Shi, P.; Lin, Q.; Jiang, Z. A thin-film temperature sensor based on a flexible electrode and substrate. *Microsyst. Nanoeng.* **2021**, *7*, 42.
(631) Swiegers, J.; Chambers, P.; Pretorius, I. Olfaction and taste: Human perception, physiology and genetics. *Aust. J. Grape Wine Res.* **2005**, *11* (2), 109−113.
(632) Wang, C.; Chen, Z.; Chan, C. L. J.; Wan, Z. a.; Ye, W.; Tang, W.; Ma, Z.; Ren, B.; Zhang, D.; Song, Z.; et al. Biomimetic olfactory chips based on large-scale monolithically integrated nanotube sensor arrays. *Nat. Electron.* **2024**, *7* (2), 157−167.
(633) Hu, J.; Liu, D.; Xia, X.; Wang, B.; Pan, D.; Cheng, Y.; Lu, Y. MXene/perovskite-based bionic human odor sensor array with machine learning. *Chem. Eng. J.* **2023**, *468*, 143752.
(634) Song, H. W.; Moon, D.; Won, Y.; Cha, Y. K.; Yoo, J.; Park, T. H.; Oh, J. H. A pattern recognition artificial olfactory system based on human olfactory receptors and organic synaptic devices. *Sci. Adv.* **2024**, *10* (21), No. eadl2882.
(635) Ghasemi-Varnamkhasti, M.; Mohtasebi, S. S.; Siadat, M. Biomimetic-based odor and taste sensing systems to food quality and safety characterization: An overview on basic principles and recent achievements. *J. Food Eng.* **2010**, *100* (3), 377−387.
(636) Rogers, K. R. Principles of affinity-based biosensors. *Mol. Biotechnol.* **1998**, *7*, 3−18.
(637) Leech, D. Affinity biosensors. *Chem. Soc. Rev.* **1994**, *23* (3), 205−213.
(638) Abdiche, Y. N.; Malashock, D. S.; Pons, J. Probing the binding mechanism and affinity of tanezumab, a recombinant humanized anti-NGF monoclonal antibody, using a repertoire of biosensors. *Protein Sci.* **2008**, *17* (8), 1326−1335.
(639) Gohlke, H.; Klebe, G. Approaches to the description and prediction of the binding affinity of small-molecule ligands to macromolecular receptors. *Angew. Chem.-Int. Ed.* **2002**, *41* (15), 2644−2676.
(640) Ryde, U.; Soderhjelm, P. Ligand-binding affinity estimates supported by quantum-mechanical methods. *Chem. Rev.* **2016**, *116* (9), 5520−5566.
(641) Katz, B. A. Structural and mechanistic determinants of affinity and specificity of ligands discovered or engineered by phage display. *Annu. Rev. Biophys. Biomol. Struct.* **1997**, *26* (1), 27−45.
(642) Kastritis, P. L.; Bonvin, A. M. On the binding affinity of macromolecular interactions: daring to ask why proteins interact. *J. R. Soc. Interface* **2013**, *10* (79), 20120835.
(643) Lochan, R. C.; Head-Gordon, M. Computational studies of molecular hydrogen binding affinities: the role of dispersion forces, electrostatics, and orbital interactions. *Phys. Chem. Chem. Phys.* **2006**, *8* (12), 1357−1370.
(644) Rodriguez-Reyes, J. C. F.; Siler, C. G.; Liu, W.; Tkatchenko, A.; Friend, C. M.; Madix, R. J. van der Waals interactions determine selectivity in catalysis by metallic gold. *J. Am. Chem. Soc.* **2014**, *136* (38), 13333−13340.
(645) Ma, W.; Yang, L.; Lv, Y.; Fu, J.; Zhang, Y.; He, L. Determine equilibrium dissociation constant of drug-membrane receptor affinity using the cell membrane chromatography relative standard method. *J. Chromatogr. A* **2017**, *1503*, 12−20.
(646) Yang, D.; Singh, A.; Wu, H.; Kroe-Barrett, R. Determination of high-affinity antibody-antigen binding kinetics using four biosensor platforms. *J. Vis. Exp.* **2017**, *122*, No. e55659.
(647) Holford, T. R.; Davis, F.; Higson, S. P. Recent trends in antibody based sensors. *Biosens. Bioelectron.* **2012**, *34* (1), 12−24.
(648) Pelosi, P.; Zhu, J.; Knoll, W. Odorant-binding proteins as sensing elements for odour monitoring. *Sensors* **2018**, *18* (10), 3248.
(649) Pelosi, P.; Zhu, J.; Knoll, W. From gas sensors to biomimetic artificial noses. *Chemosensors* **2018**, *6* (3), 32.
(650) Goldsmith, B. R.; Mitala, J. J., Jr; Josue, J.; Castro, A.; Lerner, M. B.; Bayburt, T. H.; Khamis, S. M.; Jones, R. A.; Brand, J. G.; Sligar, S. G.; et al. Biomimetic chemical sensors using nanoelectronic readout of olfactory receptor proteins. *ACS Nano* **2011**, *5* (7), 5408−5416.
(651) Barbosa, A. J.; Oliveira, A. R.; Roque, A. C. Protein-and peptide-based biosensors in artificial olfaction. *Trends Biotechnol.* **2018**, *36* (12), 1244−1258.


https://doi.org/10.1021/acs.chemrev.4c00966
*Chem. Rev.* 2025, 125, 11567−11665

(652) Boger, D. L.; Fink, B. E.; Brunette, S. R.; Tse, W. C.; Hedrick, M. P. A simple, high-resolution method for establishing DNA binding affinity and sequence selectivity. *J. Am. Chem. Soc.* **2001**, *123* (25), 5878−5891.
(653) Zhou, C.; Yang, Z.; Liu, D. Reversible regulation of protein binding affinity by a DNA machine. *J. Am. Chem. Soc.* **2012**, *134* (3), 1416−1418.
(654) Rastogi, C.; Rube, H. T.; Kribelbauer, J. F.; Crocker, J.; Loker, R. E.; Martini, G. D.; Laptenko, O.; Freed-Pastor, W. A.; Prives, C.; Stern, D. L.; Mann, R. S.; Bussemaker, H. J. Accurate and sensitive quantification of protein-DNA binding affinity. *Proc. Natl. Acad. Sci. U. S. A.* **2018**, *115* (16), No. E3692.
(655) Zhou, W.; Saran, R.; Liu, J. Metal sensing by DNA. *Chem. Rev.* **2017**, *117* (12), 8272−8325.
(656) Tang, X.; Bansaruntip, S.; Nakayama, N.; Yenilmez, E.; Chang, Y.-l.; Wang, Q. Carbon nanotube DNA sensor and sensing mechanism. *Nano Lett.* **2006**, *6* (8), 1632−1636.
(657) Lai, Q. T.; Zhao, X. H.; Sun, Q. J.; Tang, Z.; Tang, X. G.; Roy, V. A. Emerging MXene-Based Flexible Tactile Sensors for Health Monitoring and Haptic Perception. *Small* **2023**, *19* (27), 2300283.
(658) Kim, J. H.; Cho, C. H.; Shin, J. H.; Yang, J. C.; Park, T. J.; Park, J.; Park, J. P. Highly sensitive and label-free detection of influenza H5N1 viral proteins using affinity peptide and porous BSA/MXene nanocomposite electrode. *Anal. Chim. Acta* **2023**, *1251*, 341018.
(659) Hou, S.; Yu, J.; Zhuang, X.; Li, D.; Liu, Y.; Gao, Z.; Sun, T.; Wang, F.; Yu, X. Phase separation of P3HT/PMMA blend film for forming semiconducting and dielectric layers in organic thin-film transistors for high-sensitivity NO2 detection. *ACS Appl. Mater. Interfaces* **2019**, *11* (47), 44521−44527.
(660) Xie, T.; Xie, G.; Du, H.; Zhou, Y.; Xie, F.; Jiang, Y.; Tai, H. The fabrication and optimization of thin-film transistors based on poly (3-hexylthiophene) films for nitrogen dioxide detection. *IEEE Sens. J.* **2016**, *16* (7), 1865−1871.
(661) Tiwari, S.; Singh, A. K.; Joshi, L.; Chakrabarti, P.; Takashima, W.; Kaneto, K.; Prakash, R. Poly-3-hexylthiophene based organic field-effect transistor: Detection of low concentration of ammonia. *Sens. Actuator B-Chem.* **2012**, *171*, 962−968.
(662) Lu, Y.; Yao, Y.; Zhang, Q.; Zhang, D.; Zhuang, S.; Li, H.; Liu, Q. Olfactory biosensor for insect semiochemicals analysis by impedance sensing of odorant-binding proteins on interdigitated electrodes. *Biosens. Bioelectron.* **2015**, *67*, 662−669.
(663) Khadka, R.; Aydemir, N.; Carraher, C.; Hamiaux, C.; Baek, P.; Cheema, J.; Kralicek, A.; Travas-Sejdic, J. Investigating electrochemical stability and reliability of gold electrode-electrolyte systems to develop bioelectronic nose using insect olfactory receptor. *Electroanalysis* **2019**, *31* (4), 726−738.
(664) Umpleby II, R. J.; Baxter, S. C.; Rampey, A. M.; Rushton, G. T.; Chen, Y.; Shimizu, K. D. Characterization of the heterogeneous binding site affinity distributions in molecularly imprinted polymers. *J. Chromatogr. B* **2004**, *804* (1), 141−149.
(665) Saylan, Y.; Akgönüllü, S.; Yavuz, H.; Ünal, S.; Denizli, A. Molecularly imprinted polymer based sensors for medical applications. *Sensors* **2019**, *19* (6), 1279.
(666) Ramanavicius, S.; Jagminas, A.; Ramanavicius, A. Advances in molecularly imprinted polymers based affinity sensors. *Polymers* **2021**, *13* (6), 974.
(667) Shimizu, K. D.; Stephenson, C. J. Molecularly imprinted polymer sensor arrays. *Curr. Opin. Chem. Biol.* **2010**, *14* (6), 743−750.
(668) Jin, H. J.; Lee, S. H.; Kim, T. H.; Park, J.; Song, H. S.; Park, T. H.; Hong, S. Nanovesicle-based bioelectronic nose platform mimicking human olfactory signal transduction. *Biosens. Bioelectron.* **2012**, *35* (1), 335−341.
(669) Son, M.; Kim, D.; Ko, H. J.; Hong, S.; Park, T. H. A portable and multiplexed bioelectronic sensor using human olfactory and taste receptors. *Biosens. Bioelectron.* **2017**, *87*, 901−907.
(670) Park, S. J.; Kwon, O. S.; Lee, S. H.; Song, H. S.; Park, T. H.; Jang, J. Ultrasensitive flexible graphene based field-effect transistor (FET)-type bioelectronic nose. *Nano Lett.* **2012**, *12* (10), 5082−5090.
(671) Tuffery, P.; Derreumaux, P. Flexibility and binding affinity in protein-ligand, protein-protein and multi-component protein interactions: limitations of current computational approaches. *J. R. Soc. Interface* **2012**, *9* (66), 20−33.
(672) Yánez-Sedeno, P.; Pingarrón, J. M.; Riu, J.; Rius, F. X. Electrochemical sensing based on carbon nanotubes. *Trac-Trends Anal. Chem.* **2010**, *29* (9), 939−953.
(673) Liu, X.; Huang, L.; Qian, K. Nanomaterial-based electrochemical sensors: mechanism, preparation, and application in biomedicine. *Adv. NanoBiomed Res.* **2021**, *1* (6), 2000104.
(674) Bakker, E.; Telting-Diaz, M. Electrochemical sensors. *Anal. Chem.* **2002**, *74* (12), 2781−2800.
(675) Windmiller, J. R.; Wang, J. Wearable electrochemical sensors and biosensors: a review. *Electroanalysis* **2013**, *25* (1), 29−46.
(676) Pejcic, B.; De Marco, R. Impedance spectroscopy: Over 35 years of electrochemical sensor optimization. *Electrochim. Acta* **2006**, *51* (28), 6217−6229.
(677) Grieshaber, D.; MacKenzie, R.; Vörös, J.; Reimhult, E. Electrochemical biosensors-sensor principles and architectures. *Sensors* **2008**, *8* (3), 1400−1458.
(678) Van Leeuwen, H. P.; Town, R. M. Electrochemical metal speciation analysis of chemically heterogeneous samples: the outstanding features of stripping chronopotentiometry at scanned deposition potential. *Environ. Sci. Technol.* **2003**, *37* (17), 3945−3952.
(679) Vidal, J.; Yague, M.; Castillo, J. A chronoamperometric sensor for hydrogen peroxide based on electron transfer between immobilized horseradish peroxidase on a glassy carbon electrode and a diffusing ferrocene mediator. *Sens. Actuator B-Chem.* **1994**, *21* (2), 135−141.
(680) De, D.; Englehardt, J. D.; Kalu, E. E. Electroreduction of Nitrate and Nitrite Ion on a Platinum-Group-Metal Catalyst-Modified Carbon Fiber Electrode Chronoamperometry and Mechanism Studies. *J. Electrochem. Soc.* **2000**, *147* (12), 4573.
(681) Nawaz, M. A. H.; Majdinasab, M.; Latif, U.; Nasir, M.; Gokce, G.; Anwar, M. W.; Hayat, A. Development of a disposable electrochemical sensor for detection of cholesterol using differential pulse voltammetry. *J. Pharm. Biomed. Anal.* **2018**, *159*, 398−405.
(682) Guerreiro, G. V.; Zaitouna, A. J.; Lai, R. Y. Characterization of an electrochemical mercury sensor using alternating current, cyclic, square wave and differential pulse voltammetry. *Anal. Chim. Acta* **2014**, *810*, 79−85.
(683) Saputra, H. A. Electrochemical sensors: basic principles, engineering, and state of the art. *Monatshefte für Chemie-Chemical Monthly* **2023**, *154* (10), 1083−1100.
(684) Zhang, W.; Wang, R.; Luo, F.; Wang, P.; Lin, Z. Miniaturized electrochemical sensors and their point-of-care applications. *Chin. Chem. Lett.* **2020**, *31* (3), 589−600.
(685) Lan, S.; Veiseh, M.; Zhang, M. Surface modification of silicon and gold-patterned silicon surfaces for improved biocompatibility and cell patterning selectivity. *Biosens. Bioelectron.* **2005**, *20* (9), 1697−1708.
(686) Omer, K. M.; Hama Aziz, K. H.; Mohammed, S. J. Improvement of selectivity via the surface modification of carbon nanodots towards the quantitative detection of mercury ions. *New J. Chem.* **2019**, *43* (33), 12979−12986.
(687) Weng, Z.; Zaera, F. Increase in activity and selectivity in catalysis via surface modification with self-assembled monolayers. *J. Phys. Chem. C* **2014**, *118* (7), 3672−3679.
(688) DeSantis, G.; Jones, J. B. Chemical modification of enzymes for enhanced functionality. *Curr. Opin. Biotechnol.* **1999**, *10* (4), 324−330.
(689) Talbert, J. N.; Goddard, J. M. Enzymes on material surfaces. *Colloid Surf. B-Biointerfaces* **2012**, *93*, 8−19.
(690) Bai, Y.; Koh, C. G.; Boreman, M.; Juang, Y.-J.; Tang, I.-C.; Lee, L. J.; Yang, S.-T. Surface modification for enhancing antibody binding on polymer-based microfluidic device for enzyme-linked immunosorbent assay. *Langmuir* **2006**, *22* (22), 9458−9467.


https://doi.org/10.1021/acs.chemrev.4c00966
*Chem. Rev.* 2025, 125, 11567−11665

(691) Makamba, H.; Kim, J. H.; Lim, K.; Park, N.; Hahn, J. H. Surface modification of poly (dimethylsiloxane) microchannels. *Electrophoresis* **2003**, *24* (21), 3607−3619.
(692) Walsh, S. J.; Bargh, J. D.; Dannheim, F. M.; Hanby, A. R.; Seki, H.; Counsell, A. J.; Ou, X.; Fowler, E.; Ashman, N.; Takada, Y.; et al. Site-selective modification strategies in antibody-drug conjugates. *Chem. Soc. Rev.* **2021**, *50* (2), 1305−1353.
(693) Chen, Y.; Xianyu, Y.; Jiang, X. Surface modification of gold nanoparticles with small molecules for biochemical analysis. *Acc. Chem. Res.* **2017**, *50* (2), 310−319.
(694) Park, K.; Son, J.; Chung, H.; Kim, S.; Lee, C.; Kang, K.; Kim, H. G. Surface modification by silver coating for improving electrochemical properties of LiFePO4. *Solid State Commun.* **2004**, *129* (5), 311−314.
(695) Vengatesan, M. R.; Mittal, V. *Surface modification of nanomaterials for application in polymer nanocomposites: an overview*; Wiley-VCH, 2015.
(696) Ma, Z.; Shi, W.; Yan, K.; Pan, L.; Yu, G. Doping engineering of conductive polymer hydrogels and their application in advanced sensor technologies. *Chem. Sci.* **2019**, *10* (25), 6232−6244.
(697) Wang, G.; Morrin, A.; Li, M.; Liu, N.; Luo, X. Nanomaterial-doped conducting polymers for electrochemical sensors and biosensors. *J. Mater. Chem. B* **2018**, *6* (25), 4173−4190.
(698) Gao, L.; Wang, M.; Wang, W.; Xu, H.; Wang, Y.; Zhao, H.; Cao, K.; Xu, D.; Li, L. Highly sensitive pseudocapacitive iontronic pressure sensor with broad sensing range. *Nano-Micro Lett.* **2021**, *13*, 140.
(699) Chang, Y.; Wang, L.; Li, R.; Zhang, Z.; Wang, Q.; Yang, J.; Guo, C. F.; Pan, T. First decade of interfacial iontronic sensing: from droplet sensors to artificial skins. *Adv. Mater.* **2021**, *33* (7), 2003464.
(700) Li, J.; Li, J.; Tang, Y.; Liu, Z.; Zhang, Z.; Wu, H.; Shen, B.; Su, M.; Liu, M.; Li, F. Touchable gustation via a hoffmeister gel iontronic sensor. *ACS Nano* **2023**, *17* (5), 5129−5139.
(701) Xiong, Y.; Han, J.; Wang, Y.; Wang, Z. L.; Sun, Q. Emerging iontronic sensing: materials, mechanisms, and applications. *Research* **2022**, *2022*, 9867378.
(702) Li, D. Nanofluidic Iontronic Devices. In *Electrokinetic Microfluidics and Nanofluidics*; Springer, 2022; pp 201−246.
(703) Zhu, Z.; Zhao, Y.; Chang, C.; Yan, S.; Sun, T.; Gu, S.; Li, Y.; Zhang, D.; Wang, C.; Zeng, X. C. Design of artificial biomimetic channels with Na+ permeation rate and selectivity potentially outperforming the natural sodium channel. *Nano Res.* **2024**, *17* (9), 8638−8646.
(704) DuChanois, R. M.; Porter, C. J.; Violet, C.; Verduzco, R.; Elimelech, M. Membrane materials for selective ion separations at the water-energy nexus. *Adv. Mater.* **2021**, *33* (38), 2101312.
(705) Liu, K.; Epsztein, R.; Lin, S.; Qu, J.; Sun, M. Ion-ion selectivity of synthetic membranes with confined nanostructures. *ACS Nano* **2024**, *18* (33), 21633−21650.
(706) Vatanpour, V.; Madaeni, S. S.; Zinadini, S.; Rajabi, H. R. Development of ion imprinted technique for designing nickel ion selective membrane. *J. Membr. Sci.* **2011**, *373* (1−2), 36−42.
(707) Hashimoto, K.; Fujii, K.; Nishi, K.; Sakai, T.; Shibayama, M. Nearly ideal polymer network ion gel prepared in pH-buffering ionic liquid. *Macromolecules* **2016**, *49* (1), 344−352.
(708) Kataoka, T.; Ishioka, Y.; Mizuhata, M.; Minami, H.; Maruyama, T. Highly conductive ionic-liquid gels prepared with orthogonal double networks of a low-molecular-weight gelator and cross-linked polymer. *ACS Appl. Mater. Interfaces* **2015**, *7* (41), 23346−23352.
(709) Collinson, M. M. Sol-gel strategies for the preparation of selective materials for chemical analysis. *Crit. Rev. Anal. Chem.* **1999**, *29* (4), 289−311.
(710) Cowan, M. G.; Gin, D. L.; Noble, R. D. Poly (ionic liquid)/ionic liquid ion-gels with high "free" ionic liquid content: platform membrane materials for CO2/light gas separations. *Acc. Chem. Res.* **2016**, *49* (4), 724−732.
(711) Snedden, P.; Cooper, A. I.; Scott, K.; Winterton, N. Cross-linked polymer- ionic liquid composite materials. *Macromolecules* **2003**, *36* (12), 4549−4556.
(712) Butler, S. J.; Parker, D. Anion binding in water at lanthanide centres: from structure and selectivity to signalling and sensing. *Chem. Soc. Rev.* **2013**, *42* (4), 1652−1666.
(713) Hancock, R. D. The pyridyl group in ligand design for selective metal ion complexation and sensing. *Chem. Soc. Rev.* **2013**, *42* (4), 1500−1524.
(714) Singha, D. K.; Mahata, P. Highly selective and sensitive luminescence turn-on-based sensing of Al3+ ions in aqueous medium using a MOF with free functional sites. *Inorg. Chem.* **2015**, *54* (13), 6373−6379.
(715) Zhao, C.; Wang, Y.; Tang, G.; Ru, J.; Zhu, Z.; Li, B.; Guo, C. F.; Li, L.; Zhu, D. Ionic flexible sensors: mechanisms, materials, structures, and applications. *Adv. Funct. Mater.* **2022**, *32* (17), 2110417.
(716) Lee, J.; Le, Q. T.; Lee, D.; Nam, S.; Nguyen, T. H.; Song, Y.; Sung, J.; Son, S.-W.; Kim, J. Micropyramidal flexible ion gel sensor for multianalyte discrimination and strain compensation. *ACS Appl. Mater. Interfaces* **2023**, *15* (21), 26138−26147.
(717) Karawdeniya, B. I.; Damry, A. M.; Murugappan, K.; Manjunath, S.; Bandara, Y. N. D.; Jackson, C. J.; Tricoli, A.; Neshev, D. Surface functionalization and texturing of optical metasurfaces for sensing applications. *Chem. Rev.* **2022**, *122* (19), 14990−15030.
(718) Sung, S.-H.; Suh, J. M.; Hwang, Y. J.; Jang, H. W.; Park, J. G.; Jun, S. C. Data-centric artificial olfactory system based on the eigengraph. *Nat. Commun.* **2024**, *15* (1), 1211.
(719) Chen, Z.; Zhou, B.; Xiao, M.; Bhowmick, T.; Karthick Kannan, P.; Occhipinti, L. G.; Gardner, J. W.; Hasan, T. Real-time, noise and drift resilient formaldehyde sensing at room temperature with aerogel filaments. *Sci. Adv.* **2024**, *10* (6), No. eadk6856.
(720) Lim, H.; Kwon, H.; Kang, H.; Jang, J. E.; Kwon, H.-J. Semiconducting MOFs on ultraviolet laser-induced graphene with a hierarchical pore architecture for NO2 monitoring. *Nat. Commun.* **2023**, *14*, 3114.
(721) Huang, C.; Shang, X.; Zhou, X.; Zhang, Z.; Huang, X.; Lu, Y.; Wang, M.; Loffler, M.; Liao, Z.; Qi, H.; Kaiser, U.; Schwarz, D.; Fery, A.; Wang, T.; Mannsfeld, S. C. B.; Hu, G.; Feng, X.; Dong, R.; et al. Hierarchical conductive metal-organic framework films enabling efficient interfacial mass transfer. *Nat. Commun.* **2023**, *14*, 3850.
(722) Lu, L.; Liu, X.; Gu, P.; Hu, Z.; Liang, X.; Deng, Z.; Sun, Z.; Zhang, X.; Yang, X.; Yang, J.; Zu, G.; Huang, J. Stretchable all-gel organic electrochemical transistors. *Nat. Commun.* **2025**, *16*, 3831.
(723) Esteves, C.; Palma, S. I. C. J.; Costa, H. M. A.; Alves, C.; Santos, G. M. C.; Ramou, E.; Carvalho, A. L.; Alves, V.; Roque, A. C. A. Tackling Humidity with Designer Ionic Liquid-Based Gas Sensing Soft Materials. *Adv. Mater.* **2022**, *34* (8), 2107205.
(724) Chouhdry, H. H.; Lee, D. H.; Bag, A.; Lee, N.-E. A flexible artificial chemosensory neuronal synapse based on chemoreceptive ionogel-gated electrochemical transistor. *Nat. Commun.* **2023**, *14*, 821.
(725) Lei, D.; Liu, N.; Su, T.; Zhang, Q.; Wang, L.; Ren, Z.; Gao, Y. Roles of MXene in pressure sensing: preparation, composite structure design, and mechanism. *Adv. Mater.* **2022**, *34* (52), 2110608.
(726) Wang, D.; Zhang, D.; Tang, M.; Zhang, H.; Sun, T.; Yang, C.; Mao, R.; Li, K.; Wang, J. Ethylene chlorotrifluoroethylene/hydrogel-based liquid-solid triboelectric nanogenerator driven self-powered MXene-based sensor system for marine environmental monitoring. *Nano Energy* **2022**, *100*, 107509.
(727) Qian, C.; Choi, Y.; Kim, S.; Kim, S.; Choi, Y. J.; Roe, D. G.; Lee, J. H.; Kang, M. S.; Lee, W. H.; Cho, J. H. Risk-perceptional and feedback-controlled response system based on NO2-detecting artificial sensory synapse. *Adv. Funct. Mater.* **2022**, *32* (18), 2112490.
(728) Li, T.; Yu, H.; Xiong, Z.; Gao, Z.; Zhou, Y.; Han, S.-T. 2D oriented covalent organic frameworks for alcohol-sensory synapses. *Mater. Horizons* **2021**, *8* (7), 2041−2049.


https://doi.org/10.1021/acs.chemrev.4c00966
*Chem. Rev.* 2025, 125, 11567−11665

(729) Bernabei, M.; Persaud, K. C.; Pantalei, S.; Zampetti, E.; Beccherelli, R. Large-scale chemical sensor array testing biological olfaction concepts. *IEEE Sens. J.* **2012**, *12* (11), 3174−3183.
(730) Kwon, O. S.; Song, H. S.; Park, S. J.; Lee, S. H.; An, J. H.; Park, J. W.; Yang, H.; Yoon, H.; Bae, J.; Park, T. H.; et al. An ultrasensitive, selective, multiplexed superbioelectronic nose that mimics the human sense of smell. *Nano Lett.* **2015**, *15* (10), 6559−6567.
(731) Roy, S.; Rhim, J.-W. Anthocyanin food colorant and its application in pH-responsive color change indicator films. *Crit. Rev. Food Sci. Nutr.* **2021**, *61* (14), 2297−2325.
(732) Dunbar, A.; Brittle, S.; Richardson, T.; Hutchinson, J.; Hunter, C. Detection of volatile organic compounds using porphyrin derivatives. *J. Phys. Chem. B* **2010**, *114* (36), 11697−11702.
(733) Gilbertson, T. A.; Khan, N. A. Cell signaling mechanisms of oro-gustatory detection of dietary fat: advances and challenges. *Prog. Lipid Res.* **2014**, *53*, 82−92.
(734) Ye, J.; Fan, M.; Zhang, X.; Liang, Q.; Zhang, Y.; Zhao, X.; Lin, C.-T.; Zhang, D. A novel biomimetic electrochemical taste-biosensor based on conformational changes of the taste receptor. *Biosens. Bioelectron.* **2024**, *249*, 116001.
(735) del Valle, M. Electronic tongues employing electrochemical sensors. *Electroanalysis* **2010**, *22* (14), 1539−1555.
(736) Kouhi, I.; Parvizi Fard, G.; Alipour, E.; Saadatirad, A. Development of an electrochemical sensor for determination of vanillin in some food stuffs. *J. Food Process Preserv.* **2022**, *46* (2), No. e16289.
(737) Jung, H. H.; Yea, J.; Lee, H.; Jung, H. N.; Jekal, J.; Lee, H.; Ha, J.; Oh, S.; Song, S.; Son, J.; et al. Taste bud-inspired single-drop multitaste sensing for comprehensive flavor analysis with deep learning algorithms. *ACS Appl. Mater. Interfaces* **2023**, *15* (39), 46041−46053.
(738) Ciui, B.; Martin, A.; Mishra, R. K.; Nakagawa, T.; Dawkins, T. J.; Lyu, M.; Cristea, C.; Sandulescu, R.; Wang, J. Chemical sensing at the robot fingertips: Toward automated taste discrimination in food samples. *ACS Sens.* **2018**, *3* (11), 2375−2384.
(739) Mosca, A. C.; Andriot, I.; Guichard, E.; Salles, C. Binding of Na+ ions to proteins: Effect on taste perception. *Food Hydrocolloids* **2015**, *51*, 33−40.
(740) Gwac, H.; Jang, Y.; Moon, J. H.; Kim, S. J. Wearable Multi-Plied Potentiometric Sensor based on Carbon Nanotube Yarn for Electronic Tongue. *Adv. Mater. Technol.* **2024**, *9*, 2302194.
(741) Neta, E.; Johanningsmeier, S.; Drake, M.; McFeeters, R. Effects of pH adjustment and sodium ions on sour taste intensity of organic acids. *J. Food Sci.* **2009**, *74* (4), S165−S169.
(742) Schiffman, S. S.; Sattely-Miller, E. A.; Graham, B. G.; Bennett, J. L.; Booth, B. J.; Desai, N.; Bishay, I. Effect of temperature, pH, and ions on sweet taste. *Physiol. Behav.* **2000**, *68* (4), 469−481.
(743) Wei, X.; Wang, B.; Cao, X.; Zhou, H.; Wu, Z.; Wang, Z. L. Dual-sensory fusion self-powered triboelectric taste-sensing system towards effective and low-cost liquid identification. *Nat. Food* **2023**, *4* (8), 721−732.
(744) Xu, W.; He, Y.; Li, J.; Deng, Y.; Zhou, J.; Xu, E.; Ding, T.; Wang, W.; Liu, D. Olfactory visualization sensor system based on colorimetric sensor array and chemometric methods for high precision assessing beef freshness. *Meat Sci.* **2022**, *194*, 108950.
(745) Li, S.; Li, K.; Li, X.; Chen, Z. Colorimetric electronic tongue for rapid discrimination of antioxidants based on the oxidation etching of nanotriangular silver by metal ions. *ACS Appl. Mater. Interfaces* **2019**, *11* (40), 37371−37378.
(746) Im, H.; Choi, J.; Lee, H.; Al Balushi, Z. Y.; Park, D.-H.; Kim, S. Colorimetric Multigas Sensor Arrays and an Artificial Olfactory Platform for Volatile Organic Compounds. *ACS Sens.* **2023**, *8* (9), 3370−3379.
(747) Ganzevles, P. G.; Kroeze, J. H. The sour taste of acids. The hydrogen ion and the undissociated acid as sour agents. *Chem. Senses* **1987**, *12* (4), 563−576.
(748) Fujimura, S.; Koga, H.; Takeda, H.; Tone, N.; Kadowaki, M.; Ishibashi, T. Role of taste-active components, glutamic acid, 5′-inosinic acid and potassium ion in taste of chicken meat extract. *Anim. Sci. Technol. (Jpn.)* **1996**, *67* (5), 423−429.
(749) Bigiani, A. Salt taste. In *The Senses: A Comprehensive Reference*; Elsevier, Academic Press, 2020; Vol. *3*, pp 247−263.
(750) Lyall, V.; Alam, R. I.; Phan, D. Q.; Ereso, G. L.; Phan, T.-H. T.; Malik, S. A.; Montrose, M. H.; Chu, S.; Heck, G. L.; Feldman, G. M.; et al. Decrease in rat taste receptor cell intracellular pH is the proximate stimulus in sour taste transduction. *Am. J. Physiol.-Cell Physiol.* **2001**, *281* (3), C1005−C1013.
(751) Wu, X.; Tahara, Y.; Yatabe, R.; Toko, K. Taste sensor: Electronic tongue with lipid membranes. *Anal. Sci.* **2020**, *36* (2), 147−159.
(752) Tahara, Y.; Ikeda, A.; Maehara, Y.; Habara, M.; Toko, K. Development and evaluation of a miniaturized taste sensor chip. *Sensors* **2011**, *11* (10), 9878−9886.
(753) Parra, V.; Arrieta, Á. A.; Fernández-Escudero, J. A.; García, H.; Apetrei, C.; Rodríguez-Méndez, M. L.; de Saja, J. A. E-tongue based on a hybrid array of voltammetric sensors based on phthalocyanines, perylene derivatives and conducting polymers: Discrimination capability towards red wines elaborated with different varieties of grapes. *Sens. Actuator B-Chem.* **2006**, *115* (1), 54−61.
(754) Zhu, Y.; Wang, J.; Wu, Y.; Shang, Z.; Ding, Y.; Hu, A. A fluorescent sensor array-based electronic tongue for Chinese tea discrimination. *J. Mater. Chem. C* **2021**, *9* (17), 5676−5681.
(755) Khan, A.; Ahmed, S.; Sun, B.-Y.; Chen, Y.-C.; Chuang, W.-T.; Chan, Y.-H.; Gupta, D.; Wu, P.-W.; Lin, H.-C. Self-healable and anti-freezing ion conducting hydrogel-based artificial bioelectronic tongue sensing toward astringent and bitter tastes. *Biosens. Bioelectron.* **2022**, *198*, 113811.
(756) Ahn, S. R.; An, J. H.; Song, H. S.; Park, J. W.; Lee, S. H.; Kim, J. H.; Jang, J.; Park, T. H. Duplex bioelectronic tongue for sensing umami and sweet tastes based on human taste receptor nanovesicles. *ACS Nano* **2016**, *10* (8), 7287−7296.
(757) Chen, P.; Wang, B.; Cheng, G.; Wang, P. Taste receptor cell-based biosensor for taste specific recognition based on temporal firing. *Biosens. Bioelectron.* **2009**, *25* (1), 228−233.
(758) Kobayashi, Y.; Habara, M.; Ikezazki, H.; Chen, R.; Naito, Y.; Toko, K. Advanced taste sensors based on artificial lipids with global selectivity to basic taste qualities and high correlation to sensory scores. *Sensors* **2010**, *10* (4), 3411−3443.
(759) Liu, J.; Qian, J.; Adil, M.; Bi, Y.; Wu, H.; Hu, X.; Wang, Z.; Zhang, W. Bioinspired integrated triboelectric electronic tongue. *Microsyst. Nanoeng.* **2024**, *10*, 57.
(760) Siew, F. W.; Sook, M. K. Differential colorimetric nano-biosensor array as bioelectronic tongue for discrimination and quantitation of multiple foodborne carcinogens. *Food Chem.* **2021**, *357*, 129801.
(761) Chen, H.; Bian, F.; Wang, Y.; Zhao, Y.; Shang, L. Colorimetric photonic tongue for metal ions screening. *Matter* **2022**, *5* (5), 1590−1602.
(762) Hao, M.; Li, Z.; Huang, X.; Wang, Y.; Wei, X.; Zou, X.; Shi, J.; Huang, Z.; Yin, L.; Gao, L.; et al. A cell-based electrochemical taste sensor for detection of Hydroxy-α-sanshool. *Food Chem.* **2023**, *418*, 135941.
(763) Liu, J.; Zhang, N.; Li, J.; Li, M.; Wang, G.; Wang, W.; Fan, Y.; Jiang, S.; Chen, G.; Zhang, Y.; et al. A novel umami electrochemical biosensor based on AuNPs@ ZIF-8/Ti3C2MXene immobilized T1R1-VFT. *Food Chem.* **2022**, *397*, 133838.
(764) Yang, R.; Zhang, W.; Tiwari, N.; Yan, H.; Li, T.; Cheng, H. Multimodal sensors with decoupled sensing mechanisms. *Adv. Sci.* **2022**, *9* (26), 2202470.
(765) Won, S. M.; Wang, H.; Kim, B. H.; Lee, K.; Jang, H.; Kwon, K.; Han, M.; Crawford, K. E.; Li, H.; Lee, Y.; et al. Multimodal sensing with a three-dimensional piezoresistive structure. *ACS Nano* **2019**, *13* (10), 10972−10979.
(766) Lo, L.-W.; Zhao, J.; Wan, H.; Wang, Y.; Chakrabartty, S.; Wang, C. A soft sponge sensor for multimodal sensing and distinguishing of pressure, strain, and temperature. *ACS Appl. Mater. Interfaces* **2022**, *14* (7), 9570−9578.


https://doi.org/10.1021/acs.chemrev.4c00966
*Chem. Rev.* 2025, 125, 11567−11665

(767) Kumari, P.; Mathew, L.; Syal, P. Increasing trend of wearables and multimodal interface for human activity monitoring: A review. *Biosens. Bioelectron.* **2017**, *90*, 298−307.
(768) Yadav, S. K.; Tiwari, K.; Pandey, H. M.; Akbar, S. A. A review of multimodal human activity recognition with special emphasis on classification, applications, challenges and future directions. *Knowledge-Based Syst.* **2021**, *223*, 106970.
(769) Servati, A.; Zou, L.; Wang, Z. J.; Ko, F.; Servati, P. Novel flexible wearable sensor materials and signal processing for vital sign and human activity monitoring. *Sensors* **2017**, *17* (7), 1622.
(770) Zhu, H.; Luo, H.; Cai, M.; Song, J. A multifunctional flexible tactile sensor based on resistive effect for simultaneous sensing of pressure and temperature. *Adv. Sci.* **2024**, *11* (6), 2307693.
(771) Gao, F.-L.; Min, P.; Gao, X.-Z.; Li, C.; Zhang, T.; Yu, Z.-Z.; Li, X. Integrated temperature and pressure dual-mode sensors based on elastic PDMS foams decorated with thermoelectric PEDOT: PSS and carbon nanotubes for human energy harvesting and electronic-skin. *J. Mater. Chem. A* **2022**, *10* (35), 18256−18266.
(772) Li, M.; Chen, J.; Zhong, W.; Luo, M.; Wang, W.; Qing, X.; Lu, Y.; Liu, Q.; Liu, K.; Wang, Y.; et al. Large-area, wearable, self-powered pressure-temperature sensor based on 3D thermoelectric spacer fabric. *ACS Sens.* **2020**, *5* (8), 2545−2554.
(773) Chen, L.; Chang, X.; Wang, H.; Chen, J.; Zhu, Y. Stretchable and transparent multimodal electronic-skin sensors in detecting strain, temperature, and humidity. *Nano Energy* **2022**, *96*, 107077.
(774) Zhang, X.; Li, J.; Lin, J.; Li, W.; Chu, W.; Zhang, M.; Lu, Y.; He, X.; Zhao, Q. Highly stretchable electronic-skin sensors with porous microstructure for efficient multimodal sensing with wearable comfort. *Adv. Mater. Interfaces* **2023**, *10* (8), 2201958.
(775) Yu, Y.; Nassar, J.; Xu, C.; Min, J.; Yang, Y.; Dai, A.; Doshi, R.; Huang, A.; Song, Y.; Gehlhar, R.; Ames, A. D.; Gao, W. Biofuel-powered soft electronic skin with multiplexed and wireless sensing for human-machine interfaces. *Sci. Robot.* **2020**, *5* (41), No. eaaz7946.
(776) Kim, S. H.; Basir, A.; Avila, R.; Lim, J.; Hong, S. W.; Choe, G.; Shin, J. H.; Hwang, J. H.; Park, S. Y.; Joo, J.; et al. Strain-invariant stretchable radio-frequency electronics. *Nature* **2024**, *629*, 1047−1054.
(777) Wang, S.; Xu, J.; Wang, W.; Wang, G.-J. N.; Rastak, R.; Molina-Lopez, F.; Chung, J. W.; Niu, S.; Feig, V. R.; Lopez, J.; et al. Skin electronics from scalable fabrication of an intrinsically stretchable transistor array. *Nature* **2018**, *555* (7694), 83−88.
(778) Zhong, D.; Wu, C.; Jiang, Y.; Yuan, Y.; Kim, M.-g.; Nishio, Y.; Shih, C.-C.; Wang, W.; Lai, J.-C.; Ji, X.; et al. High-speed and large-scale intrinsically stretchable integrated circuits. *Nature* **2024**, *627* (8003), 313−320.
(779) Massetti, M.; Jiao, F.; Ferguson, A. J.; Zhao, D.; Wijeratne, K.; Würger, A.; Blackburn, J. L.; Crispin, X.; Fabiano, S. Unconventional thermoelectric materials for energy harvesting and sensing applications. *Chem. Rev.* **2021**, *121* (20), 12465−12547.
(780) Russ, B.; Glaudell, A.; Urban, J. J.; Chabinyc, M. L.; Segalman, R. A. Organic thermoelectric materials for energy harvesting and temperature control. *Nat. Rev. Mater.* **2016**, *1*, 16050.
(781) Briscoe, J.; Dunn, S. Piezoelectric nanogenerators-a review of nanostructured piezoelectric energy harvesters. *Nano Energy* **2015**, *14*, 15−29.
(782) Sezer, N.; Koç, M. A comprehensive review on the state-of-the-art of piezoelectric energy harvesting. *Nano Energy* **2021**, *80*, 105567.
(783) Toprak, A.; Tigli, O. Piezoelectric energy harvesting: State-of-the-art and challenges. *Appl. Phys. Rev.* **2014**, *1* (3), 031104.
(784) Slabov, V.; Kopyl, S.; Soares dos Santos, M. P.; Kholkin, A. L. Natural and eco-friendly materials for triboelectric energy harvesting. *Nano-Micro Lett.* **2020**, *12*, 42.
(785) Ahmed, A.; Hassan, I.; El-Kady, M. F.; Radhi, A.; Jeong, C. K.; Selvaganapathy, P. R.; Zu, J.; Ren, S.; Wang, Q.; Kaner, R. B. Integrated triboelectric nanogenerators in the era of the internet of things. *Adv. Sci.* **2019**, *6* (24), 1802230.
(786) Zou, Y.; Raveendran, V.; Chen, J. Wearable triboelectric nanogenerators for biomechanical energy harvesting. *Nano Energy* **2020**, *77*, 105303.
(787) Chang, S.-Y.; Cheng, P.; Li, G.; Yang, Y. Transparent polymer photovoltaics for solar energy harvesting and beyond. *Joule* **2018**, *2* (6), 1039−1054.
(788) Abdin, Z.; Alim, M. A.; Saidur, R.; Islam, M. R.; Rashmi, W.; Mekhilef, S.; Wadi, A. Solar energy harvesting with the application of nanotechnology. *Renew. Sust. Energy Rev.* **2013**, *26*, 837−852.
(789) Scrosati, B. Paper powers battery breakthrough. *Nat. Nanotechnol.* **2007**, *2* (10), 598−599.
(790) Huang, Y.; Zhong, M.; Huang, Y.; Zhu, M.; Pei, Z.; Wang, Z.; Xue, Q.; Xie, X.; Zhi, C. A self-healable and highly stretchable supercapacitor based on a dual crosslinked polyelectrolyte. *Nat. Commun.* **2015**, *6*, 10310.
(791) Jung, Y.; Pyun, K. R.; Min, J.; Yoon, H.; Lee, M.; Kim, B.-W.; Lee, J.; Ko, S. H. An Ag-Au-PANI core-shell nanowire network for visible-to-infrared data encryption and supercapacitor applications. *J. Mater. Chem. A* **2023**, *11* (13), 7264−7275.
(792) Yin, L.; Cao, M.; Kim, K. N.; Lin, M.; Moon, J.-M.; Sempionatto, J. R.; Yu, J.; Liu, R.; Wicker, C.; Trifonov, A.; et al. A stretchable epidermal sweat sensing platform with an integrated printed battery and electrochromic display. *Nat. Electron.* **2022**, *5* (10), 694−705.
(793) Kim, H.; Pyun, K. R.; Lee, M. T.; Lee, H. B.; Ko, S. H. Recent advances in sustainable wearable energy devices with nanoscale materials and macroscale structures. *Adv. Funct. Mater.* **2022**, *32* (16), 2110535.
(794) Van Meerbeek, I.; De Sa, C.; Shepherd, R. Soft optoelectronic sensory foams with proprioception. *Sci. Robot.* **2018**, *3* (24), No. eaau2489.
(795) Sundararajan, K.; Georgievska, S.; te Lindert, B. H. W.; Gehrman, P. R.; Ramautar, J.; Mazzotti, D. R.; Sabia, S.; Weedon, M. N.; van Someren, E. J. W.; Ridder, L.; Wang, J.; van Hees, V. T. Sleep classification from wrist-worn accelerometer data using random forests. *Sci. Rep.* **2021**, *11*, 24.
(796) Hargrove, L. J.; Li, G.; Englehart, K. B.; Hudgins, B. S. Principal components analysis preprocessing for improved classification accuracies in pattern-recognition-based myoelectric control. *IEEE Trans. Biomed. Eng.* **2009**, *56* (5), 1407−1414.
(797) Sempionatto, J. R.; Lasalde-Ramírez, J. A.; Mahato, K.; Wang, J.; Gao, W. Wearable chemical sensors for biomarker discovery in the omics era. *Nat. Rev. Chem.* **2022**, *6* (12), 899−915.
(798) Fortino, V.; Wisgrill, L.; Werner, P.; Suomela, S.; Linder, N.; Jalonen, E.; Suomalainen, A.; Marwah, V.; Kero, M.; Pesonen, M.; et al. Machine-learning-driven biomarker discovery for the discrimination between allergic and irritant contact dermatitis. *Proc. Natl. Acad. Sci. U. S. A.* **2020**, *117* (52), 33474−33485.
(799) Shim, J.; Fleisch, E.; Barata, F. Wearable-based accelerometer activity profile as digital biomarker of inflammation, biological age, and mortality using hierarchical clustering analysis in NHANES 2011−2014. *Sci. Rep.* **2023**, *13* (1), 9326.
(800) Radha, M.; Fonseca, P.; Moreau, A.; Ross, M.; Cerny, A.; Anderer, P.; Long, X.; Aarts, R. M. A deep transfer learning approach for wearable sleep stage classification with photoplethysmography. *npj Digit. Med.* **2021**, *4*, 135.
(801) LaViola, J. J., Jr A discussion of cybersickness in virtual environments. *ACM SIGCHI Bull.* **2000**, *32* (1), 47−56.
(802) Tang, C.; Xu, M.; Yi, W.; Zhang, Z.; Occhipinti, E.; Dong, C.; Ravenscroft, D.; Jung, S.-M.; Lee, S.; Gao, S.; Kim, J. M.; Occhipinti, L. G. Ultrasensitive textile strain sensors redefine wearable silent speech interfaces with high machine learning efficiency. *npj Flex. Electron.* **2024**, *8*, 27.
(803) Rojas-Munoz, E.; Lin, C.; Sanchez-Tamayo, N.; Cabrera, M. E.; Andersen, D.; Popescu, V.; Barragan, J. A.; Zarzaur, B.; Murphy, P.; Anderson, K.; Douglas, T.; Griffis, C.; McKee, J.; Kirkpatrick, A. W.; Wachs, J. P. Evaluation of an augmented reality platform for austere surgical telementoring: a randomized controlled crossover study in cricothyroidotomies. *npj Digit. Med.* **2020**, *3*, 75.


https://doi.org/10.1021/acs.chemrev.4c00966
*Chem. Rev.* 2025, 125, 11567−11665

(804) Su, Y.-P.; Chen, X.-Q.; Zhou, T.; Pretty, C.; Chase, G. Mixed reality-enhanced intuitive teleoperation with hybrid virtual fixtures for intelligent robotic welding. *Appl. Sci.* **2021**, *11* (23), 11280.
(805) Huang, F.; Yang, X.; Yan, T.; Chen, Z. Telepresence augmentation for visual and haptic guided immersive teleoperation of industrial manipulator. *ISA Trans.* **2024**, *150*, 262−277.
(806) Di Pasquale, V.; De Simone, V.; Miranda, S.; Riemma, S. Smart operators: How Industry 4.0 is affecting the worker's performance in manufacturing contexts. *Procedia Comput. Sci.* **2021**, *180*, 958−967.
(807) Malik, A. A.; Masood, T.; Bilberg, A. Virtual reality in manufacturing: immersive and collaborative artificial-reality in design of human-robot workspace. *Int. J. Comput. Integr. Manuf.* **2020**, *33* (1), 22−37.
(808) Doolani, S.; Wessels, C.; Kanal, V.; Sevastopoulos, C.; Jaiswal, A.; Nambiappan, H.; Makedon, F. A review of extended reality (xr) technologies for manufacturing training. *Technologies* **2020**, *8* (4), 77.
(809) Helsel, S. Virtual reality and education. *Educ. Technol.* **1992**, *32* (5), 38−42.
(810) Kavanagh, S.; Luxton-Reilly, A.; Wuensche, B.; Plimmer, B. A systematic review of virtual reality in education. *Themes Sci. Technol. Educ.* **2017**, *10* (2), 85−119.
(811) Kim, J.; Lee, M.; Shim, H. J.; Ghaffari, R.; Cho, H. R.; Son, D.; Jung, Y. H.; Soh, M.; Choi, C.; Jung, S.; et al. Stretchable silicon nanoribbon electronics for skin prosthesis. *Nat. Commun.* **2014**, *5* (1), 5747.
(812) Zwoliński, G.; Kamińska, D.; Laska-Leśniewicz, A.; Haamer, R. E.; Vairinhos, M.; Raposo, R.; Urem, F.; Reisinho, P. Extended reality in education and training: Case studies in management education. *Electronics* **2022**, *11* (3), 336.
(813) Hunt, C. L.; Sun, Y.; Wang, S.; Shehata, A. W.; Hebert, J. S.; Gonzalez-Fernandez, M.; Kaliki, R. R.; Thakor, N. V. Limb loading enhances skill transfer between augmented and physical reality tasks during limb loss rehabilitation. *J. NeuroEng. Rehabil.* **2023**, *20*, 16.
(814) Sveistrup, H. Motor rehabilitation using virtual reality. *J. NeuroEng. Rehabil.* **2004**, *1*, 10.
(815) Schultheis, M. T.; Rizzo, A. A. The application of virtual reality technology in rehabilitation. *Rehabil. Psychol.* **2001**, *46* (3), 296.
(816) Laver, K. E.; Lange, B.; George, S.; Deutsch, J. E.; Saposnik, G.; Crotty, M. Virtual reality for stroke rehabilitation. *Cochrane Database Syst. Rev.* **2017**, *11* (11), CD008349.
(817) Kim, Y.; Kim, H.; Kim, Y. O. Virtual reality and augmented reality in plastic surgery: a review. *Arch. Plast. Surg.* **2017**, *44* (03), 179−187.
(818) Aïm, F.; Lonjon, G.; Hannouche, D.; Nizard, R. Effectiveness of virtual reality training in orthopaedic surgery. *Arthroscopy* **2016**, *32* (1), 224−232.
(819) Jung, T.; tom Dieck, M. C.; Lee, H.; Chung, N. Effects of virtual reality and augmented reality on visitor experiences in museum. In *Information and Communication Technologies in Tourism 2016: Proceedings of the International Conference in Bilbao, Spain, February 2−5, 2016*; Springer, 2016; pp 621−635.
(820) Wen, F.; Sun, Z.; He, T.; Shi, Q.; Zhu, M.; Zhang, Z.; Li, L.; Zhang, T.; Lee, C. Machine learning glove using self-powered conductive superhydrophobic triboelectric textile for gesture recognition in VR/AR applications. *Adv. Sci.* **2020**, *7* (14), 2000261.
(821) Tussyadiah, I. P.; Wang, D.; Jia, C. Virtual reality and attitudes toward tourism destinations. In *Information and Communication Technologies in Tourism 2017: Proceedings of the International Conference in Rome, Italy, January 24−26, 2017*; Springer; 2017; pp 229−239.
(822) McLean, G.; AlYahya, M.; Barhorst, J. B.; Osei-Frimpong, K. Examining the influence of virtual reality tourism on consumers' subjective wellbeing. *Tour. Manag. Perspect.* **2023**, *46*, 101088.
(823) Lee, J.; Kim, J.; Choi, J. Y. The adoption of virtual reality devices: The technology acceptance model integrating enjoyment, social interaction, and strength of the social ties. *Telemat. Inform.* **2019**, *39*, 37−48.
(824) McMahan, R. P.; Bowman, D. A.; Zielinski, D. J.; Brady, R. B. Evaluating display fidelity and interaction fidelity in a virtual reality game. *IEEE Trans. Vis. Comput. Graph.* **2012**, *18* (4), 626−633.
(825) Lee, H.; Jung, T. H.; tom Dieck, M. C.; Chung, N. Experiencing immersive virtual reality in museums. *Inf. Manage.* **2020**, *57* (5), 103229.
(826) Fida, B.; Cutolo, F.; di Franco, G.; Ferrari, M.; Ferrari, V. Augmented reality in open surgery. *Updates Surg.* **2018**, *70* (3), 389−400.
(827) Yoon, J. W.; Chen, R. E.; Kim, E. J.; Akinduro, O. O.; Kerezoudis, P.; Han, P. K.; Si, P.; Freeman, W. D.; Diaz, R. J.; Komotar, R. J.; Pirris, S. M.; Brown, B. L.; Bydon, M.; Wang, M. Y.; Wharen, R. E.; Quinones-Hinojosa, A. Augmented reality for the surgeon: systematic review. *Int. J. Med. Robot. Comput. Assist. Surg.* **2018**, *14* (4), No. e1914.
(828) Jensen, L.; Konradsen, F. A review of the use of virtual reality head-mounted displays in education and training. *Educ. Inf. Technol.* **2018**, *23*, 1515−1529.
(829) Sacks, R.; Perlman, A.; Barak, R. Construction safety training using immersive virtual reality. *Constr. Manag. Econ.* **2013**, *31* (9), 1005−1017.
(830) Qin, Z.; Tai, Y.; Xia, C.; Peng, J.; Huang, X.; Chen, Z.; Li, Q.; Shi, J. Towards virtual VATS, face, and construct evaluation for peg transfer training of box, VR, AR, and MR trainer. *J. Healthc. Eng.* **2019**, *2019*, 6813719.
(831) Yiannakopoulou, E.; Nikiteas, N.; Perrea, D.; Tsigris, C. Virtual reality simulators and training in laparoscopic surgery. *Int. J. Surg.* **2015**, *13*, 60−64.
(832) Larsen, C. R.; Oestergaard, J.; Ottesen, B. S.; Soerensen, J. L. The efficacy of virtual reality simulation training in laparoscopy: a systematic review of randomized trials. *Acta Obstet. Gynecol. Scand.* **2012**, *91* (9), 1015−1028.
(833) Andrews, C.; Southworth, M. K.; Silva, J. N.; Silva, J. R. Extended reality in medical practice. *Curr. Treat. Option Cardiovasc. Med.* **2019**, *21*, 18.
(834) Ha, M.; Lee, J.; Cho, Y.; Lee, M.; Baek, H.; Lee, J.; Seo, J.; Chun, S.; Kim, K.; Kim, J.-G.; Lee, W. G. A hybrid upper-arm-geared exoskeleton with anatomical digital twin for tangible metaverse feedback and communication. *Adv. Mater. Technol.* **2024**, *9* (2), 2301404.
(835) Acuña Luna, K. P.; Hernandez-Rios, E. R.; Valencia, V.; Trenado, C.; Peñaloza, C. Deep learning-enhanced motor training: A hybrid VR and exoskeleton system for cognitive-motor rehabilitation. *Bioengineering* **2025**, *12* (4), 331.
(836) Bach-y-Rita, P.; Kercel, S. W. Sensory substitution and the human-machine interface. *TRENDS COGN. SCI.* **2003**, *7* (12), 541−546.
(837) Auvray, M.; Myin, E. Perception with compensatory devices: From sensory substitution to sensorimotor extension. *Cogn. Sci.* **2009**, *33* (6), 1036−1058.
(838) Shull, P. B.; Damian, D. D. Haptic wearables as sensory replacement, sensory augmentation and trainer-a review. *J. NeuroEng. Rehabil.* **2015**, *12*, 59.
(839) De Bruyn, N.; Saenen, L.; Thijs, L.; Van Gils, A.; Ceulemans, E.; Essers, B.; Lafosse, C.; Michielsen, M.; Beyens, H.; Schillebeeckx, F.; et al. Sensorimotor vs. motor upper limb therapy for patients with motor and somatosensory deficits: a randomized controlled trial in the early rehabilitation phase after stroke. *Front. Neurol.* **2020**, *11*, 597666.
(840) Cesari, V.; Melfi, F.; Gemignani, A.; Menicucci, D. Sensory substitution increases robotic surgical performance and sets the ground for a mediating role of the sense of embodiment: a systematic review. *Heliyon* **2023**, *9* (11), No. e21665.
(841) Vaitkevičius, A.; Taroza, M.; Blažauskas, T.; Damaševičius, R.; Maskeliūnas, R.; Woźniak, M. Recognition of American sign language gestures in a virtual reality using leap motion. *Appl. Sci.* **2019**, *9* (3), 445.
(842) Weissmann, J.; Salomon, R. Gesture recognition for virtual reality applications using data gloves and neural networks. In


https://doi.org/10.1021/acs.chemrev.4c00966
*Chem. Rev.* 2025, 125, 11567−11665

*IJCNN'99. International Joint Conference on Neural Networks. Proceedings (Cat. No. 99CH36339)*; IEEE, 1999; Vol. 3, pp 2043−2046.
(843) Chen, Z.; Min, H.; Wang, D.; Xia, Z.; Sun, F.; Fang, B. A review of myoelectric control for prosthetic hand manipulation. *Biomimetics* **2023**, *8* (3), 328.
(844) Murray, C. D.; Pettifer, S.; Howard, T.; Patchick, E. L.; Caillette, F.; Kulkarni, J.; Bamford, C. The treatment of phantom limb pain using immersive virtual reality: three case studies. *Disabil. Rehabil.* **2007**, *29* (18), 1465−1469.
(845) Trost, Z.; France, C.; Anam, M.; Shum, C. Virtual reality approaches to pain: toward a state of the science. *Pain* **2021**, *162* (2), 325−331.
(846) Park, M. J.; Kim, D. J.; Lee, U.; Na, E. J.; Jeon, H. J. A literature overview of virtual reality (VR) in treatment of psychiatric disorders: recent advances and limitations. *Front. Psychiatry* **2019**, *10*, 505.
(847) Yao, S.; Kim, G. The effects of immersion in a virtual reality game: Presence and physical activity. In *HCI in Games: First International Conference, HCI-Games 2019, Held as Part of the 21st HCI International Conference, HCII 2019, Orlando, FL, USA, July 26−31, 2019, Proceedings 21*; Springer, 2019; pp 234−242.
(848) Checa, D.; Bustillo, A. A review of immersive virtual reality serious games to enhance learning and training. *Multimed. Tools Appl.* **2020**, *79* (9), 5501−5527.
(849) Kim, G.; Biocca, F. Immersion in virtual reality can increase exercise motivation and physical performance. In *Virtual, Augmented and Mixed Reality: Applications in Health, Cultural Heritage, and Industry: 10th International Conference, VAMR 2018, Held as Part of HCI International 2018, Las Vegas, NV, USA, July 15−20, 2018, Proceedings, Part II 10*; Springer, 2018; pp 94−102.
(850) Kwon, Y.-T.; Kim, Y.-S.; Kwon, S.; Mahmood, M.; Lim, H.-R.; Park, S.-W.; Kang, S.-O.; Choi, J. J.; Herbert, R.; Jang, Y. C.; Choa, Y.-H.; Yeo, W.-H. All-printed nanomembrane wireless bioelectronics using a biocompatible solderable graphene for multimodal human-machine interfaces. *Nat. Commun.* **2020**, *11*, 3450.
(851) Zallio, M.; Clarkson, P. J. The ethics of the metaverse and digital, virtual and immersive environments: Metavethics. In *The Future of Metaverse in the Virtual Era and Physical World*; Springer, 2023; pp 93−103.
(852) Schulteis, M.; Rothbaum, B. O. Ethical issues for the use of virtual reality in the psychological sciences. *Ethical Iss. Clin. Neurophysiol.* **2002**, *243* (80), 5.
(853) Yoo, S.-S.; Kim, H.; Filandrianos, E.; Taghados, S. J.; Park, S. Non-invasive brain-to-brain interface (BBI): establishing functional links between two brains. *PLoS One* **2013**, *8* (4), No. e60410.
(854) Millán, J. d. R.; Carmena, J. Invasive or noninvasive: understanding brain-machine interface technology; Institute of Electrical and Electronics Engineers, 2010.
(855) Kim, H.; Kim, J. H.; Lee, Y. J.; Lee, J.; Han, H.; Yi, H.; Kim, H.; Kim, H.; Kang, T. W.; Chung, S.; Ban, S.; Lee, B.; Lee, H.; Im, C.-H.; Cho, S. J.; Sohn, J. W.; Yu, K. J.; Kang, T. J.; Yeo, W.-H. Motion artifact-controlled micro-brain sensors between hair follicles for persistent augmented reality brain-computer interfaces. *Proc. Natl. Acad. Sci. U. S. A.* **2025**, *122* (15), No. e2419304122.
(856) Prapas, G.; Angelidis, P.; Sarigiannidis, P.; Bibi, S.; Tsipouras, M. G. Connecting the Brain with Augmented Reality: A Systematic Review of BCI-AR Systems. *Appl. Sci.* **2024**, *14* (21), 9855.
(857) Regas, I.; Loisel, F.; Haight, H.; Menu, G.; Obert, L.; Pluvy, I. Functionalized nerve conduits for peripheral nerve regeneration: A literature review. *Hand Surg. Rehabil.* **2020**, *39* (5), 343−351.
(858) Fenno, L.; Yizhar, O.; Deisseroth, K. The development and application of optogenetics. *Annu. Rev. Neurosci.* **2011**, *34* (1), 389−412.
(859) Deisseroth, K. Optogenetics and psychiatry: applications, challenges, and opportunities. *Biol. Psychiatry* **2012**, *71* (12), 1030−1032.
(860) Deisseroth, K. Optogenetics. *Nat. Methods* **2011**, *8* (1), 26−29.
(861) Booth, L. C.; Yao, S. T.; Korsak, A.; Farmer, D. G.S.; Hood, S. G.; McCormick, D.; Boesley, Q.; Connelly, A. A.; McDougall, S. J.; Korim, W. S.; Guild, S.-J.; Mastitskaya, S.; Le, P.; Teschemacher, A. G.; Kasparov, S.; Ackland, G. L.; Malpas, S. C.; McAllen, R. M.; Allen, A. M.; May, C. N.; Gourine, A. V. Selective optogenetic stimulation of efferent fibers in the vagus nerve of a large mammal. *Brain Stimul.* **2021**, *14* (1), 88−96.
(862) Kalmbach, A.; Hedrick, T.; Waters, J. Selective optogenetic stimulation of cholinergic axons in neocortex. *J. Neurophysiol.* **2012**, *107* (7), 2008−2019.
(863) Entcheva, E.; Kay, M. W. Cardiac optogenetics: a decade of enlightenment. *Nat. Rev. Cardiol.* **2021**, *18* (5), 349−367.
(864) Delbeke, J.; Hoffman, L.; Mols, K.; Braeken, D.; Prodanov, D. And then there was light: perspectives of optogenetics for deep brain stimulation and neuromodulation. *Front. Neurosci.* **2017**, *11*, 663.
(865) Losey, D. M.; Stocco, A.; Abernethy, J. A.; Rao, R. P. N. Navigating a 2D virtual world using direct brain stimulation. *Front. Robot. AI* **2016**, *3*, 72.
(866) Yousif, N.; Liu, X. Modeling the current distribution across the depth electrode-brain interface in deep brain stimulation. *Expert Rev. Med. Devices* **2007**, *4* (5), 623−631.
(867) Liu, X.; Zhu, H.; Zhang, M.; Wu, X.; Richardson, A. G.; Sritharan, S. Y.; Ge, D.; Shu, Y.; Lucas, T. H.; Van der Spiegel, J. A fully integrated wireless sensor-brain interface system to restore finger sensation. In *2017 IEEE International Symposium on Circuits and Systems (ISCAS)*; IEEE, 2017; pp 1−4.
(868) Ron-Angevin, R.; Díaz-Estrella, A. Brain-computer interface: Changes in performance using virtual reality techniques. *Neurosci. Lett.* **2009**, *449* (2), 123−127.
(869) Lécuyer, A.; Lotte, F.; Reilly, R. B.; Leeb, R.; Hirose, M.; Slater, M. Brain-computer interfaces, virtual reality, and videogames. *Computer* **2008**, *41* (10), 66−72.
(870) Williams, N. R.; Okun, M. S. Deep brain stimulation (DBS) at the interface of neurology and psychiatry. *J. Clin. Invest.* **2013**, *123* (11), 4546−4556.


https://doi.org/10.1021/acs.chemrev.4c00966
*Chem. Rev.* 2025, 125, 11567−11665